SECURITY CLASSIFICATION OF THIS PAGE UNCLASSIFIED

AD-A208 840

(2)

REPORT DOCUMENTATION PAGE

1a. REPORT SECURITY CLASSIFICATION	1b. RESTRICTIVE MARKINGS
2a. SECURITY CLASSIFICATION AUTHORITY	3. DISTRIBUTION / AVAILABILITY OF REPORT: Approved for public release, distribution unlimited
2b. DECLASSIFICATION / DOWNGRADING SCHEDULE	
4. PERFORMING ORGANIZATION REPORT NUMBER(S)	5. MONITORING ORGANIZATION REPORT NUMBER(S): AFOSR-TR- 87-2033
6a. NAME OF PERFORMING ORGANIZATION: Dept of Aerospace Engineering	6b. OFFICE SYMBOL (If applicable):
6c. ADDRESS (City, State, and ZIP Code): Texas A&M University, College Station, TX 77843-3141	7a. NAME OF MONITORING ORGANIZATION: AFOSR/NA
	7b. ADDRESS (City, State, and ZIP Code): Bolling Air Force Base Bldg. 410, Washington DC, 20332
8a. NAME OF FUNDING / SPONSORING ORGANIZATION: AFOSR	8b. OFFICE SYMBOL (If applicable): NA
8c. ADDRESS (City, State, and ZIP Code): Bolling AFB Bldg. 410, Washington, DC, 20332	9. PROCUREMENT INSTRUMENT IDENTIFICATION NUMBER: AFOSR-84-0066
	10. SOURCE OF FUNDING NUMBERS: PROGRAM ELEMENT NO. 61102F; PROJECT NO. 2308; TASK NO. B2; WORK UNIT ACCESSION NO.

11. TITLE (Include Security Classification)

Ultrasonic Nondestructive Evalustion of Damage in Continuous Fiber Composites

12. PERSONAL AUTHOR(S)

Vikram K. Kinra

13a. TYPE OF REPORT	13b. TIME COVERED	14. DATE OF REPORT (Year, Month, Day)	15. PAGE COUNT
Final	FROM ~~2/1/84 TO 1/31/87~~ 1984-1988	~~November 1987~~ 1989	

16. SUPPLEMENTARY NOTATION

17. COSATI CODES			18. SUBJECT TERMS (Continue on reverse if necessary and identify by block number)
FIELD	GROUP	SUB-GROUP	Velocity, Attenuation, Composites, Damage, Ultrasonic, Nondestructive Evaluation.

19. ABSTRACT (Continue on reverse if necessary and identify by block number)

A new technique for measuring the wavespeed and attenuation in the thickness direction, in extremely thin laminates, and the excitation and detection of Lamb waves in the lengthwise direction has been developed. Thus, both in-plane and out-of-plane measurements can be made. Damage in the form of transverse cracking in cross-ply graphite/epoxy laminates has been studied by the use of these two techniques. For through-the-thickness measurements the stiffness was found to be insensitive to transverse cracking. The attenuation, however, was found to be quite sensitive and, therefore, has been shown to be a reliable damage metric. For the complementary case of Lamb wave propagation in the lengthwise direction, both the stiffness and the attenuation were observed to be sensitive damage parameters.

20. DISTRIBUTION / AVAILABILITY OF ABSTRACT	21. ABSTRACT SECURITY CLASSIFICATION
☐ UNCLASSIFIED/UNLIMITED ☐ SAME AS RPT ☐ DTIC USERS	
22a. NAME OF RESPONSIBLE INDIVIDUAL: Lt. Col. George K. Haritos	22b. TELEPHONE (Include Area Code): (202) 767-0463
	22c. OFFICE SYMBOL: NA

DD FORM 1473, 84 MAR 83 APR edition may be used until exhausted. All other editions are obsolete.

SECURITY CLASSIFICATION OF THIS PAGE UNCLASSIFIED

89 5 15 124

AFOSR TR-87-2033

Ultrasonic nondestructive evaluation of fibre-reinforced composite materials – a review

VIKRAM K KINRA and VINAY DAYAL

Department of Aerospace Engineering and Mechanics and Materials Center, Texas A&M University, College Station, Texas 77843, USA

Abstract. This paper reviews various ultrasonic nondestructive evalu-

Reprinted from

SĀDHANĀ

Academy Proceedings in Engineering Sciences

Sādhanā, Vol. 11, Parts 3 & 4, December 1987, pp. 419–432. © Printed in India

Ultrasonic nondestructive evaluation of fibre-reinforced composite materials – a review

VIKRAM K KINRA and VINAY DAYAL

Department of Aerospace Engineering and Mechanics and Materials Center, Texas A&M University, College Station, Texas 77843, USA

Abstract. This paper reviews various ultrasonic nondestructive evaluation techniques applicable to fibre-reinforced composites. The techniques are briefly described and key references are cited. Methods to evaluate the reduced stiffness of composites due to micro-damage are described. Results show that for composites through-the-thickness attenuation increases and stiffness does not change due to transverse cracks, but in-plane stiffness and attenuation changes are substantial and can be measured by the Lamb wave techniques.

Keywords. Ultrasonics; nondestructive evaluation; composites; thin laminates.

1. Introduction

The excellent strength-to-weight ratio and the flexibility in tailoring the strength and stiffness of fibre-reinforced materials have made composites an indispensable structural material. Mixing of brittle but high strength fibres (e.g. graphite fibre, $\sigma_u = 2{\cdot}5\ \mathrm{GN/m^2}$) with viscoelastic and low strength (e.g. epoxy $\sigma_u = 0{\cdot}10\ \mathrm{GN/m^2}$) matrices, however, has created some very complex damage mechanism problems. Damage initiation and propagation are very different in composites from those in metals. The effect of mechanical, thermal or humidity loading is very complex in composites. Nondestructive evaluation (NDE) of in-service components is important because the damage initiation and growth mechanisms are not fully understood.

Various NDE techniques such as X-ray radiography, dye-penetrant tests, ultrasonics, thermography, acoustic emission, holography etc. have been successfully used to characterize damage in composites. This review is restricted to ultrasonic NDE of composites. It will also cover the technique of acoustic emission as well as the more recently developed method of acousto-ultrasonics.

In metals when damage is initiated, it becomes the nucleating site for further damage growth. On the other hand, Reifsnider *et al* (1983, pp. 399–420) have shown that in fibre-reinforced composites, a very different phenomenon takes place. Invariably, the first mode of damage in composites is matrix cracking. The fibres, being much stronger than the matrix, are able to carry the extra load due to the redistribution of stresses in

the vicinity of the matrix cracks. Fibres also act as matrix crack arresters. Stresses in the vicinity of the first crack are relieved and the next crack forms where the stresses again develop to a critical value. As a result the entire structure develops microcracks without endangering the integrity of the structure. Up to this stage of damage, identification of individual cracks does not serve any useful purpose. But due to these cracks the stiffness of the structure is reduced and hence the interest lies in the determination of the residual stiffness and the attenuation of the material. The transverse cracks in the 90°-plies are arrested by the 0°-plies. The point of crack arrest also becomes a point of stress concentration and, therefore, a nucleating site for the delaminations. At this stage of damage development microcracks have lost their significance and the attention is turned to the detection of macro-damage. The damage size and location are also of interest during manufacturing since any foreign material, such as dust, grease or oil left on the surface of the lamina during fabrication can result in debonding. Thus all NDE techniques can broadly be categorized as (1) techniques for detection, sizing and location of damage, and (2) evaluation of mechanical properties such as stiffness and ultrasonic attenuation.

2. Detection of damage, size and location

According to Krautkramer & Krautkramer (1983), Sokolov (1929) used a through-the-thickness transmission technique for flaw detection in metals. In regions where cracks exist, the sound intensity is small compared to the undamaged regions. Firestone (1945) utilized the pulse-echo method for the detection of flaws in materials. The ultrasonic pulses reflected from the flaws are detected to map out the flaws. The time taken for the waves to travel from the transmitting transducer to the receiving transducer gives the depth of the flaw if the wave speed in the material is accurately known. Today, using

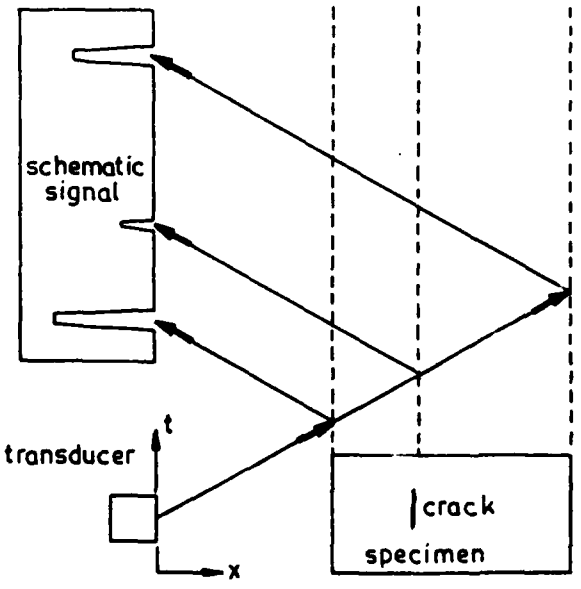

Figure 1. Schematic of the C-scan principle. The signal reflected from the crack is seen as a smaller signal between the reflections from the front and back surfaces.

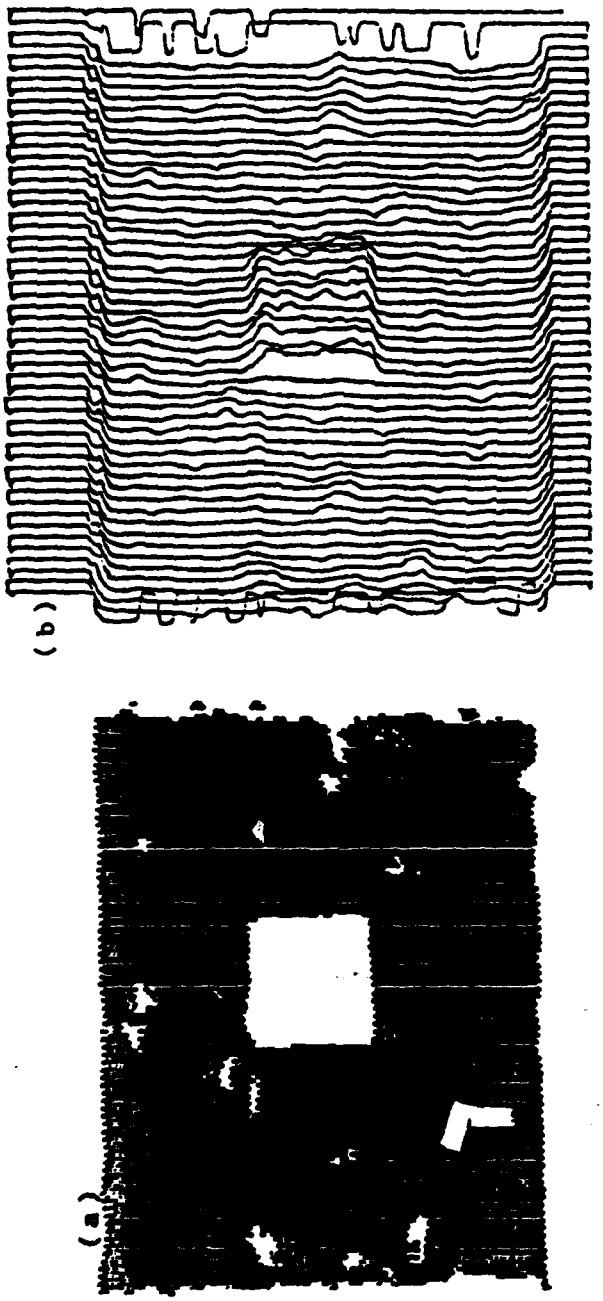

Figure 2. Representative C-scan of the graphite/epoxy laminate with an initial flaw in the form of an embedded inter-ply square film patch. (a) Pen-lift scan, (b) analog scan (Daniel *et al* 1981).

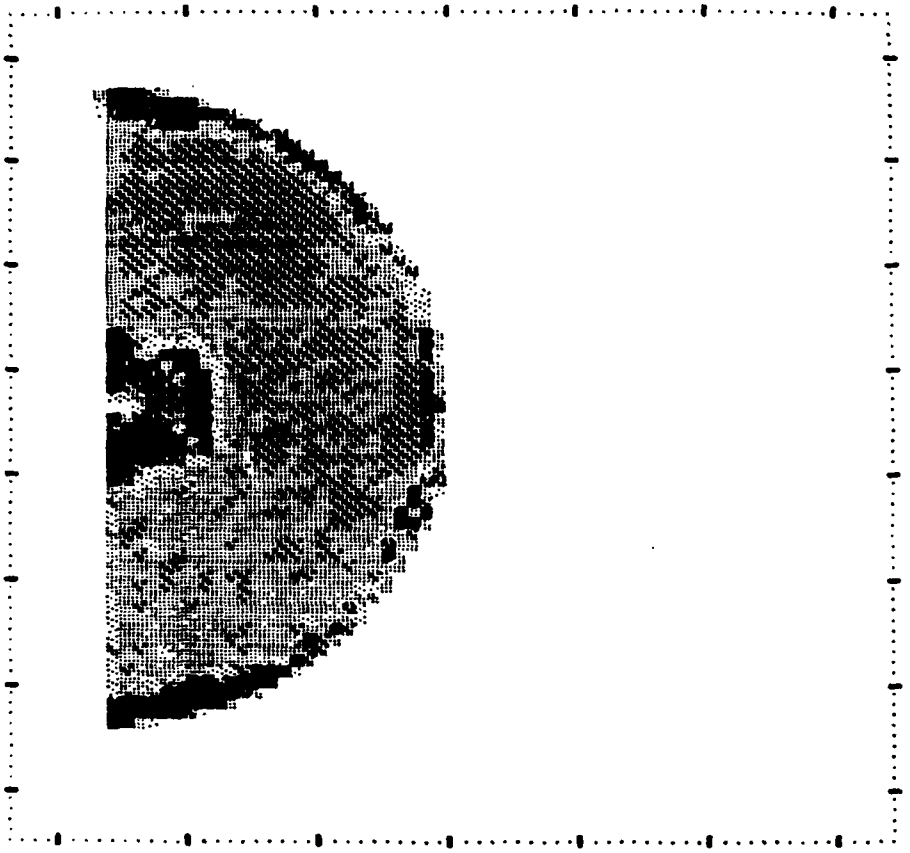

Figure 3. Digital C-scan of a 32-ply graphite/epoxy laminate with central and circumferential damage as well as thickness variation across the specimen (R A Blake, private commun.) (magnification = 0·8 ×; scan line spacing = 0·082 in.; scan time = 61 s).

computers with multicolored plotting facilities, a very detailed picture of the damage can be obtained. This pulse-echo technique is now better known as the "C-scan" technique. The basic concept behind this technique is shown in figure 1. The same transducer is used for production and reception of the waves. A typical signal trace is also shown. The first pulse is the front surface reflection, the second is reflection from the crack, and the third pulse is from the back surface. The presence of central pulse indicates a flaw in the material. The depth h of the crack can be obtained by an accurate measurement of time t and prior knowledge of the wavespeed c in the material: $h = ct/2$. Bar-Cohen *et al* (1979) have used this technique to detect 1 mm diameter delaminations in graphite/epoxy laminates with an accuracy of $\pm 0{\cdot}2$ mm in depth measurements. Daniel *et al* (1981) have used the C-scan for monitoring fatigue damage in composites; a typical C-scan picture from his work is reproduced in figure 2. Blake (1982, 1983) and Blake & Hartman (1984) have used computers for digital analysis and presentation of the damage pictures; see figure 3 for a digital C-scan picture.

Acoustic emission (AE) is another technique which is used for the detection of the onset of damage, its size and location. The deformation of a structure takes place under loading. This deformation eventually results in the generation of cracks or discontinuities in the structure. During the initiation and development of these cracks energy is released as sound waves. Thus the instant of initiation of damage can be recorded by detecting the AE waves. By a simple triangulation technique the location of damage can also be estimated fairly accurately. This is an excellent on-board technique, and although not a nondestructive technique, it is able to pinpoint the onset of failure.

Liptai (1972) found that in composites the acoustic emission takes place in two categories, the low level emission generated by plastic deformation of matrix and fibres, and the higher level emission generated by fibre failure, matrix cracking, interface failure and fibre pullout. Acoustic emission techniques have been used to study the real-time behavior of composite materials during fatigue loading by William & Reifsnider (1977). They have shown that AE data can be combined with video-thermography and dynamic recording of compliance to get meaningful results for the real-time NDE. Becht *et at* (1976) and Baily *et al* (1980) have used AE to investigate flaw formation and propagation in graphite reinforced plastic (GRP) pressure tubes, and to evaluate the fracture behavior of notched-bend specimens in flexural and fatigue experiments. They have reported some success in identifying fibre failure from matrix failure by amplitude distribution analysis. Arora & Tangri (1981) have used AE count rate (number of times the amplitude crosses the threshold) to estimate the growth rate of cracks in Zr-2·5% Nb. William & Egan (1979) and Belchamber *et al* (1983) have used spectral analysis of the AE signal to analyse fibre composite failure mechanisms. Since various types of damage may occur at the same time, it is rather difficult to differentiate between them. In this work, groups of AE events are treated as random data and are statistically analysed to identify group characteristics of different failure modes.

Vary & Bowles (1977, pp. 242–258) and Vary (1982) have combined AE with ultrasonics and developed the acousto-ultrasonic technique for characterization of fibre reinforced composites. The acoustic emission is stimulated by passing ultrasonic waves in structures. These AE waves are then detected by the usual AE procedures. These complex waves have been quantified by the "stress wave factor" (SWF) technique which will be described next. Talreja *et al* (1984, pp. 1099–1106) have used the technique developed by Vary to assess stiffness degradation in graphite/epoxy laminates.

The stress wave factor technique was proposed by Vary & Bowles (1977, pp. 242–258). The SWF is defined as; $SWF = g*r*n$, where g is the time interval over which the signal is recorded, r is the repetition rate of simulated AE waves and n is the number of oscillations each AE burst exceeds a fixed threshold voltage. Vary & Lark (1979) have shown that SWF can be correlated with the variations of the tensile and shear strengths of composite materials. William & Lampert (1980) have used a modified SWF for the degradation studies of impact damage in graphite-fibre composites. SWF is considered to be a measure of goodness of the material; a high SWF indicates a less damaged specimen. Obviously, SWF is inversely proportional to the attenuation in the material.

3. Acoustic parameters (wavespeed and attenuation) for the NDE of composites

It is well-known that the wavespeed of sound in a material is related to its stiffness:

$c^2 = E/\rho$ where c is the speed of sound, E is an approximate stiffness and ρ is the density. The presence of defects (e.g. voids, cracks, particles etc.) changes the effective stiffness of the material. When a mechanical wave of wavelength large in comparison to the crack size is propagated through such a medium, the change in stiffness is manifested as a change in the sound velocity according to the above equation. Furthermore, the defects act as wave scatterers. As a result, the defect population also manifests itself in the attenuation of the wave passed through the material. Kinra *et al* (1980, 1982), Kinra & Anand (1982), Kinra & Ker (1982, 1983) and Kinra (1984, pp. 983–991) have measured c and α (attenuation coefficient) for a variety of particulate composites. As expected both c and α were found to depend strongly on the volume fraction of inclusions. An unexpected result was that near a critical frequency, c and α were also found to be highly sensitive functions of frequency. This was attributed to the excitation of the fundamental resonance of the particles or voids.

The anisotropy of composites can greatly complicate the interpretation of the received ultrasonic signals. Kriz & Ledbetter (1983) and Kinra & Eden (1984) have obtained the solution of the Christoffel's equations given by Musgrave (1970) to graphically depict stiffness, longitudinal wave velocity and shear velocity variations in graphite/epoxy laminates. Some results obtained by Kinra & Eden (1984) are shown in figure 4. Here, slowness is the inverse of velocity. Shown also on the plot are the group velocity vectors (energy propagation directions) which are always perpendicular to the slowness surface.

Various researchers have used ultrasonics for the NDE of composites by relating the damage to the acoustic parameters. Ultrasonic waves have been used to measure the stiffness parameters in composites by Tauchert & Guzelsu (1971, 1972) Kriz & Stinchcomb (1979), Mann *et al* (1980), William *et al* (1980a) and Ueda *et al* (1983). Reynold & Wilkinson (1979) have used the measurement of difference in wave velocities for the estimation of porosity in composite materials. Heyman and Cantrell (1979, pp. 45–56) used a phase-insensitive transducer to study the effect of material inhomogeneity on ultrasonic measurements. Ultrasonic attenuation has been used to characterize damage in fibre composites by Hayford & Henneke (1979, pp. 184–200), Lee & Williams (1980), William *et al* (1980b, 1982), William & Doll (1980), Ulman &

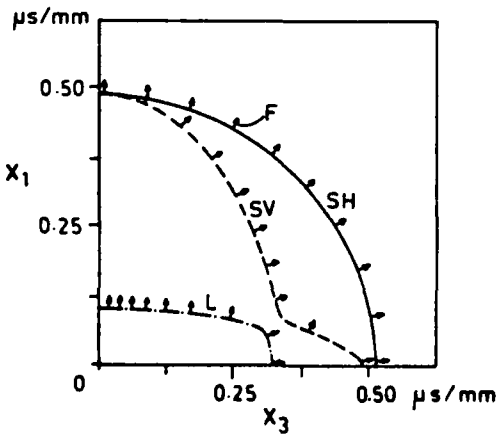

Figure 4. Slowness surfaces for a unidirectional graphite/epoxy composite. L: quasi-longitudinal, SV: quasi-shear (vertical), and SH: quasi-shear (horizontal) surfaces. F is the energy propagation direction.

Henneke (1982, pp. 323–342) and Hale & Ashton (1985). Ringermacher (1980, pp. 957–960) has utilized the changes in wavespeed to characterize damage in composites. He has shown that wavespeed is not a useful parameter to characterize damage in fibre composites. Cantrell *et al* (1980, pp. 1003–1005) have measured both attenuation and wavespeed and reached the same conclusion that while attenuation is a very sensitive measure of damage, wavespeed or stiffness is not. Eden (1985) has tested transverse cracks generated in $[0_6 90_4 0_2]_s$ graphite/epoxy specimens under static loading. He has used the pulse-echo spectroscopic technique to measure both wavespeed and attenuation. He has shown that as the damage increases, the pulses become broad (dispersive effect) and it becomes increasingly difficult to make good measurements of the acoustic parameters. He has also shown that when the waves propagate normal to the plane of the plate then the interaction between the cracks and waves is small. Hence wavespeed does not change but the increase in attenuation is appreciable.

4. Research of the present authors

We now summarize the principal research carried out by us. A detailed literature survey revealed that there was no method available to measure the acoustic parameters for thin specimens. We expect that aerospace structures will be thin and so Dayal *et al* (1986, pp. 899–904) have developed ultrasonic techniques for the measurement of acoustic parameters in thin specimens. When the specimen is thin the wave reflections from the two surfaces interfere and the classical time-of-flight method breaks down. In our technique the data is transformed from the time domain to the frequency domain by the use of fast fourier transforms (FFT). The techniques are fully computer-controlled and hence can be very easily adapted for automation and remote control. These techniques have been applied to the monitoring of damage in fibre-reinforced composites by Dayal & Kinra (1986). We found that attenuation is a very sensitive parameter of damage while wavespeed is rather insensitive. Results also show that the technique is very accurate and highly reproducible.

4.1 *Through-the-thickness measurement of acoustic parameters*

Let an infinite elastic plate be immersed in an elastic fluid (water). The time-versus-distance diagram of various reflected and transmitted pulses is shown in figure 5. If the plate is thick enough then 2 and 6 or 4 and 6 can be separated in the time domain. The available techniques (toneburst, pulse-superposition, pulse-echo etc.) are adequate to calculate the wavespeed and attenuation (though not very accurate for attenuation). If the plate is thin then 2, 6, 10 etc. or 4, 8, 12 etc. interfere and acoustic parameters cannot be calculated using any of the currently available techniques. The technique developed by us removes these restrictions and we have been successful in measuring wavespeed for aluminium plates down to 0·258 mm (10 mil) thickness. The equations used to reduce the data for these measurements are as follows. The first case we consider is when the plate thickness is such that a single pulse of signal is used and the various reflected or transmitted pulses can be separated in the time domain. Then,

$$(G^*/F^* - 1) = -T_{12}T_{21}\exp(-i2kh), \tag{1}$$

where G^* is the FFT of pulses 2 + 6 and F^* is the FFT of pulse 2; T_{12} is the transmission

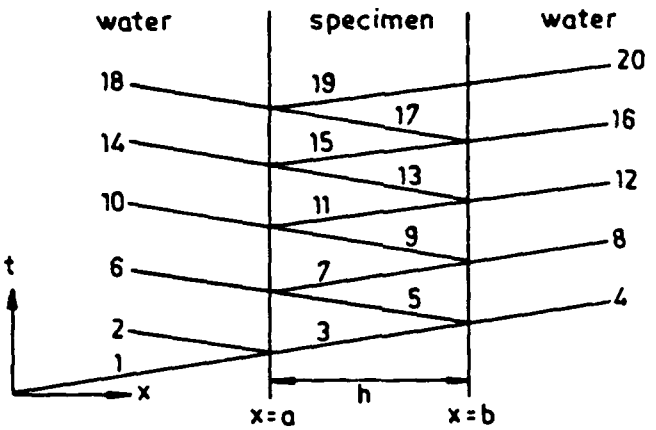

Figure 5. Time-versus-distance diagram for a plate immersed in a fluid.

coefficient for wave from water to plate and T_{21} is the transmission coefficient from plate to water; $k = k_1 + ik_2$ is the complex wavenumber, $k_1 = \omega/c$, ω is the circular frequency and c is the wavespeed, k_2 is the attenuation coefficient; and h is the plate thickness. Then,

$$c = 4\pi h/(-\phi/f) \quad \text{and} \quad k_2 = \ln M/2h, \tag{2}$$

where ϕ is the phase of $(G^*/F^* - 1)$ and $M = |(G^*/F^*)/T_{12}T_{21}|$.

The wavespeed is calculated by plotting the phase-versus-frequency plot and the slope is obtained by fitting a least squares straight line through the points. Attenuation is obtained from the ratio of the magnitudes.

If the transmitted signal is used then the equations are,

$$G^*/F^* = R_{21}^2 \exp(-i2kh) \tag{3}$$

where G^* is the FFT of pulse 8 and F^* is the FFT of pulse 4.

The wavespeed and attenuation are calculated from (2) with $M = |(G^*/F^*)/R_{12}^2|$.

Now the case where the pulses cannot be separated is considered. If the reflected field is recorded by the transducer then the governing equation is

$$\beta/(1+\beta) = R_{21}^2 \exp(-i2kh) \tag{4}$$

where $\beta = R_{12}R_{21}(G^*/F^* - 1)/T_{12}T_{21}$ and $R_{12}(R_{21})$ is the reflection coefficient of a wave in water (plate) from plate (water). G^* is the FFT of pulses $2 + 6 + 10 + \ldots \infty$ and F^* is the FFT of a reference signal obtained by replacing the specimen by a thick plate of the same material and surface conditions.

If the transmitted signal is recorded by the transducer,

$$G^*/F^* = T_{12}T_{21} \exp\{-ih(k - k_0)\}/\{1 - R_{21} \exp(-i2kh)\} \tag{5}$$

where k_0 is the wavenumber of the wave in water, G^* is the FFT of pulses $4 + 8 + 12 + \ldots \infty$ and F^* is the FFT of signal when there is no specimen between the transducers. Note that this is a quadratic equation in $\exp(-ikh)$.

These equations are equally valid for longitudinal and shear waves and have been used to measure both types of waves. They have been applied to a variety of specimens

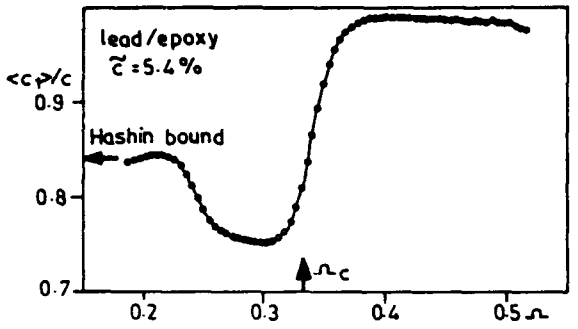

Figure 6. Normalized phase velocity as a function of frequency in a lead/epoxy particulate composite. Note large variations in velocity around the cut-off frequency Ω_c. Circles are digitized data points.

and the results are shown in table 1. The thickness of a plate of aluminium was reduced by careful machining and the wavespeed calculated at various thickness. The results show excellent repeatability and accuracy. It may be mentioned here that although the derivation assumed that the plate is elastic it is not difficult to show that these equations are rigorously valid for linear viscoelastic and dispersive materials provided attenuation is small, i.e., $k_2 \ll k_1$, which is generally the case. As an illustration of the efficacy of our technique in measuring k_1 and k_2 of highly dispersive and attenuative media, we tested random particulate composites consisting of lead spheres in an epoxy matrix. Figure 6 shows the phase velocity as a function of frequency in this specimen. Below the cut-off frequency, where the wavelength is large in comparison to the ball radius, the wavespeed is weakly dependent on frequency. Again at high frequencies, where the wavelength is small in comparison to the ball radius, the wavespeed is sensibly independent of the frequency. Around the cut-off frequency the wavespeed fluctuates very rapidly with increase in frequency. Here, cut-off frequency is the frequency that corresponds to the excitation of the rigid-body-translation resonance of the spheres. *It is emphasized that the entire dispersion curve was obtained in a single experiment.*

Next the results are presented for the NDE of fibre reinforced, graphite/epoxy, AS4/3502 composites. A $[0_6 90_4 0_2]_s$ laminate was tested. A static load was applied to the specimen and transverse cracks were produced in the 90°-plies. The test was interrupted at regular intervals and the number of cracks was determined by the edge replication technique. The specimen was then subjected to ultrasonic investigation. Figure 7 shows the results for tests at three different frequencies for attenuation as a function of applied loads. Shown also are the line sketches of the edge replications at different damage stages. A dramatic increase in attenuation is observed at all the frequencies. Figure 8 shows that for the same test there is practically no change in wavespeed. These results show that for the through-the-thickness measurements attenuation is a very good damage metric while wavespeed is not.

All the above measurements of wavespeed and attenuation have been made in the through-the-thickness direction where the crack-wave interaction is the weakest. This interaction is strongest when a wave travels perpendicular to the crack faces. This provided the motivation for examining the propagation of Lamb waves, which are described next.

4.2 *Lamb wave technique for the NDE of composites*

When Lamb waves are propagated in plates immersed in water, the displacement of the

Table 1. Longitudinal and shear wave speeds of different specimens.

Sample	Test frequency (MHz)	Thickness (mm)	c_1^a (mm μs)	c_2^b (mm μs)	σ_c^c(%)	ε_c^d(%)	k_2	σ_a^e(%)	Technique
Ni-based alloys	5	18·848	5·273	2·737	0·02	0·2	—	—	Sec/first
	5	6·365	5·877	3·163	0·02	0·2	—	—	Sec/first
	5	6·263	5·872	3·162	0·02	0·2	—	—	Sec/first
Epon	1	1·869	2·874	--	0·10	—	0·1340	1·4	All/first
	5	1·869	2·884	—	0·14	—	0·0940	1·5	All/first
	10	1·869	2·915	—	0·08	—	0·0975	1·0	All/first
	10	1·869	2·915	—	0·24	—	0·0979	2·2	Tonebrust
Aluminium	10	2·807	6·357	—	—	0·2	—	—	Toneburst
	10	2·807	6·324	—	0·013	0·2	—	—	Sec/first
	10	2·807	6·327	—	0·010	0·2	—	—	All/first
	10	1·686	6·346	—	0·040	0·2	—	—	All/first
	10	1·001	6·354	—	0·030	0·2	—	—	All/first
	10	0·613	6·359	—	0·130	0·2	—	—	All/first
	10	0·256	6·323	—	0·140	0·2	—	—	All/first

[a] c_1 longitudinal wavespeed; [b] σ_c standard deviation in c; [c] ε_c error in c; [d] c_2 shear wavespeed; [e] σ_a standard deviation in attenuation.

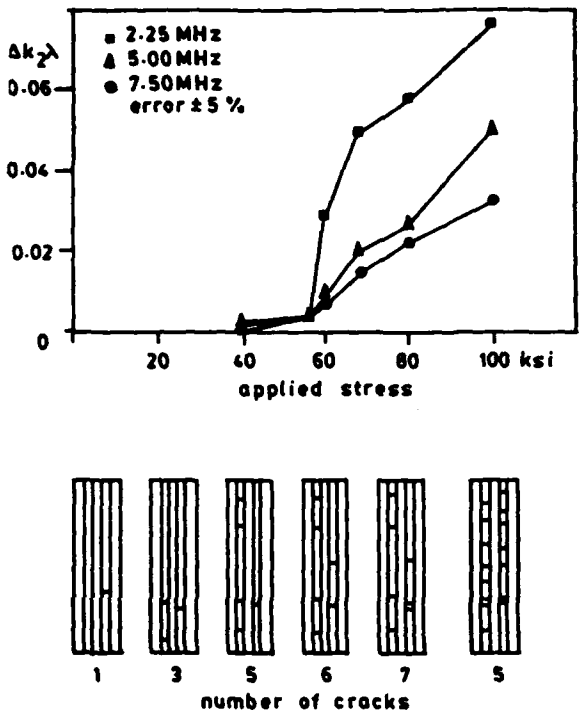

Figure 7. Attenuation increases dramatically with transverse cracks in a $[0_6 90_4 0_2]_s$ laminate at all three frequencies tested. The extent of damage and number of cracks are shown in the edge replication sketches.

two surfaces of the plate generates waves in water, hence the terminology "leaky Lamb waves". Since these waves travel in the plane of the plate, in-plane stiffness governs the wavespeed of Lamb waves. Leaky Lamb waves were used by Bar-Cohen & Chimenti (1985) for the NDE of damage in composites. They have shown that various forms of damage can be identified by a null-zone measurement method. When a wave is incident upon a plate, it results in the excitation of a Lamb wave in the plate as well as a specular reflection. Due to phase change in the leaky wave, the specular reflection and the leaky wave interfere and a well-defined null zone is observed. The movement of the null zone has been related to the defects in their work. In our work we have adopted a different approach. The transducers are placed such that specular reflection is avoided and only

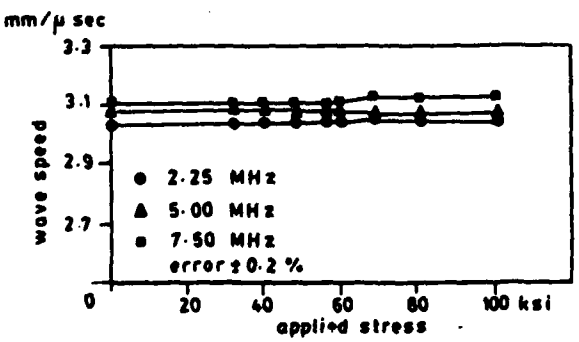

Figure 8. Longitudinal wavespeed remains unchanged with damage. Laminate is the same as in Figure 7.

the leaky Lamb waves are sensed. We measured the wavespeed and attenuation of the leaky Lamb waves.

The angle at which a Lamb wave is generated in the plate is governed by Snell's Law,

$$\sin(\theta_i)/\sin(\theta_r) = c_w/c_L, \tag{8}$$

where θ_i is the angle of incidence, $\theta_r = \pi/2$ is the angle of refraction, c_w is the wavespeed in water and c_L is the Lamb wavespeed. Habegar *et al* (1979) have shown by a rigorous analysis that at low frequencies (wavelength $\gg$ plate thickness) the Lamb wavespeed can be related to the in-plane stiffness (E_1) as

$$c_L^2 = E_1/\{\rho(1 - \nu_{12}\nu_{21})\} \tag{9}$$

where ν_{12} and ν_{21} are the two Poisson's ratios for the composite plate. Since for the cross-ply composites that we have tested, $\nu_{12}\nu_{21} \ll 1$, (8) reduces to

$$c_L^2 = E_1/\rho. \tag{10}$$

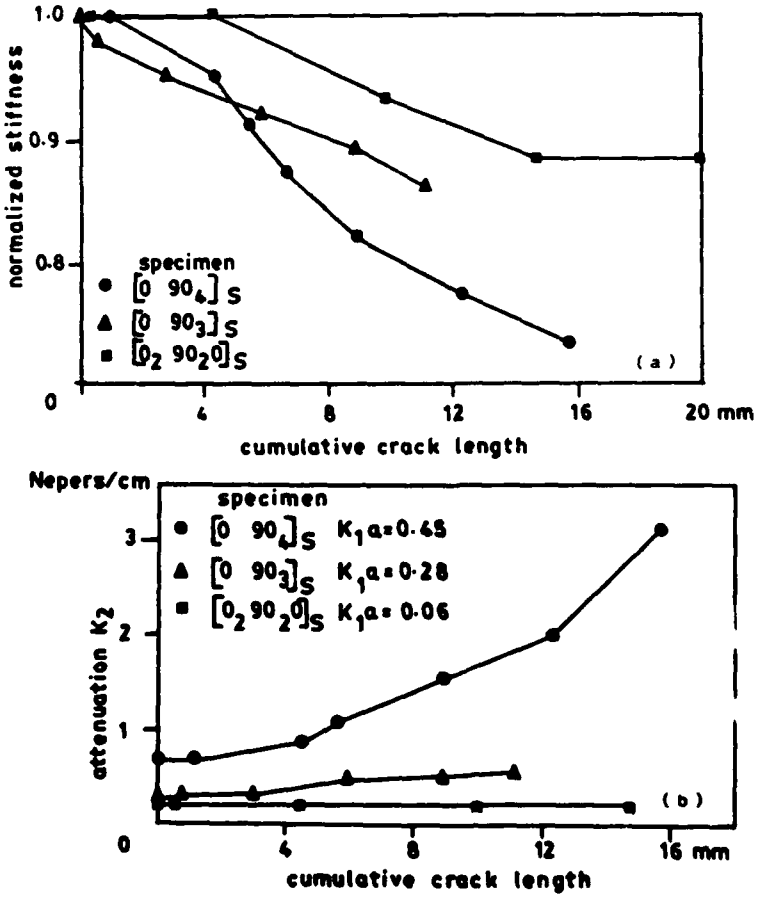

Figure 9. (a) Reduction of in-plane stiffness, and (b) increase in attenuation of leaky Lamb waves with damage, in three graphite/epoxy laminates.

Thus by the measurement of the Lamb wavespeed from (7) and substituting it in (9) the in-plane stiffness E_1 can be calculated. The results for a variety of graphite/epoxy laminates (Dayal & Kinra 1987) are reproduced here. Figure 9 shows the reduction in stiffness for three different laminate layups: $[0\ 90_4]_s$; $[0\ 90_3]_s$; and $[0_2 90_2 0]_s$. Let $2a$ be the length of the crack which is the same as the thickness of the contiguous 90°-plies. Let N be the linear density of the transverse cracks in the direction of wave propagation. In the absence of a more suitable measure of damage, we define cumulative crack length $L = 2aN$ and use it as a damage metric. Note that four 90°-plies contribute more to the overall stiffness of the laminate in comparison to three 90°-plies and hence their failure results in a larger stiffness reduction. The third laminate $[0_2 90_2 0]_s$ has four 90°-plies but they are divided in two and also the laminate has four 0°-plies. Thus the stiffness contribution of the 90°-plies is very low and hence it shows much lower stiffness reduction on damage. The increase in attenuation for the three laminates is shown in figure 9b. All tests were conducted at the same frequency of 0·5 MHz. The scattering cross-section of $[0\ 90_4]_s$ laminate is the largest ($k_1 a = 0{\cdot}45$) and hence the attenuation increase is maximum. When $k_1 a \ll 1$, as for the $[0_2\ 90_2\ 0]_s$ laminate ($k_1 a = 0{\cdot}06$), the wavelength is very large as compared to the crack length and the wave does not "see" the crack and the increase in attenuation is very low.

The results obtained by the authors thus show that for the through-the-thickness measurements the change in attenuation is a good measure of matrix cracking while wavespeed is not. But in the in-plane measurements both wavespeed and attenuation are sensitive measures of matrix cracks.

References

Arora A, Tangari K 1981 *Exp. Mech.* 21: 261–267

Baily C D, Freeman C D, Hamilton J M 1980 *Mater. Eval.* 38: 21–26

Bar-Cohen Y, Arnon U, Meron M 1978 *SAMPE J.* 14: 4–9

Bar-Cohen Y, Chimenti D E 1985 *Proc. 15th Symp. NDE, San Antonio, Texas*

Becht J, Schwalbe H J, Eisenblaetter J 1976 *Composites* 245–248

Belchamber R M, Betteridge D, Chow Y T, Hawkes A G, Cudby M E A, Wood D G M 1983 *J. Compos. Mater.* 17: 420–435

Blake R A Jr 1982 *Proc. MICRO-DELCON* pp. 30–36

Blake R A Jr 1983 Ultrasonic Image Histogram Evaluation and Enhancement, *IEEE Proc. of the 6th Annual MICRO-DELCON Conf.*

Blake R A Jr, Hartman H S 1984 *Compos. Technol. Rev.* 6 (3): 118–123

Cantrell J H Jr, Winfree W P, Heyman J S, Whitcomb J D 1980 *Proc. IEEE Ultrasonic Symp.* Boston pp. 1003–1005

Daniel I M, Schramm S W, Liber T 1981 *Mater. Eval.* 39: 834–839

Dayal V, Kinra V K 1986 *Proc. 3rd US Japan Conf. on Compos. Mater., Tokyo*

Dayal V, Kinra V K 1987 Non-Destructive Evaluation of Transverse Cracks in Fibre-Reinforced Composites by Ultrasonics. *16th NDE Symp., San Antonio, Texas*

Dayal V, Kinra V K, Eden J G 1986 *Proc. Int. Symp. Compos. Mater. Struct., Beijing* (ed.) T T Loo and C T Sun pp. 899–904

Eden J G 1985 *The application of ultrasonics to assess damage in composite materials*, M S thesis, Texas A&M University

Firestone F A 1945 *J. Acoust. Soc. Am.* 17: 287–299

Habegar C C, Mann R W, Baum G A 1979 *Ultrasonics* 57–62

Hale J M, Ashton J N 1985 *Br. J. Non-Destr. Test.* 27(2): 83–87

Hayford D T, Henneke E G II 1979 *Compos. Mater. Test Design (Fifth Conf.), ASTM STP 674* (ed.) S W Tsai (Philadelphia: ASTM) pp. 184–200

Heyman J S, Cantrell J H 1979 *NDE flaw criticality Compos. Mater., ASTM STP* 692, (ed.) R B Pipes (Philadelphia: ASTM) pp. 45–56
Kinra V K 1984 *Rev. Progr. Quant. NDE Eval.* (eds) D O Thompson, D E Chimenti (New York: Plenum Publishing Corp.) B3: 983–991
Kinra V K, Anand A 1982 *Int. J. Solids Struct.* 18 (5): 367–380
Kinra V K, Eden J G 1984 Propagation of Elastic waves in Unidirectional Fibre Reinforced Composites, AFOSR Contract Report MM4875-84-19, Dept. of Aerospace Engg., Texas A&M University, College Station, TX, USA
Kinra V K, Ker E L 1982 *J. Compos. Mater.* 16: 117–138
Kinra V K, Ker E L 1983 *Int. J. Solids Struct.* 19: 393–410
Kinra V K, Ker E L, Datta S K 1982 *Mech. Res. Commun.* 9 (2): 109–114
Kinra V K, Petraitis M S, Datta S K 1980 *Int. J. Solids Struct.* 16: 301–312
Krautkramer J, Krautkramer H 1983 *Ultrasonic testing of materials* 3rd edn (Berlin: Springer Verlag) chap. 10–11
Kriz R D, Stinchcomb W W 1979 *Exp. Mech.* 19 (2): 41–49
Kriz R D, Ledbetter H M 1983 Elastic Representation Surfaces of Unidirectional Graphite/Epoxy Composites, Fracture and Deformation Div., National Bureau of Standards, Boulder, Colorado
Lee S S, Williams J H Jr 1980 *J. Non-Destr. Eval.* 1 (4): 277–285
Liptai R G 1972 *Compos. Mater. Test. Design* (*Second Conf.*) *ASTM STP* (*Philadelphia*: ASTM) pp. 497: 285
Mann R W, Baum G A, Habegar C C 1980 *Tappi* 63: 163–166
Musgrave M J P 1970 *Crystal acoustics* (San Franscisco, CA: Holden-Day)
Reifsnider K L, Henneke E G, Stinchcomb W W, Duke J C 1983 *Mechanics of composite materials* (eds) Z Hashin, C T Herakovich (London: Pergamon Press) pp. 399–420
Reynolds W N, Wilkinson S J 1978 *Ultrasonics* 16: 159–163
Ringermacher H 1980 *Proc. of IEEE Ultrasonic Symp. Boston* pp. 957–960
Sokolov S Ya 1929 Zur Frage der Fortpflanzung ultraakustischer Schwinggungen in verschiedenen Korpern, ENT 6: 454–461
Talreja R, Govada A, Henneke E G II 1984 *Review of research in quantitative nondestructive evaluation* (New York: Plenum Press) vol. 2, pp. 1099–1106
Tauchert T R, Guzelsu A N 1971 *J. Compos. Mater.* 5: 549–552
Tauchert T R, Guzelsu A N 1972 *J. Appl. Mech.* 98–102
Vary A, Bowles K J 1977 *Proc. 11th Symp. on NDT, Am. Soc. NDT and Southwest Res. Inst., San Antonio, TX* pp. 242–258 (Also report NASA TMX-73646, 1977)
Vary A, Lark R F 1979 *J. Test. Eval.* 7 (4): 185–191
Vary A 1982 *Mater. Eval.* 40: 650–654
Ueda M, Ikudome K, Igarashi Y 1983 *Trans. JSCM* 9 (1): 25–30
Ulman D A, Henneke E G II 1982 *Compos. Mater. Test. Design* (*Sixth Conf.*), *ASTM STP 787* (ed.) I M Daniel (Philadelphia: ASTM) pp. 323–342
William J H Jr, Doll B 1980 *Mater. Eval.* 38: 33–37
William J H Jr, Egan D M 1979 *Mater. Eval.* 37 (1): 43–47
William J H Jr, Lampert N R 1980 *Mater. Eval.* 38: 68–72
William J H Jr, Lee S S, Nayeb-Hashimi H 1980b *J. Nondestr. Eval.* 1 (3): 191–199
William J H Jr, Nayeb-Hashimi H, Lee S S 1980a *J. Nondestr. Eval.* 1 (2): 137–148
William J H Jr, Yuce H, Lee S S 1982 *Mater. Eval.* 40: 560–565
William R S, Reifsnider K L 1977 *Mater. Eval.* 35 (8): 50–54

Final - October 1987

A NEW TECHNIQUE FOR ULTRASONIC NDE OF THIN SPECIMENS

by

V.K. Kinra

and

V. Dayal

Mechanics and Materials Center

and

Aerospace Engineering Department
Texas A&M University
College Station, TX 77843

Accepted for Publication by Experimental Mechanics

LIST OF SYMBOLS

$F^*(\omega)$	fourier transform of f(t)
$G^*(\omega)$	fourier transform of g(t)
M	magnitude of a complex number
N	number of digitizing points
R_{ij}	Reflection coefficient in medium i from medium j
T	sampling interval in time domain, ns
T_o	signal length, μsec
T_{ij}	Transmission coefficient for a wave incident in medium i and transmitted into medium j
a	a characteristic length; half crack length or particle radius, mm
c, c_l	longitudinal phase velocity in specimen, mm/μsec
c_o	longitudinal phase velocity of wave in immersion medium (water), mm/μsec
c_g	group velocity in specimen, mm/μsec
f	frequency, MHz
f_c	cut-off frequency, MHz
Δf	frequency resolution, MHz
h	plate thickness, mm
i =	$\sqrt{-1}$
k	complex wavenumber = $k_1 + ik_2$, mm^{-1}
k_o	wavenumber in water, real, mm^{-1}
k_1	= ω/c, wavenumber in specimen, mm^{-1}
k_2	attenuation coefficient, nepers/mm
m	integer; number of complete round trips taken by the wave across the plate thickness
t	time, μsec
u	particle displacement
x	distance
Ω	normalized frequency, $2\pi fa/c_1$
λ	wavelength, mm
ζ	normalized wavenumber, $2\pi fa/\langle c_1 \rangle$
ρ	density of specimen, g/ml
ρ_o	density of water, g/ml
ϕ	phase of a complex number
ω	circular frequency, rad/μsec
< >	aggregate property of composite

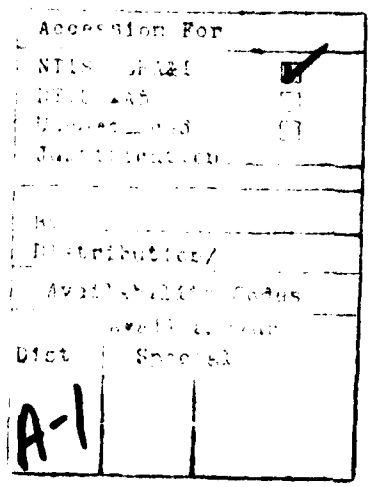

1. INTRODUCTION

The classical method of measuring the speed of sound in non-dispersive media is the time-of-flight method, see Reference[1] for example. We note that in non-dispersive media the phase velocity and the group velocity are identical[2]. When the material is either dispersive or attenuative this method breaks down and a suitable method then is the so-called toneburst method. Here, a burst of pure tone, typically about ten cycles in duration is used; this places a constraint on the specimen thickness; it must be thick enough so that the toneburst reflections from the two faces of the specimen can be clearly separated in time-domain i.e. it should be roughly five-wavelength thick. For example, in steel at, say, one MHz frequency the required minimum thickness would be about 30 mm. There are many situations of practical importance where one must carry out an ultrasonic examination of considerebly thinner specimens. For example, aircraft and aerospace structures using graphite/epoxy or metal-matrix composites employ panels as thin as one mm. Chang, et.al[3] have developed a technique for the measurement of phase velocity in thin laminates. They carry out an FFT of the front-surface and the back-surface reflections of a signal. The amplitude-vs-frequency curve is characterized by a series of resonance peaks; the peak spacing yields the phase velocity which is the same as the group velocity, for it is assumed that the material is non-dispersive. This method requires human analysis of data (it cannot be computer automated). Further, one cannot measure attenuation by this method. More recently Heyman[4] has developed a technique called phase insensitive toneburst spectroscopy. Although this technique yields excellent results, it requires the use of rather specialized and sophisticated transducers called acousto-electric transducers (AET) which are not yet commercially available.

By combining standard FFT methods with conventional ultrasonics (using commercially available broad band piezoelectric transducers) we have been able to develop a method by which one can measure the phase velocity, the group velocity and the attenuation in ultra-thin specimens (sub-millimeter or sub-wavelength in thickness). There are many situations in which one cannot obtain a series of resonance peaks required by the method of Chang, et.al[3]. Our method works even in the absence of a single resonance peak. A detailed description of this technique is the central objective of this paper. We will illustrate the use of this technique on four rather disparate materials: aluminum, an epoxy, a particulate composite and graphite-fiber/epoxy composite. It will be demonstrated that this technique works equally well for thin or thick specimens, and for dispersive as well as non-dispersive media.

2. THEORY

Consider an infinite elastic plate immersed in an elastic fluid (water). A Lagrangian diagram indicating the space-time location of a wavefront which occupied the position x=0 at time t=0 is shown in Fig. 1. A plane-fronted finite-duration pulse, ray 1, is normally incident on the plate. This results in an infinite series of reflected and transmitted pulses. The expressions for the reflection and transmission coefficients of a displacement wave for perfectly elastic media may be found in Achenbach's book[5].

Let the displacement in the incident field be given by

$$u^{inc} = f_0(\omega t - k_0 x)$$

where $f_o(s) \equiv 0$ for $s<0$. (1)

For the time being ω and k_o can be any two constants connected by $c_o = \omega/k_o$, where c_o is the phase velocity of wave in water. Later ω and k_o will be identified with the circular frequency and wavenumber of a monochromatic harmonic wave. The displacement field along the various reflected rays may be written as

$$u^2 = R_{12} f_o(s-s_2);\ s_2 = 2k_o a$$

$$u^6 = T_{12} R_{21} T_{21} f_o(s-s_6);\ s_6 = 2k_o a + 2kh \qquad (2)$$

$$u^{10} = T_{12} R_{21}^2 T_{21} f_o(s-s_{10});\ s_{10} = 2k_o a + 4kh$$

etc.

Here, $s = \omega t + k_o x$, $h = b-a$ is the plate thickness, R_{ij} is the reflection coefficient in medium i from medium j, T_{ij} is the transmission coefficient for a wave incident in medium i and transmitted into medium j, $k=\omega/c$, c is the phase velocity in the plate, and

$$R_{12} = \frac{\rho_o c_o - \rho c}{\rho_o c_o + \rho c} = -R_{21},$$

$$T_{12} = \frac{2\rho_o c_o}{\rho_o c_o + \rho c} = 2 - T_{21}, \qquad (3)$$

where ρ_o and ρ are, respectively, the density of water and the plate material. The entire reflected field, $u^r = u^2 + u^6 + u^{10} + \ldots\ldots\infty$, may be written as

$$u^r = R_{12} f_o(s-s_2) + T_{12} R_{21} T_{21} \sum_{m=1}^{\infty} R_{21}^{m-1} \; f_o(s-s_m) \qquad (4)$$
$$s_m = 2\, k_o a + m\, 2kh$$

In an exactly analogous manner, one can write down the expressions for the transmitted pulses. With $s = \omega t - k_o x$

$$u^4 = T_{12} T_{21} f_o(s-s_4);\; s_4 = h(k-k_o)$$

$$u^8 = T_{12}\, R_{21}^2\, T_{21}\, f_o(s-s_8);\; s_8 = h(3k-k_o) \qquad (5)$$

$$u^{12} = T_{12}\, R_{21}^4\, T_{21}\, f_o(s-s_{12});\; s_{12} = h(5k-k_o)$$

etc.

The total transmitted field may be written as

$$u^t = T_{12}\, T_{21} \sum_{m=0}^{\infty} R_{21}^{2m} \; f_o(s-s_m);\; s_m = h\,[(2m+1)\,k-k_o] \qquad (6)$$

In eqs (4) and (6) m is the number of <u>complete round trips</u> taken by the wave across the plate thickness h.

The Fourier transform of a function f(t) is defined as

$$F^*(\omega) = \frac{1}{\sqrt{2\pi}} \int_{-\infty}^{\infty} f(t)\, e^{-i\omega t} dt, \quad -\infty < \omega < \infty \tag{7a}$$

with the associated inverse transform given by,

$$f(t) = \frac{1}{\sqrt{2\pi}} \int_{-\infty}^{\infty} F^*(\omega)\, e^{i\omega t} d\omega \tag{7b}$$

2.1 Analysis for Thick Specimens

We first consider the case of a relatively thick specimen such that various pulses in Fig. 1 can be clearly separated from each other in the time-domain. Let f(t) be the signal corresponding to ray 2 and g(t) be the signal corresponding to rays 2 and 6 combined sensed by a transducer at x=0. (This is the so-called pulse-echo mode). Then

$$f(t) = R_{12}\, f_o(\omega t - 2k_o a) \tag{8}$$

and

$$g(t) = T_{12}R_{21}T_{21} f_o(\omega t - 2k_o a - 2kh) + f(t). \tag{9}$$

Let $F^*(\omega)$, $G^*(\omega)$ and $F_o^*(\omega)$ be the Fourier transforms of f(t), g(t) and $f_o(t)$, respectively. Then,

$$F^*(\omega) = R_{12}\, e^{-i2k_o a} F_o^*(\omega) \tag{10}$$

$$G^*(\omega) = R_{12} F_o^*(\omega)\, e^{-i2k_o a} [1 - T_{12}T_{21} e^{-i2kh}] \tag{11}$$

and

$$\frac{G^*(\omega)}{F^*(\omega)} = 1 - T_{12}T_{21} e^{-i2kh} \tag{12}$$

It is emphasized that in the foregoing it is assumed that the plate behaves in a perfectly elastic manner i.e. the wavenumber k is real and $c=\omega/k$ is a constant. The key term in eqs (11) and (12) is e^{-i2kh} or $e^{-i2h\omega/c}$. Thus, in eq (11) if one plots $|G^*(\omega)|$ vs ω it will be characterized by a series of resonance peaks whose spacing is given by $\Delta(2h\omega/c) = 2\pi$, or in view of $\omega = 2\pi f$

$$c = 2h\,\Delta f \tag{13}$$

Measurement of c in aluminum using eq (13) is illustrated in Fig. 2. Here $F(\omega) = |F^*(\omega)|$ and $G(\omega) = |G^*(\omega)|$. Note that $G(\omega)$ consists of the transducer response, $F(\omega)$ superimposed by an oscillation due to $e^{-i2h\omega/c}$ term.

A further improvement in the measurement method can be achieved by plotting $(G^*(\omega)/F^*(\omega) - 1)$, eq (12). This is illustrated in Fig. 3. By taking out the shape of the transducer response we are left with oscillations due to the constructive and destructive interference between the front-surface (ray 2) and back-surface reflections (ray 6).

Even though eq (12) is derived for an elastic material it is rigorously valid for a linear viscoelastic material provided the damping is small i.e. in $k=k_1+ik_2$, $k_2/k_1<<1$. This elementary proof is deferred to the appendix. We rewrite eq (12) as

$$e^{-i2kh} = -(G^*(\omega)/F^*(\omega) - 1)/T_{12}T_{21} = Me^{i\phi} \tag{14a}$$

Then, $$k_1(\omega) = -\phi/2h$$

and

$$k_2(\omega) = (\ln M)/2h, \tag{14b}$$

where $M = |((G^*(\omega)/F^*(\omega)) - 1)/T_{12}T_{21}|$

Since $k_1(\omega) = \omega/c$ and $\omega = 2\pi f$

$$c = \frac{4\pi h}{(-\phi/f)} \text{ and } k_2(\omega) = (\ln M)/2h. \tag{15}$$

These are the desired equations for calculating the phase velocity and the attenuation.

Now consider the transmitted field for a thick specimen. Two measurements are made. In the first, the specimen is removed from the water path i.e. the wave travels solely through water. Let the receiving transducer be located at some $x = l > b$. Then $u^{inc}(l,t) \equiv f(t) = f_o(\omega t - k_o l)$ The specimen is now inserted in the wavepath and the signal due to ray 4 alone is recorded. Thus, $u^4(l,t) \equiv g(t) = T_{12}T_{21}f_o(\omega t - k_o l - 2k_o a - kh)$. Then,

$$\frac{G^*(\omega)}{F^*(\omega)} = T_{12}T_{21}e^{-i(kh+k_o h)} \tag{16}$$

If $\dfrac{G^*(\omega)e^{ik_o h}}{F^*(\omega)T_{12}T_{21}}$ is set equal to $Me^{i\phi}$ then

$$k_1(\omega) = -\phi/h \tag{17a}$$

and $$k_2(\omega) = (\ln M)/h \tag{17b}$$

where $M = \left|\frac{G^*(\omega)}{F^*(\omega)}\right| / T_{12}T_{21}$

Substituting $k_1 = 2\pi f/c$, we get

$$c = \frac{2\pi h}{(-\phi/f)} \text{ and } k_2(\omega) = \ln M/h \tag{18}$$

Another variation of this technique is when signals for both rays 4 and 8 are quite large. Then the following approach yields more accurate results because the data reduction can be done from a single experiment. Let f(t) and g(t) be the signals corresponding to rays 4 and 8, let $F^*(\omega)$ and $G^*(\omega)$ be their Fourier transforms then

$$\frac{G^*(\omega)}{F^*(\omega)} = R_{21}^2 \, e^{-i2kh} \tag{19}$$

As before, if we set $G^*(\omega)/F^*(\omega)\ R_{21}^2 = Me^{i\phi}$ then, Eq. (15) can be used to calculate the wavespeed and attenuation. In the following for brevity, these methods will be referred to as Second/First method.

We note that this method is equally effective for <u>dispersive</u> media. From eq (14) one plots k_1 vs. ω. A secant to the curve yields inverse of the phase velocity (phase slowness). For dispersive media a quantity of interest is the group velocity. This is the speed with which energy propagates in a medium, $c_g = \partial\omega/\partial k_1$; this too can be computed from the phase plot, and eq (14b) yield frequency dependent attenuation. Finally, we introduce a normalized attenuation $k_2\lambda$. This is the attenuation of a wave over one wavelength. The motivation for this particular normalization is that for a linear viscoelastic material $k_2\lambda$ is independent of frequency.

2.2 Analysis for Thin* Composites

The <u>total</u> reflected field comprising rays 2, 6, 10, 14 ..... ∞ at x=0 is given by eq (12) as

$$u^r(o,t) \equiv g(t) = R_{12} f_o(\omega t - 2k_o a)$$

$$+ T_{12} R_{21} T_{21} \sum_{m=1}^{\infty} R_{21}^{2(m-1)} f_o(\omega t - 2k_o a - m2kh) \qquad (20)$$

Note that ray 2 cannot be used as the reference signal. One has to conduct a separate experiment as follows: the thin coupon is replaced by a thick coupon with the front surface precisely at x=a. Let the front surface reflection be labeled f(t), then

$$f(t) = R_{12} f_o(\omega t - 2k_o a)$$

$$F^*(\omega) = R_{12} e^{-i2k_o a} F_o^*(\omega)$$

$$G^*(\omega) = F^*(\omega) + T_{12} R_{21} T_{21} \sum_{m=1}^{\infty} R_{21}^{2(m-1)} F_o^*(\omega) \cdot e^{-i[2k_o a + m\,2kh]} \qquad (21)$$

Let $Z = R_{21}^2 \, e^{i2kh}, \; |Z| < |, \qquad (22)$

---

*In this paper the qualifiers "thick" and "thin" are used in the following sense. When various reflections or transmissions corresponding to a short-duration pulse can be separated in the time-domain, the specimen is considered thick. But the duration of the pulse depends on the center-frequency of the transducer. Hence the use of the word thick is quite arbitrary.

Then,
$$\frac{G^*}{F^*} - 1 = \frac{T_{12}T_{21}}{R_{12}R_{21}} \sum_{m=1}^{\infty} Z^m$$

Observing that for $|Z| < 1$, $(1-Z)^{-1} = 1+Z+Z^2 + \ldots\infty$, and defining

$$\beta = \frac{R_{12}R_{21}}{T_{12}T_{21}}\left(\frac{G^*(\omega)}{F^*(\omega)} - 1\right) \quad \text{we get}$$

$$Z = \frac{\beta}{1+\beta} \tag{23}$$

From Z one can readily calculate the complex-valued wavenumber $k(\omega)$.

For completeness we include here a variation of this method. Suppose a thick coupon to obtain a reference signal is not available (this difficulty will be discussed later). One can then use a thick specimen of some other material; we have used a block of aluminum. Let the acoustic impedance of this material be $\rho_1 c_1$. Let the front-surface reflection be $f(t) = R\, f_o(wt-2k_o a)$ where the reflection coefficient $R = (\rho_o c_o - \rho_1 c_1)/(\rho_o c_o + \rho_1 c_1)$, and g(t) is still given by eq (18). As before with

$$\beta = \frac{R_{12}R_{21}}{T_{12}T_{21}}\left[\frac{R}{R_{12}} \frac{G^*(\omega)}{F^*(\omega)} - 1\right], \tag{24}$$

$$Z = R_{21}^2\, e^{-ikh} = \beta/(1+\beta) \tag{25}$$

In the following for brevity these methods will be referred to as All/First method.

We now consider the transmitted field. Here a second transducer is used as a receiver at some $x = l>b$. To obtain a reference signal the specimen is removed and the signal through water is recorded.

$$f(t) = u^{inc}(1,t) = f_o(wt-k_o1)$$

Let g(t) be the <u>total</u> transmitted field, rays 4, 8, 12, ...∞ then from eq (6)

$$g(t) = T_{12}T_{21} \sum_{m=0}^{\infty} R_{21}^{2m} f_o[\omega t-k_o1-h\{(2m+1)k-k_o\}] \tag{26}$$

$$\frac{G^*(\omega)}{F^*(\omega)} = \frac{T_{12}T_{21}\bar{e}^{ih(k-k_o)}}{1-R_{21}^2\,\bar{e}^{i2kh}} \tag{27}$$

We note one major difference between eqs (23) and (27). Unlike eq (23), eq (27) is a <u>quadratic</u> in Z = exp(-ikh). This presents some additional numerical problems. These are discussed next. Equation (27) may be rewritten as

$$Z^2 + ZY - D_o = 0$$

where

$$Y = \frac{T_{12}T_{21}}{R_{21}Z_o}\frac{F^*(\omega)}{G^*(\omega)} \tag{28}$$

$$Z_o = \exp(-ihk_o)$$

$$D_o = 1/R_{21}^2$$

and k_o is the wavenumber in water. Since the phase velocity in water is known, Z_0 is known a priori. If the acoustic impedance of the plate, ρc, was known, one could calculate T_{ij} and R_{ij}. However, c is precisely the unknown we are seeking to measure. This problem could be solved by a simple iteration procedure. An approximate phase velocity was initially used in the algorithm to estimate T_{ij} and R_{ij}. The quadratic equation (28) is solved and two roots

of Z are obtained. The correct root is chosen based on the fact that the phase of Z decreases as frequency increases (for the other root the reverse is true). This velocity is used for the next iteration cycle. This procedure converges very rapidly. When we purposely supplied an initial phase velocity with a very large error (30%), the convergence was found to occur in about five iterations. More realistically, the wavespeed can be estimated to within five percent. Here convergence to within 0.01 percent occurs within three or four iterations. When the value of c obtained by this procedure was substituted back into eq (28) to calculate attenuation, $k_2\lambda$ was found to be an oscillatory function of frequency for a linear viscoelastic material, namely, an epoxy. Now, it is well-known that for a such a material $k_2\lambda$ is a constant. The oscillating nature of $k_2\lambda$ could, however, be readily explained as follows. A detailed numerical examination of eq (28) revealed that the calculation of $k_2\lambda$ is very sensitive to small variation in the phase velocity c. The oscillations were due to the fact that the measured velocity was different from the true velocity. This problem could be resolved in the following manner. If one takes the absolute value of both sides, eq (25) can be re-written as follows:

$$\cos \frac{4\pi hf}{c} + \frac{1}{2}\left(\frac{T_{12}T_{21}}{R_{21}}\right)^2 \left|\frac{F^*(\omega)}{G^*(\omega)}\right| = \frac{1}{2}\left[R_{21}^2 e^{qf} + \frac{1}{R_{21}^2 e^{qf}}\right] \qquad (29)$$

where $q = 2h\, k_2\lambda/c$.

The terms in eq (29) have been separated judiciously as follows. The left hand side (LHS) is a function of wavespeed only while the right hand side (RHS) depends on both, the wavespeed as well as the attenuation. The RHS is a sum of two exponentials and, therefore, is not an oscillatory function of frequency f. On the other hand, the LHS is the sum of a cosine function of

frequency and the experimentally determined $F^*(\omega)/G^*(\omega)$ which was found to be oscillatory. Now if the correct value of c is not used in eq (29) the periods of the two terms do not match and the oscillatory parts do not cancel each other as they would for the correct value of c. With this in mind, the RHS is viewed as the reference curve and a numerical search is made around the value of c obtained by the iterative procedure described earlier, to minimize the root-sum-square of the LHS. This fixes c. Now we view the LHS as the reference curve and conduct a numerical search over a range of $k_2\lambda$ so as to minimize the root-sum-square between the LHS and the RHS. This fixes k_2.

Finally, it is noted that the theoretical procedures developed in this section are equally valid for both the longitudinal as well as the shear disturbances.

3. EXPERIMENTAL PROCEDURES

3.1 Measurement Procedures

A schematic of the apparatus is shown in Fig. 4. The heart of the system is a pair of accurately-matched, broad-band, water-immersion, piezoelectric transducers. An experiment is initiated at time t=0 by a triggering pulse produced by a pulser/receiver; the pulse is used to trigger a digitizing oscilloscope; simultaneously the pulser/receiver produces a short-duration (about 100 ns) large-amplitude (about 200 volts) spike which is applied to the transmitting transducer. In the reflection mode it also acts as a receiver. The received signal is post-amplified (to about one volt) and then digitized with maximum sampling rate of 100 MHz (or 10 nanoseconds per point). To reduce the ubiquitous random errors, each measurement is averaged over a sample size of 64. A laboratory computer controls <u>all</u> operations of the digital oscilloscope through an IEEE bus. The built-in signal processor of

the oscilloscope performs FFT on the acquired signals and the relevant parts of the data are then transferred to the computer for further analysis.

3.2 Calibration Procedures

Since our objective in this research is to estimate damage in composite materials from a measurement of the ultrasonic parameters, accuracy is of prime importance. For example, one percent error in estimating the phase velocity may, for some typical laminates, correspond to a ten percent error in estimating the remaining fatigue life. At present, we can measure velocity in monolithic materials to an accuracy of 0.1%, and velocity and attenuation in heterogenous materials to an accuracy of 0.2% and 2%, respectively. In order to achieve this accuracy the measurement system was subjected to systematic calibration procedures; these are described next.

3.2.1 Sampling Interval

The analog signal from the transducer is digitized at a specified sampling interval by the digitizing oscilloscope. The object of this study was to determine an upper bound on the sampling interval below which the harmonic distortion was considered acceptable. We quote here the limits on the sampling interval as specified by the sampling theorem [7], "If the sampling interval T is chosen equal to $1/2f_c$, where f_c is the highest frequency component of the signal, aliasing will not occur". Aliasing is defined as "The distortion of the desired Fourier transform of a sampled function". An experimental verification of this statement is given here. Figures 5 and 6 show the amplitude and phase response of a 10 MHz transducer at sampling intervals of 10 nS (100 MHz), 20 nS (50 MHz), 40 nS (25 MHz), and 100 ns (10 MHz). The highest frequency content of this signal is about 10 MHz and so the

sampling interval of 50 nS would be acceptable from the viewpoint of aliasing. It is obvious from Fig. 5 that at 10 nS or 20 nS sampling intervals the frequency content of the signal is essentially the same. However, at 40 nS sampling intervals significant distortion of the amplitude is observed; but the phase remains relatively unaffected. At 100 nS, both the amplitude and the phase plots are completely distorted. This would come as no surprise for here we are sampling only one point per cycle. In this work we have used either 10 or 20 nS sampling interval.

3.2.2 Frequency Resolution

It is seen from eqs (15) and (18) that wavespeed can be calculated if the slope (ϕ/f) of the phase vs. frequency curve can be obtained. The FFT algorithm provides the real and imaginary components of the transformed signals and from these the phase is calculated. Computer can provide the phase angle in the range of $-\pi/2$ to $+\pi/2$ from which the angle in the range of 2π can be deduced very easily, depending on the quadrant in which the phaser lies. Hence we obtain a sawtooth type phase vs. frequency plot. It was observed that for the signal under consideration, phase increases monotonically with the frequency. Thus the sawtooth plot has to be converted to a continuous phase vs. frequency curve before its slope can be obtained to calculate the wavespeed. The computer algorithm developed by us tracks the rotation of the phase vector and 2π radians are added to the phase each time the vector completes a cycle.

Let the sampling interval be T and the total number of sampled points be N. The total length of the signal is $T_0 = (N-1)T$. Let the frequency resolution be Δf, then $\Delta f = 1/T_0 = 1/(N-1)T$. The consideration of aliasing fixes T. Hence N is the only parameter that can be adjusted to obtain the

desired frequency resolution. For example, if the desired Δf=0.05 MHz/point, T is 10 nS, then N=2000 or 2048. The length of a signal can be readily increased simply by adding zeros at the end of the signal. Of course, this is accompanied by an increased computation time.

3.2.3 Transducer Response

The frequency response of a transducer with a center-frequency of 10 MHz is shown in Fig. 7. Experience indicated that satisfactory measurements can be made over a frequency range (or band width) given by 25% of the peak amplitude response as shown in the figure. It was observed that the phase vs frequency curve over this range is a straight line; outside it becomes non-linear.

4. RESULTS AND DISCUSSIONS

4.1 Wave Propagation in Non-dispersive Media

The main objective of this work is to develop techniques suitable for very thin specimens. Therefore, we subjected our techniques to the following critical test. A thick aluminum plate (2.807 ± 0.0025 mm) was first tested using the conventional toneburst method. Then the thickness was gradually machined down to 0.258 mm (about 10 mil, a very thin foil) in five steps. In non-dimensional terms the thickness was reduced from about 4.4 to 0.4 wavelengths; a frequency of 10 MHz was used. At each step c was measured. We could have used five different samples. Instead we adopted the foregoing procedure in order to ensure that we are always testing exactly the same material. The density was measured by the Archimedes principle. Our estimate of the error in density is ± 0.015%. The results are presented in Table 1. The first measurement was made using the conventional toneburst method[8,9].

The time-domain signal is shown in Fig. 8(a). A particular peak (say the fourth peak) near the center of the toneburst is selected as the reference peak. The twice-transit-time, 2h/c could be measured to an accuracy of 1 nS. Our estimate of error in the phase velocity is 0.2%; see Ref.[10] for a detailed error analysis. In the second measurement the toneburst was reduced to about one cycle; see Fig. 8(b). Note that the pulses can be clearly separated. The Second/First method, eq (15) was used to analyze this data. Since only the first two pulses are needed for data analysis, the remaining pulses are electronically gated out or nulled. In the third measurement, the data analysed remains the same i.e. Fig. 8(b). However, the All/First method, eq (27), is used. In other words, g(t) is now viewed as the sum of all transmissions. For the remaining measurements the specimen was gradually machined down. All/First Method was used to analyze the data. The pulses for h=1.686 mm are shown in Fig. 8(c). Note that the conventional toneburst method can no longer be used; though both methods developed in this work can be used, we used the All/First method. The pulse for the next three thicknesses, h=1.001, 0.613 and 0.258 mm are shown in Figs. 8d, 8e, 8f, respectively. Because of the reduced thickness the pulses cannot be separated in the time domain. Therefore, even the Second/First method cannot be used; here we have to use the All/First method. For the thinnest specimen the round trip time is only 82 nS; the pulse duration is roughly 200 nS. This given rise to what appears to be "ringing" in Fig. 8f.

With reference to Table 1, the average of all the measurements is 6.342 mm/μsec ± 0.25%. We conclude that the All/First method developed for ultra-thin (sub-wavelength) specimens and the Second/First method for moderately thin (about one wavelength) specimens yield results which agree to 0.25% with the conventional toneburst method. (We hesitate to make absolute claims on

accuracy because for the given piece of aluminum we do not know the true value of the phase velocity).

The ideal method for "calibrating" a new experimental technique is to use it to measure a quantity which is known with a ten times better accuracy. Unfortunately, the National Bureau of standards has not yet developed a standard for acoustic velocity (or elastic modulii). Our laboratory did, however, participate in a six-laboratory ASTM round-robin conducted by Dr. Alan Wolfenden[11], (Department of Mechanical Engineering, Texas A&M University, College Station, Texas 77843). This allowed us an opportunity to compare our error-estimates with those of the others. The material tested were two nickel-based alloys; see Table 2 for a material and geometric description. Since these specimens are very very "thick" (several wavelengths), the Second/First method, eq (15), was used. Furthermore, shear velocity was also measured. Here a shear (or Y cut) transducer was directly cemented onto the metal specimen using a shear couplant. Ignoring the "main bang," the remaining reflected signal was collected. From the measurements of the longitudinal and shear velocity, c_1 and c_2, and density ρ, the elastic constants E and ν can be readily calculated. The results of the round-robin test are presented in Table 3. Reasonably good agreement (within 2.5%) is observed between the results obtained in different laboratories using different techniques.

Next, we have tested our experimental method on a medium which is non-dispersive but attenuative. An epoxy (EPON 828Z) was selected for this purpose. The results are presented in Table 4. Note that three frequencies, spanning nearly a decade, were used. The phase velocity measured by the toneburst method on a thick specimen is 2.915 mm/μsec and agrees very well with that measured with the All/First technique.

4.2 Wave Propagation in Dispersive Media

Finally, we have tested our experimental procedures on a material which is simultaneously highly dispersive as well as highly attenuative. Towards this end we tested a random particulate composite consisting of lead spheres in an epoxy matrix. These composites have been described in [12,13]. Transducers with 0.25 MHz center-frequency were employed. Second/First method in through-transmission mode, eq (16), was used.

Kinra[13] has shown that wave propagation in these composites occurs along two separate branches: (1) The low-frequency, slower, acoustical branch along which the particle motion is essentially in phase with the excitation and (2) The high-frequency, faster, optical branch along which the particle motion is essentially out of phase with the excitation. The two are separated by a cut-off frequency which corresponds to the excitation of the rigid-body-translational resonance of the heavy inclusions; this occurs when $k_1 a = O(1)$, where a is the inclusion radius. Around the cut-off frequency both the phase velocity and the attenuation change dramatically with frequency. This is what makes this composite such an interesting material to study using our technique which was developed especially for dispersive media.

The results for a dispersive material are presented now. In Fig. 9 $F^*(\omega)$ is the received signal with the specimen removed while $G^*(\omega)$ is the signal with the specimen in place; $\tilde{c}$ is the volume fraction of inclusions. The dip in the amplitude of $G^*(\omega)$ corresponds to the cut-off frequency. The present measurement, f_c=0.21 MHZ., agrees quite well with the earlier measurement[12] using the conventional tone-burst method. We now introduce a normalized frequency $\Omega \equiv k_1 a = 2\pi fa/c_1$ and a normalized wavenumber $\xi = \langle k_1 \rangle a = 2\pi fa/\langle c_1 \rangle$ where $\langle\ \rangle$ refers to an aggregate property of the

composite (an ensemble average). Fig. 10 shows the frequency vs wavenumber plot. As expected[12], along the acoustical branch at low frequencies the behavior is non-dispersive; a straight line fitted through the data points passes through the orgin ($\langle c_1 \rangle / c_1 = \Omega/\xi$). Same was noted at high frequencies along the optical branch. These two observations serve as critical checks on the accuracy of our measurement. The normalized phase velocity is given by the slope of the secant, $\langle c_1 \rangle / c_1 = \Omega/\xi$, and the group velocity is given by the slope of the tangent, $\langle c_g \rangle / c_1 = d\Omega/d\xi$. The discrete toneburst data from the earlier work[12-14] is also plotted; the agreement is considered quite satisfactory. The present technique is tremendously faster; the entire dispersion and attenuation curve is produced in a single experiment. Another major advantage of this method is as follows. When one uses the toneburst method, each point suffers a scatter due to random errors; see Fig. 10. In the present method the <u>whole curve</u> may shift up or down but the <u>shape</u> of the curve will not be altered by the random errors. Here we are mainly interested in the shape of the dispersion curve. Fig. 11 shows the normalized phase velocity versus frequency. The arrow labelled HASHIN is the velocity calculated from the lower (appropriate) <u>static</u> bound due to Hashin and Shtrikman[15]. The agreement between the theory and the low-frequency results is considered quite satisfactory. As Ω increases the effective inertia of the lead spheres ($\sim \rho\omega^2$) increases and the phase velocity decreases. At very high frequencies (it is conjectured) the inertia becomes so large that the spheres become essentially motionless. Thus they no longer contribute to the inertia of the composite as perceived by the effective wave. Hence the velocity increases dramatically across the cut-off frequency and becomes frequency-independent at very high frequencies. Fig. 11b shows the group velocity i.e. the speed with which energy flows in a composite. As

expected, the group velocity is essentially constant at low and high frequencies; around the cut-off frequency, Ω_c, it undergoes large fluctuations. Theoretically, $c_g \to \infty$ at two points around the cut-off frequency. Perhaps the most interesting feature is that the group velocity becomes negative around Ω_c, i.e. as the wave propagates in the positive x-direction, the energy flows in the negative x-direction. In Fig. 10 this corresponds to those points on the curve where the slope is negative.

In Fig. 12 we have plotted attenuation versus frequency. The peak in the curve defines the cut-off frequency. For comparison $k_2\lambda$ for the neat epoxy alone is 0.13 which is negligibly small compared to the peak attenuation. Thus all of $k_2\lambda$ may be attributed to the scattering effects.

4.3 *QNDE of Damage in Composite Materials*

We now demonstrate the application of our technique to fiber-reinforced composite materials. Graphite/Epoxy AS4/3502 crossply $[0_6/90_4/0_2]_s$ laminates were tested. These were subjected to monotonic tensile loading. As a result transverse cracks develop. Edge replication was made to obtain a record of the transverse cracks. The loading was interrupted at several points along the load axis, the coupon was subjected to an ultrasonic examination and the loading was resumed. The Second/First method in the reflection mode, eq (15), was used. In Fig. 13 we have also shown the portion of the edge replication which is insonified by the ultrasonic beam. The number of cracks seen by the beam is also listed. Note that we have not plotted the attenuation $k_2\lambda$ but rather the changes in $k_2\lambda$ caused by this damage. To guard against for fortuitous results three different frequencies were used, namely, 2.25, 5.00 and 7.50 MHz. We note that attenuation changes quite significantly and

monotonically with the number of transverse cracks. We also note that in the range of frequency tested, the attenuation decreases with frequency. This may be attributed to the fact that these experiments were conducted at k_1a=1.23, 2.70 and 4.02, where a is the half-crack-length, at 2.25, 5.00 and 7.50 HHz, respectively. Fig. 14 shows the longitudinal phase velocity at the same three frequencies. Within the errors of measurement, ±0.2%, the phase velocity remains constant with damage. This is not at all surprising, in view of the fact that here the wave-vector (or the particle displacement vector) is parallel to the crack face i.e. the crack-wave interaction is very weak. Thus we conclude that for the present case while the attenuation is a good measure of the damage, velocity is not.

5. CONCLUSIONS

We have described a new experimental technique which can be used to measure phase velocity and attenuation of ultrasonic waves in very thin plates (down to a thickness which is three orders of magnitude smaller than the wavelength). We emphasize that in the development of this technique we have taken a "black-box" approach i.e. it would work for any material so long as it behaves in a linear viscoelastic material and the attenuation is not large.

6. ACKNOWLEDGEMENTS

This research is supported by the Air Force Office of Scientific Research Contract No. F49620-83-C-0067. The continuing encouragement of Major Glasgow and Major Haritos is gratefully acknowledged.

APPENDIX

Consider one-dimensional monochromatic, time-harmonic wave propagation along a rod made up of a linear viscoelastic material, $e^{i(\omega t-kx)}$. At any frequency ω the complex-valued wavenumber is $k(\omega) = k_1(\omega) + ik_2(\omega)$. If attenuation is small the phase velocity $c = \omega/k_1$; k_2 is the attenuation i.e. the amplitude of the wave decays as $e^{-k_2 x}$. Now suppose a pulse is propagating down this rod and is given at x=0 by f(t).

Let

$$F^*(\omega) = \frac{1}{\sqrt{2\pi}} \int_{-\infty}^{\infty} f(t)\, e^{-i\omega t} dt \qquad \text{(A 1)}$$

Then

$$f(t) = \frac{1}{\sqrt{2\pi}} \int_{-\infty}^{\infty} F^*(\omega)\, e^{i\omega t} d\omega \qquad \text{(A 2)}$$

For the sake of this discussion f(t) may be viewed as an infinite sum of wavelets of the type,

$$f(t) = \left(\frac{F^*(\omega)\Delta\omega}{\sqrt{2\pi}}\right) e^{i\omega t} \qquad \text{(A 3)}$$

Consider a propagating monochromatic "wavelet" of complex-amplitude, $\frac{F^*(\omega)\Delta\omega}{\sqrt{2\pi}} e^{i(\omega t-kx)}$. In eq (A3) f(t) may be viewed as an infinite sum of such "wavelets" at x=0. Furthermore, at some arbitrary x the wavelets may be summed up to yield

$$g(t) = \int_{-\infty}^{\infty} \left(\frac{F^*(\omega)d\omega}{\sqrt{2\pi}}\, e^{-ikx}\right) e^{i\omega t}$$

If $G^*(\omega)$ is the Fourier transform of g(t) then

$$G^*(\omega) = F^*(\omega)\, e^{-ikx}$$

or

$$\frac{G^*(\omega)}{F^*(\omega)} = e^{-ikx}$$

We have shown, therefore, that eq (12) which was originally derived for a perfectly elastic material is valid for a linear viscoelastic material provided the attenuation is small ($k_2/k_1 < 0.1$) which is generally the case with engineering materials and certainly is the case for all materials tested during this work.

REFERENCES

1. T.R. Tauchert, and A.M. Guzelsu,, "An Experimental Study of Dispersion of Stress Waves in a Fiber-Reinforced Composite," ASME Journal of Applied Mechanics, 39, 98-102 (1972).

2. H. Kolsky,, "Stress Waves in Solids," DOVER (1953)

3. F.H. Chang, J.C. Couchman, and B.G.W. Yee, "Ultrasonic Resonance Measurements of Sound Velocity in Thin Composite Laminates," J. Comp. Matl. 8, 356-363 (Oct. 1974).

4. J.S. Heyman, "Phase Insensitive Acoustoelectric Transducer," J. Acoust. Soc. Am., 64(1), 243-249 (July 1968).

5. J.D. Achenbach, "Wave Propagation in Elastic Solids," North-Holland Publishing Company (1973).

6. H. Kolsky, "The Propagation of Stress Pulses in Viscoelastic Solids" The Philoscophical Magazine, 8(1), 693 (Aug. 1956).

7. E.O. Brigham, "The Fast Fourier Transform," Prentice Hall (1974).

8. V.K. Kinra, M.S. Petraites, and S.K. Datta "Ultrasonic Wave Propagation in a Random Particulate Composite," Int. J.Solids Structures, 16, 301-312 (1980).

9. V.K. Kinra, and A. Anand, "Wave Propagation in a Random Particulate Composite at Long and Short Wavelength," Int. J. Solids, Structures, 18(5), 367-380 (1982).

10. V.K. Kinra, and E.L. Ker, "Effective Elastic Moduli of a Thin-Walled Glass Microsphere/PMMA Composite," J.Comp. Matl, 16, 117-188 (Mar. 1982).

11. A. Wolfenden, M.R. Harmouche, G.V. Blessing, Y.T. Chen, P. Terranora, V.K. Kinra, V. Dayal, J.W. Lemmens, R. Phillips, J.S. Smith and R.J. Wann, "Dynamic Young's Modulus Measurements in Nickel-Based Alloys: Six Methods," to appear, J. Testing Evaluation.

12. V.K. Kinra, and P.N. Li, "Resonant Scattering of Elastic Waves by a Random Distribution of Inclusions," Int. J. Solids Structures, 22(1), 1-11, (1986).

13. V.K. Kinra, "Dispersive Wave Propagation in Random Particulate Composites," Recent Advances in Composites in the United States and Japan, ASTM STP 864, J.R. Vinson and M. Taya, Eds., 309-325 (1985).

14. V.K. Kinra and C.Q. Rousseau, "Acoustical and Optical Branches of Wave Propagation: Some Additional Results," Proc. Multiple Scattering of Waves in Random Media and Random Rough Surfaces, The Pennsylvania State Univ., Ed. V.K. Vardan and V.V. Vardan, 603-613 (1985).

15. Z. Hashin and S. Shtrikman, "A Variational Approach to the Theory of The Elastic Behavior of Multiphase Materials," J. Mech. Phys. Solids, 11, 127-140 (1963).

TABLE 1. Test Results on Aluminum Sample

Material: Aluminum
Wave Type: Longitudinal
Mode: Transmission
Frequency: 10 MHz
Density: 2.8177 ± 0.0004 g/ml

h mm	h/λ	c mm/μsec	$\bar{\sigma}$/c %	Technique	Reference Figure
2.807	4.4	6.3572		Toneburst	8a
2.807	4.4	6.3239	0.013	Second/First	8b
2.807	4.4	6.3275	0.010	All/First	8b
1.686	2.7	6.3461	0.040	All/First	8c
1.001	1.6	6.3538	0.030	All/First	8d
0.613	0.96	6.3594	0.130	All/First	8e
0.258	0.4	6.3231	0.140	All/First	8f

TABLE 2: Results of ASTM Round-Robin Tests of Ni based alloys

Sample 1 : INCONEL ALLOY 600
Composition: Ni 37.46, C 0.01, Co 14.38, Nb 4.71, Ti 1.46, Fe 41.98
Test Frequency: 5.0 MHz
Mode: Reflection

Sample 2 : INCOLOY ALLOY 907
Composition: Ni 74.91, Cr 15.48, C 0.08, Fe 9.53

SAMPLE	h mm	ρ g/ml	c_1 mm/μsec	c_2 mm/μsec	E GN/m^2	ν
1.2*	6.263	8.371	5.872	3.161	216.9 ± 0.14%	0.2960 ± 0.20%
1.4	6.365	8.373	5.877	3.163	216.6 ± 0.15%	0.2960 ± 0.20%
2.1	18.848	8.267	5.273	2.7308	163.0 ± 0.26%	0.3153 + 0.18%

* The first digit (1 or 2) refers to the alloy while the second digit (1-4) is merely to identify different physical specimens.

TABLE 3: Comparison of ASTM Round Robin Tests for the Young's Modulus, E

SAMPLE/LAB	1.1	1.2	1.3	1.4	2.1	2.2	2.3
1	218.0 218.0 218.1	216.9	218.5	-	161.5	159.9	157.2
2	210.5	209.2	-	-	164.1	-	155.7
3	218.8	216.0	217.5 217.0 216.2 217.3	-	162.0 161.8 160.8	- -	158.4
4	212.0	-	205.0	-	156.0	-	172.0
5	215.6	-	214.2	-	156.0	-	162.0
6[This Work]	-	216.9	-	216.6	163.0	-	-
7	203.0	-	210.3	-	156.8	-	155.8 158.0

Units for above values: GN/m^2

Techniques: -

LAB. 1, 2, 7 Free-Free Beam
LAB. 3 Impulse Fourier
LAB. 4 Pulse-Echo-Overlap Ultrasonic
LAB. 5 Piezoelectric Ultrasonic Oscillation (PUCOT)
LAB. 6 This work

TABLE 4: Test Results on Epon 828-Z Epoxy

Material: Epon 828-Z epoxy
Wave Type: Longitudinal
Mode: Transmission

Specimen thickness 1.869 mm ± 0.0025
Specimen density 1.2069 ± 0.0004 g/ml

Test Frequency MHz	Wavespeed mm/μsec	$\bar{\sigma}$ %	$k_2\lambda$	$\bar{\sigma}$ %	Technique
1.0	2.874	0.1	0.1340	1.4	All/First
5.0	2.884	0.14	0.0924	1.5	All/First
10.0	2.915	0.08	0.0975	1.0	All/First
10.0	2.915	0.24	0.0979	2.2	Toneburst

List of Figures

Fig. 1 Various reflections and transmissions from a plate immersed in water.

Fig. 2 Magnitudes of Fourier Transforms of f(t) and g(t) when pulses can be separated

Fig. 3 Magnitude of $G^*(\omega)/F^*(\omega)$ -1, from Fig. 2. Resonance spacing can be measured easily from the zero line crossings.

Fig. 4 Block diagram of the experimental set up.

Fig. 5 Amplitude response of a 10 MHz transducer at different digitizing intervals.

Fig. 6 Phase response of a 10 MHz transducer at different digitizing intervals.

Fig. 7 Useful frequency range of a 10 MHz transducer.

Fig. 8 10 MHz signal through aluminum plates of different thickness. (a) is for toneburst Others are for a single pulse of signal. Plate thickness given on each signal.

Fig. 9 Magnitude of $F^*(\omega)$ [FFT of signal through polystyrene delay rod] and $G^*(\omega)$ [FFT of signal through polystyrene and Lead/Epoxy specimen]. Note the dip in amplitude at the cut-off frequency, fc.

Fig. 10 Frequency; $\Omega = k_1 a$ and wavenumber; $\xi = \langle k_1 \rangle a$ curve for a dispersive Lead/Epoxy specimen. Circled points are data from reference 12-14.

Fig. 11a Normalized phase velocity and frequency curve for the dispersive Lead/Epoxy specimen.

Fig. 11b Normalized group velocity and frequency curve for Lead/Epoxy specimen.

Fig. 12 Normalized attenuation and frequency curve. Note a very high attenuation (large energy absorption) due to dispersion at the cut-off frequency, Ω_c.

Fig. 13 Attenuation increases dramatically with transverse cracks in Gr/Ep, $[0_6 90_4 0_2]_s$ laminate at all three frequencies tested. Extent of damage is shown in the edge replication sketches.

Fig. 14 Longitudinal wavespeed variation at three different frequencies with transverse cracks in a Gr/Ep, $[0_2 90_4 0_2]_s$ laminate.

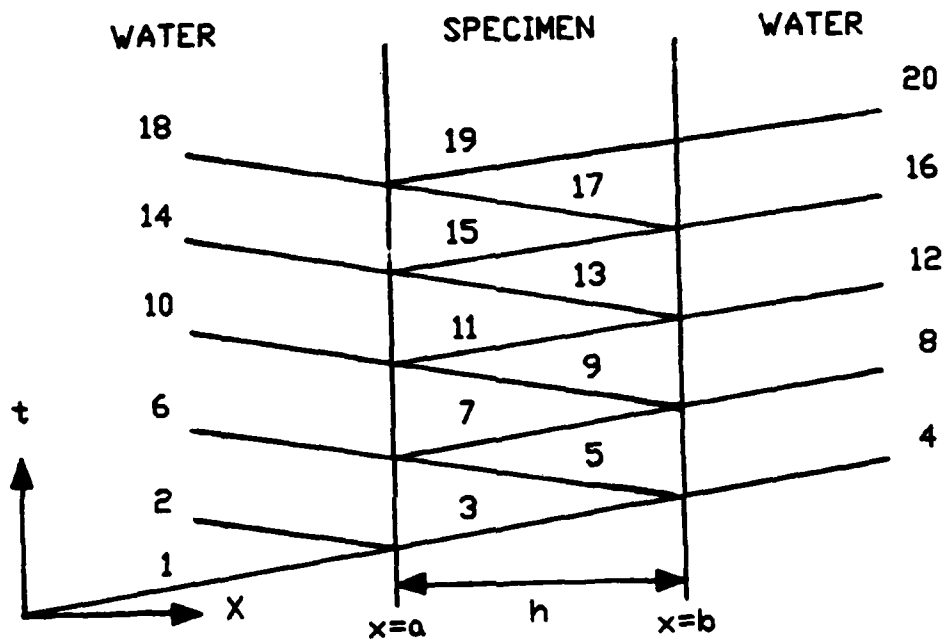
WATER
SPECIMEN
WATER
20
18
19
16
17
14
15
12
13
10
11
8
9
t
6
7
4
5
2
3
1
X
x=a
h
x=b

Figure 1

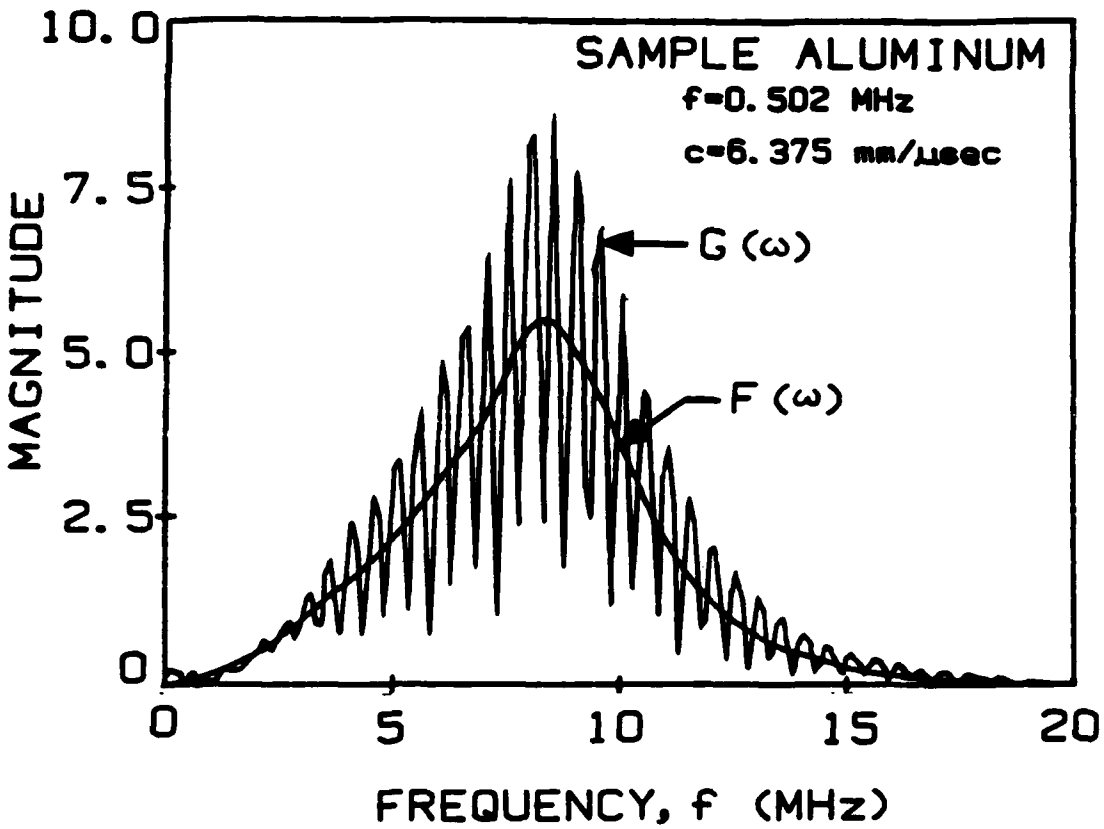
SAMPLE ALUMINUM
f=0.502 MHz
c=6.375 mm/μsec
G (ω)
F (ω)
MAGNITUDE
10.0
7.5
5.0
2.5
0
0
5
10
15
20
FREQUENCY, f (MHz)

Figure 2

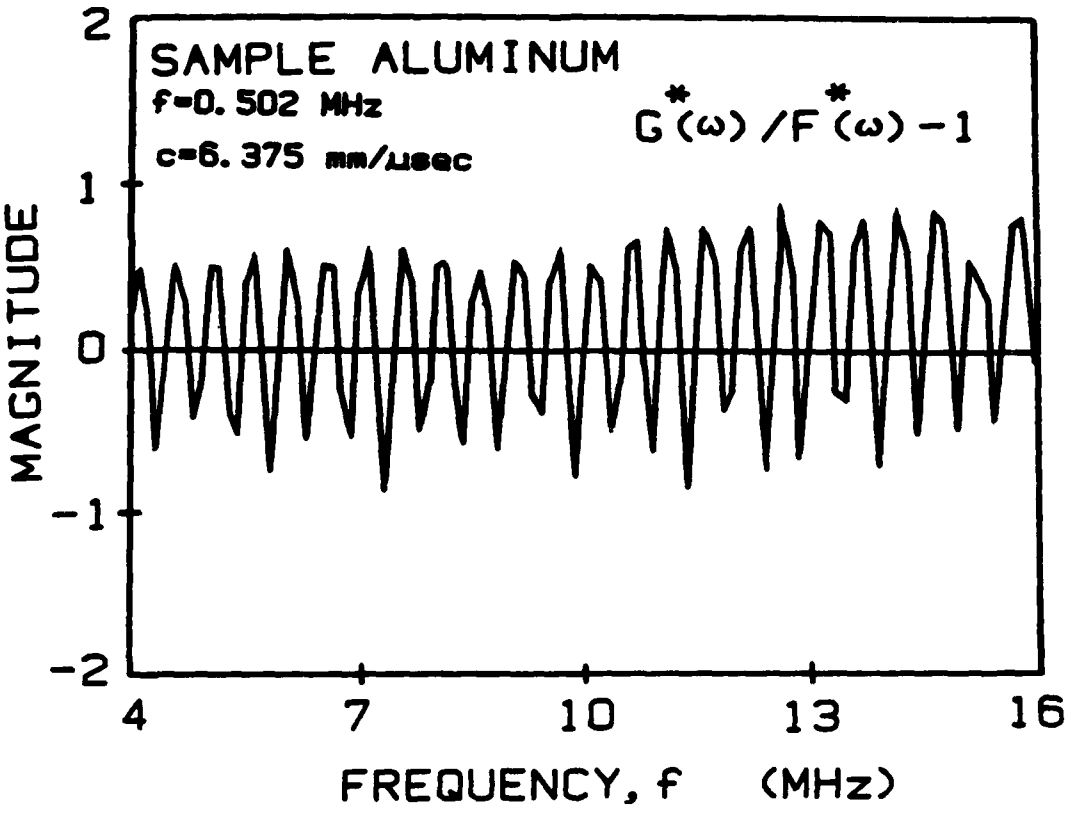
SAMPLE ALUMINUM
f=0.502 MHz
c=6.375 mm/μsec
G*(ω)/F*(ω)-1
MAGNITUDE
2
1
0
-1
-2
4
7
10
13
16
FREQUENCY, f (MHz)

Figure 3

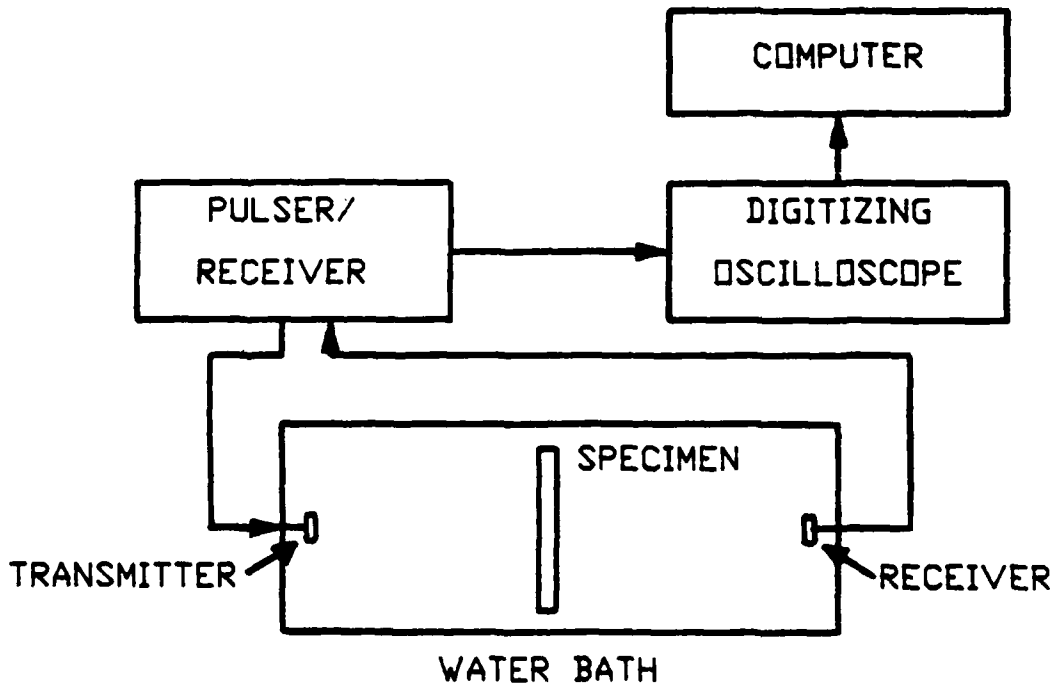
COMPUTER
PULSER/
RECEIVER
DIGITIZING
OSCILLOSCOPE
SPECIMEN
TRANSMITTER
RECEIVER
WATER BATH

Figure 4

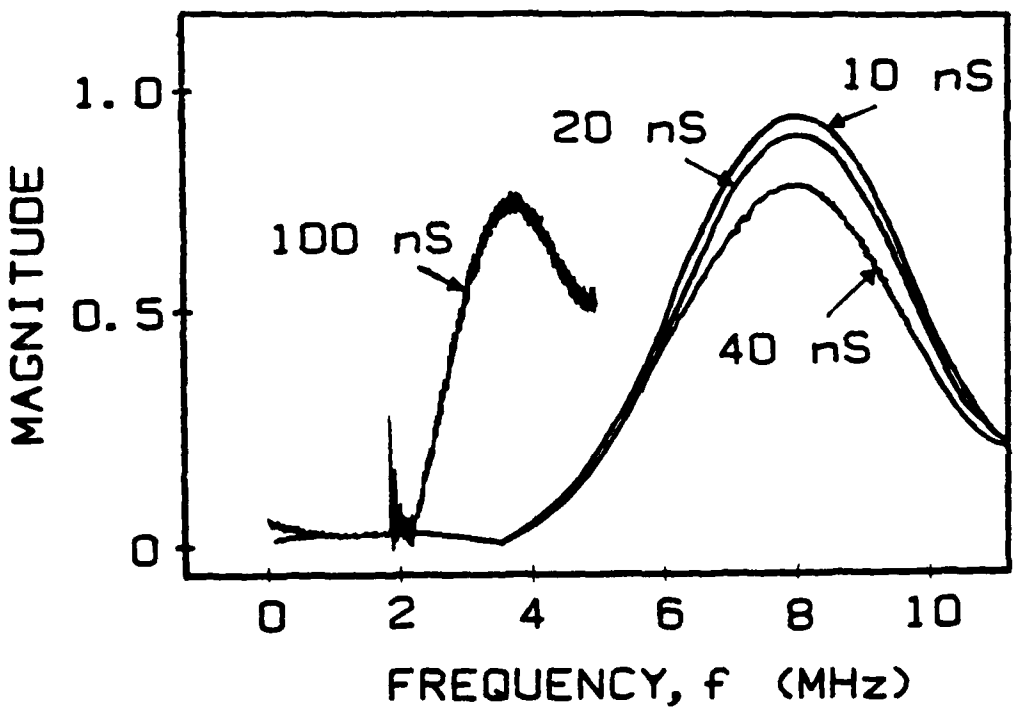
1.0
0.5
0
MAGNITUDE
10 nS
20 nS
100 nS
40 nS
0
2
4
6
8
10
FREQUENCY, f (MHz)

Figure 5

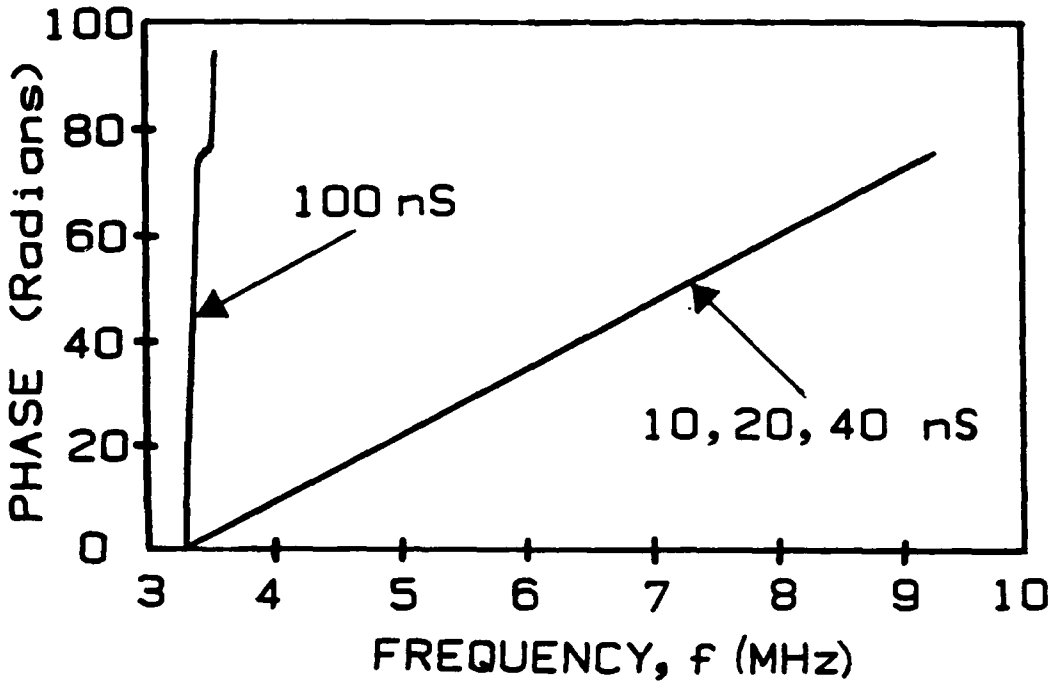
100
80
60
40
20
0
PHASE (Radians)
100 nS
10, 20, 40 nS
3
4
5
6
7
8
9
10
FREQUENCY, f (MHz)

Figure 6

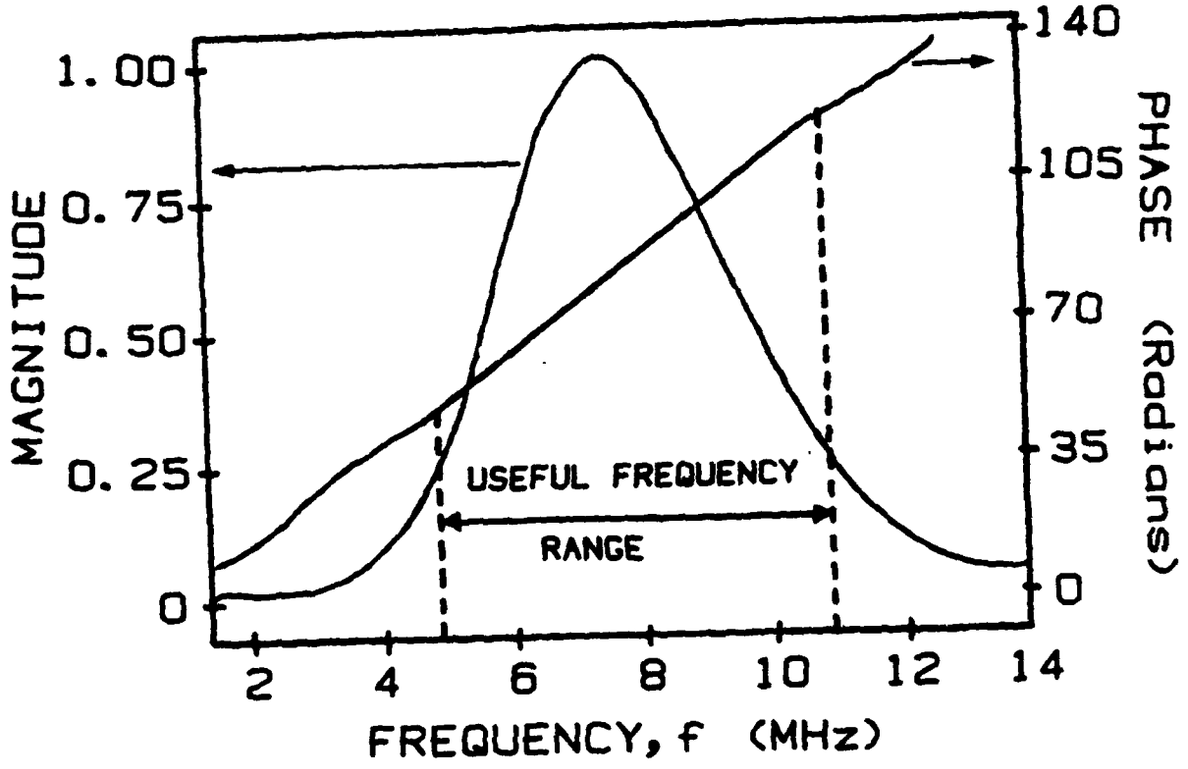
1.00
0.75
0.50
0.25
0
MAGNITUDE
140
105
70
35
0
PHASE (Radians)
USEFUL FREQUENCY
RANGE
2
4
6
8
10
12
14
FREQUENCY, f (MHz)

Figure 7

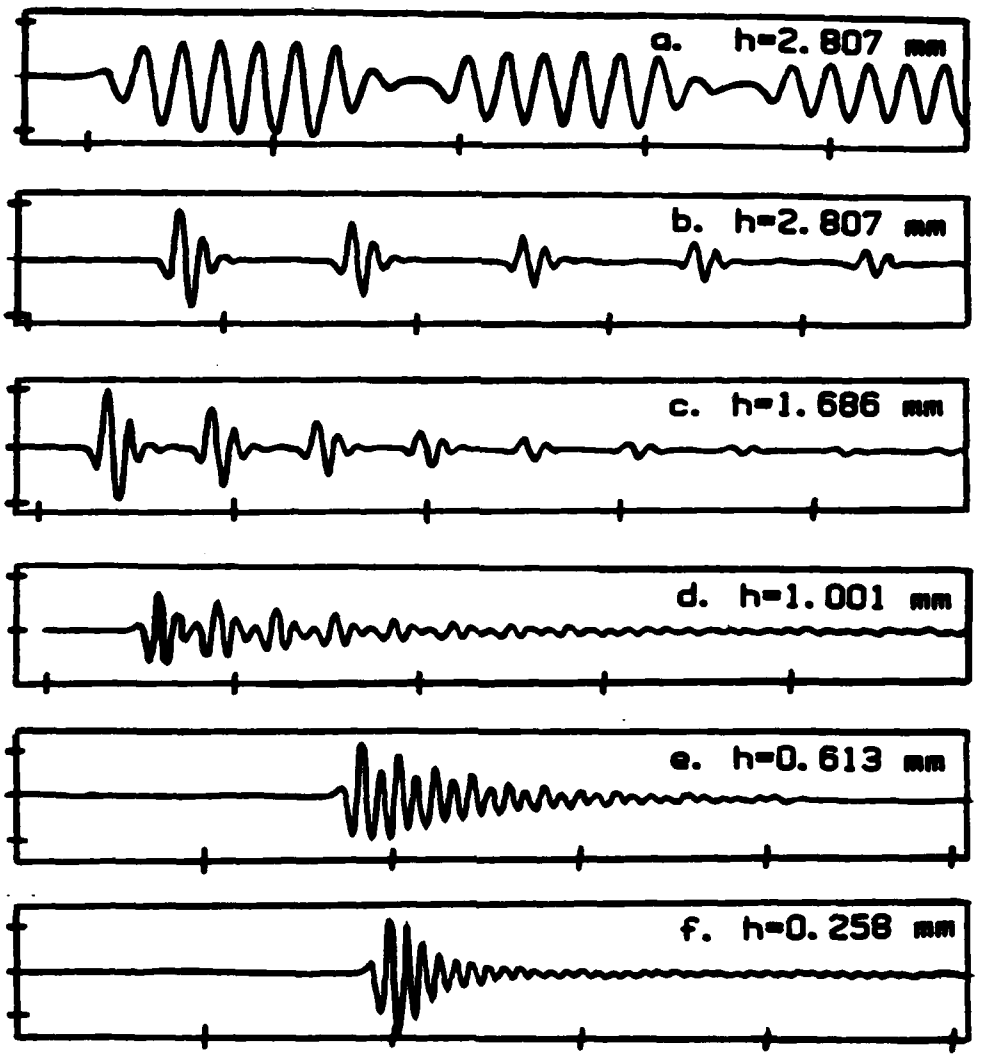

Figure 8

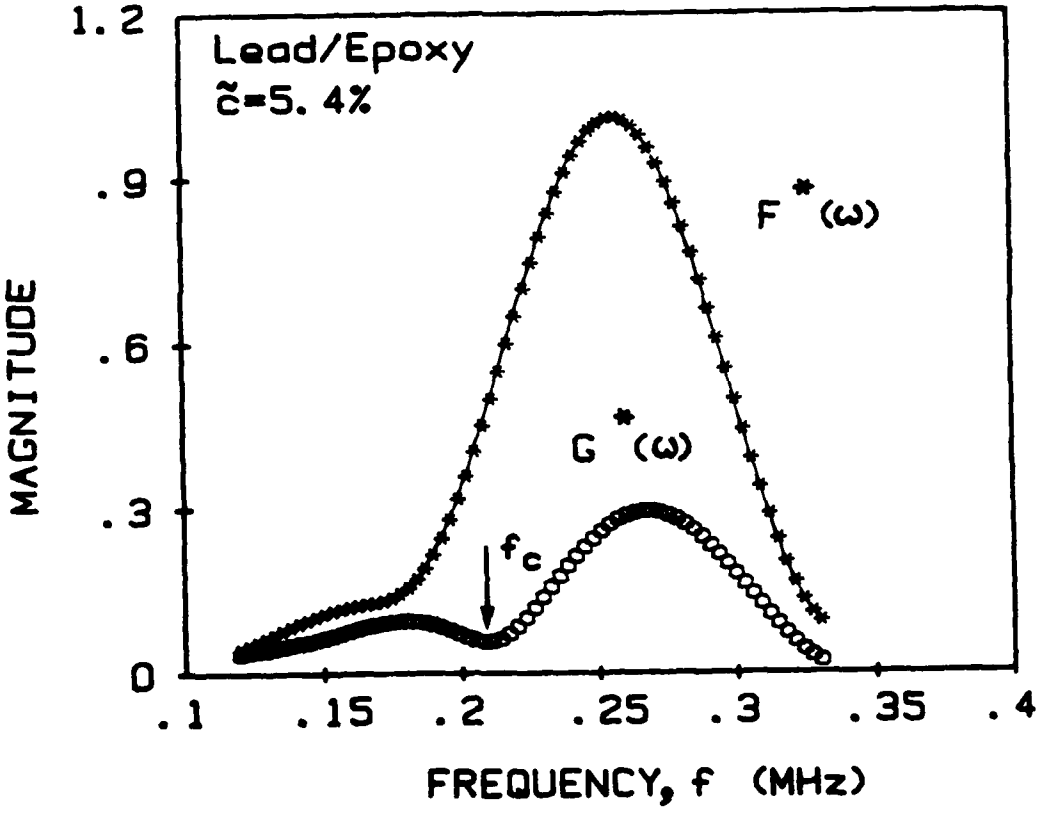
Lead/Epoxy
c̃=5.4%
F*(ω)
G*(ω)
fc
MAGNITUDE
FREQUENCY, f (MHz)
1.2
.9
.6
.3
0
.1
.15
.2
.25
.3
.35
.4

Figure 9

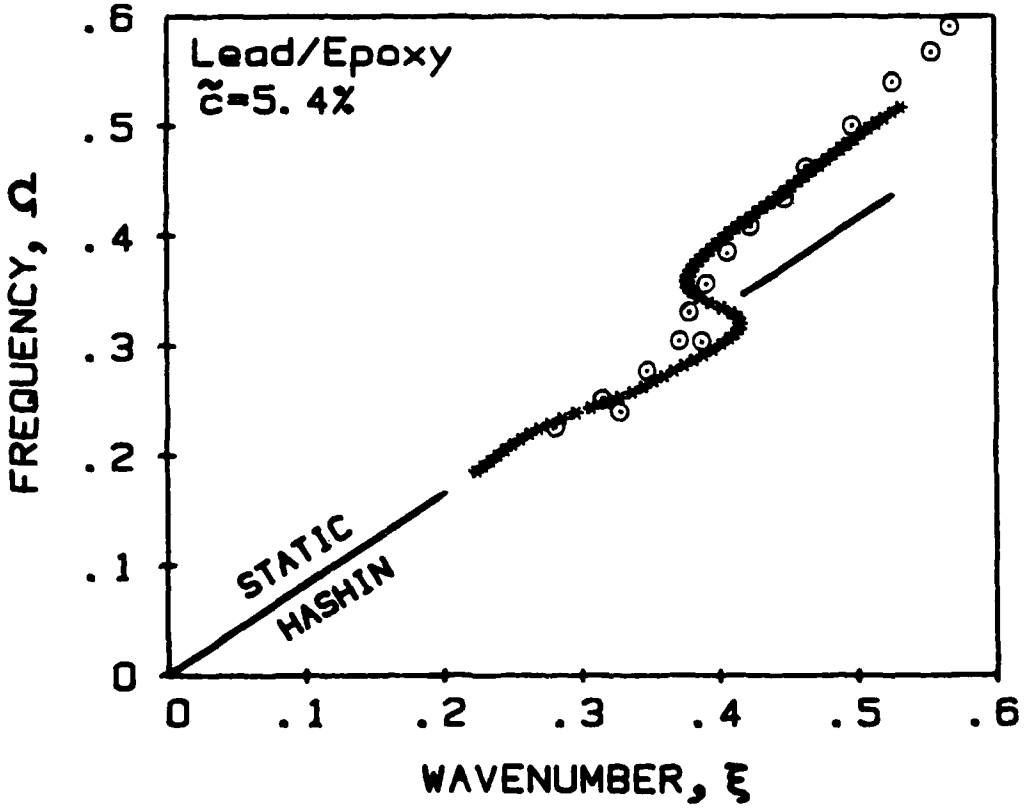
Lead/Epoxy
c̃=5.4%
STATIC
HASHIN
FREQUENCY, Ω
WAVENUMBER, ξ
0
.1
.2
.3
.4
.5
.6

Figure 10

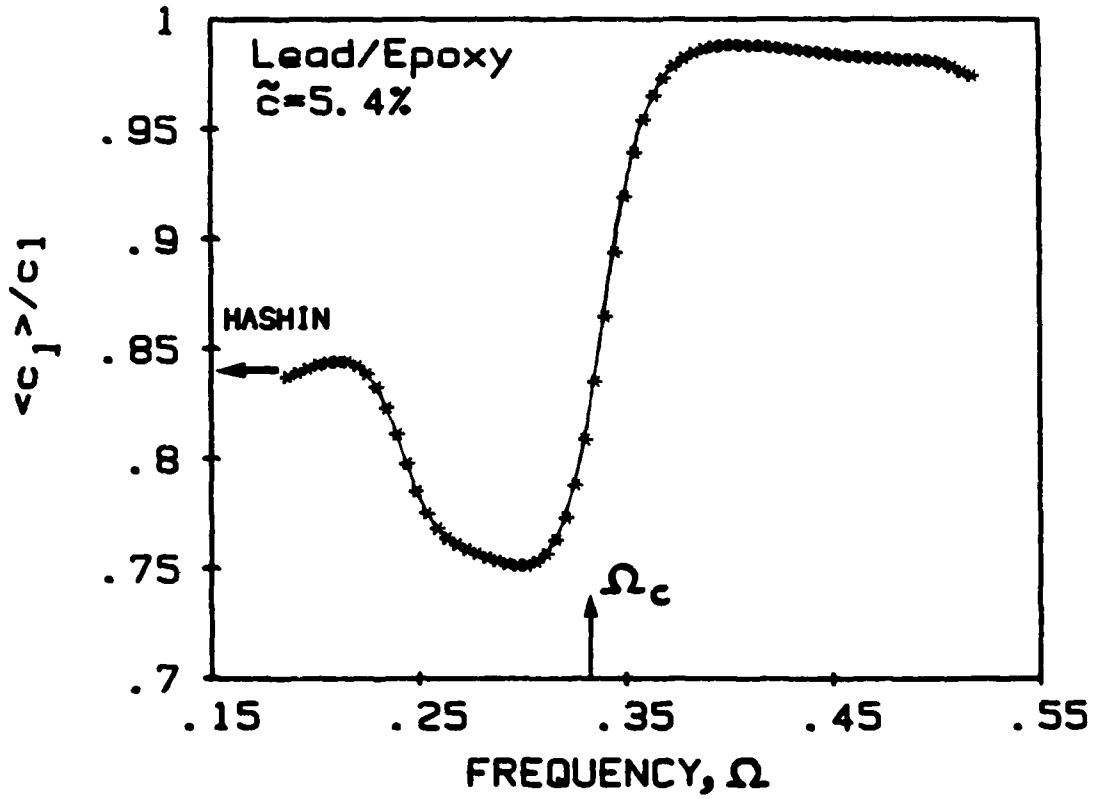
Lead/Epoxy
c̃=5.4%
HASHIN
Ω_c
$\langle c_1 \rangle / c_1$
1
.95
.9
.85
.8
.75
.7
.15
.25
.35
.45
.55
FREQUENCY, Ω

Figure 11a

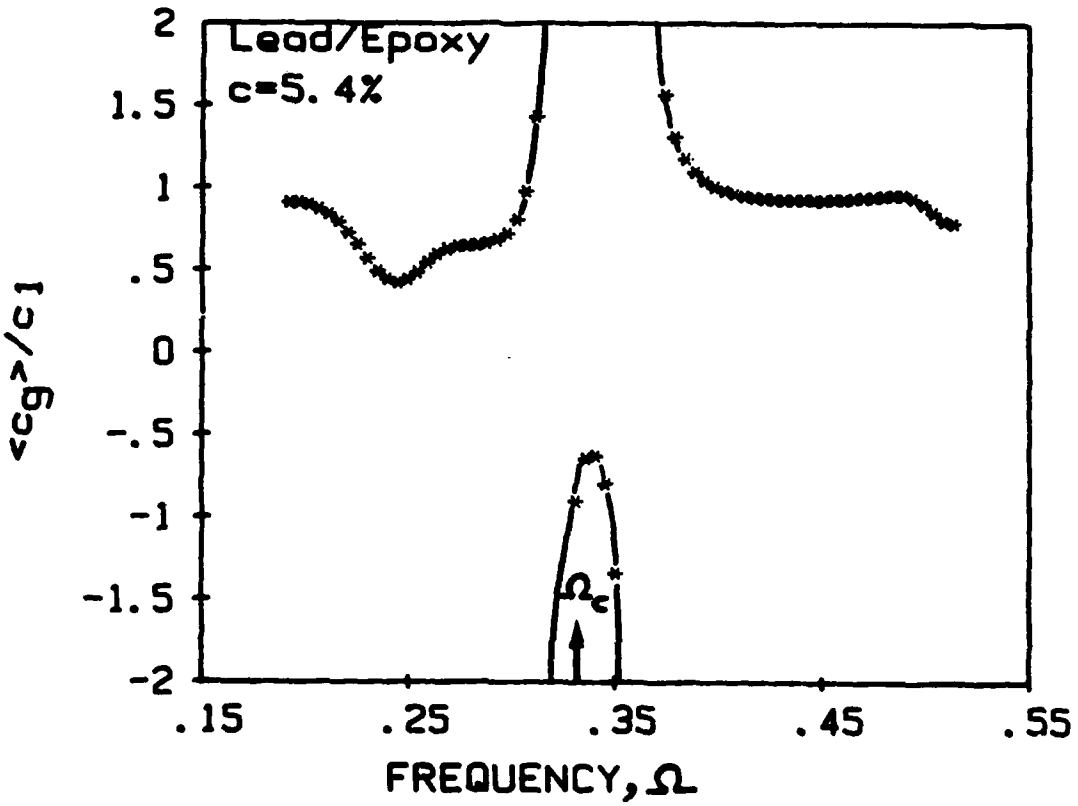

Figure 11b

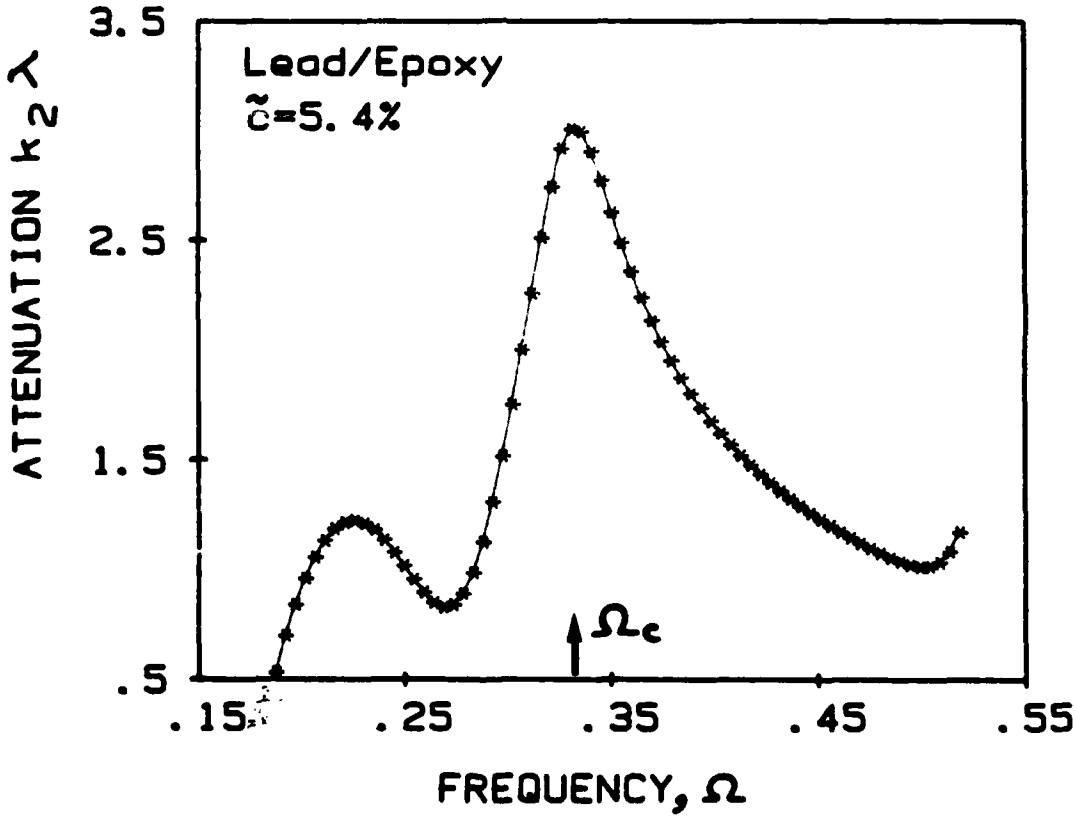
Lead/Epoxy
$\tilde{c}$=5.4%
ATTENUATION $k_2\lambda$
3.5
2.5
1.5
.5
.15
.25
.35
.45
.55
Ω_c
FREQUENCY, Ω

Figure 12

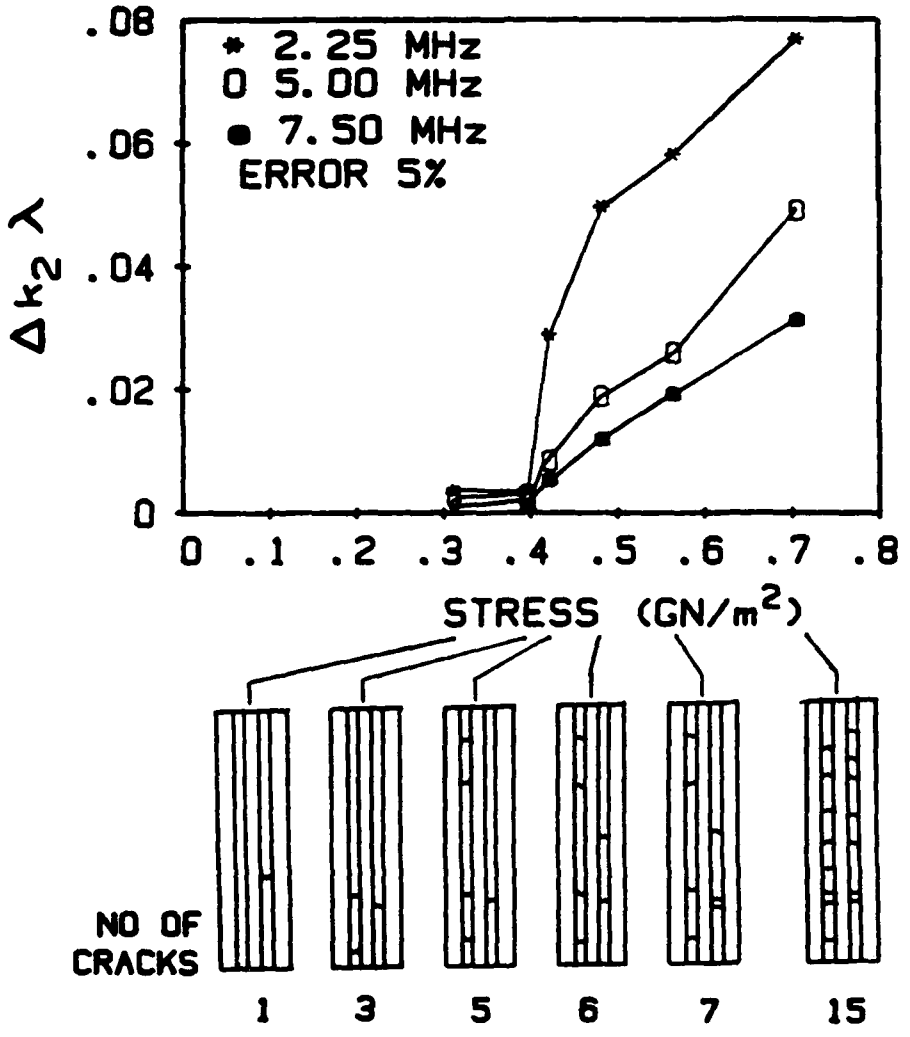
.08
.06
.04
.02
0
$\Delta k_2 \lambda$
* 2.25 MHz
O 5.00 MHz
● 7.50 MHz
ERROR 5%
0 .1 .2 .3 .4 .5 .6 .7 .8
STRESS (GN/m^2)
NO OF CRACKS
1 3 5 6 7 15

Figure 13

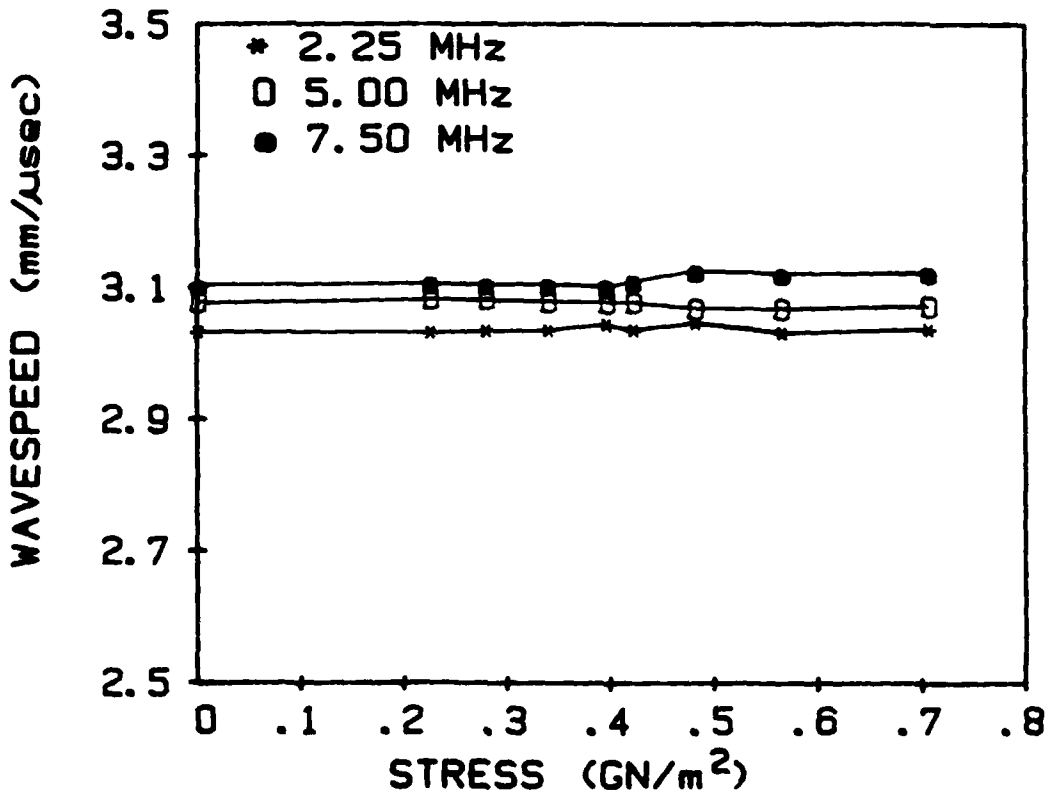
3.5
3.3
3.1
2.9
2.7
2.5
WAVESPEED (mm/μsec)
* 2.25 MHz
O 5.00 MHz
● 7.50 MHz
0
.1
.2
.3
.4
.5
.6
.7
.8
STRESS (GN/m²)

Figure 14

Ultrasonic Nondestructive Testing of Fiber Reinforced Composite Materials

VINAY DAYAL* AND V. K. KINRA**
Texas A&M University
College Station, Texas, U.S.A.

J. G. EDEN***
General Dynamics
Fort Worth, Texas, U.S.A.

ABSTRACT A fully computerized technique for the measurement of wavespeed and attenuation has been developed. The technique can be applied to a thin specimen . It has been used to measure damage in specimens made of Magnamite AS4/3502 Graphite/ Epoxy. It has been observed that attenuation is a reliable measure of damage due to microcracks. To the best of our knowledge this is the first technique which can be used to interrogate very thin specimens.

INTRODUCTION It is well known that fiber-reinforced composite materials develop a complex damage state when subjected to mechanical or thermal loading. The residual strength or fatigue life depends upon the current state of damage. When the damage occurs, it has two effects upon the propagation of a mechanical wave through the composite:1.It affects the stiffness and, therefore, the speed of wave propagation; 2.It increases the attenuation of the wave. Thus the ultrasonic parameters,wavespeed and attenuation, are a measure of the damage of the composite.

A new technique of ultrasonic NDE of composites is presented here. Ultrasonic NDE has been around for years. However, none of the existing techniques work satisfactorily for thin laminates for the following reason: the wave reflection from laminate faces are too close in the time domain and interfere with each another. A new technique has been developed based on the following theorem of the theory of Fourier transforms: the closer two events are in the time domain, the farther apart are the corresponding events in the frequency domain. The technique developed here yields accurate measurements of wavespeed (or stiffness) and attenuation (or damping) of longitudinal and shear waves in the thickness direction.

The development of the technique and some results from its application to fiber-reinforced composite,Graphite/Epoxy AS4/3502 laminates, of a variety of stacking sequences are presented.

---

* Grad Student Aerospace Engg.,Texas A&M Univ.,Coll. St. TX 77843
** Assoc. Prof Aerospace Engg.,Texas A&M Univ.,Coll. St. TX 77843
*** Engineer,Adv.Methods Gr.,General Dynamics,Fort Worth TX 76101

THEORETICAL ANALYSIS Consider a plate of a linear viscoelastic material sandwiched between two half-spaces of perfectly elastic materials. Consider also, a finite duration pulse,ray 1,incident at the viscoelastic plate as shown in fig.1.

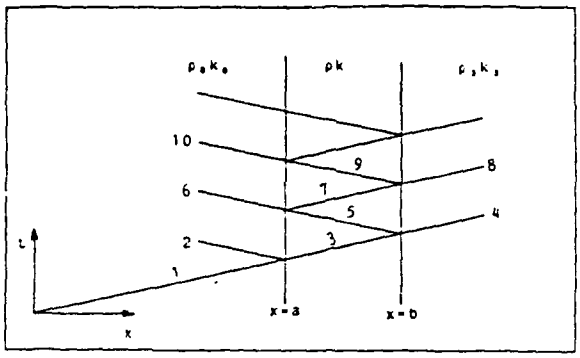

Fig.1 Pulse reflection and transmission by a plate.

Due to the mismatch in the acoustic impedence of the three materials, there will be an infinite series of reflected and transmitted pulses. These pulses contain information about the acoustic properties of the viscoelastic material.

Let the displacement field along the incident ray 1 be given by $u^{inc}=f(\omega t-k_0 x)$, where $f(s)\equiv 0$ for $s<0$ and ω and k_0 are circular frequency and wavenumber of the first half-space,respectively. The total reflected field is the sum of the following rays, with ($h=b-a$ and $s=\omega t+k_0 x$).

$u^2=R_{12}f(s-s_2)$; $s_2=2k_0a$

$u^6=T_{12}R_{23}T_{21}f(s-s_6)$; $s_6=2k_0a+2kh$

$u^{10}=T_{12}R_{23}R_{21}R_{23}T_{21}f(s-s_{10})$; $s_{10}=2k_0a+4kh$

where T_{ij} = Transmission coefficient from medium i to j

R_{ij} = Reflection coefficient from interface of media i&j with wave incident in medium i

The sum of these rays is

$$u^r=R_{12}f(s-2k_0a)+T_{12}R_{23}T_{21}\sum_{m=0}^{\infty}(R_{12}R_{23})^{m-1}f(s-s_m);\ s_m=2k_0a+m2kh \quad (1)$$

Similarly, the sum of the transmitted field can be written as

$$u^t=T_{12}T_{23}\sum_{m=0}^{\infty}(R_{21}R_{23})^m f(s-s_m);\quad s_m=a(k_0-k_3)+h[(2m+1)k-k_3] \quad (2)$$

It is to be noted here that k for a viscoelastic plate is a complex wavenumber.

If we consider a plate immersed in water then in the above analysis, the two half spaces are identical and the equations (1) and (2) reduce to

$$u^r=R_{12}f(s-2k_0a)+T_{12}R_{21}T_{21}\sum_{m=1}^{\infty}R_{21}^{2(m-1)}f(s-s_m);\quad s_m=2k_0a+m2kh$$

$$u^t=T_{12}T_{21}\sum_{m=0}^{\infty}R_{21}^{2m}f(s-s_m);\quad s_m=h[(2m+1)k-k_0]$$

Let us define the Fourier Transforms as

$$F^*(\omega)=\frac{1}{\sqrt{2\pi}}\int_{-\infty}^{\infty}f(t)e^{-i\omega t}dt$$

$$F_0^*(\omega)=\frac{1}{\sqrt{2\pi}}\int_{-\infty}^{\infty}f_0(t)e^{-i\omega t}dt$$

from these we get

$$F_0^*(\omega)=e^{i2k_0a}F^*(\omega)$$

If the incident field is $u^{inc}=f_0(\omega t-k_0x)$, the reflected field is given by $u^r=Rf_0(\omega t-k_0x-2k_0a)$ where $R=(\rho_0c_0-\rho c)/(\rho_0c_0+\rho c)$. Let the reflected signal as sensed by the transducer be $f(t)$, then $f(t)=f_0(\omega t-2k_0a)$. It can be readily shown that at $x=0$, the total reflected field is given by

$$u^r(0,t)=\frac{1}{\sqrt{2\pi}}\int_{-\infty}^{\infty}F_0^*(\omega)d\omega e^{i\omega t}\left[R_{12}e^{-i2k_0a}+\sum_{m=1}^{\infty}\beta_m e^{-i\{2k_0a+2mkh\}}\right]$$

where $\beta_m=T_{12}R_{21}T_{21}R_{21}^{2(m-1)}$

Let $u^r(0,t)=g(t)$ and $G^*(\omega)$ be the Fourier transform of $g(t)$, then

$$\sum_{m=1}^{\infty}\beta_m e^{-i2mkh}=\left[\frac{G^*}{F^*}e^{2ik_0a}-R_{12}\right] \tag{3}$$

Since $1+z+z^2+z^3+\text{----}=1/(1-z)$ for $|z|<1$

Equation (3) can be written in the form

$$R_{21}^2e^{-i2kh}=\frac{\beta}{1+\beta},\ \text{where}\ \beta=\frac{R_{12}R_{21}}{T_{12}T_{21}}\left[\frac{G^*}{F^*}-1\right] \tag{4}$$

By measuring F^* (FFT of the front surface reflection and G^* (FFT of the total signal with all reflections) the complex valued $k(\omega)=k_1+ik_2$ can be obtained from eq.(4).

Similarly, from the transmitted field it can be shown that

$$\frac{e^{-ih(k-k_0)}}{1-R_{12}^2e^{-i2kh}}=\frac{G^*(\omega)}{T_{12}T_{21}F^*(\omega)} \tag{5}$$

Here r^* is the FFT of the signal at the receiver when there is no sample and G^* is the FFT of the total signal after the sample has been introduced in the path.

The preceeding analysis is useful even when the sample is thin and the pulses in the received signal are indistinguishable from each other. However, if the pulses can be seperated out then any two pulses can be used to obtain

$$\frac{G^*}{F^*}-1=T_{12}T_{21}\,e^{-i2kh} \tag{6}$$

where F^* is the FFT of the first pulse and G^* is the FFT of two pulses. Substituting $k=k_1+ik_2$ into eq.(6), where $k_1=2\pi f/c$, k_2 is attenuation, c is wavespeed and f is frequency and comparing the real and imaginary terms on the two sides we get $k_1=2\pi f/c=\phi/2h$ or $c=4\pi hf/\phi$ and attenuation $k_2=[\ln M-\ln(T_{12}T_{21})]$ where ϕ is the phase of G^*/F^*-1 and $M=|G^*/F^*-1|$. Detailed derivation of these equations is given in [1].

TECHNIQUE DEVELOPMENT Keeping in view the tremendous speed and reliability which can be achieved by using computers for collection and analysis of data, the equations dev-

eloped above were interpreted in a way most suitable for computer analysis. Several potential sources of errors were studied next. These are:(1) Sampling interval,(2) Frequency resolution,(3) Transducer response and (4) Adequacy of pulse seperation. The first factor is the digitizing interval for the signal. FFT of a 10 MHz signal at 10ns(100 MHz), 20ns(50 MHz) and 40 ns(25 MHz) sampling intervals was studied. It was observed that at 10 or 20 ns the frequency content of the signal is essentially the same. However, at 40 ns sampling interval the signal loses some of its high frequency content. The second factor considered was the resolution of the signal in the frequency domain. A sampling frequency of 50 MHz or higher is being used and a resolution of 0.1 MHz or less on the frequency domain is considered adequate. The third factor considered was the useful range of the transducer frequency response. The FFT of the first pulse is shown in Fig. 2b. It was found that satisfactory measurements can be obtained over a frequency range given by 25% of the peak amplitude. Fourthly, with reference to Fig.2a, another source of error is that the operator has to decide where the first pulse ends and the second one starts. Hence as described in the theoretical analysis section, methods have been developed where the full signal is analysed as given in eqs.(4) and (5). For further details see [1]. The work presented here is for specimens where the two pulses can be seperated.

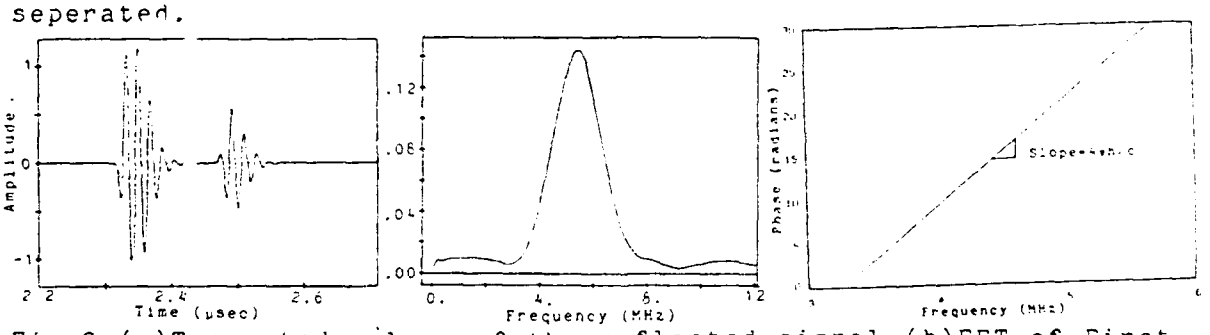

Fig.2 (a)Two gated pulses of the reflected signal (b)FFT of First pulse (c) Phase vs frequency for aluminum specimen.

EXPERIMENTAL PROCEDURE The block diagram of the experimental setup is as shown in fig. 3a. The specimens were fabricated using Magnamite AS4/3502 graphite prepreg tape made by Hercules Inc. All specimens were of 11"x1"x variable thickness. The specimens were loaded on Instron Model 1125. The tests were conducted at a crosshead speed of 0.05 in/min. Edge replication was done with the specimens under a nominal load to open up the transverse cracks.

In order to insure that each transducer was interrogating the same area, a square window was attached to the circular transducer as shown in fig.3b. These windows were made of room-temperature-curing silicone-rubber mixed with PMMA particles. To ensure that the tests were not affected by the temperature variations, the bath temperature was controlled to ±0.5°C. To eliminate the water absorption by microcracks, the edges of the cracked specimens were coated by strippable lacquer (Sherwin Williams). To avoid the spatial irregularities of the composite (ie matrix

or fiber rich regions, thickness variations, surface marks etc), to effect the measurements, tabs were provided on the specimen to replace it in the water bath to within ±0.001 in., after each mechanical loading.

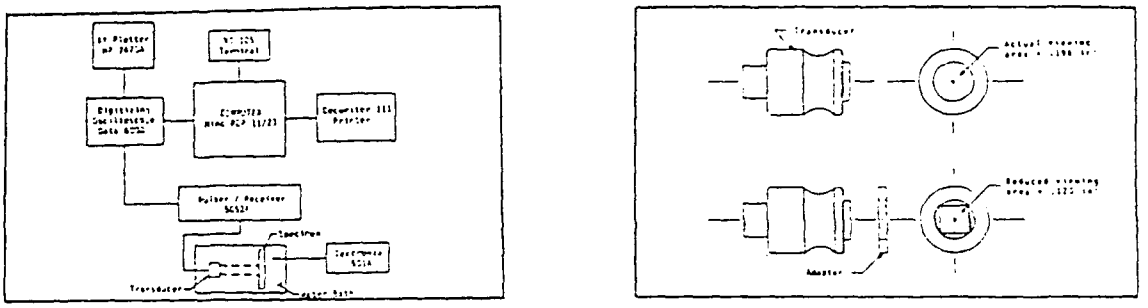

Fig.3(a) Block diagram of the experimental setup.
(b) Window attachment on the transducer.

RESULTS The technique developed here was first applied to an aluminium sample. Fig.2a shows the first and second gated pulse for the aluminium sample and the phase vs frequency plot is shown in fig. 2c. The phase as calculated by the computer is modulo 2Π. It is converted to a continuous phase by adding 2Π after each cycle completion. Slope of the phase vs frequency plot gives the group velocity. It was found that for the samples tested, the group velocity was very close to the phase velocity as the phase vs freq. plot was essentially a straight line. The wavespeed calculated from this plot was precise to ±0.02% when the specimen was not moved. If the specimen was removed between tests and replaced the precision is reduced to ±0.1%. The same tests were repeated with heavily damaged composite specimen and the precision of the tests was found to be ±0.2%.

The errors in the measurement of attenuation were larger. It was found that the attenuation could be measurement with a precision of ±1.0%. All the results are presented with attenuation in the non-dimensional form ie $k_2\lambda$. Fig.4 shows the edge replications of the damage states and the corresponding attenuation vs frequency curves. At lower frequencies the attenuation is more sensitive to the damage than at higher frequencies. It is observed that the attenuation gives a very good measure of the extent of microdamage in the off-axis plies.

Fig.5 shows the variation of the attenuation as the crack length increases. Here, the crack length is the measure of the number of cracks and is the total length of the cracks in the field of measurement.

When there are less cracks in the specimen then there is some amount of scatter in the attenuation measured, but as the total crack length increases the measurement becomes steady. For details of these results see [2].

CONCLUSIONS A new technique for the measurement of wave speed and attenuation of ultrasonic waves has been developed. To the best of our knowledge this is the first technique that gives satisfactory results even for very thin specimen.

The technique has been applied to fiber-reinforced composite material specimens. It was found that whereas the wave speed (or stiffness) is rather insensitive to transverse cracking, the through-the-thickness attenuation is a sensitive measure of the damage state and hence is a potential damage metric.

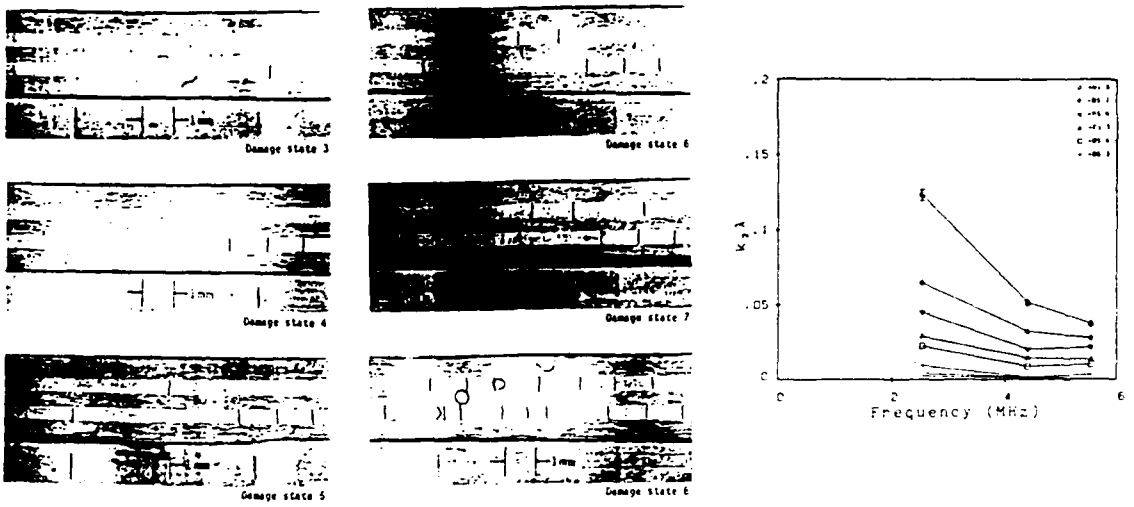

Fig.4 Edge replications of damage state and attenuation vs frequency plot.

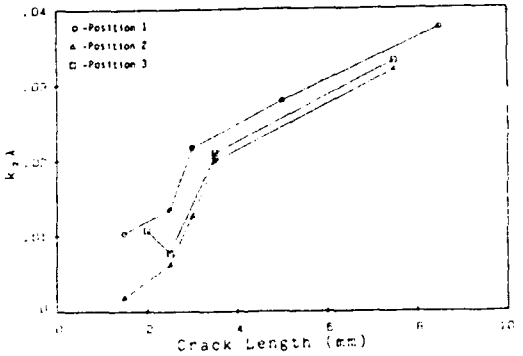

Fig.5 Attenuation vs crack length for a graphite/epoxy specimen.

REFERENCES 1. Kinra V.K.,"Ultrasonic Nondestructive Evaluation of damage in Continuous Fiber Composites".Annual Technical Report. Project AFOSR-84-0066,Apr 85.
2. Eden J.G.,"The application of Ultrasonics to assess damage in composite Materials". M.S. Thesis. Dec 85. Texas A&M University.

ACKNOWLEDGEMENTS This research is supported by the Air Force Office of Scientific Research Contract No. F49620-83-C-0067.

"Composites'86: Recent Advances in Japan and the United States"
Kawata, S. Umekawa & A. Kobayashi, Ed., Proc. Japan-U.S. CCM-III, Tokyo, 1986.

Ultrasonic Nondestructive Testing of Composite Materials

Vinay Dayal and V. K. Kinra

Graduate Student and Associate Prof., Respectively, Aerospace Engg. Dept., Texas A&M University, College Station, TX 77840, U.S.A.

ABSTRACT

Wavespeed and attenuation, the ultrasonic parameters are affected by the internal structure or damage of the material. Accurately measured ultrasonic parameters, in a composite coupon are thus an indicator of the extent of the cumulative damage in the coupon. A through-transmission water-immersion technique has been developed for the measurement of the ultrasonic parameters. The method utilizes the Fast Fourier Transforms to convert the time domain signal to the Frequency domain signal. Computers are used for the acquisition and analysis of data, for accuracy and speed. This technique can be used to measure the ultrasonic parameters of coupons of any thickness and material. The technique presented here has been used to measure damage in specimen made of Magnamite AS4/3502 Graphite/Epoxy. It has been observed that attenuation increase due to microcracks is a reliable measure of the damage in the composites. To the best of our knowledge, this is the first technique which can be used to interrogate specimens of any thickness.

INTRODUCTION

Fiber-Reinforced-Composites have been in use as structural members for a considerable amount of time and various methods are available for their testing. A detailed review of the methods and techniques available may be found in (1).

The complex damage state developed due to the loading (mechanical or thermal) of composite materials, changes the stiffness and the damping characteristics of the material. When an ultrasonic wave is passed through the composite, the wavespeed and attenuation measurements give the stiffness and damping of the material. Changes in wavespeed and attenuation are thus a measure of the damage in the composites. It is our endeavour to develop techniques to measure these ultrasonic parameters accurately, repeatably and quickly. We have used computers for the collection and analysis of data, with least human

intervention, so that the techniques can be automated.

The toneburst method has been the most basic method of the wavespeed measurement. Since broad bursts of the signal(about 5 cycles) are used in this method, it cannot be used when the reflections from the front and back surfaces of the specimen interfere. A computerized pulse technique was presented in (2) for the measurement of wavespeed and attenuation. This method also depends on the seperation of pulses and though thinner specimens could be tested, since a single pulse is being used, the technique failed when the pulses started interfering.

We present here a technique which can be applied to specimen of any thickness. A pitch-catch signal pulse of a 1 MHz transducer is shown in Fig 1a. When a 10 ply composite specimen is introduced in the path, the total signal received is shown in Fig 1b. The technique presented here is capable of calculating wavespeed and attenuation from the signals of Fig 1.

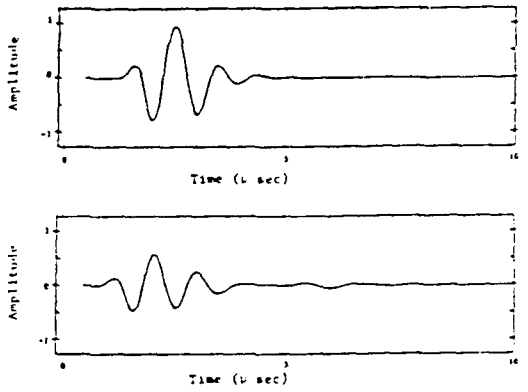

Fig. 1a. Pitch-Catch signal of a 1 MHz transducer, b. Signal when a 10 ply composite specimen introduced in the path.

The development of the technique and some results from its application to fiber reinforced composite Graphite/Epoxy AS4/3502 laminates with stacking sequences $[0,90_4]_s$ are presented.

THEORETICAL ANALYSIS

Consider a plate of a linear viscoelastic material sandwiched between two half-spaces of perfectly elastic materials. Consider also, a finite duration pulse,ray 1,incident at the viscoelastic plate as shown in Fig 2.

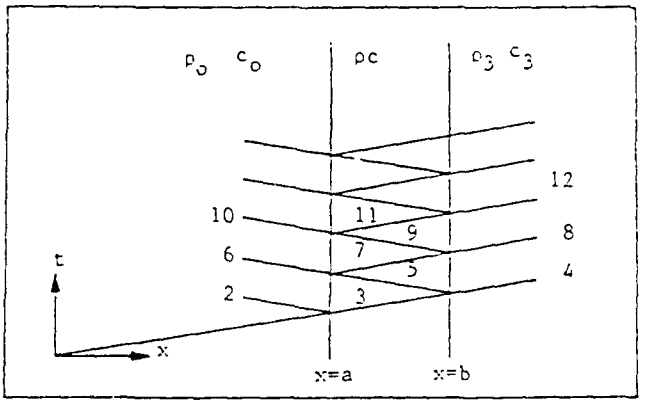

Fig.2 A series of Pulses reflected and transmitted by a plate.

Due to the mismatch in the acoustic impedence of the three materials, there will be an infinite series of reflected and transmitted pulses. These pulses contain information about the acoustic properties of the viscoelastic material.

Let the displacement field along the incident ray 1 be given by $u^{inc}=f(\omega t-k_0 x)$, where $f(s)\equiv 0$ for $s<0$ and ω and k_0 are circular frequency and wavenumber of the first half space. The total reflected field is the sum of the following rays, with $h=b-a$ and $s=\omega t+k_0 x$.

$u^2=R_{12}f(s-s_2)$; $\quad s_2=2k_0a$

$u^6=T_{12}R_{23}T_{21}f(s-s_6)$; $\quad s_6=2k_0a+2kh$

$u^{10}=T_{12}R_{23}R_{21}T_{21}f(s-s_{10})$; $\quad s_{10}=2k_0a+4kh$

where T_{ij}=Transmission coefficient from medium i to j

R_{ij}=Reflection coefficient from interface of media i&j with wave incident in medium i

The sum of these rays is

$$u^r=R_{12}f(s-2k_0a)+T_{12}R_{23}T_{21}\sum_{m=0}^{\infty}(R_{12}R_{23})^{m-1}f(s-s_m);\ s_m=2k_0a+m2kh \quad (1)$$

Similarly, the sum of the transmitted field can be written as

$$u^t=T_{12}R_{23}\sum_{m=0}^{\infty}(R_{12}R_{23})^m f(s-s_m);\ s_m=a(k_0-k_1)+h[(2m+1)k-k_1] \quad (2)$$

It is to be noted here that k for a viscoelastic plate is a complex wavenumber.

If we consider a plate immersed in water then in the above analysis, the two half spaces are identical and the equations (1) and (2) reduce to

$$u^r=R_{12}f(s-2k_0a)+T_{12}R_{21}T_{21}\sum_{m=1}^{\infty}R_{21}^{2(m-1)}f(s-s_m);\ s_m=2k_0a+m2ka$$

$$u^t=T_{12}T_{21}\sum_{m=0}^{\infty}R_{21}^{2m}f(s-s_m);\ s_m=h[(2m+1)k-k_0]$$

Let us define the Fourier Transforms as

$$F^*(\omega)=\frac{1}{\sqrt{2\pi}}\int_{-\infty}^{\infty}f(t)e^{-i\omega t}dt$$

$$F^*(\omega)=\frac{1}{\sqrt{2\pi}}\int_{-\infty}^{\infty}f_0^*(t)e^{-i\omega t}dt$$

from these we get

$$F_0^*(\omega)=e^{i2k_0a}F^*(\omega)$$

If the incident field is $u^{inc}=f_0(\omega t-k_0x)$, the reflected field is given by $u^r=Rf_0(\omega t-k_0x-2k_0a)$ where $R=(\rho_0c_0-\rho c)/(\rho_0c_0+\rho c)$. Let the reflected signal as sensed by the transducer be f(t), then $f(t)=f_0(\omega t-2k_0a)$. It can be readily shown that at x=0, the total reflected field is given by

$$u^r(0,t)=\frac{1}{\sqrt{2\pi}}\int_{-\infty}^{\infty}F_0^*(\omega)d\omega e^{i\omega t}\left[R_{12}e^{-i2k_0a}+\sum_{m=1}^{\infty}\beta_m e^{-i\{2k_0a+2mkh\}}\right]$$

where $\beta_m=T_{12}R_{21}T_{21}R_{21}^{2(m-1)}$

Let $u^r(0,t)=g(t)$ and $G^*(\omega)$ be the Fourier transform of g(t), then

$$\sum_{m=1}^{\infty}\beta_m e^{-i2mkh}=\left[\frac{G^*}{F^*}e^{2ik_0a}-R_{12}\right] \qquad (3)$$

Since $1+z+z^2+z^3+\cdots=1/(1-z)$ for $|z|<1$
Equation (3) can be written in the form

$$R_{21}^2 e^{-i2kh}=-\frac{\beta}{1+\beta}, \text{ where } \beta=\frac{R_{12}R_{21}}{T_{12}T_{21}}\left[\frac{G}{F^*}-1\right] \qquad (4)$$

By measuring F^* (FFT of the front surface reflection and G^* (FFT of the total signal with all reflections) the complex valued $k(\omega)=k_1+ik_2$ can be obtained from eq.(4).

Similarly, from the transmitted field it can be shown that

$$\frac{e^{-ih(k-k_0)}}{1-R_{12}^2e^{-i2kh}}=\frac{G^*(\omega)}{T_{12}T_{21}F^*(\omega)} \qquad (5)$$

Here F^* is the FFT of the signal at the receiver when there is no sample and G^* is the FFT of the total signal after the sample has been introduced in the path. Detailed derivation of these equations is given in (3).

Equation (5) can now be written in the following form

$$Z^2+ZY-c_0=0. \qquad (6)$$

where $Z=e^{-ihk}$
$k=k_1+ik_2$
$k_1=\omega/c$
k_2=coefficient of attenuation

$Y=(T_{12}T_{21}/R_{21})(F^*/G^*)Z_0$

$Z_0=e^{-ihk_0}$
k_0=wavenumber in the elastic mediums.
$c_0=1./R_{21}$

In (6) both Z and Y are complex.

In the water immersion case which is the one we are going to use for the tests, Z_0 can be easily calculated if the wavespeed in water is accurately known. The transmission and reflection coefficients can be calculated if the densities of the two mediums and longitudinal wavespeeds in them are known. But the wavespeed in the plate is the unknown which we want to measure. Hence to overcome this dilemma, an iteration procedure was followed where an approximate wavespeed is provided as an input to estimate the various reflection and transmission coefficients. The quadratic equation (6) is then solved to give two roots of Z. The correct root is chosen based on the fact that as the frequency increases as the phase of Z decreases. The wavespeed is calculated from the phase of Z. This wavespeed is then used to re-estimate the reflection and transmission coefficients. This iterative procedure converges rapidly to the correct wavespeed. It was estimated that even with an initial descrepancy of ±30% in wavespeed, the solution converged in fewer than 5 iterations.

EXPERIMENTAL PROCEDURE

The block diagram of the experimental setup is as shown in Fig 3.

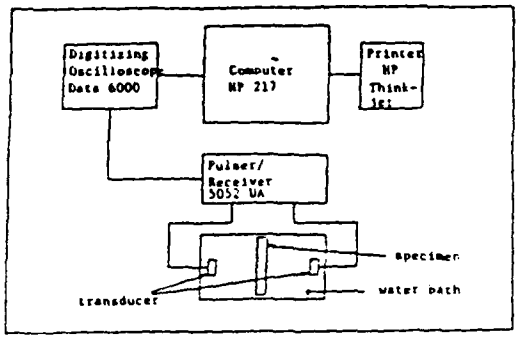

Fig.3 Block diagram of the experimental setup.

The analog signal is collected by the Pulser-Receiver (Panametrics 5052 UA) and is fed into the Digital Oscilloscope (Data 6000). The signal is digitized in the oscilloscope. The signal processing unit of this oscilloscope then performs Fast Fourier Transform on the signal. The useful portion of the transformed signal is then acquired by the computer for the calculation of the wavespeed and the attenuation. In these steps several potential sources of errors can affect the results. These are: (1) Sampling interval, (2) Frequency Resolution and (3) Transducer Response. The first factor is the digitizing interval of the acquired signal. FFT of a 1 MHz signal at 10,20,40,100 nS sampling intervals was studied. It was observed that at 10,20 or 40 nS sampling interval the frequency content of the signal is essentially the same. However, at 100 nS sampling interval, the signal loses some of its high frequency contents. The useful digitizing intervals depend on the frequency of the transducer being used. For example for 10 MHz frequency, at 40 nS interval some of the high frequency contents are lost. The second factor considered was the resolution of the signal in the frequency domain. A sampling interval of 40 nS or less with a frequency resolution of 0.05 MHz or less is considered adequate. This factor is also transducer frequency related. The third factor considered was the useful range of the transducer frequency response. It was found that satisfactory measurements can be obtained over a frequency range given by 25% of the peak response amplitude. For further details see (4).

The specimens were fabricated using Magnamite AS4/3502 graphite prepreg tape made by Hercules Inc. All specimen were of 11"x1"x .05" size. The specimens were loaded on Instron Model 1125. The tests were conducted at a crosshead speed of 0.05 in/min. The transverse cracks were opened by a nominal load on the specimen and edge replications were taken to keep a record of the cracks. To eliminate the water absorption by the microcracks while testing by ultrasounds, the edges of the cracked specimens were coated by Strippable Lacquer (Sharvin Williams).

RESULTS

First of all, the accuracy of the measurement technique reported here was estimated. The technique was applied to a heavily damaged composite specimen. This was done to account for

measurements under the worst conditions of damage. It was estimated that the precision of the measurement was ±0.3% for wavespeed and ±1.5% for attenuation. It is to be noted here that the accuracy of the measurement will depend on the accuracy of the predetermined input parameters viz. the densities of the water and specimen and the wavespeed of ultrasound in water.

The results presented here are for Gr/Epoxy $[0/90_4]_s$ specimens tested by a broad band 5 MHz transducer. In the results presented, attenuation k_2 has been non-dimensionalized to $k_2\lambda$. Line sketches of the edge replications, where the measurements were made, are shown in fig 4. The variation of attenuation, as the applied load is increased, is shown in Fig 5. Numbers on the curves denote the location number on the specimen. The specimen were surveyed along the length for each load step to identify any preferred localization of defects. It was observed that for the layup tested, the damage was evenly distributed. As is evident from the edge replications, very few cracks are developed for stresses upto 35 ksi, and hence the increase in attenuation is also low. When the stresses were increased further, multiple cracks developed and this resulted in a large increase in the attenuation values.

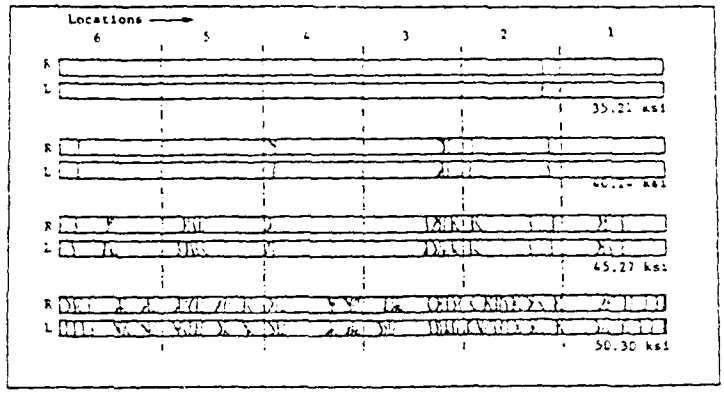

Fig 4. Line sketch of the edge replications of a $[0/90_4]_s$ Gr/Epoxy Specimen. L&R denote left & right sides of the specimen

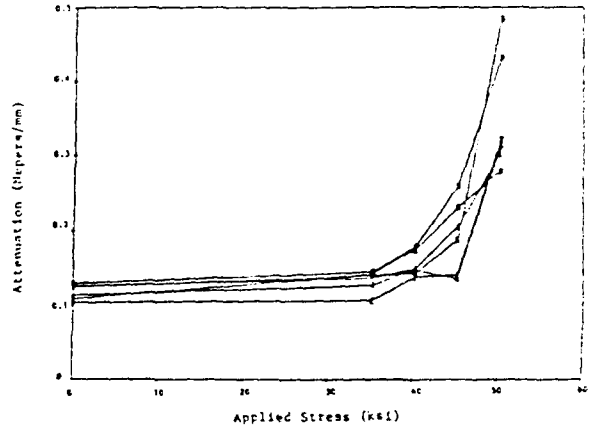

Fig 5. Variation of Attenuation as a function of Applied Stress at 6 different locations of the specimen.

It can be seen from the edge replications that the damage is evenly distributed along the specimen and no preffered sites of damage were observed. The specimen failed near the grips.

As expected, for the tests conducted, no significant variation in wavespeed was observed. The reason is that in this configuration of the testing, the wavefront is perpendicular to the plane of the crack, or the wave propagation direction is in the plane of the crack. Hence, the cracks do not change the wavespeed appreciably.

CONCLUSIONS

A new technique for the measurement of wave speed and attenuation of ultrasonic waves has been developed. This technique is fully computerized and does not need any human interference except the placing and removing the specimen from the ultrasonic path. To the best of our knowledge this is the first technique that gives satisfactory results for specimen of any thickness.

The technique has been applied to fiber-reinforced composite material specimens. It was found that whereas the wave speed (or stiffness) is rather insensitive to transverse cracking, the through-the-thickness attenuation is a sensitive measure of the damage state and hence is a potential damage metric.

ACKNOWLEDGEMENTS

This research is supported by the Air Force Office of Scientific Research Contract No. F49620-83-C-0067.

REFERENCES

1. Bar-Cohen, Y.,"NDE of Fiber-Reinforced Composite Materials - A Review",Materials Evaluation, Vol.44, No.4, Mar. 1986, pp446-454.
2. Dayal, V., Kinra, V.K., Eden, J.G.,"Ultrasonic NDT of Fiber Reinforced Materials", Proc. of the International Symposium on Composite Materials '86, Beijing, China.
3. Kinra V.K.,"Ultrasonic Nondestructive Evaluation of damage in Continuous Fiber Composites".Annual Technical Report. Project AFOSR-84-0066,Apr 85.

ULTRASONIC NDE OF COMPOSITES FOR TRANSVERSE CRACKING

Dayal,V. and Kinra,V.K.
Graduate Student and Assoc. Prof.,respectively,
Dept. Of Aerospace Engg.
Texas A&M University.
College Station, TX 77840.

INTRODUCTION

When fiber-reinforced composites are loaded either mechanically or thermally, a very complex damage state is developed. The damage consists of matrix cracking, longitudinal cracking, delamination, debonding, fiber pullout, fiber breaking and void formation etc. As the damage progresses, the mechanical behavior of the composite changes. This change manifests itself in the form of reduction in the overall stiffness and an increase in the damping characteristics of the composites. The wavespeed and attenuation of a mechanical wave launched in the specimen depend on the stiffness and the damping properties of the material, respectively. Thus, the acoustic properties (wavespeed and attenuation) of the waves passed through the composites are affected by the damage.

The total damage picture in composites is very complex. One or more of the damage mechanisms mentioned above may be present at the same location in the composites. Though it would be an ideal goal to develop a method which can give the total damage picture, the NDE community has been unable to do so until now. Before trying to achieve this goal we have to study and understand each damage mode individually. Keeping this in view, in this work we have attempted to study the transverse cracking phenomenon. The reasons behind this choice are: it is the most common damage mode; it is generally the first step in development of other damage modes; and it is easy to generate without the interference of other damage modes. Though each type of damage mode will affect the overall stiffness of the composites, in this study we have used the layups which promote the transverse cracking as the dominant damage mode.

The conventional method of measuring the acoustic parameters is the toneburst method [1]. If the specimens are thin, the reflection from the faces of the specimen interfere. This renders the toneburst technique useless, as one cannot identify individual maximums in the signal. Since the most commonly used laminates in the aerospace structures are expected to be rather thin (~2 mm) we undertook the task of developing a new technique especially suited for thin laminates. The use of computers for data collection and analysis make the technique very attractive for automation, with high degree of accuracy and repeatability.

A computerized pulse technique was presented in [2] for the measurement of the acoustic parameters. The digitized signal in time domain is transformed to frequency domain by the use of Fast Fourier Transforms (FFT). The acoustic parameters are then computed from the phase shift and loss of amplitude between two pulses in the reflected signal . This method could be used for specimen where the pulses could be separated. The toneburst method requires about 10 cycles of signal, whereas the technique developed by us required only one cycle, hence, though separation of signals was required in both the methods, thinner samples can be interrogated with the new technique.

An extension of this technique was presented in [3] where the separation of pulses is not required. Hence this technique could be applied to specimen of any thickness. This technique could be applied to both reflection or through-transmission methods. In the reflection method precise replacement of the specimen is very critical for the correct measurement. The through-transmission method does not suffer from this restriction and hence was used by us. A pitch-catch signal from a 1 MHz transducer is shown in Fig.1a. When a 10 ply composite specimen is introduced in the

path, the total signal received is shown in Fig.1b. This technique is capable of calculating the acoustic parameters from these signals.

The above mentioned two techniques have been applied to the analysis of transverse cracking. We present here the salient features of the two techniques for completeness. Some results are then presented from the application of the techniques to Graphite/Epoxy AS4/3502 laminates. Interested reader is referred to [4] for further details. The results show that although the through-the-thickness measurement of attenuation is very sensitive to transverse cracks, wavespeed is not. A plausible explanation is that in this configuration of tests, the waves are moving parallel to the plane of the cracks. When the waves move normal to the cracks we should expect a larger reduction in the wavespeed.

In the Lamb wave mode of wave motion in a plate, the waves move in the plane of the plate, and hence are normal to the transverse cracks. We have tested the specimens with transverse cracks using Lamb waves. Results show that the changes in wavespeed and hence the changes in longitudinal stiffness of the specimen can best be detected by the use of Lamb waves.

THEORETICAL ANALYSIS

Consider an ultrasonic pulse in water, incident upon a composite plate. This pulse will suffer successive reflections at the two interfaces, these reflections are shown in Fig.2. It has been shown in [2] that

$$G^*/F^* - 1 = T_{12}T_{21}\,Exp(-2ikh) \qquad (1)$$

where G^* is the Fourier Transform of the pulse 6.
F^* if the Fourier Transform of the pulse 2.
T_{12} is the Transmission Coeff. from water into specimen.
T_{21} is the Transmission Coeff. from specimen into water.
$k = k_1 + ik_2$ is the Complex Wavenumber in the specimen.
$k_1 = \omega/c$
k_2 is the attenuation coefficient.
ω is the circular frequency of the input signal.
c is the wavespeed in the specimen.
h is the specimen thickness.

This equation has been used to develop the technique where signal pulses 2 and 6 can be separated. The phase of $G^*/F^* - 1$ gives the wavespeed and $\log|(G^*/F^* - 1)/T_{12}T_{21}|$ gives the attenuation for the ultrasonic waves in the specimens.

In the second technique pulses 4,8,12 of Fig.2, cannot be separated. It has been shown in [3] that

$$Z^2 + ZY - C_0 = 0 \qquad (2)$$

where $Z = Exp(-ihk)$
$Y = (T_{12}T_{21}/R_{21})(F^*/G^*)Z_0$
$Z_0 = Exp(-ihk_0)$
k_0 = wavenumber in medium 1
$C_0 = 1/R_{12}$
R_{12} = Reflection coefficient in medium 2 from the 2/1 interface.
k, T_{12}, T_{21}, h are same as defined earlier for eqn.(1)

Note that in this equation both Z and Y are complex. This complex quadratic equation is solved at each point of the waveform. The correct root is chosen based on the fact that as the frequency increases, the phase of Z decreases. The wavespeed is calculated from the phase of Z. The reflection and the transmission coefficients are dependent on the wavespeed in the specimen, which is precisely what we want to measure. This dilemma was resolved by an iterative procedure. Wavespeed for the undamaged specimen is used to estimate the reflection and transmission coefficients and a value of wavespeed is calculated from eqn. (2). This wavespeed is used as the next guess in the estimate of the coefficients. It was found that even with an initial error of 30 % in wavespeed, the solution converged in less than 5 iterations.

For the Lamb wave tests we have used only very low frequencies i.e. long wavelengths. The reason is that when the wavelength is large compared to the thickness of the specimens, a few Lamb modes are generated and so are easy to identify. At the low frequencies used, only the fundamental symmetric and anti-

symmetric modes are excited. We have used the symmetric mode of Lamb waves where the particle displacement is uniform across the plate.

EXPERIMENTAL PROCEDURE

The block diagram of the experimental setup is shown in Fig.3. The pulse generator triggers the signal generator which produces a single cycle of sinusoical signal. This pulse is amplified by the power amplifier and the signal is fed into the ultrasonic transducer. The transmitter launches a mechanical wave in water. This wave travels through the specimen and is received by the receiving transducer. The signal from the receiver is amplified by the signal amplifier and fed into the Digitizing Oscilloscope. The analog signal is digitized and stored in the oscilloscope. The built-in signal processor of the oscilloscope provides the computer with the FFT of the signal. The ultrasonic parameters are then calculated by the computer.

For the Lamb wave application, a trigger pulse is fed into the signal generator which, in the gated mode, produces a toneburst of signal of about 10 cycles. Rest of the circuit description remains same as before. As shown in the block diagram, the transducers are mounted on precisely controlled travelling mechanisms. The specimen is mounted on a turntable. The vernier of the turntable is graduated to 0.1° rotation. This type of arrangement is required so that when the specimen is rotated, the transducers are suitably moved to ensure that the same area of the specimen is interrogated throughout the test. The procedure followed for these tests is as follows. Lamb Waves are generated in the specimen by launching a toneburst of longitudinal waves through the water. The specimen is rotated and the signal received by the receiving transducer is recorded. Critical Lamb angles are identified by the sharp peaks in the received signal. The Lamb angles are confirmed by a very simple test. An elementary calculation which, for brevity, is omitted here, shows that if the receiving transducer is moved in a straight line parallel to the zero degree orientation of the specimen, there should be no change in the arrival time of the signal. Since the wave travels a longer distance in the specimen the attenuation can be measured. From the angle of the specimen the wavespeed is calculated by the Snell's law;

$$\mathrm{Sin}(\theta_i)/V_w = \mathrm{Sin}(\pi/2)/C \qquad (3)$$

where θ_i is the angle of incidence.
V_w is the wavespeed in water.
C is the wavespeed in the specimen.

The longitudinal stiffness is calculated from the relation $E=\rho C^2$ where ρ is the density of the specimen, E is the longitudinal stiffness and C the Lamb wavespeed. As the damage is induced in the specimen, decrease in the stiffness of the specimen results in an increase in the Lamb angle.

RESULTS AND DISCUSSION

First we present some results from the application of the technique where separation of pulses was possible. In all the results presented here we have used the non-dimensional form of attenuation($k_2\lambda$) where λ is the wavelength of the signal. The variation of attenuation as the load is increased to induce the transverse cracks is shown in Fig.4 for the specimen of $[0_4,90_4,0_4]_s$ layup. It is observed that for all damage states the attenuation decreases with an increase in the frequency. The maximum variation in attenuation is observed at a frequency of 2.25 MHz. This figure also shows a very dramatic increase in the attenuation as the damage is induced in the specimen. The variation of attenuation, at three locations on the specimen, as the total crack length in the field of observation increases, is shown in Fig.5. In the early stages of damage when there are a few cracks, some scatter in the attenuation is observed. As more cracks are generated, the attenuation variation becomes steady. The reason is that when there are a few cracks then their location, in the field of the transducer, is critical. A crack in the center of the transducer field will scatter the waves much more than the crack at the edge of the field. But when there are a number of cracks then their effect is averaged out and a fairly uniform response is obtained.

Further tests were performed on a $[0/90_4]_s$ specimen at 5 MHz. The purpose of these tests was twofold. First, these being thin specimen, were tested to check the second technique developed by us, where the various reflections need not be separated. Secondly, we were interested in studying that as the transverse cracks are

developed, is there any preferred site of damage accumulation and if so, could it be detected ultrasonically. These tests were performed on several specimens. Results from one specimen are presented in Fig.6. The variation of attenuation with the applied loads is shown at six different location on the specimen. Initially there are some preferred sites of damage, but as the damage increases it is evenly distributed all over the specimen. In the specimens tested the failure always took place at the grips and hence no precursor of final failure could be detected.

Now, when a damaged specimen is unloaded some of the transverse cracks may be partially closed. Such closure would tend to decrease the attenuation. Our objective in the next set of tests was to experimentally determine whether or not the cracks are partially closed. The through-the-thickness attenuation was monitored as the load on the specimen was increased. The maximum applied stress was about 15% of the ultimate strength and was sufficiently low so as not to cause any additional cracking. The main problem in these tests was to prevent water from entering the open cracks. A thin coating of a rubbery adhesive was used to seal the edges. Presented in Fig.7 is the variation in the attenuation as two cycles of load are applied to open the cracks and Fig.8 shows the wavespeed variation during the same loading. The attenuation increases as the cracks open and follow essentially the same path over the two cycles of loading and unloading. The scatter bounds of 1.0 % in attenuation and 0.5 % in wavespeed measurement are shown in the figures. This shows that even though the cracks open, as is evident from the increase in attenuation, there is no measurable change in wavespeed.

Now we shift our attention to the testing of the transverse cracks by Lamb waves. All the tests have been conducted on $[0/90_3]_s$ and $[0/90_5]_s$ specimens at a frequency of 0.5 MHz. Decrease in stiffness as the crack length in the interrogation area increases is shown in Fig.9. A steady decrease in the stiffness is observed as the transverse cracks increase. Variation of attenuation as the damage increases is shown in Fig.10. As expected, attenuation increases monotonically with damage. Since attenuation can be measured with an accuracy of ± 10%, the four-fold increase in attenuation observed in these tests is quite appreciable.

CONCLUSIONS

The effect of transverse cracks on the acoustic parameters depends on the direction of the wave propagation relative to the cracks. In the case of through-the-thickness measurements where the wave propagation direction is in the plane of the cracks, the attenuation measurement is sensitive to damage while the wavespeed is not. Conversely, when the waves travel normal to the cracks, as in the case of Lamb waves then, for the configuration tested, both the and the attenuation are sensitive to cracks.

REFERENCES

1.Kinra,V.K. and Anand,A."Wave Propagation in a Random Particulate composite at Long and Short Wavelengths", Intl. J. of Solids and Structures, 18(5), 1982, 1982,pp.367-380.

2.Dayal,V., Kinra,V.K.,Eden,J.C., "Ultrasonic NDT of fiber reinforced composite materials" Proc. of the Intl. Symposium on Composite Materials '86,Beijing, China.

3.Dayal,V., Kinra,V.K., "Ultrasonic NDT of Composite Materials" Pro. of 3rd US Japan Conf. on Comp. Matl. '86,Tokyo.

4.Eden,J.C., "The application of Ultrasonics to assess damage in composite materials.",M.S. Thesis, Texas A&M University.

ACKNOWLEDGEMENTS

This research was supported by the Air Force Office of Scientific Research under Contract # F49620-83-C-0067 to Texas A&M University, College Station, Texas

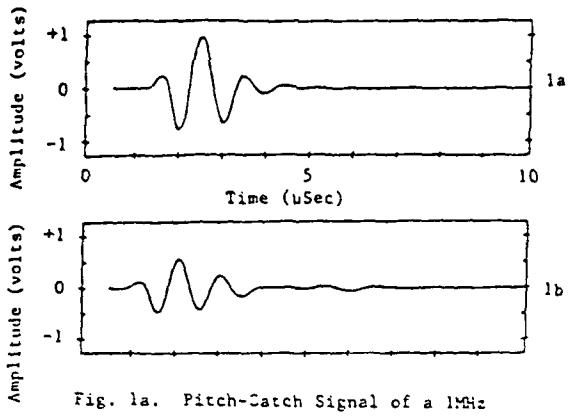

Fig. 1a. Pitch-Catch Signal of a 1MHz transducer b. through a 10 ply specimen

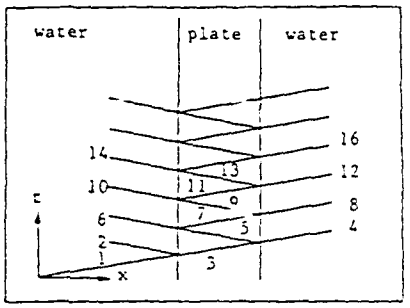

Fig. 2. A series of pulses reflected and transmitted by a plate

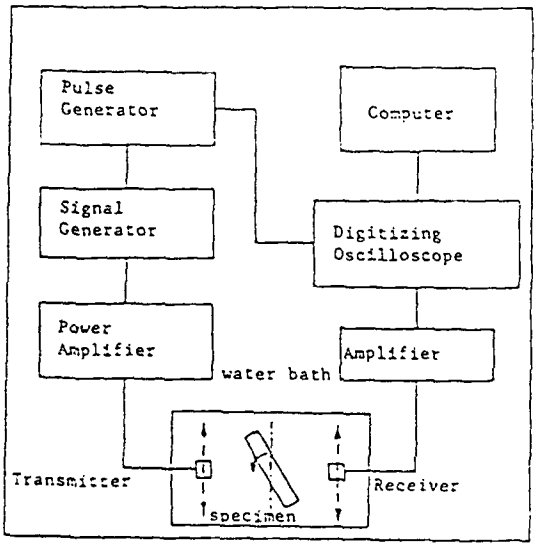

Fig. 3. Block diagram of the Experimental Setup

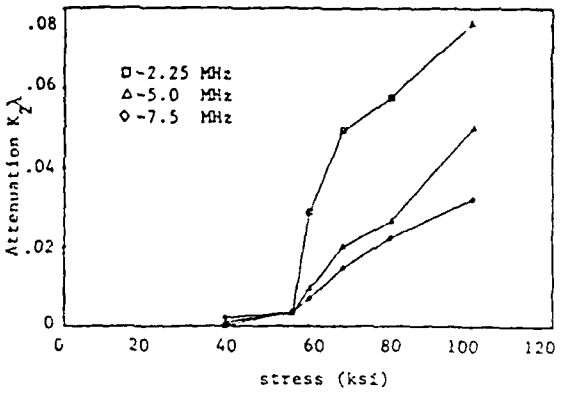

Fig. 4. Increase in attenuation as stress to induce transverse cracking increased.

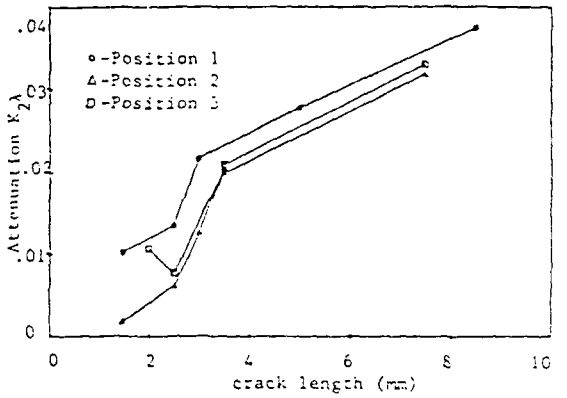

Fig. 5. Increase in attenuation vs. total crack length of transverse cracks.

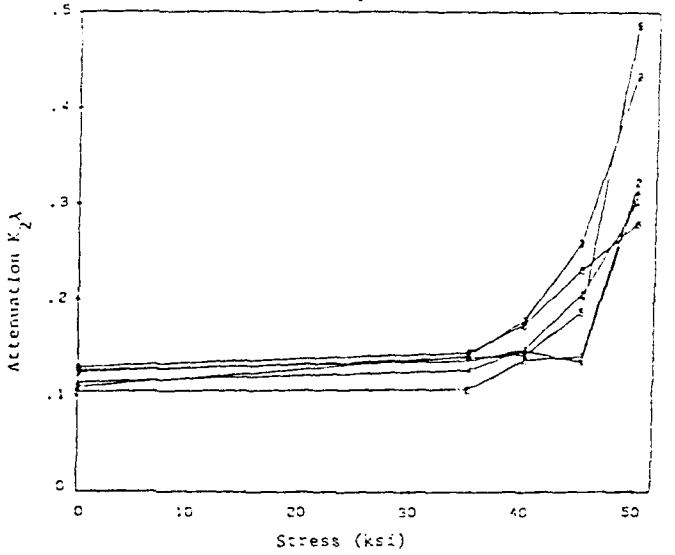

Fig. 6. Variation of attenuation as a function of Applied Stress at 6 different locations of the specimen.

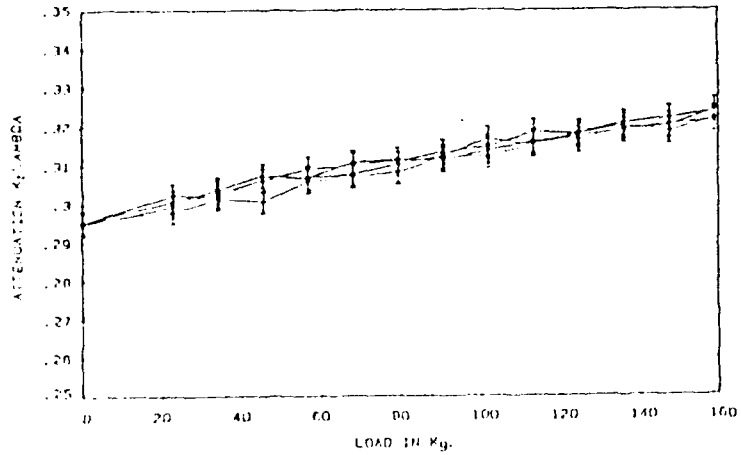

Fig. 7. Attenuation variation as load applied to open cracks.

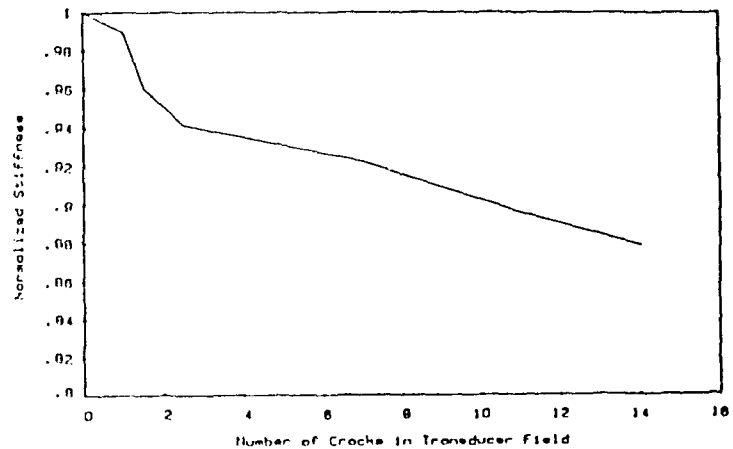

Fig. 9. Decrease in stiffness as damage increases. (Lamb Wave Method)

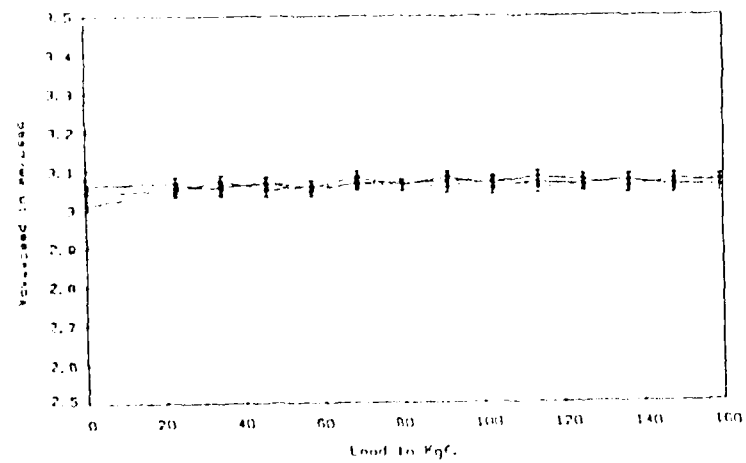

Fig. 8. Wavespeed variation as load applied to open cracks.

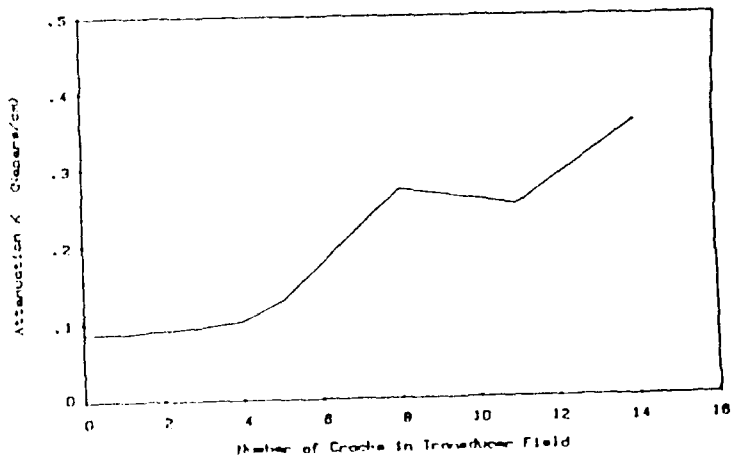

Fig. 10. Attenuation variation as damage increases. (Lamb Wave Method)

NONDESTRUCTIVE EVALUATION OF COMPOSITE MATERIAL USING ULTRASOUND

V. K. Kinra and V. Dayal

Aerospace Engineering Department and
Mechanics and Materials Center Texas A&M University
College Station, TX 77843

ABSTRACT

Fiber-reinforced composites are finding an increasing use in the aerospace industry. Initially the FRP components constituted only the non-critical components of the structure. Now the composites are being used in the primary load bearing members. After undergoing a certain amount of usage, the mechanical, thermal and environmental loading produces a complex damage state which includes transverse cracks, longitudinal splits, delaminations, debonding, etc. Almost all the NDT techniques are geared towards the estimation of the extent of damage to the structure. From these results it is expected that the damage modelers will be able to estimate the residual stiffness and residual strength and life of the structure. We have used ultrasonic waves to study the changes in stiffness of the structure as the damage progresses. This work will help the damage modelers in furthering their analysis.

The ultrasonic waves passing through a composite specimen interact with the various defects, and in turn, these defects affect the basic ultrasonic parameters; wavespeed and attenuation. It is well known that wavespeed is directly related to the stiffness, and attenuation is a measure of the damping characteristics of the material. A very important stiffness component is the in-plane stiffness of the plate. Hence, we propagate the waves in the plane of the plate to measure the in-plane stiffness. The mode of propagation is called the Lamb wave or Plate wave mode. The plate is immersed in a fluid and the Lamb waves leaking into the fluid are called the leaky Lamb waves. These leaky waves have been used to determine the wavespeed and attenuation of the Lamb waves traveling in the plate.

Damage is gradually introduced in the composite plate. In the work presented here, we have limited the mode of damage to transverse cracks only. The changes in the wavespeed and attenuation are measured as a function of damage. We present here some results from the tests of cross-ply and angle-ply graphite/epoxy laminates. The reduction in the in-plane stiffness and an increase in the attenuation is observed as the number of transverse cracks increase.

INTRODUCTION

The growth of damage in composite materials is very different from that in homogeneous materials. In homogeneous materials once the damage is initiated, any further loading tends to increase the existing damage. On the other hand, in composites the damage relieves the stresses in its vicinity such that the next cracking takes place at some other location. It is only when the microcracks become densely populated that they initiate larger damage such as interior delaminations. The study of damage growth in cross-ply laminates due to cyclic loading[1] has shown that first the transverse cracks appear in the 90° -plies. These cracks are restrained in their growth and hence further loading results in the axial split in the 0° -plies due to the Poisson's effect. The intersection of the transverse cracks and the longitudinal splits becomes the nucleation site for the interior delamination between the plies.

When an ultrasonic wave is passed through a damaged composite, the interaction between the wave and the damage can affect the wave in two ways: (1) Damage will, in general, reduce stiffness and since wavespeed is directly proportional to the square-root of stiffness, damage will reduce the wavespeed, and (2) The attenuation will increase because the crack-wave interaction results in an incoherent scattering of the waves. Thus the effect of damage on the overall behavior of the composite can be studied by measuring the acoustic parameters of the ultrasound passed through the specimen.

We have developed two new techniques[2] for the measurement of acoustic parameters in thin laminates which are expected to be used in aerospace structures. With the first of these techniques, one is able to measure the acoustic parameters when the pulses reflected from two surfaces of a plate specimen can be separated in time domain. With the second technique one can make the measurements even when the pulses are inseparable. Here, the signal in time domain is transferred to the frequency domain by the use of fast Fourier transforms (FFT). The data in the frequency domain is used in an

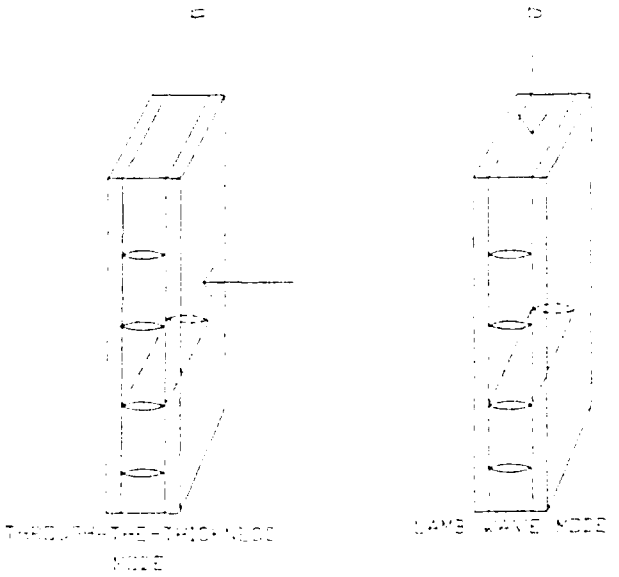

Fig. 1. Wave Propagation Direction Relative to Transverse Crack Plane.

algorithm developed by us to measure the complex-valued wavenumber $k = k_1 + k_2$, where $k_1 = \omega/c$, ω is the circular frequency of the signal used, c is the phase velocity and k_2 is the attenuation coefficient. Figure 1a shows that in this mode of wave motion the wave travels in the plane of the crack and, hence, there is a weak interaction between the waves and the crack. Results show that although the changes in attenuation are substantial, the effect on wavespeed is immeasurably small.

Figure 1b shows the Lamb wave mode where the wave travels normal to the transverse cracks. Here the interaction between the wave and the crack is stronger, and therefore, a larger effect on the acoustic parameters was observed. In this mode of wave motion, the longitudinal stiffness of the plate determines the wavespeed. Hence, the effect of the transverse cracks on the longitudinal in-plane stiffness of the composite laminates could be studied. We present here some results from the testing of the composite laminates with transverse cracks by the Lamb wave technique. The results show that both the wavespeed and the attenuation are significantly affected by the transverse cracks.

THEORY

For the Lamb wave tests we have used the fundamental symmetric mode of wave propagation. The reason behind this choice is that in this mode the wave travels with a plane wavefront. The relation between the material properties and wavespeed in the fundamental symmetric mode[3] is

$$C_L^2 = E_1/[\rho(1-\nu_{12}\nu_{21})] \qquad (1)$$

where C_L is the Lamb wavespeed, E_1 is the in-plane modulus, ν_{12} is the major Poisson's ratio, and ν_{21} is the minor Poisson's ratio.

For the composites used by us $\nu_{12} = 0.28$ and $\nu_{21} = 0.018$. Thus $\nu_{12}\nu_{21} << 1$ and to a first approximation eq. (1) is:

$$C_L^2 = E_1/\rho \qquad (2)$$

The relation between the angle of incidence of the wave on the plate, θ_i, and the wavespeed (C_L) of the Lamb wave is governed by the Snell's Law:

$$\sin(\theta_i)/v_w = \sin(\pi/2)/C_L \qquad (3)$$

where V_w is the wavespeed in water.

EXPERIMENTAL SETUP

The block diagram of the experimental setup is shown in Fig. 2. The specimen, the transmitter and the receiver are immersed in the water bath. The specimen is mounted on a turn table and can be rotated about a vertical axis in steps of 0.1°. This rotation is required to set the specimen for the through-the-thickness and Lamb wave measurements. The transducers are mounted on precision traveling mechanisms. In the through-the-thickness measurements the specimen is normal to the incident wave and the two transducers are in the same line.

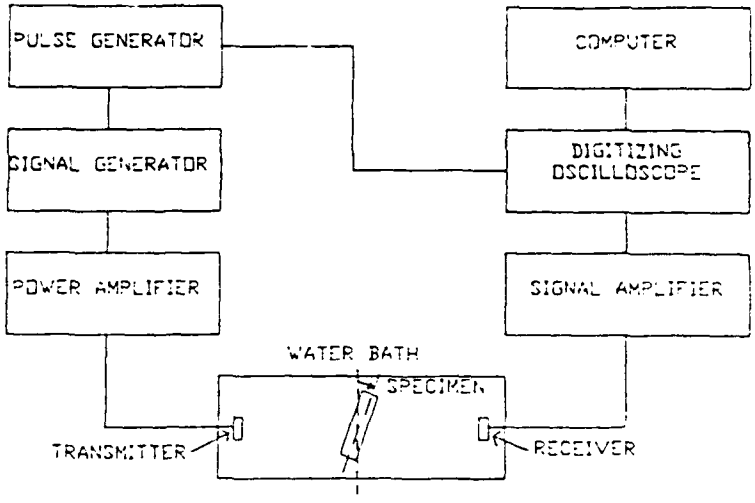

Fig. 2. Block Diagram of the Experimental Setup.

The pulse generator triggers the signal generator which produces a single cycle of sinusoidal wave for through-the-thickness measurements and a tone burst for the Lamb wave measurements. This signal is amplified by the power amplifier and the signal is fed into the wide band transmitting transducer. The wave launched into the water travels through the specimen and sensed by the receiving transducer. The signal from the receiver is amplified by the signal amplifier and fed into the digitizing oscilloscope (Data 6000 by Data Precision). The analog signal is digitized and stored in the oscilloscope. The built-in signal processor of this oscilloscope provides the computer with the amplitude and location of a characteristic point of the toneburst signal e.g. a maximum of a sine wave. The signal amplitude at different angles of incidence is recorded, and critical Lamb angle is identified by the peak in the received signal. A very simple test is sufficient to check for the correct Lamb angle. It can be shown by an elementary calculation that if the receiver is moved in a straight line perpendicular to the line joining the two transducers then there should be no change in the arrival time of the

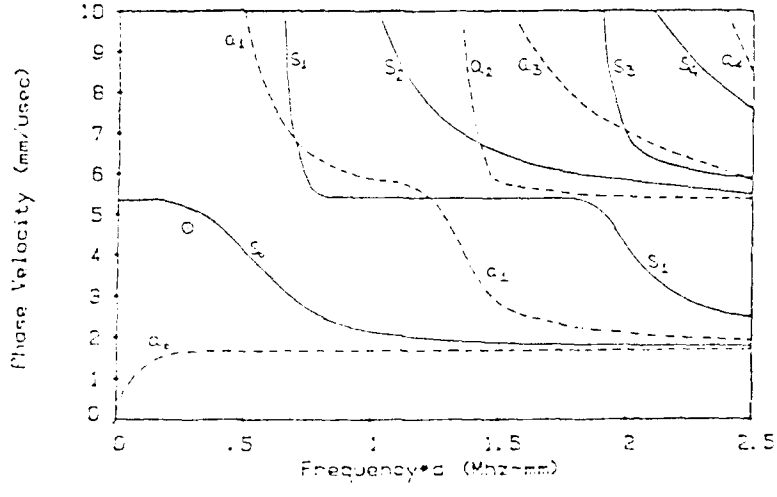

Fig. 3. Dispersion Curve for $[0/90_3]_s$ Gr/Ep Laminate.

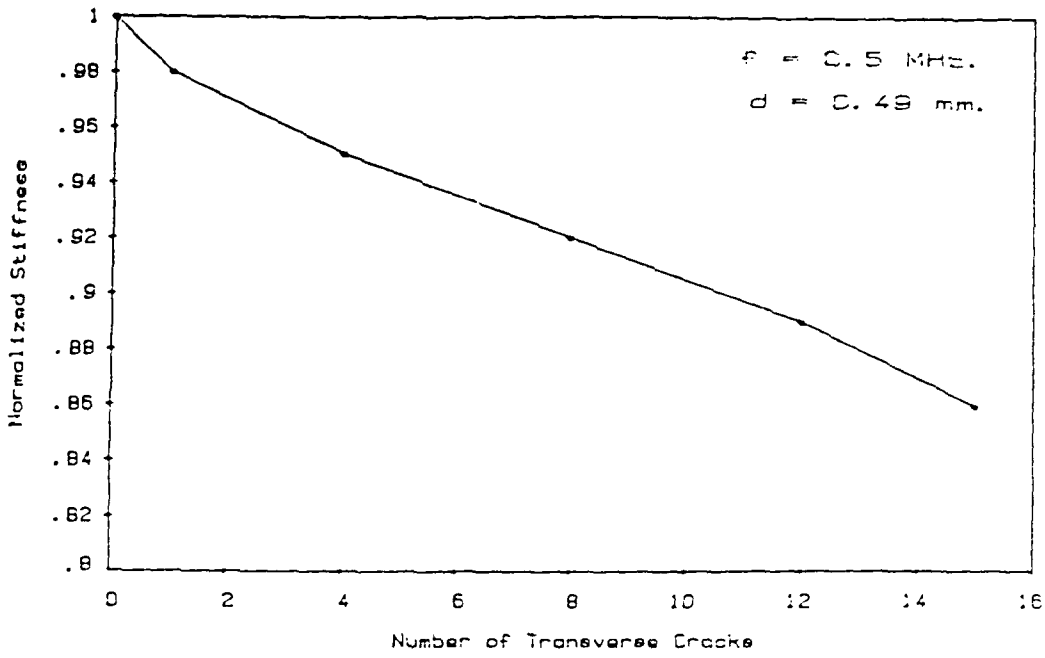

Fig. 4. Stiffness Variation with Damage in $[0/90_3]_s$ Laminate.

signal at the receiver provided the specimen is oriented at the correct Lamb angle. When the transducer is moved for this check, the wave spends more time in the specimen and less time in water and hence the attenuation can be measured.

All the specimens for which the results are presented here are made of AS4/3502 graphite/epoxy laminates. The specimens are 11" x 1" coupons.

RESULTS AND DISCUSSIONS

Now we present some results from the testing of $[0/90_3]_s$ and $[0/90_4]_s$ laminates by the Lamb wave method when transverse cracks are introduced. The cracks are generated in these specimens by displacement controlled monotonic loading at a displacement rate of .02"/min.

We have carried out a theoretical analysis of Lamb wave propagation in a symmetrical balanced composite laminate[4]. The dispersion curves reproduced here are from that work. Fig. 3 shows the dispersion curve for the $[0/90_3]_s$ specimen. Phase velocity of the Lamb waves is plotted against the product of signal frequency and d, where 2d is the plate thickness. The symmetric and antisymmetric modes are shown in solid and discontinuous lines, respectively. The frequency at which the tests were performed (0.5 MHz), is indicated by a circle; s_0 represents the fundamental symmetric mode. The normalized reduction in stiffness as the number of cracks increases in the transducer field are shown in Fig. 4. The stiffness is normalized with respect to the stiffness of the virgin specimen (i.e. no damage). There is a steady decrease in the stiffness and the overall reduction is about 12%. The increase in the attenuation for this specimen is shown in Fig. 5. A four fold increase in attenuation can be observed in this test. Figure 6 shows the dispersion curve for $[0/90_4]_s$ laminate and the tests were conducted at

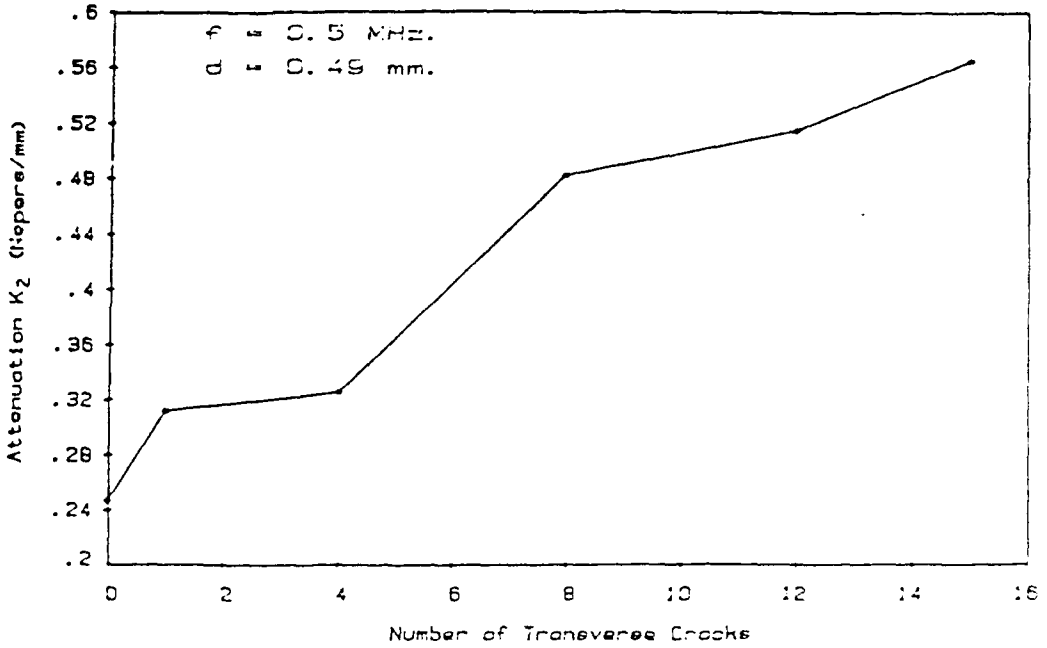

Fig. 5. Attenuation Variation with Damage in $[0/90_3]_s$ Laminate.

the frequency indicated by the circled point. The line diagram of the state of damage is shown in Fig. 7. The location of the transmitter (TR) and the receiver (R) are shown in the figure. The reduction in the stiffness of this laminate when the transverse cracks are introduced, is shown in Fig. 7. Observe that going from the damage state 3 to 4 though there was a substantial increase in the number of cracks in the specimen, the number of cracks in the local region interrogated by the transducer did not increase and hence the changes in the stiffness of the specimen were not observed. This is very reassuring for it demonstrates that our measurement reflects local changes in the stiffness. For this specimen the reduction in stiffness of about 30% was observed. The increase in the attenuation is shown in Fig. 8 which shows almost a six fold increase in attenuation.

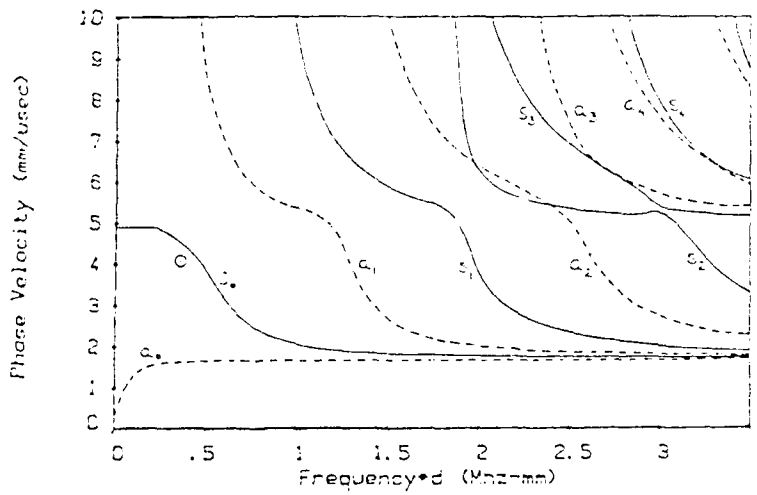

Fig. 6. Dispersion Curve for $[0/90_4]_s$ Gr/Ep Laminate.

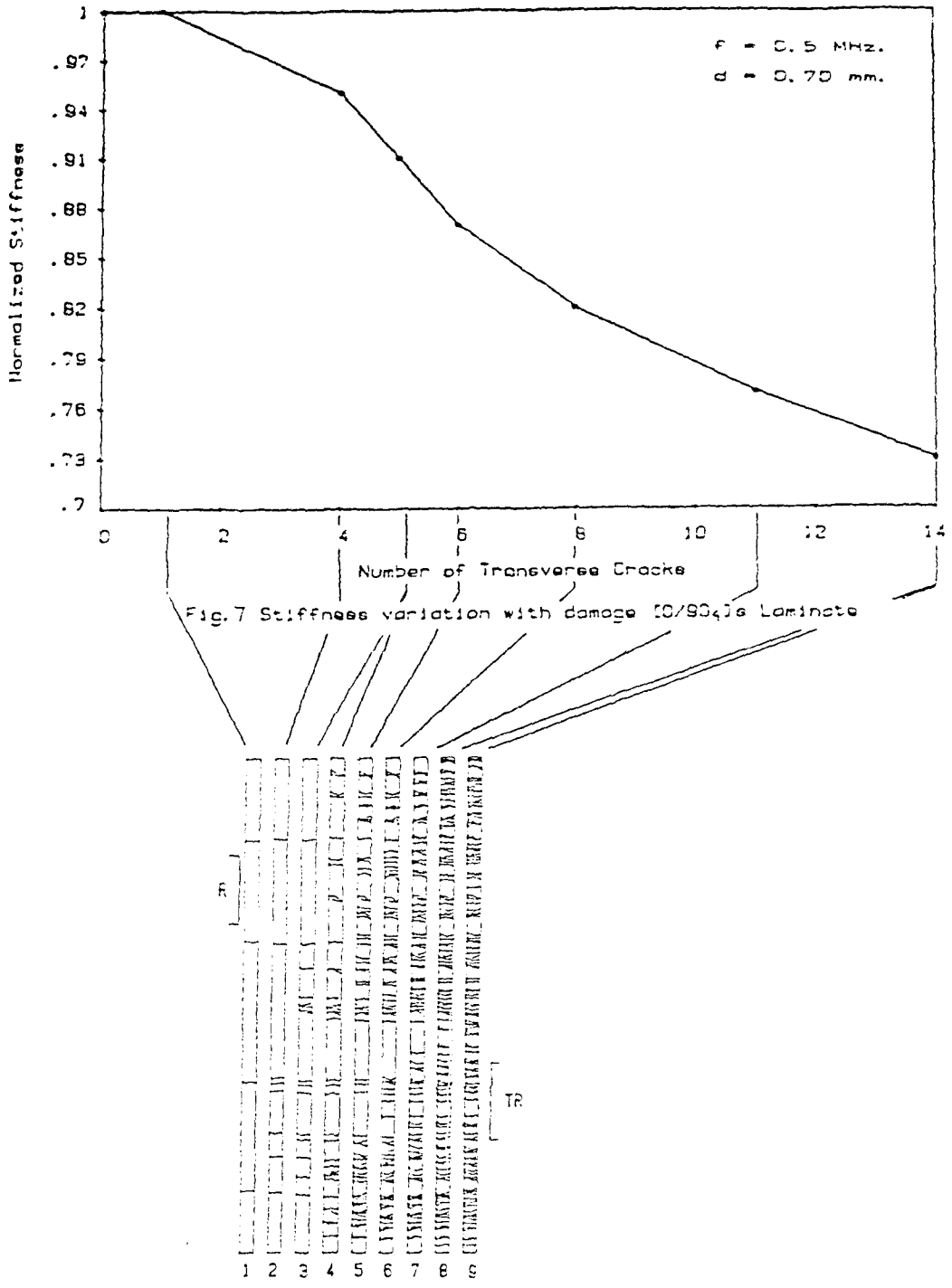

Fig. 7. Stiffness Variation with Damage for $[0/90_4]_s$ Laminate.

CONCLUSIONS

The use of two techniques for ultrasonic nondestructive evaluation of damage (transverse cracking) in laminated composites has been demonstrated. In the first, a longitudinal wave is propagated in the thickness direction. Here the crack-wave interaction is weak. As expected, the wavespeed does not change measurably while the attenuation increases with transverse cracking.

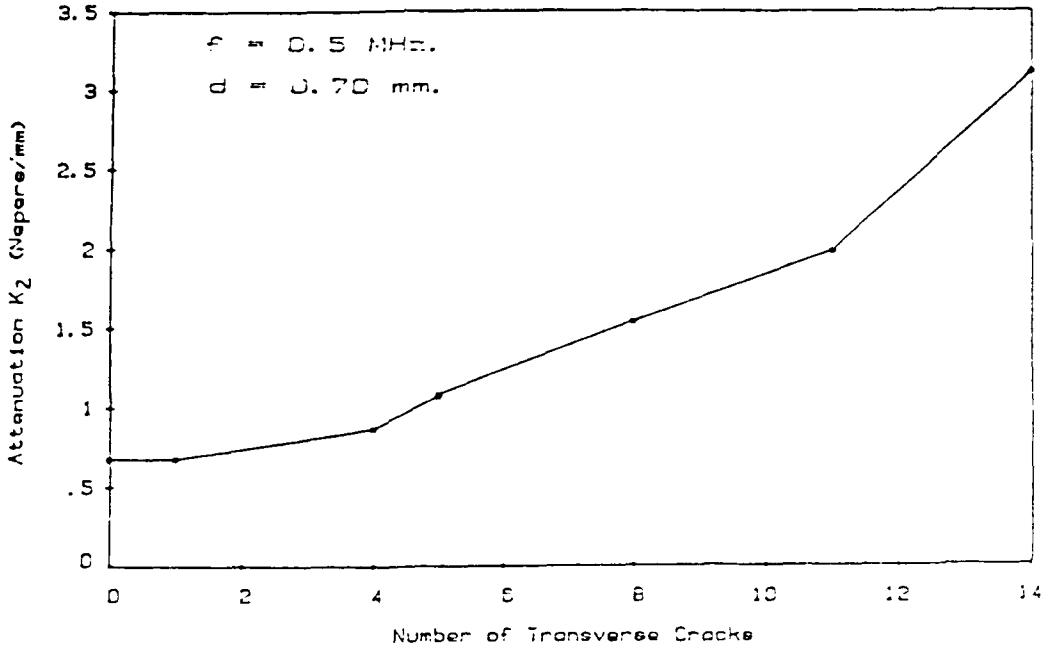

Fig. 8. Attenuation Variation with Damage $[0/90_4]_s$ Laminate.

In the second technique, Lamb waves are propagated along the length of the specimen. Here, the crack-wave interaction is the strongest; both the wave-speed and the attenuation change appreciably with damage. The Lamb wave method, therefore, is a much more effective method for the detection of transverse cracks.

ACKNOWLEDGEMENTS

This research is supported by the Air Force Office of Scientific Research Contract No. F49620-83-C-0067.

REFERENCES

1. K. L. Reifsnider, E. G. Henneke, W. W. Stinchcomb, and J. C. Duke, Damage Mechanics and NDE of Composite Laminates, in: "Mechanics of Composite Materials," Z. Hashin and C. T. Herakovich, eds. Pergamon Press, New York (1983).
2. V Dayal and V. K. Kinra, Ultrasonic NDE of Composite Transverse Cracking, in: "Proceedings of SEM Fall Conference," Society for Experimental Mechanics (1986).
3. C. C. Habegar, R. W. Mann, and G. A. Baum, Ultrasonic Plate Waves in Paper, Ultrasonics 3:57 (1979).
4. V. Dayal and V. K. Kinra, "Lamb Waves in Anisotropic Plates Immersed in a Fluid--An Exact Numerical Solution," (unpublished results).

A. Wolfenden,[1] *M. R. Harmouche,*[1] *G. V. Blessing,*[2] *Y. T. Chen,*[3] *P. Terranova,*[3] *V. Dayal,*[4] *V. K. Kinra,*[5] *J. W. Lemmens,*[6] *R. R. Phillips,*[7] *J. S. Smith,*[8] *P. Mahmoodi,*[9] *and R. J. Wann*[9]

Dynamic Young's Modulus Measurements in Metallic Materials: Results of an Interlaboratory Testing Program

REFERENCE: Wolfenden, A., Harmouche, M. R., Blessing, G. V., Chen, Y. T., Terranova, P., Dayal, V., Kinra, V. K., Lemmens, J. W., Phillips, R. R., Smith, J. S., Mahmoodi, P., and Wann, R. J., **"Dynamic Young's Modulus Measurements in Metallic Materials: Results of an Interlaboratory Testing Program,"** *Journal of Testing and Evaluation*, JTEVA, Vol. 17, No. 1, Jan. 1989, pp. 2-13.

ABSTRACT: The results of a round-robin testing study are presented for measurements of dynamic Young's modulus in two nickel-based alloys. The Interlaboratory Testing Program involved six types of apparatus, six different organizations, and specimens from a well-documented source. All the techniques yielded values of dynamic Young's modulus that agreed within 1.6% of each other. For Inconel alloy 600 the dynamic modulus was 213.5 GPa with a standard deviation of 3.6 GPa; for Incoloy alloy 907 the corresponding values were 158.6 and 2.2 GPa, respectively. No significant effect of frequency over the range 780 Hz to 15 MHz was found.

KEY WORDS: elastic modulus, dynamic, Young's modulus, metals, interlaboratory, frequency dependence

In engineering and science elastic modulus is of fundamental and technological importance. It has applications in areas such as load-deflection, buckling, thermoelastic stresses, elastic instability, fracture mechanics, creep, interatomic potentials, lattice defects, thermodynamic equations of state, free energy, and thermal expansion.

In reflection of this wide-ranging importance of modulus, several standards organizations around the world have formulated procedures for the determination of static and dynamic modulus of certain types of materials. For example, ASTM has published Standard Methods for Young's Modulus, Shear Modulus, and Poisson's Ratio for Glass and Glass-Ceramics by Resonance (ASTM C 623), Young's Modulus, Shear Modulus, and Poisson's Ratio for Ceramic Whitewares by Resonance (ASTM C 848), Moduli of Elasticity and Fundamental Frequencies of Carbon and Graphite Materials by Sonic Resonance (ASTM C 747), and Fundamental Transverse, Longitudinal, and Torsional Frequencies of Concrete Specimens (ASTM C 215). In addition, there is the well-known standard test method for determining static Young's modulus of metallic tensile specimens (ASTM E 111). In view of the considerable amount of work devoted by members of standards organizations to the formulation and publication of these recognized testing methods for specific materials, it is very surprising that *there is no recognized testing method for the determination of dynamic Young's modulus in metallic materials.* There is, however, a large contribution towards a recognized testing method for dynamic modulus in ASTM Practice for Measuring Ultrasonic Velocity in Materials (E 494). The main aim of this paper is to be a part of a movement to fill this lacuna.

As background history to the preparation of this paper, it is pertinent to mention that in the early 1980s, within the framework of ASTM Subcommittee E28.03 on Elastic Properties and Definitions on Mechanical Testing, an Interlaboratory Testing Program was set up to address measurements of dynamic Young's modulus in metals. This program or task group carries the identification E28.03.05; its active members and their laboratories are listed in Table 1. The paper is the first full report resulting from the testing program and documents the alloys used as specimens, some details on the various testing techniques in the laboratories, the experimental results, a detailed analysis of the results (with discussion), and the conclusions of the study.

Specimens

For the Interlaboratory Testing Program special care was devoted to specimen selection and preparation. An early discussion of the ASTM E28.03.05 group resulted in a consensus that the materials chosen should be of technological interest and that the preference of one of the laboratories for a magnetic material should be respected. One of the group members made the resources of his company available in this regard. Thus Inco Alloys International provided both the materials and the machining facilities. The metallic materials chosen for the tests were Inconel alloy 600 (UNS N06600; designated Alloy A) and Incoloy alloy 907 (UNS N19907;

Manuscript received 3/15/87; accepted for publication 7/15/88.

[1]Mechanical Engineering Department, Texas A&M University, College Station, TX 77843.

[2]Ultrasonics Standards Group, National Bureau of Standards, Gaithersburg, MD 20899. (The National Bureau of Standards is now the National Institute of Standards and Technology.)

[3]Corporate R&D, % Zell #1, Pitney Bowes, Walter H. Wheeler, Jr. Dr., Stamford, CT 06904.

[4]Department of Mechanical Engineering, North Carolina A&T State University, Greensboro, NC 27411.

[5]Aerospace Engineering Department, Texas A&M University, College Station, TX 77843.

[6]Elektronika N.V., Research Park 62, B-3030 Leuven, Belgium.

[7]348 Center Street, St. Marys, PA 15857.

[8]Inco Alloys International, Inc., P.O. Box 1958, Huntington, WV 25720.

[9]Corporate Research Laboratories/3M, 3M Center, St. Paul, MN 55133.

0090-3973/89/0001-0002$00.00

TABLE 1—*List of the personnel taking part in the interlaboratory testing program and their laboratories or company names, and of the trade names or acronyms (where available) for the apparatus used and the physical principle of operation.*

Laboratory	Personnel	Trade Name or Acronym	Physical Principle
1. Inco Alloys International	J. S. Smith		Free-free Beam (F)
2. Pitney Bowes	Y. T. Chen R. R. Phillips P. Terranova		Free-free Beam (F)
3. J. W. Lemmens Electronika	J. W. Lemmens	Grindo-Sonic	Impulse Excitation (F)
4. National Bureau of Standards (NBS)	G. V. Blessing		Velocity Measurements of Ultrasonic Wave Pulses (T)
5. Texas A&M University	A. Wolfenden M. R. Harmouche	PUCOT (Piezoelectric Ultrasonic Composite Oscillator Technique)	Piezoelectric Ultrasonic Oscillation (F)
6. Texas A&M University	V. K. Kinra V. Dayal		Ultrasonic Pulse Spectroscopy (P)
7. 3M Company	P. Mahmoodi R. J. Wann		Free-free Beam (F)
8. Texas A&M University	A. Wolfenden M. R. Harmouche	Modul-R	Magnetically Excited Resonance (F)

F: Denotes that the apparatus is designed to measure frequency of the specimen.
T: Denotes that the apparatus is designed to measure the transit time for ultrasonic pulses.
P: Denotes that the apparatus is designed for ultrasonic pulse spectroscopy.

the magnetic material, designated Alloy B).[10] The chemical compositions, thermomechanical treatments, and sizes of the specimens of Alloys A and B are given in Table 2. The specimen sizes reflect to a great extent the optimum or convenient sizes pertinent to the particular measuring techniques at the various laboratories. To examine the possibility that the specimens were *not* isotropic, X-ray diffraction pole figures (powder patterns) were obtained for filings from the specimens and for pieces of the specimens. For Inconel alloy 600 (Alloy A), no significant texture effects were detected. However, for Incoloy alloy 907 (Alloy B), small traces of (311) and (222) textures were found.

Experimental Procedures

All experimental methods of measuring dynamic Young's modulus E use, in some form or other, the basic wave equation for the propagation of a longitudinal elastic wave in an elastic medium:

$$E = \rho v^2 \tag{1}$$

where ρ is the mass density of the medium and v is the wave speed.

[10]Inconel and Incoloy are trademarks for products of the Inco family of companies (Inco Alloys International, Inc.).

Thus the methods that are concerned with measurements of transit time t (and hence velocity) of ultrasonic pulses over a known distance L in an elastic medium apply Eq 1 directly ($v = L/t$), assuming that ρ is known or can be measured also. In the case of the methods that utilize measurements of resonant frequency of standing or decaying elastic waves in an elastic medium a modified form of Eq 1 is applied:

$$E = \rho v^2$$

$$= \rho(f\lambda)^2 \tag{2}$$

where f is the resonant frequency and λ is the wavelength. The specific geometrical details of the specimen usually determine λ. For example, for a uniform beam resonating in its fundamental longitudinal mode, the wavelength is twice the length L of the beam. Therefore Eq 2 becomes

$$E = 4\rho L^2 f^2 \tag{3}$$

Again, in the frequency methods ρ must be known or measured. All but one of the experimental procedures used in the Interlabora-

TABLE 2—*Chemical compositions, thermomechanical treatments, and sizes of the specimens of Alloys A and B.*

	Alloy A (Inconel Alloy 600)	Alloy B (Incoloy Alloy 907)
Composition (wt%)		
Ni	74.91	37.46
Cr	15.48	...
Fe & others	balance	balance
C	0.08	0.01
Co	...	14.38
Nb	...	4.71
Ti	...	1.46
Treatment		
	Cold drawn Mill annealed[a] 31.75 mm (1.25 in.) diameter	Hot rolled 17.78 by 101.6 mm (0.7 by 4 in.) flat
Specimen Sizes		
Round	6.35 mm (0.25 in.) diameter by 79.38 mm (3.125 in.) long	
Strip	2.03 mm (0.080 in.) by 6.35 mm (0.25 in.) by 106.65 mm (4.199 in.)	
Special #1	25.4 mm (1.000 in.) diameter by 101.6 mm (4.000 in.)	
Special #2		50.8 by 50.8 by 19.05 mm (2 by 2 by 0.750 in.) 25.4 mm diameter by 19.05 mm (1 in. diameter by 0.750 in.)

[a]In the range 980 to 1038°C.

tory Testing Program fell into these two basic categories for determining dynamic Young's modulus. The third basic technique, newly developed, is ultrasonic pulse spectroscopy. The techniques will be described in this section of the paper in the following sequence: free-free beam, impulse excitation, wave velocity measurements, ultrasonic pulse spectroscopy, piezoelectric ultrasonic oscillation, and magnetically excited resonance.

Free-Free Beam Technique

Three of the laboratories mentioned in Table 1 incorporated the free-free beam test method [*1–3*]. While the details of the apparatus at the three locations vary, the basic principle of operation is the same. For brevity, an apparatus will be described which may be regarded as typical for the technique.

The test method is patterned after the technique of Spinner and Tefft [*2*] of the National Bureau of Standards. Figure 1 shows schematically the instrumentation and the test configuration. The rectangular or cylindrical specimen is suspended near its nodal points by pure silk or cotton-covered polyester thread. The nodal points for beams of uniform section in a free-free suspension are at distances from the free ends of approximately $0.22L$ and $0.78L$ [*4*]. For the rectangular specimen the cotton threads are positioned at opposite sides as indicated by Spinner and Tefft [*2*] and suspended from Astatic X 26 crystal cutters used as both drive and pickup transducers. This configuration of opposite side suspension excites both the flexural and torsional modes of vibration. Cylindrical specimens are suspended in a similar manner except for the obvious off-setting of the suspension positions. Alternatively, the better

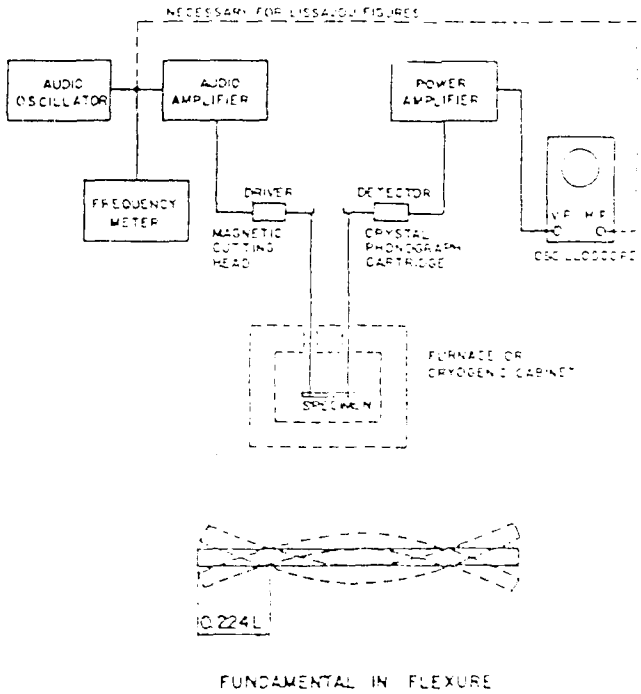

FIG. 1—*Schematic diagram of the instrumentation used in the free-free beam test method and of the test configuration. The specimen is suspended at or near the nodal points.*

string suspension system known as the loop method may be used [5].

The sine wave signal from a function generator is fed to a power amplifier and then to the driver transducer. The pickup transducer has a 10× gain preamplifier. The signal from the pickup is analyzed on a suitable analyzer, which is configured in a peak averaging mode using exponential averaging. The function generator is swept manually through the frequency range of interest while the output signal is examined. The fundamental frequency is quite easily determined in this manner.

Physical measurements such as length, width, diameter, or thickness are measured with a machinist's caliper. The density of the specimen is determined using mass and volume calculated from the measured dimensions.

The equations used for calculating Young's modulus are [4]

$$\text{Cylindrical:} \quad E = 64\pi^2 f^2 L^4 \rho / A^2 d^2 \tag{4}$$

$$\text{Rectangular:} \quad E = 48\pi^2 f^2 L^4 \rho / A^2 h^2 \tag{5}$$

where

f = fundamental frequency,
L = free length,
ρ = density,
d = diameter,
h = thickness, and
A = constant depending on the shape of the specimen.

Impulse Excitation Technique

The test method entails (*a*) the excitation of the test specimen by means of a light mechanical impulse (a tap) and (*b*) the analysis of the resultant transient vibration. An electronic circuit is used to isolate the harmonics and the fundamental resonant frequency from the spectrum of noise, and to measure the period corresponding to the fundamental frequency. The result is displayed in digital form. A block diagram for the method is shown in Fig. 2.

The specimen is supported preferably at the nodes of the desired vibrational mode. By positioning correctly the location of the exciting impulse, each mode can be induced easily. Whatever the mode, the instrument will identify the fundamental resonant frequency of the vibration. Very little exciting energy is required, even for very large specimens, because the measurement is performed at a very low strain amplitude. Hence only a very light tap is sufficient to initiate the measurement.

The most versatile means of detecting the vibrational motion is provided by a hand-held piezoelectric probe. It is used to analyze signals from about 20 Hz to 80 kHz in frequency. Acoustic, optical, or electromagnetic detectors can be used for specialized purposes, such as testing materials at high temperatures. With the fundamental resonant frequency thus obtained and the density determined by the Archimedes method, the moduli and Poisson's ratio can be calculated for regular shaped specimens using well-known equations [2].

Velocity of Ultrasonic Wave Pulses

This technique is one of the better known methods for measuring dynamic moduli in materials. A brief account of the theory behind the technique and of the experimental arrangement is given.

For ultrasonic wavelengths less than the dimensions of the specimens, two normal modes of wave propagation in isotropic media prevail. They are the longitudinal and shear modes, with respective velocities V_L and V_s (see, for example, Refs 6 and 7 and ASTM E 494). Longitudinal waves, sometimes referred to as compressional waves, alternately compress and dilate the material lattice (i.e., generate compressive and tensile strains) as they pass by. The re-

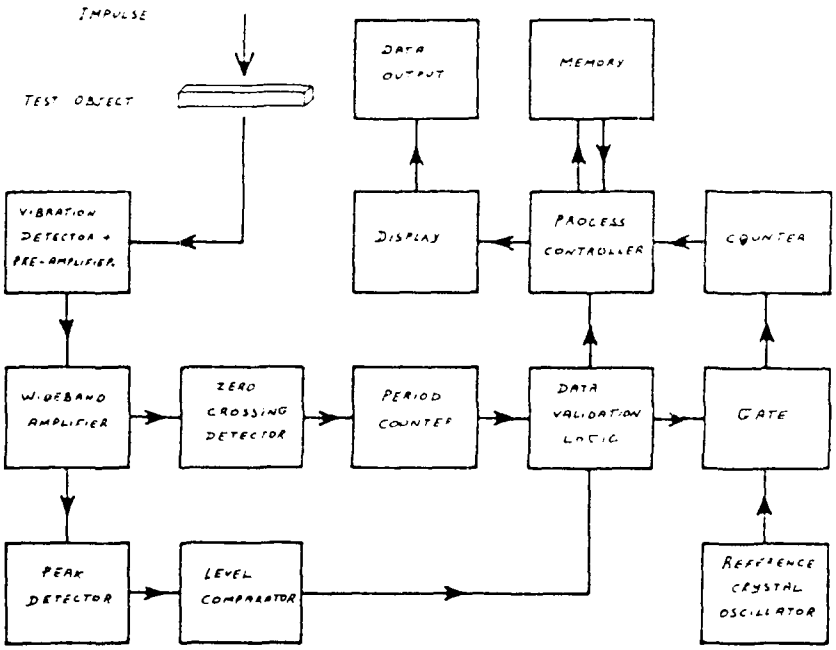

FIG. 2—*Block diagram of the impulse excitation technique.*

sulting particle motion of the material is parallel to the direction of wave propagation. Shear waves, on the other hand, generate particle displacements perpendicular to the propagation direction, causing the material lattice to shear as the waves pass by.

From these two wave speeds and the density ρ, all the elastic parameters of the material can be calculated: the Young's, bulk, and shear moduli, and Poisson's ratio (P.R.). Their relationships are given by

$$\text{Young's modulus} = \rho V_S^2(3V_L^2 - 4V_S^2)/(V_L^2 - V_S^2) \quad (6)$$

$$\text{Bulk modulus} = \rho\,(V_L^2 - (4/3)V_S^2) \quad (7)$$

$$\text{Shear modulus} = \rho V_S^2 \quad (8)$$

$$\text{P.R.} = (V_L^2 - 2V_S^2)/(2V_L^2 - 2V_S^2) \quad (9)$$

Anisotropy and inhomogeneity in the specimen may be conveniently evaluated ultrasonically. If a specimen is inhomogeneous, different wave speeds will be observed at different positions in the specimen; if the specimen is anisotropic, different wave speeds will be observed for different propagation directions in the specimen. Furthermore, shear waves may be used to evaluate anisotropy in the specimen by propagating them in the same direction and rotating the transducer's particle displacement (polarization) vector.

The wave speed V in the specimen is determined by measuring the transit time t of an ultrasonic pulse over a known path L in the specimen, and by calculating $V = L/t$. It is important to note that the distinction between phase and group velocities becomes irrelevant for non-dispersive media, such as the specimens tested here. This is pointed out empirically in the following section. The necessary measurements to differentiate between group and phase values were not made. The measurement techniques applied here could span the difference between the two values. In any event, the difference between the values is probably less than the measurement precision quoted for the metal samples studied: one part in a thousand, or 0.1%. Typically, L is twice some usable dimension in the specimen, such as the cylinder bar length or the thickness of a flat strip. The factor of two derives from the round-trip distance for the pulse when making pulse-echo measurements using a single transducer. The pulse-echo-overlap technique is convenient for making precise transit time measurements [8]. With this technique, at least two echoes (with a single transducer) are needed to provide an overlap of successive echoes on the oscilloscope by means of time-delaying circuitry, from which the transit times in the specimen are determined.

The ultrasonic velocity measurements are made at frequencies ranging from 5 to 15 MHz for the specimen dimensions in these tests, with the higher frequencies being used for shorter path lengths. All measurements are made at a nominal room temperature of 21°C. Figure 3 illustrates the principal components used for a majority of the measurements. (Some data are taken using a through-transmission technique wherein a second transducer attached to the opposite face of the specimen receives the ultrasonic pulse.) A pulser/receiver unit transmits a very short (less than 0.1 μs) spike voltage to a transducer, generating a broad-band ultrasonic wave of short duration—less than 1.0 μs, for example, at 5 MHz. A typical broad-band wave shape is illustrated in Fig. 3. For the rod sample, it should be noted that the errors in determining wave speed can be very significant due to sidewall reflections using the pulse-echo-overlap (or through transmission) technique [9]. Alternatively, the transducer may be driven by a multi-cycle sinusoidal voltage burst, usually at the transducer's resonant frequency, which results in a relatively narrow band ultrasonic wave packet of longer duration—several microseconds, for example, at 5 MHz. The transducer converts the excitation into a mechanical oscillation or sound wave which is coupled into the specimen to propagate at the sound velocity. The coupling is significantly enhanced by use of a thin layer (much less than an ultrasonic wavelength) of liquid or elastomer material. (Other coupling techniques exist which do not require direct mechanical contact of transducer to specimen [7].) Commercially available transducers have a casing that houses a piezoelectric element and often an impedance matching circuit, which are designed for convenient electrical attachment to the pulser/receiver via coaxial cable and standard connectors. The piezoelectric elements of the transducers used in this work range from 4 to 13 mm diameter.

After entering the specimen, the ultrasonic pulse echoes back and forth between the faces of the specimen, while constantly decaying in amplitude due to scattering, absorption, and boundary

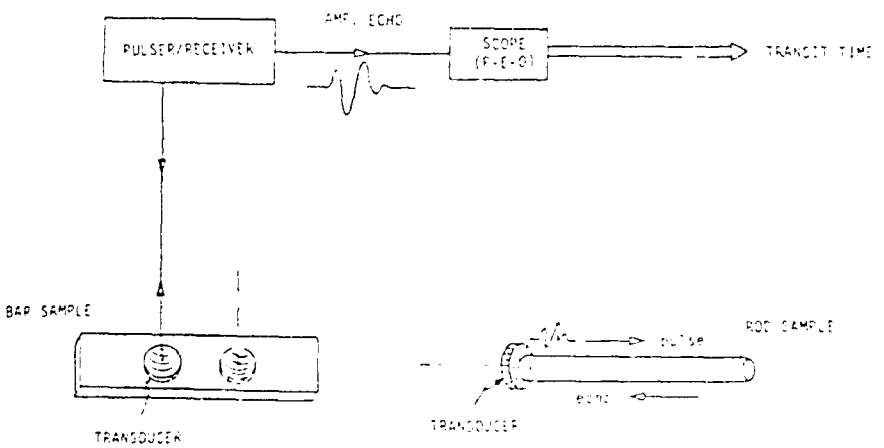

FIG. 3—*Ultrasonic velocity measurement system with direct contact of transducer on specimen. The transit time of the ultrasonic pulse is measured by the pulse echo overlap technique.*

interface losses. Each time the wave pulse is incident at the transducer/specimen interface, a portion of the elastic wave energy is converted into an electrical signal by the transducer. This received signal is then amplified and displayed on an oscilloscope so that the transit time measurements can be made. Electronic techniques exist to automate the measurements with direct computer control. The accuracy of these measurements depends on the dimensions of the specimen (path length, end-face parallelism, etc.), the particular ultrasonic coupling technique, and the signal-to-noise ratio. Typically, the accuracy for these transit time measurements is ± 0.1% or better. The accuracy could be increased (if desired) by taking into account (*a*) the effects of beam spreading (diffraction) and (*b*) the small but finite effect of the bond layer thickness on the phase shift upon each reflection from the specimen-transducer boundary, as noted elsewhere [*10,11*]. However, in discussing these potentially high accuracies, the limitations imposed by the *inhomogeneity* and anisotropy of the specimens should be kept in mind. Indeed, in Specimen 2.3 (Incoloy alloy 907) a noticeable anisotropy of about 10% for the shear modulus was detected at both Positions 1 and 2 (see Fig. 3, bar sample). This anisotropy effect on the modulus most likely arises from the texture observed in Alloy B (see Specimens section). The densities of the specimens for this study were determined by the Archimedes method, by which the density of the specimen is measured relative to that of distilled water. The latter density is known from published tables.

Ultrasonic Pulse Spectroscopy for the Measurement of Phase Velocity and Attenuation

As discussed earlier in this paper, all the elastic parameters of a material can be calculated from the measurement of longitudinal and shear phase velocities. The technique described in the previous section is the conventional method of measuring the wave speed. If the specimen is thick (where the reflections can be separated in time domain), the transit time method is the easiest and very efficient. However, if the specimen is thin that method breaks down and cannot be used. Even when applicable, the conventional method requires human judgment and interference to make good measurements. The measurement of attenuation is not at all accurate and by this method only group velocity can be measured.

We have developed techniques which have eliminated all the above mentioned limitations. A fully computerized technique has been developed which can measure phase velocity and attenuation for thick as well as thin specimens. The digitized signal in time domain is transformed to the frequency domain by the use of Fast Fourier Transforms (FFT). If two pulses can be separated, then acoustic parameters, phase velocity, and attenuation are computed from the phase shift and loss of amplitude between two pulses in the reflected or transmitted signal. If the pulses cannot be separated, the complete signal is transformed by FFT and, by deconvolving the signal with respect to a reference signal, the acoustic parameters are computed. For details of these techniques readers are referred to Refs *12* and *13*.

The techniques can be used both in the transmission and reflection mode. They can be used in direct contact or water immersion with a minor change in the governing equations. The techniques measure phase velocity and attenuation over a range of frequencies from which the group velocity can be obtained. Due to the fact that attenuation can be measured accurately, a variety of potential applications of this technique are envisaged. The effect of temperature up to the melting point of a material can be studied. The uniformity of the specimen and its porosity can be estimated. In composite materials we are able to assess damage due to mechanical and thermal loading. Brief accounts of the theory behind the technique, the procedure, and the results follow.

If the pulses can be separated in the time domain the following equation is obtained [*13*] for the water immersion reflection case:

$$G^*/F^* = 1 + T_{12}T_{21}\exp(-i2kh) \tag{10}$$

and for the direct contact reflection case:

$$G^*/F^* = 1 + R_{21}^2\exp(-i2kh) \tag{11}$$

where

G^* = FFT of two pulses,
F^* = FFT of the first pulse,
T_{ij} = transmission coefficient from medium i to j,
R_{ij} = reflection coefficient when the wave travelling in medium i reflects from i/j interface,
h = specimen thickness,
$k = k_1 + ik_2$ is the complex wavenumber,
$k_1 = \omega/c$ is the wavenumber,
ω = circular frequency,
c = wave speed, and
k_2 = attenuation.

Substituting $k = k_1 + ik_2$ into Eqs 10 and 11 and comparing the real and imaginary parts of the two sides, we obtain

$$k_1 = 2f/c = \phi/2h$$

$$\text{or} \quad c = 4h/(\phi/f)$$

$$\text{and} \quad k_2 = \ln(M)$$

where ϕ = phase of $G^*/F^* - 1$, and

$$M = \begin{cases} |G^*/F^* - 1|/(T_{12}T_{21}) & \text{in water immersion} \\ |G^*/F^* - 1|/R_{21}^2 & \text{in direct contact} \end{cases}$$

Similarly, if the pulse cannot be separated, then for the reflection field:

$$\exp(-i2kh) = [\beta/(1 + \beta)]R_{21}^2$$

where $\beta = R_{12}R_{21}[G^*/F^* - 1]/(T_{12}T_{21})$. Here G^* is the FFT of the entire reflected field and F^* is the FFT of the reference signal.

For the transmitted field:

$$\frac{\exp(-ih(k - k_0))}{1 - R_{21}^2\exp(-i2kh)} = \frac{G^*}{T_{12}T_{21}F^*}$$

Here F^* is the FFT of the signal at the receiver when there is no sample between the two transducers and G^* is the FFT of the total transmitted signal after the specimen is introduced in the acoustic path.

Since fairly thick specimens were tested in the tests reported here, Eq 11 has been used in the measurements.

The block diagram of the experimental setup is as shown in Fig. 4. The analog signal is collected by the pulser-receiver and is fed

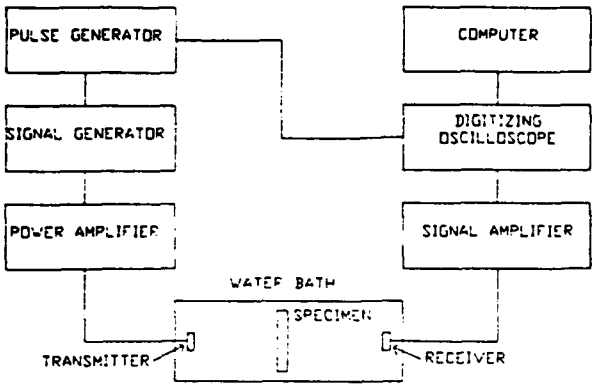

FIG. 4—*Schematic diagram of the ultrasonic pulse spectroscopy technique.*

into the digital oscilloscope. The signal is digitized in the oscilloscope. The signal processing unit of this oscilloscope performs Fast Fourier Transform on the signal. The useful portion of the transformed signal is then acquired by the computer for the calculation of the wave speed and the attenuation. In these steps several potential sources of errors can affect the results: (1) sampling interval, (2) frequency resolution, and (3) transducer response. The first factor is the digitizing interval of the acquired signal. The FFT of a 1 MHz signal at 10, 20, 40, and 100 ns sampling intervals was studied. It was observed that at the 10, 20, or 40 ns sampling interval the frequency content of the signal is essentially the same. However, at the 100 ns sampling interval, the signal loses some of its high frequency contents. The useful digitizing intervals depend on the frequency of the transducer being used. For example, for 10 MHz frequency, at the 40 ns interval some of the high frequency contents are lost. The second factor considered was the resolution of the signal in the frequency domain. A sampling interval of 40 ns or less with a frequency resolution of 0.05 MHz or less is considered adequate. This factor is also transducer frequency related. The third factor considered was the useful range of the transducer frequency response. It was found that satisfactory measurements can be obtained over a frequency range given by 25% of the peak response amplitude.

Three specimens were tested by the technique described above. The phase versus frequency plot for these specimens was a straight line; hence it can be deduced that the phase velocity ($\equiv \omega/k$) is equal to the group velocity ($\equiv d\omega/dk$) for these specimens.

The measurement of the wave speed is estimated to be accurate to $\pm 0.05\%$. The results obtained for three specimens are presented in Tables 3 and 4. The density for Specimens B2.2 and A1.3 was measured by the Archimedes principle; the density of Specimen A1.1 was measured by direct measurement of dimensions and mass. This resulted in a larger uncertainty in the measurement of density of Specimen A1.1 and consequently in a larger error in the value of E.

Piezoelectric Ultrasonic Composite Oscillator Technique (PUCOT)

Essentially, the apparatus for the PUCOT consists of piezoelectric quartz drive (D) and gage (G) crystals to excite longitudinal or torsional ultrasonic (kHz) resonant stress waves in the test specimen (S) of appropriate resonant length via a fused quartz spacer rod (Fig. 5). The components are joined with Loctite or ceramic cement as test temperature dictates. The spacer rod may be omitted for measurements near ambient temperatures. The resonant system is driven by a closed-loop oscillator which maintains a constant (preselected) gage voltage and hence a constant maximum strain amplitude in the specimen. During a test, values of the resonant period of the DGS (drive-gage-specimen) system are recorded and standard equations (Table 5) are used to calculate Young's modulus E. The validity of the measured value for E is determined from the ratio R of the period in the specimen to that of the quartz crystals. Ideally the ratio should be unity. However, ratios between 0.97 and 1.03 yield equally valid results. More detailed descriptions of the PUCOT have been given elsewhere [*14-16*].

The PUCOT is limited to frequencies between 20 and 200 kHz. Therefore specimens that resonate beyond this frequency range cannot be tested. The test specimen may be cylindrical or a parallelepiped, but the cross section can vary in size and shape. The ratio of specimen length to the largest dimension in the cross section must exceed five to prevent dispersion of the ultrasonic wave. The strain amplitude is in the range 10^{-8} to 10^{-4}.

The density of the specimens for the PUCOT study was determined by the Archimedes method.

Magnetically Excited Resonance

Magnetically excited resonance involves the use of an instrument known as the Modul-R which measures the longitudinal resonant frequency of a specimen of ferromagnetic material near 25 kHz. This frequency has been selected because it permits use of a convenient specimen length of about 100 mm. For convenience of calculations the specimen size is 104.63 by 6.35 mm. Thicknesses may vary from 0.203 to 2.03 mm. The specimen must be ferromagnetic because both the specimen drive and pickup signals are derived from magnetostriction in the specimen.

A schematic diagram of the apparatus is given in Fig. 6. The method of operation is as follows. The specimen is placed in the coil assembly where it is supported by the bias coil frame at its midlength location. A magnetic pulse initiates the vibration, setting up a field in the pickup coil from which a small signal is amplified and fed into the drive coil. An alternating current passing through the drive coil produces an alternating field in the interior of the coil. In the presence of this field, the specimen alternately contracts and extends longitudinally. These vibrations traverse the specimen with the velocity of sound and appear as vibrations in the part of the specimen encircled by the pickup coil. These changes in strain alter the permeability of the specimen and its magnetic flux density. The altered magnetic flux density induces an alternating current in the pickup coil by amplifying the pickup signal and feeding it back to the drive coil in the correct phase relationship with the mechanical vibrations initiated by the bias coil. The specimen becomes the frequency-controlling element of the magnetostrictive oscillator, and only the fundamental longitudinal resonant frequency is displayed on the digital output counter. On the basis of the results obtained for modulus with this technique, the magnetic field imposed on the specimen is small enough to avoid the ΔE effect.

For this interlaboratory study only Specimen B2.3 (ferromagnetic and of required dimensions) was tested with the Modul-R. The density of the specimen was determined by the Archimedes method.

TABLE 3—*ASTM E28.03.05 dynamic Young's modulus interlaboratory study.*

Alloy A		Raw Data Table		
Laboratory	Specimen	*E*, GPa	Density, g/cm³	
1	1.1	218.0	8.43	IAI
	1.1	218.0	8.43	
	1.1	218.1	8.43	
	1.2	216.9	8.43	
	1.3	218.5	8.43	
2	1.1	210.5	8.376	Chen/Phillips
	1.3	209.2	8.339	
3	1.1	31.4*	8.43	Lemmens
	1.1	218.8	8.43	
	1.2	216.0	8.43	
	1.3	217.5	8.43	
	1.3	217.0	8.43	
	1.3	216.2	8.43	
	1.3	217.3	8.43	
4	1.1	212.0	8.36	NBS/Parallel
	1.3	205.0	8.36	NBS/Parallel
	1.3	215.0	8.36	NBS/Perpendicular, pos. 1**
	1.3	207.0	8.36	NBS/Perpendicular, pos. 2**
5	1.2	216.9	8.371	Texas A&M (PUCOT)
	1.4	216.6	8.373	
6	1.1	215.6	8.38	Texas A&M (Kinra)
	1.3	214.2	8.37	
7	1.1	203.0	8.25	3M
	1.3	210.3	8.37	

*Reject this value (wrong harmonic).
**See Fig. 3 for these positions.
Density listed for Laboratory 3 was determined at Laboratory 1.
Material: Inconel alloy 600, 25.4 mm diameter, hot-rolled annealed rod.
Specimens:
1.1: 6.35 mm diameter cylinder.
1.2: 25.4 mm diameter cylinder.
1.3: 3.18 by 6.35 by 101.6 mm flat strip.
1.4: 25.4 mm diameter cylinder (separate specimen for Laboratory 6).

Results

The results from the Interlaboratory Testing Program are quite voluminous. The data received from the various laboratories by the senior author were converted into values of Young's modulus by use of the various equations presented in the Experimental Procedures section. These values of modulus (and density) are listed in SI units in Tables 3 and 4. Finally, bar graphs of the Young's modulus measurements and the percentage deviations from the average values of the moduli for Materials A and B are presented in Figs. 7 to 10.

Analysis of Results and Discussion

Considering the wide variety of apparatus used in the eight laboratories, the results for dynamic Young's modulus of the two alloys are encouraging. Tables 3 and 4 show that the modulus ranges from 203 to 219 GPa for Material A and from 156 to 172 GPa for Material B. The mean and standard deviation for Material A are 213.91 and 4.46 GPa, respectively. It is interesting to note that the deviations about the mean for Material A (Fig. 8) are all positive or all negative for a particular laboratory. While this result may suggest particular systematic errors associated with the apparatus at any given laboratory, this suggestion tends to be negated by an inspection of the deviations about the mean for Material B (Fig. 10). Here the deviations for four of the eight laboratories are both positive and negative.

A closer examination of Table 4 reveals that one of the results (2.3) for Laboratory 4 is outlying. Indeed, this was precisely the datum for which a poor signal was noted during testing (see section also for the comments on anisotropy and texture). Therefore it seems appropriate to discard this outlying result. When this is done, the deviations about the mean for Material B group closely (Fig. 10). The mean and standard deviation for the dynamic Young's modulus are 159.16 and 2.84 GPa, respectively, for Material B.

In connection with the adjustment of the data a very important point arises. The determination of the density of the specimen is an intrinsic part of modulus determination for *all* the techniques used. Therefore it is necessary to consider the density results from

TABLE 4—*ASTM E28.03.05 dynamic Young's modulus interlaboratory study.*

Alloy B		Raw Data Table		
Laboratory	Specimen	*E*, GPa	Density, g/cm³	
1	2.1	161.5	8.34	IAI
	2.2	159.9	8.34	
	2.3	157.2	8.34	
2	2.1	164.1	8.392	Chen/Phillips
	2.3	155.7	8.225	
3	2.1	162.0	8.34	Lemmens
	2.1	161.8	8.34	
	2.1	160.8	8.34	
	2.3	158.4	8.34	
4	2.1	156.0*	8.25	NBS
	2.3	172.0**	8.25	
5	2.1	156.0	8.27	Texas A&M (PUCOT)
	2.3	162.0	8.26	
6	2.2	163.0	8.27	Texas A&M (Kinra)
7	2.1	156.8	8.20	3M
	2.3	155.8	8.17	
	2.3	158.0	8.17	
8	2.3	159.2	8.26	Modul-R

Density listed for Laboratory 3 was determined at Laboratory 1.
Material: Incoloy alloy 907, 19.05 mm thick, hot-rolled flat.
Specimens: 2.1: 6.35 mm diameter cylinder.
2.2: 25.4 mm diameter cylinder.
2.3: 1.91 by 6.35 by 101.6 mm flat strip.
*Wave propagation parallel to the length of the specimen.
**Wave propagation perpendicular to the length of the specimen.

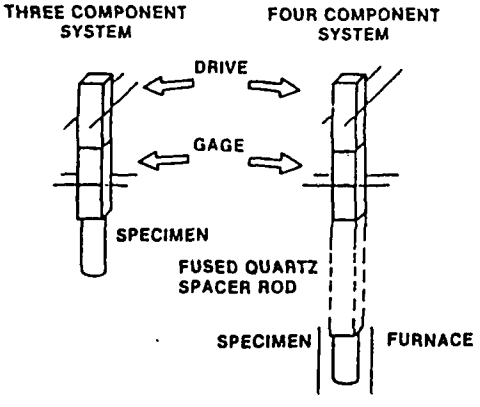

FIG. 5—*Schematic diagram of the PUCOT. Left-hand side: three-component system for measurements at room temperature; right-hand side: four-component system for measurements at temperatures above room temperature. Shown is the arrangement with longitudinal quartz crystals.*

TABLE 5—*PUCOT equations for the three-component system.*

$$L = (1/2f)(E/\rho)^{1/2} = \lambda/2$$
$$\tau(S) = m(S)^{1/2}\tau(DG)\tau(DGS)/A$$
$$A = \{\tau(DG)^2 m(DGS) - \tau(DGS)^2 m(DG)\}^{1/2}$$
$$E = 4\rho L^2/\tau(S)^2$$

L = specimen length
f = frequency
E = Young's modulus
ρ = density
λ = wavelength
τ = resonant period
S = specimen
D = drive crystal
G = gage crystal
m = mass

all the laboratories in more detail. Figures 11 and 12 show bar charts of density for Materials A and B. For Material A the mean density was found to be 8.361 g/cm³ with a standard deviation of 0.048 g/cm³; the corresponding values for Material B are 8.263 and 0.072 g/cm³. Again it must be remembered that at some of the laboratories the Archimedes method of density determination was used, while at others the density was determined from masses and physical dimensions of the specimens. That the deviations about the means for densities are mostly less than 0.08% is encouraging.

To proceed with the final adjustment of the dynamic Young's modulus data we have used what we term *common density* and *common mathematics*. *Common density* for the material is the value obtained by Laboratory 4 (NBS): Alloy A, 8.36 g/cm³; Alloy B, 8.25 g/cm³. (These values are very close to the means given in Figs. 11 and 12.) *Common mathematics* is a term indicating application of the same equations (including certain correction factors for shape and aspect ratio of the specimens, given by Spinner and

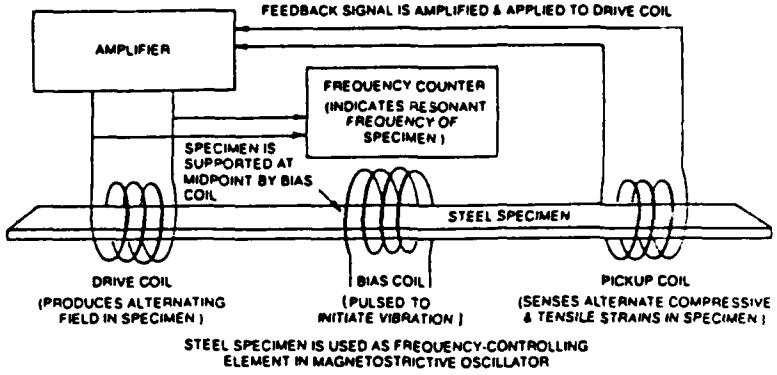

FIG. 6—*Schematic diagram of the magnetically excited resonance system known as the Modul-R.*

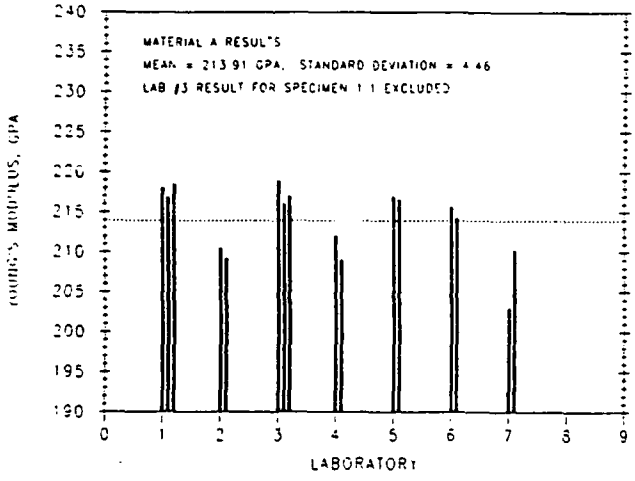

FIG. 7—*Values of dynamic Young's modulus for Material A measured in the laboratories taking part in the testing program.*

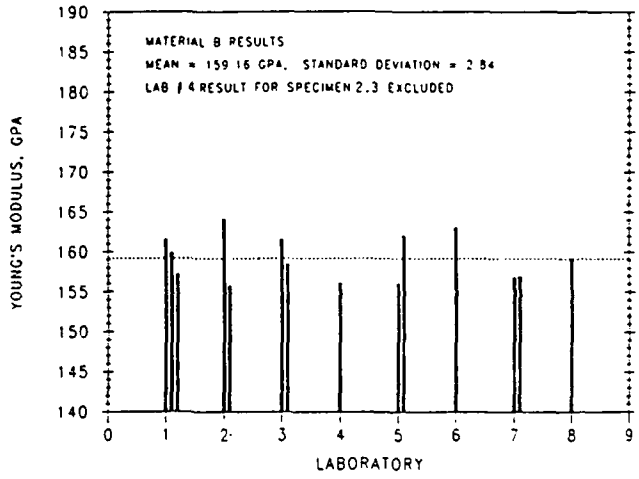

FIG. 9—*Values of dynamic Young's modulus for Material B measured in the laboratories taking part in the testing program.*

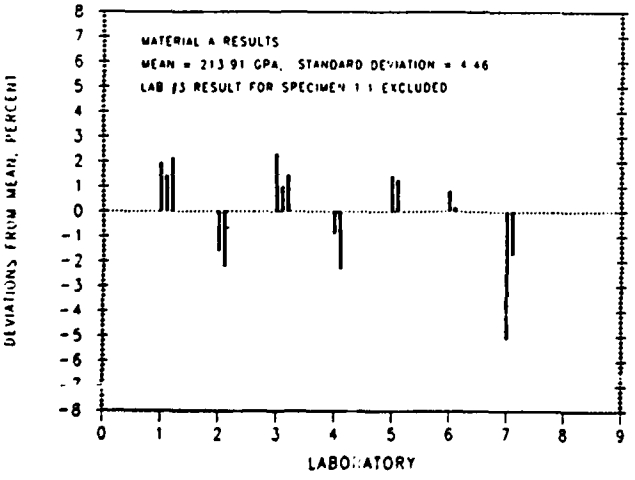

FIG. 8—*Percentage deviations from the mean value of dynamic Young's modulus for Material A.*

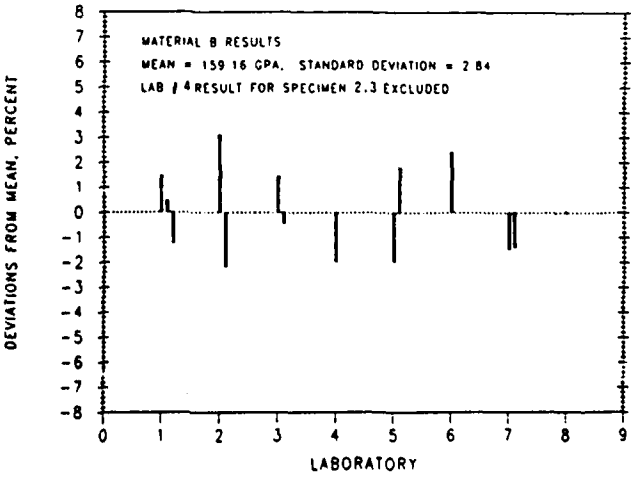

FIG. 10—*Percentage deviations from the mean value of dynamic Young's modulus for Material B.*

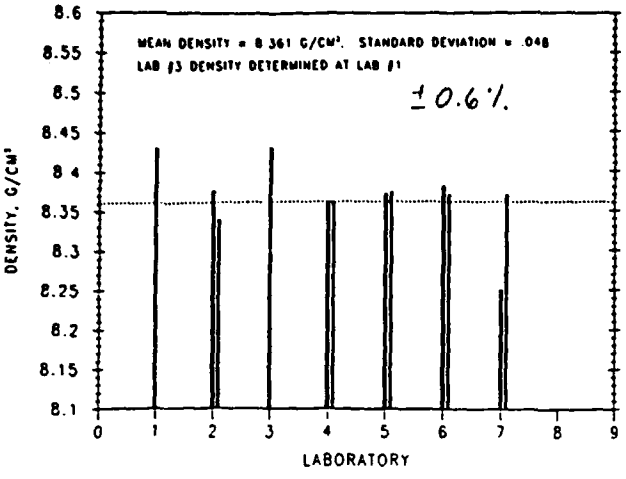

FIG. 11—*Values of density determined for Material A at the various laboratories.*

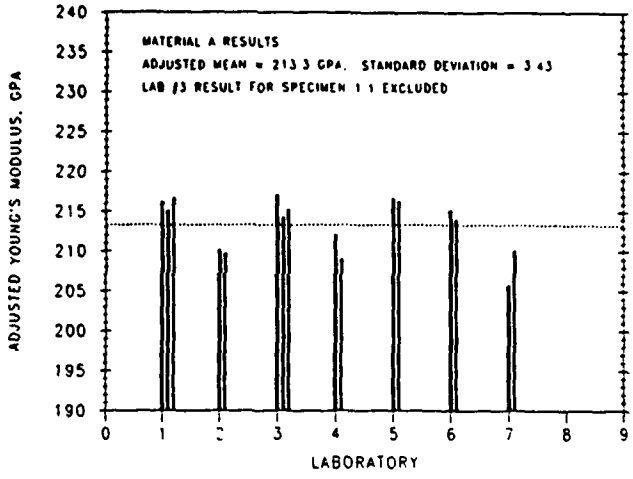

FIG. 13—*Dynamic Young's modulus results for Material A with adjustments for common density and common mathematics.*

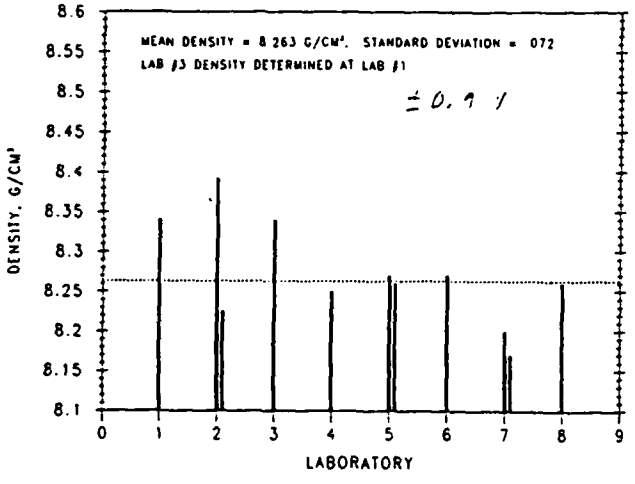

FIG. 12—*Values of density determined for Material B at the various laboratories.*

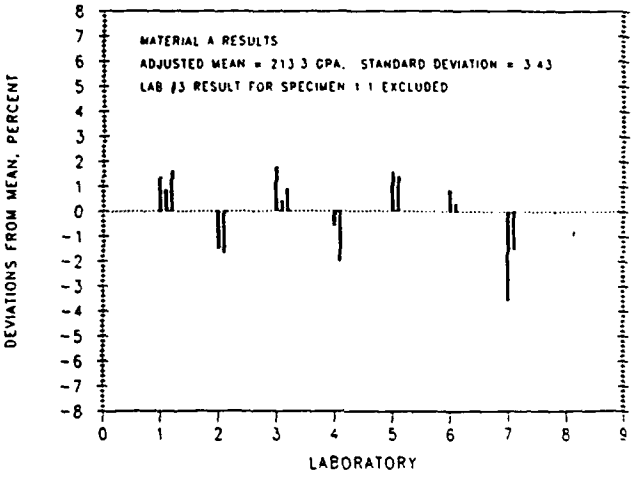

FIG. 14—*Percentage deviations from the mean value of dynamic Young's modulus for Material A with adjustments for common density and common mathematics.*

Tefft [2]) to convert measured values of frequency to values of modulus for the free-free beam technique (Laboratories 1, 2, and 7) and for the impulse technique (Laboratory 3). With these adjustments, the final results are presented in Figs. 13 to 16. For Alloy A the mean value of dynamic Young's modulus is 213.3 GPa with a standard deviation of 3.43 GPa (1.6%). The corresponding values for Alloy B are 160.59 and 2.37 GPa (1.5%), with the result for Specimen 2.3 from Laboratory 4 removed.

A further comment on the final adjustments of the dynamic Young's modulus data is in order. The value of modulus for Specimen A1.3 measured at Laboratory 7 was obtained using the first overtone rather than the fundamental. This would cause a lowering of the precision of the modulus value. The standard deviations (1.5 and 1.6%) about the means mentioned above are therefore larger than are potentially realizable by the dynamic techniques used.

To put a perspective on the quality of the results from this Interlaboratory Testing Program for dynamic Young's modulus, it is instructive to look at the results from the earlier round-robin study done at seven laboratories for static Young's modulus [17]. For the static modulus on a steel specimen the mean value was 211.3 GPa with a standard deviation of 5.1 GPa or 2.4%.

There does not appear to be any significant effect of frequency on the value of dynamic Young's modulus in the materials examined. Specifically, frequencies as low as 780 Hz (Laboratory 1) and as high as 15 MHz (Laboratory 4) were used for the modulus measurements, but no frequency dependence was established.

Conclusions

From this study of dynamic Young's modulus measurements, performed as an Interlaboratory Testing Program involving six types of apparatus, six different organizations, and specimens

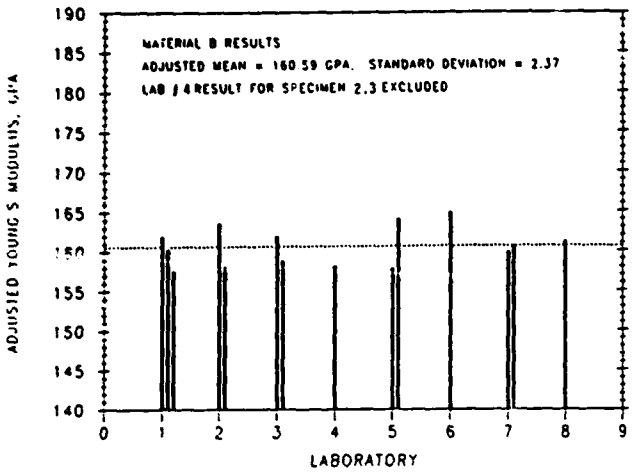

FIG. 15—*Dynamic Young's modulus results for Material B with adjustments for common density and common mathematics.*

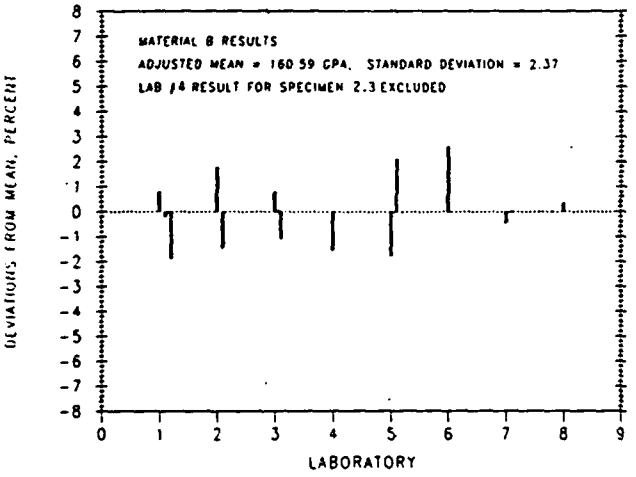

FIG. 16—*Percentage deviations from the mean value of dynamic Young's modulus for Material B with adjustments for common density and common mathematics.*

from a well-documented source, we can draw the following conclusions:

1. All the measurements of dynamic Young's modulus involved the basic wave equation (Eq 1) for the propagation of an elastic wave in an elastic medium.

2. The determination of the mass density of the specimens was an intrinsic part of the determination of dynamic Young's modulus for all the techniques used in this study.

3. All the techniques (free-free beam, impulse excitation, wave travel time, ultrasonic pulse spectroscopy, piezoelectric oscillation, and magnetically excited resonance) yielded values of dynamic Young's modulus that agreed closely with each other (to within 1.6%).

4. The mean value for dynamic Young's modulus for Inconel 600 (Alloy A) was determined as 213.3 GPa with a standard deviation of 3.4 GPa, while the corresponding values for Incoloy 907 (Alloy B) were 160.6 and 2.4 GPa, respectively. These modulus values are based on the density values of 8.36 and 8.25 g/cm^3 for Materials A and B, respectively, measured at NBS, and on common mathematical equations for certain techniques used in this study.

5. There does not appear to be any significant effect of frequency on dynamic Young's modulus in the materials tested for the frequency range 780 Hz to 15 MHz.

Acknowledgments

We are grateful to the following colleagues, most of them members of ASTM, who have contributed valuable time and advice during the period of the Interlaboratory Study: A. Fox, R. Willoughby, M. E. Lieff, J. A. Millane, T. Mellon, R. Kennedy, E. Dietrich, E. W. Filer, G. Hickcock, D. Dineff, R. Gassner, R. G. Baughan, D. DeMiglio, W. T. Groor, D. Scanlon, R. S. Strimel, S. B. Helms, W. Engelmaier, D. Germano, W. Pearce, J. E. Amaral, J. Moch, A. Perlov, N. L. Carroll, G. Foster, R. Papirno, W. Stange, T. Finke, D. Bray, J. D. Whittenberger, G. M. Ludtka, and L. Mordfin. Special thanks go to Inco Alloys International (IAI) for provision of specimens, to Dr. P. Ganesan for texture information, and to R. S. Davis of NBS for the values of common density used in the final analysis. M. D. Wyrick was responsible for the modulus measurements at IAI. Two of us (V.K.K. and V.D.) acknowledge financial support by the Air Force Office of Scientific Research under Contract F49620-83-C-0067 to Texas A&M University, College Station, Texas. The authors are most grateful to the reviewers of the manuscript for many helpful suggestions for its improvement.

References

[1] Pickett, G. in *Proceedings of ASTM*, Vol. 45, 1945, pp. 846-865.
[2] Spinner, S. and Tefft, W. E. in *Proceedings of ASTM*, Vol. 61, 1961, pp. 1221-1238.
[3] Wagel, R. L. and Walther, H., *Physics*, Vol. 6, 1935, pp. 141-157.
[4] Harris and Crede, *Shock and Vibration Handbook*, Vol. 1, pp. 1-14.
[5] Dickson, R. W. and Spinner, S., *Journal of Materials*, Vol. 3, Sept. 1968, pp. 716-724.
[6] Kolsky, H., *Stress Waves in Solids*, Dover Publications, New York, 1963.
[7] Szilard, J. in *Ultrasonic Testing: Non-Conventional Testing Techniques*, J. Szilard, Ed., Chapters 1, 2, and 9, Wiley, New York, 1982.
[8] Papadakis, E. P. in *Physical Acoustics Principles and Methods*, W. P. Mason and R. N. Thurston, Eds., Vol. 12, Chapter 5, Academic Press, New York, 1976.
[9] Papadakis, E. P., *Transactions of IEEE*, Vol. SU-16, 1969, pp. 210-218.
[10] Papadakis, E. P. in *Physical Acoustics Principles and Methods*, W. P. Mason and R. N. Thurston, Eds., Vol. 11, Chapter 3, Academic Press, New York, 1975.
[11] Papadakis, E. P., *Journal of the Acoustical Society of America*, Vol. 42, 1967, pp. 1045-1051.
[12] Dayal, V., Kinra, V. K., and Eden, J. G., "Ultrasonic Nondestructive Testing of Fiber Reinforced Composites," in *Proceedings*, International Symposium on Composite Materials, Beijing, 1986, pp. 899-904.
[13] Kinra, V. K. and Dayal, V., "A New Technique for Ultrasonic NDE of Thin Specimens," *Experimental Mechanics*, Sept. 1988, pp. 288-297.
[14] Marx, J., *Review of Scientific Instruments*, Vol. 22, 1951, pp. 503-509.
[15] Robinson, W. H. and Edgar, A., *IEEE Transactions of Sonics and Ultrasonics*, Vol. SU-21, 1974, pp. 98-105.
[16] Harmouche, M. R. and Wolfenden, A., *Journal of Testing and Evaluation*, Vol. 13, 1985, pp. 424-428.
[17] ASTM Static Modulus Study (E28.03).

(A)

NON-DESTRUCTIVE EVALUATION OF MATRIX CRACKS IN FIBER-REINFORCED COMPOSITES BY LEAKY LAMB WAVES

V. Dayal and V.K. Kinra

Mechanics and Materials Center and Aerospace Engineering Department Texas A&M University, College Station, TX-77843, USA

Leaky Lamb waves have been used for the non-destructive evaluation of fiber-reinforced composites. Two fundamental acoustic properties of the Lamb waves, namely, the wavespeed and attenuation have been measured. Stiffness is deduced from the wavespeed. The damage mode selected for this study is matrix cracking. Matrix cracks are introduced in the cross-ply laminate by static loading. Wavespeed and attenuation are measured after each damage state. As expected, the in-plane stiffness decreases and the attenuation increases as the damage increases. It was observed that the stiffness reduction was dependent on the stacking sequence while the attenuation was dependent on the scattering cross-section of the cracks, $k_1 a$.

INTRODUCTION

Matrix cracking generally is the first mode of failure in fiber-reinforced composites. This is a micro- be monitored, changes in stiffness should be measured.

ure in fiber-reinforced composites. This is a micro-level failure and not being self sustaining mechanism, is distributed throughout the structure. The strong fibers act as crack arresters and stress relieving takes place in the vicinity of the cracks. As a result the crack does not grow but creates a situation where next cracking takes place somewhere else. Though the integrity of the structure is not lost, overall stiffness of the structure is reduced, and its damping is increased.

Composites are being used as load bearing members, especially in the aerospace structures because of their excellent strength-to-weight ratio and the ability to tailor there directional properties. Reduction in stiffness can result in change in response of the structure upon loading, which is critical from the designers point of view. Hence, a non-destructive evaluation of the composite structure is necessary where even before large size defects can

ured.

Ultrasonic NDE was used for the through-the-thickness evaluation of cross-ply fiber-reinforced composites(1-3). It was found that though the ultrasonic attenuation was a very sensitive damage metric, wavespeed was not. Hence attenuation can be used as a sensitive damage metric. Master curves of attenuation as a function of crack length, obtained in (3) show such a possibility of NDE applications.

From the designers point of view, out-of-plane stiffness is not an important design factor. In-plane stiffness is an important design criteria and hence we have used Lamb waves to measure it in the work reported here. Ultrasonic waves travelling in the plane of the plate have been used to measure the changes in wavespeed and attenuation. This mode of propagation is called the Lamb wave (or plate wave) mode. When the plate is immersed in a fluid, the Lamb

(A)

waves travelling in the plate leak energy into the surrounding fluid. These waves in the fluid have been named "leaky Lamb waves". These leaky Lamb waves are sensed and the wavespeed and attenuation in the plate material is measured. In the Lamb wave mode of wave propagation attenuation in undamaged specimens is due to energy leaked into the fluid. Bar-Cohen and Chementi (4) have utilized the leaky Lamb waves for the NDE of damage in fibre-reinforced composites. They have shown that various forms of damage can be identified by a null-zone movement method. When a wave is incident upon the plate, the specular reflection from the plate takes place along with the generation of Lamb waves in the plate. Due to phase change in the leaky waves, the specular reflection and the leaky wave interfere and a well defined null zone is observed; the movement of the null zone has been related to various defects. This movement is used in a C-Scan type setup to map the damage. The work here takes an entirely different course. The receiving transducer is placed in such a position that the specular reflection is avoided and only the leaky

$$c^2 = E_1/\rho(1-\nu_{12}\nu_{21}) \qquad (1)$$

where f is the test frequency, 2d is the plate thickness, c is the Lamb wavespeed, E_1 is an in-plane modulus, and ν_{12} and ν_{21} are the two in-plane Poisson's ratios. For the composites tested during this investigation $\nu_{12}\nu_{21} \ll 1$ and hence eq (1) reduces to

$$c^2 = E_1/\rho \qquad (2)$$

The refraction of ultrasonic waves through a plate can be schematically shown in Fig. 2. From Snell's law

$$\mathrm{Sin}(\theta_i)/\mathrm{Sin}(\theta_r) = v_w/c \qquad (3)$$

where v_w is the wavespeed in water, θ_i and $\theta_r = \pi/2$ are the angles of incidence and refraction, respectively. Thus,

$$c = v_w/\mathrm{Sin}(\theta_i) \qquad (4)$$

specular reflection is avoided and only the leaky waves are sensed. Shown in Fig. 1 are the two configurations of the receiver; first, the transmission and second, the reflection. We have used the transmission mode in all our work. The wavespeed and attenuation in the specimen are measured from the received signal. The specimen is damaged and transverse cracks are introduced in the cross-ply laminates. We present here some results for the NDE of cross-ply laminates by leaky Lamb waves.

THEORY

The detailed derivation of the dispersion equations for a general balanced symmetrical composite laminate immersed in a fluid are reported in (5). The basic symmetrical mode (s_0) has been selected for the tests. In this mode it can be shown (6) that when f.d is small

$$c = v_w/\mathrm{Sin}(\theta_i) \tag{4}$$

combining eq (4) with eq (1),

$$E_1 = \rho[v_w/\mathrm{Sin}(\theta_i)]^2 \tag{5}$$

This equation is used for the measurement of the in-plane stiffness in this work.

It is obvious from eq (5) that the measurement of θ_i will be an important factor in the accuracy of measurement. A very simple but elegant method has been devised to accurately ascertain the Lamb angle. As shown in Fig. 3 the receiver is moved by a distance, x. A very elementary calculation shows that at the correct Lamb angle total travel time is independent of x. In other words the moving of the receiver does not change the arrival time of the signal at the receiving transducer; on the scope a difference of even 0.1 degrees in θ_i resulted in a measurable shift of the signal on the time axis. The decrease in the

amplitude of the signal as the receiver is moved, is recorded and by fitting an exponential curve through the points, the attenuation coefficient is calculated. It may be pointed out here that in the undamaged specimen, at the frequency tested, attenuation was found to be negligibly small. When the damage is introduced substantial increase in attenuation is observed. Thus it is safe to assume that the measured attenuation is entirely due to the damage. The accuracy of measurement of modulus is estimated to be 2%, and for attenuation it is about 10%.

EXPERIMENTAL PROCEDURE

The block diagram of the experimental setup is shown in Fig. 4. The pulse generator produces a trigger signal which is used to trigger the signal generator and also set the initial time for the digitizing oscilloscope. The pulse generator produces a train of sinusoidal signal. Since these signals are typically of a few volts in amplitude, a power amplifier is used to amplify the signal to about 200 Volts. This amplified signal is then fed into the transmitting transducer. The transducer produces an ultrasonic

the correct Lamb angle, the length of the specimen between the transducer is increased. To offset this increase, the two transducers are moved laterally, as shown in Fig. 5, such that same length of the specimen is interrogated throughout the experiments. Since repeatability is very important in our measurements, the specimen holder is designed so that exact replacement of the specimen is achieved every time. A tab is fixed on the specimen holder and the specimen is butted against it every time.

All composite specimens are made of Magnamite AS4/3502 graphite/epoxy prepreg tapes manufactured by Hercules Inc. Transverse cracks were chosen to be the mode of damage for all the studies reported here. Towards this end cross-ply laminates with layups of the type $[0_n 90_m]_s$ were fabricated. Typically the specimen are plates of 1"X11" size.

All loading to induce damage in the specimen was performed on INSTRON Model 125 equipped with a 20,000 lb load cell. The tests were conducted in the stroke-control mode. The cross-head speed used was 0.05 in/min. in the initial stages of damage. When nearing

of a few volts in amplitude, a power amplifier is used to amplify the signal to about 200 Volts. This amplified signal is then fed into the transmitting transducer. The transducer produces an ultrasonic wave which is transmitted through the water and specimen to the receiving transducer. The receiver sends the signal to the signal amplifier, which provides the oscilloscope with a signal of about one volt. The digitizing oscilloscope averages the signal over 64 samples and stores the average. On demand from the computer, the necessary information is provided by the oscilloscope over an IEEE-488 bus. The wavespeed and attenuation are then calculated. Entire operation of the oscilloscope is controlled by the computer.

Water is used as an acoustic couplant; the transducers are mounted inside a water bath. Transmitter and receiver are mounted on two travelling mechanisms graduated to 0.001 inch and the specimen is placed in a holder mounted on a turntable which is graduated to 0.1 degrees. When the specimen is rotated to achieve

[illegible] on INSTRON model [illegible]

load cell. The tests were conducted in the stroke-control mode. The cross-head speed used was 0.05 in/min. in the initial stages of damage. When nearing the ultimate strength of the specimen the speed was reduced to 0.02 in/min.

The edges of the specimens were polished with 5 and 1 micron alumina powder. This is done to get good quality edge replications. A record of the cracks developed in the specimen was maintained in the form of edge replications. In order to open the cracks, the specimens are loaded in the INSTRON machine to about 500 lbs. The replicating tape is softened by acetone and pressed against the edge of the specimen. The tape material flows into the crack and hardens in about 30 seconds. The tape is removed and the replica of the cracks can be viewed under a microfiche reader.

In the early stages of this work, water seepage into

the cracks was found to be a major source of error and this was prevented by coating the edges with a strippable coat.

RESULTS

Although dispersion equations for Lamb waves in homogeneous materials were available in the published literature, these works were based on the assumption that the attenuation due to leakage is negligibly small. This assumption is reasonably valid as long as $\rho'/\rho \gg 1$ where ρ' and ρ are the densities of the plate and the immersion fluid, respectively. If one is studying steel/water, ρ'/ρ is, in fact, large compared to one. However, for the fiber-reinforced composites studied in this work, $\rho'/\rho=1.53$ and therefore, neglecting the inertial loading of water will result in gross error in the dispersion curves. Therefore, we have derived an exact solution for the dispersion equations for an anisotropic plate immersed in a fluid and have obtained the dispersion curves as well as the attenuation curves. As a calibration step we have calculated the dispersion and attenuation curves for aluminum and these are shown in Fig. 6a and 6b.

received and is shown as amplitude peak in the signal. At $k_t d=2.25$, for this test, three peaks are obtained. Converted to wavespeeds these points are shown as discrete points on the dispersion curves in Fig. 6a. The measurement of attenuation is made as follows. The specimen angle is fixed at the Lamb angle of interest with the transducers suitably placed. Next, the receiver is moved away by 0.5 inch in steps of 0.05 inch and the amplitude at a particular peak is recorded. An exponential decay curve is passed through these points and by a least-square-error, the attenuation coefficient is obtained.

Attenuation coefficient calculated at the three Lamb angles are shown as discrete points on Fig. 6b. Notice that for a_0 and s_1 modes the comparison between theory and experiment is excellent but for s_0 mode there is some error. This error can be easily explained by the fact that since at s_0 the attenuation is very high, the energy dissipation into water is very high and in a very short distance, the energy at the receiver becomes very low; this results in larger errors. On the other hand for a_0 and s_1 modes the signal is fairly high and hence excellent comparison with theory. These tests were repeated at dif-

fluid and have obtained the dispersion curves as well as the attenuation curves. As a calibration step we have calculated the dispersion and attenuation curves for aluminum and these are shown in Fig. 6a and 6b.

The experiment performed on an aluminum plate is as follows. The plate is mounted in the rotating specimen-holder and the transducers are set such that they are not directly facing each other. The transmitter is excited with a sinusoidal wave-train of about 20 cycles at the frequency of interest. The waves sensed at the receiver are recorded and the voltage and time at a particular peak of the signal (about tenth) are measured. The angle of the specimen is changed. Since the length of the specimen between the transducers is increased due to the rotation, the transducers are moved closer so that exactly the same length of the specimen is under test throughout. Typical angle of incidence and the peak amplitude signal is shown in Fig. 7. At the angle of incidence when the Lamb wave can be sustained in the specimen a large signal is

is very high and in a very short [illegible]

at the receiver becomes very low; this results in larger errors. On the other hand for a_0 and s_1 modes the signal is fairly high and hence excellent comparison with theory. These tests were repeated at different frequencies and the results are shown as discrete points on Figs. 6a and 6b. Thus the experiment verifies the theory and vice versa. The importance of the attenuation curves is also spelled out correctly. Tests should be performed at low attenuation to get reliable results.

Before embarking on the NDE of composites, we have performed some theoretical studies to find out the effect of stiffness degradation on the theoretically calculated Lamb wavespeeds. The four elastic constants c_{11}, c_{33}, c_{55} and c_{13} are the contributors to the dispersion equations. In this study one stiffness coefficient is degraded at a time and the Lamb wavespeed calculated. The studies are made on a $[0\ 90_4]_s$ laminate. The effects of the degradation in stiffness

constants on the basic symmetric and asymmetric modes, s_0 and a_0 respectively, are studied. The results for the symmetric mode at a f.d=0.25 MHz-mm are shown in Fig. 8. Only c_{11} contributes to the reduction in the wavespeed. The effect of c_{33} and c_{13} is very small and the effect of c_{55} is practically zero. A very interesting result is that if the degradation takes place in c_{13} then the wavespeed increases. Shown in Fig. 9 is the effect of stiffness degradation on the a_0 mode at f.d=0.5 MHz-mm. It is observed that the major contributor in this case is c_{55} but contributions due to c_{11} and c_{33} are not negligible. The c_{33} behaved in such a way that its decrease results in an increase in Lamb wavespeed. But c_{13} does not contribute to the change in wavespeed. The conclusions of this study are that the Lamb wave technique is useful in measuring the degradation in c_{11}, which can be made with tests in s_0 mode. To some extent, by using the a_0 mode the degradation in c_{55} can be studied. Since contributions from other modes can affect the results, the confidence level for the results from a_0 mode will be lower.

Based on the above study and the theoretical estimates it was decided that the measurements of in-

laminate is obtained by the tensile testing and the corresponding wavespeed is shown as an arrow on the figure.

The first specimen tested to study the effect of transverse cracks on the Lamb wavespeed and attenuation is $[0\ 90_3]_s$ laminate. The tests are conducted at a frequency of 0.5 MHz with f.d=0.275 MHz-mm. The reduction in the normalized stiffness as a function of number of cracks per inch as damage progresses is shown in Fig. 11. The normalized stiffness is defined as E/E_0 where E_0 is the stiffness of the undamaged laminate and E is the stiffness of the damaged laminate. The increase in attenuation in the laminate during this test is shown in Fig. 12. The attenuation coefficient, k_2, is plotted against the number of cracks. Attenuation increases steadily as the damage increases. This result is as expected since higher the number of cracks, the larger is the cumulative scattering cross-section and hence larger is the increase in attenuation.

The second set of tests was performed on a $[0\ 90_4]_s$ laminate. The test is performed at 0.5 MHz with f.d=0.355 MHz-mm. The reduction in stiffness for this

c_{55} can be studied. Since contributions from other modes can affect the results, the confidence level for the results from a_0 mode will be lower.

Based on the above study and the theoretical estimates it was decided that the measurements of in-plane stiffness, c_{11}, can be accurately made from the s_0 mode. This is the mode which is used in all the results presented in the following.

Next, the tests were performed on a $[0\ 90_3]_s$ graphite/epoxy composite. The dispersion curves for this specimen are shown in Fig. 10a. The solid lines are for symmetric mode and dashed lines for asymmetric modes. The attenuation curves for various modes are shown in Fig. 10b. The tests for Lamb wavespeed and attenuation as described earlier are performed and the results are shown as discrete points on Figs.10a and 10b. The theoretical curves are from stiffness values calculated by the rule of mixtures(8) and hence some discrepancy between theory and experiments is to be expected. The static stiffness of the scattering cross-section and hence larger [illegible] increase in attenuation.

The second set of tests was performed on a $[0\ 90_4]_s$ laminate. The test is performed at 0.5 MHz with f.d=0.355 MHz-mm. The reduction in stiffness for this laminate is shown in Fig. 13. Also shown in the figure is the damage state and the position of the transmitter (TR) and receiver (R). Observe that in going from damage state 3 to state 4, though there was a substantial increase in the total number of cracks in the specimen, the number of cracks in the region interrogated by the transducer did not increase. As a consequence no change in the stiffness of the specimen was recorded. This is very reassuring for it demonstrates that our measurement reflects local changes in the stiffness. For this specimen, stiffness reduced by about 30 % as compared to the virgin state. In comparison to the reduction for the $[0\ 90_3]_s$ laminate it is observed that the stiffness reduction for this laminate is larger. The reason for this is that the net contribution of the eight-90°

plies to the overall stiffness is more than the contribution of six-90° plies and hence failure of plies in the $[0\ 90_4]_s$ laminates results in a higher reduction in relative stiffness.

The next set of tests were performed on a $[0_2 90_2 0]_s$ laminate. The reduction in stiffness as transverse cracks are introduced is shown in Fig. 14. Observe a smaller reduction in stiffness. Even though this laminate has four-90# plies, they are divided into groups of two, and also, the total number of 0# plies in this laminate is increased three times. Thus the total contribution of the 90# plies to the overall stiffness is very low and hence their failure results in less reduction in stiffness.

The attenuation increase in the three laminates tested are combined together and shown in Fig. 15. Shown also in the figure are the k_1a for the three laminates. The purpose of this presentation is to demonstrate the effect of the normalized scattering cross-section of the cracks on the attenuation. In $[0_2 90_2 0]_s$ laminate $k_1a=0.06$. As is well known this is the so-called Rayleigh scattering regime; thus the scattering cross-section of the cracks is very small. The waves pass through the plate without seeing the ply laminates. The stiffness decrease with damage in the three laminates; the extent of stiffness reduction depending on the laminate layup. Attenuation was very sensitive to damage and an increase in attenuation was measured for the three laminates. It was observed that attenuation increase was higher in laminates with k_1a closer to one. From the purposes of NDE both wavespeed and attenuation variations are good damage metrics.

REFERENCES

1. Ringermacher, H.I., 'Ultrasonic velocity characterization of fatigue damage in graphite/epoxy composites', Proc. IEEE 1980 Ultrasonic Symp., Boston, pp 957-960 (Nov 1980)

2. Cantrell, J.H.,Jr., Winfree,W.P., Heyman,J.H., and Whitcomb,J.D., 'Multiparameter characterization of fatigue damage in graphite/epoxy composite material', Proc. IEEE 1980 Ultrasonic Symp., Boston, pp1003-1005 (Nov 1980)

3. Eden, J.G., 'The application of Ultrasonics to assess damage in composite materials', M.S. Tnesis 1985, Texas A&M University, College Station, Tx 77843 (1985)

4. Bar-Cohen, Y., Chementi, D.E., 'NDE of defects in composites using leaky Lamb waves',Proc. 15th. Symp. on NDE Sponsored by NTIAC & SWRI and South Texas Section of ASNT, San Antonio, TX, (Apr 1985)

5. Dayal, V., 'Non-destructive evaluation of fiber-reinforced composites by ultrasound', Ph.D. thesis, Texas A&M University, College Station, TX 77843, (1987)

6. Habegar,C.C., Mann,R.W., and Baum,G.A. 'Ultrasonic plate waves in paper', Ultrasonics, pp 57-62, (Mar. 1979)

cross-section of the cracks on the attenuation. In $[0_2 90_2 0]_s$ laminate $k_1 a=0.06$. As is well known this is the so-called Rayleigh scattering regime; thus the scattering cross-section of the cracks is very small. The waves pass through the plate without seeing the cracks and as a result the increase in attenuation is very low. For $[0\ 90_3]_s$ $k_1 a=0.26$ and the cracks are able to scatter the waves to a considerable extent. For the $[0\ 90_4]_s$ laminate $k_1 a=0.45$ and the observed increase in attenuation is very high.

CONCLUSIONS

Stiffness degradation due to damage is an important design criteria and through-the-thickness measurements show that, as expected, out-of-plane stiffness does not change due to matrix cracks in cross-ply laminates. The in-plane stiffness measurements were made to record the stiffness degradation due to matrix cracks by the use of Lamb waves in three cross-

on NDE Sponsored by NTIAC & SwRI and South Texas Section of ASNT, San Antonio, TX, (Apr 1985)

5. Dayal, V., 'Non-destructive evaluation of fiber-reinforced composites by ultrasound', Ph.D. thesis, Texas A&M University, College Station, TX 77843, (1987)

6. Habegar,C.C., Mann,R.W., and Baum,G.A. 'Ultrasonic plate waves in paper', Ultrasonics, pp 57-62, (Mar. 1979)

7. Agarwal,B.D., Broutman,L.J.,Analysis and Performance of Fiber Composites, John Wiley & Sons, NY, p20, (1980)

ACKNOWLEDGEMENT

The financial support of the Air Force Office of Scientific Research under Grant No. AFOSR-84-0066 is gratefully acknowledged.

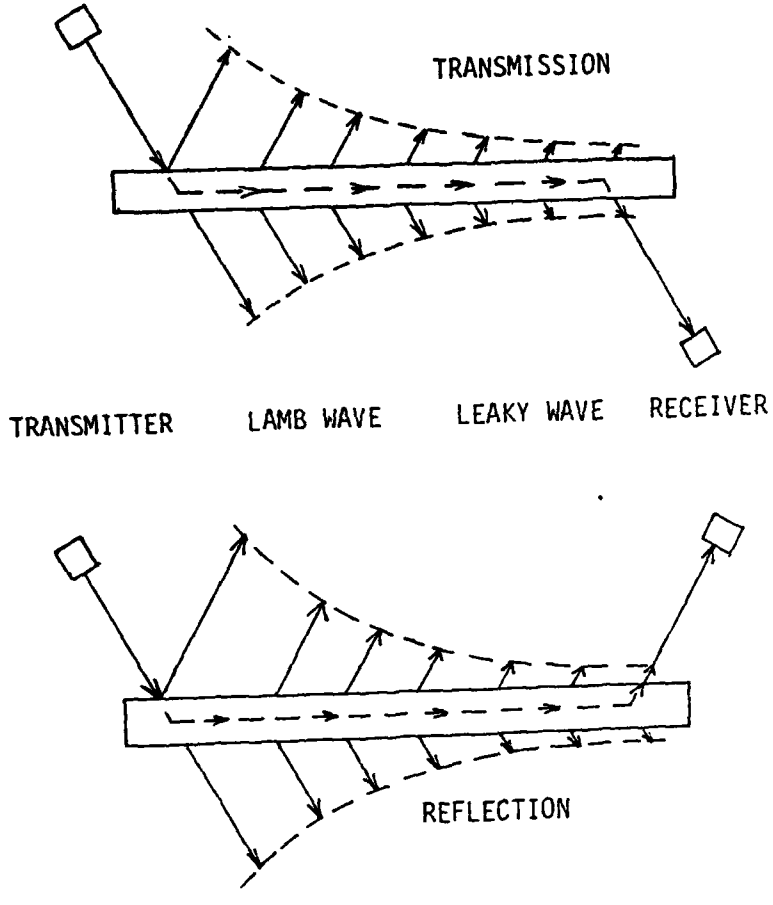

Figure 1 Generation and propagation of leaky Lamb waves immersed in a fluid.

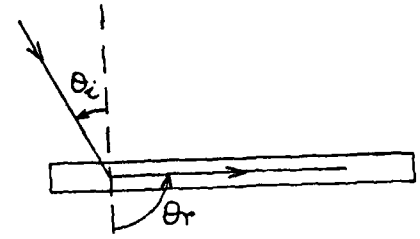

Figure 2 Refraction of wave in a plate

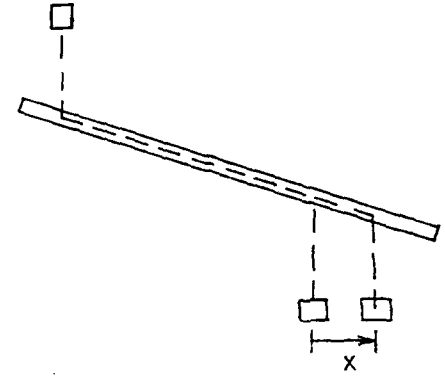

Figure 3 Receiver movement to check for Lamb angle and measure attenuation.

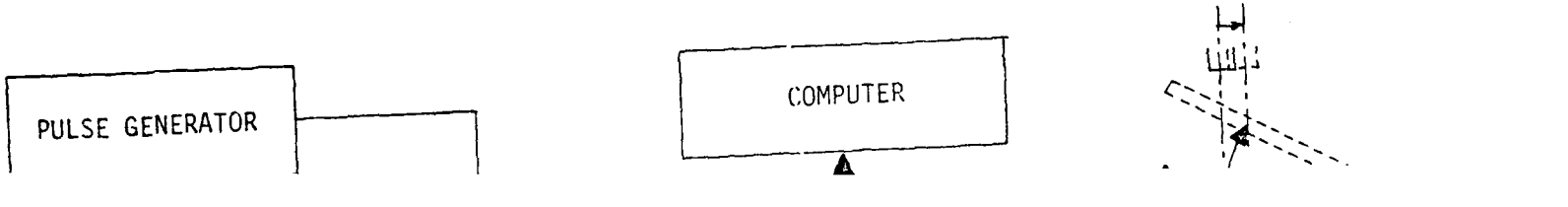

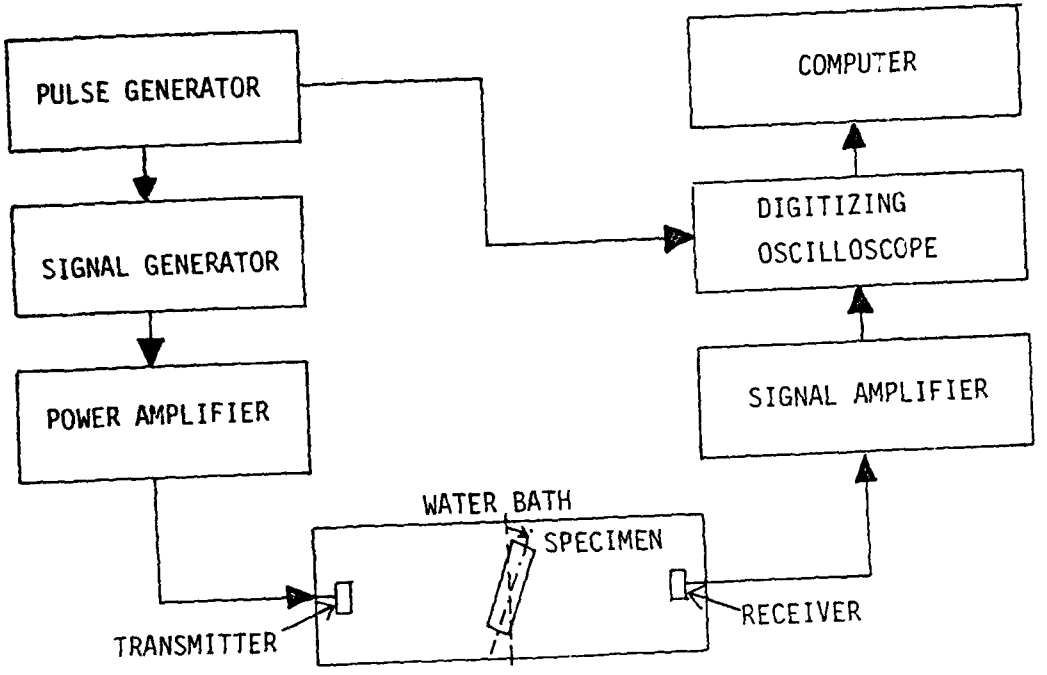

Figure 4 Block diagram of the experimental setup

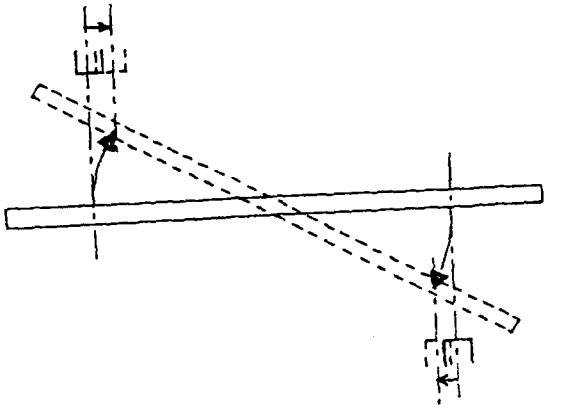

Figure 5 Transducer movement to compensate for specimen rotation

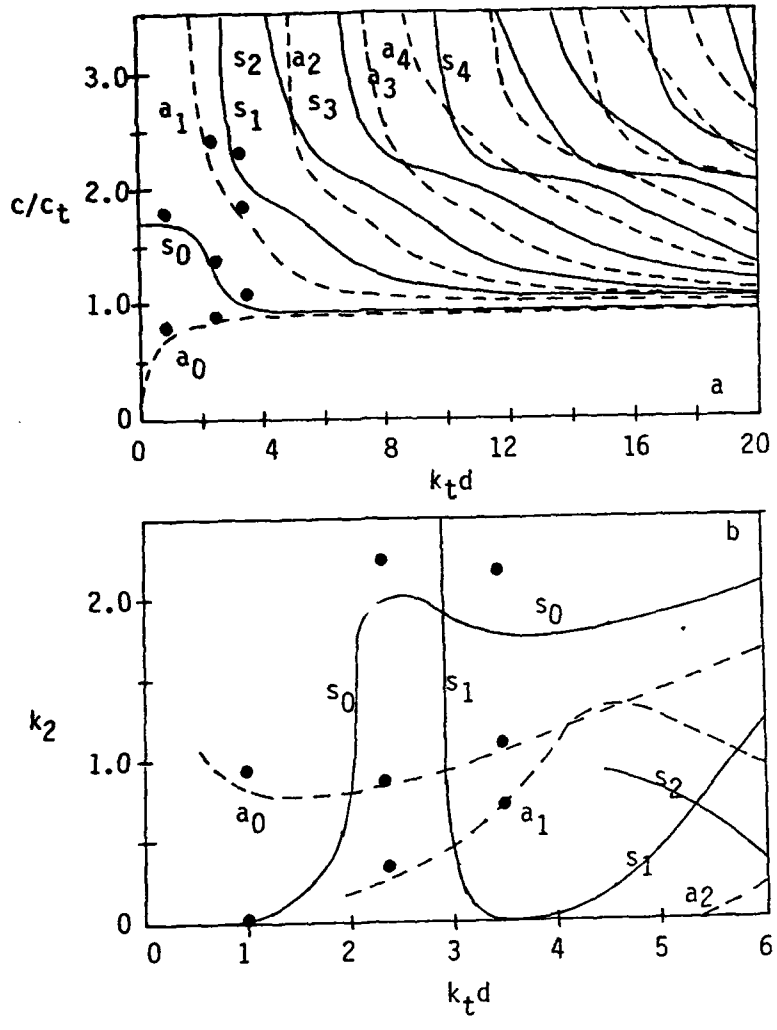

Figure 6 (a) Dispersion curve, (b) attenuation curve k_2(Nepers/cm) for aluminum in water

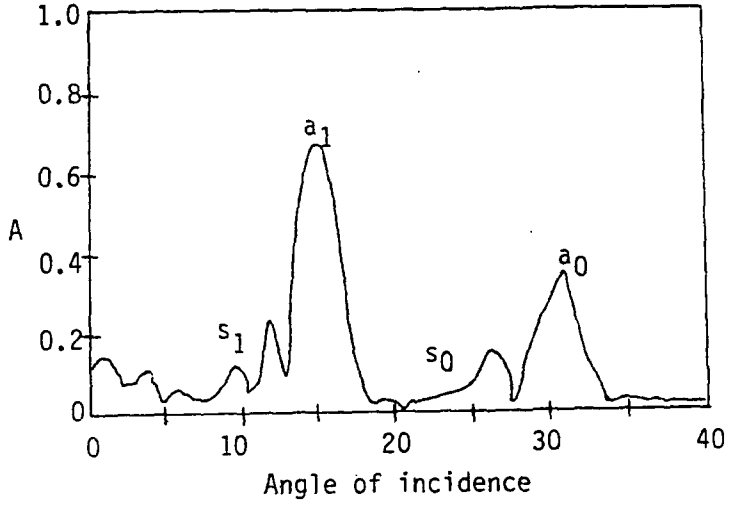

Figure 7 Received signal amplitude (A) as a function of angle of incidence, aluminum $k_t d$=2.25

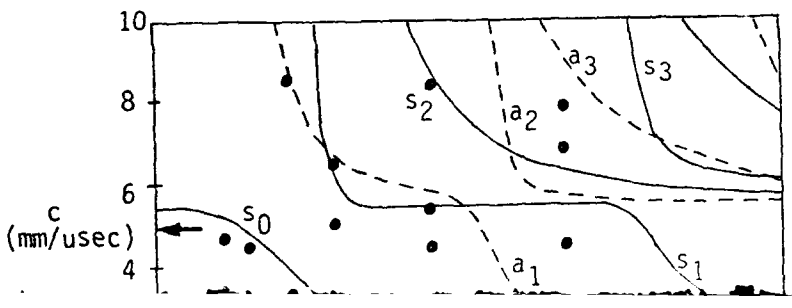

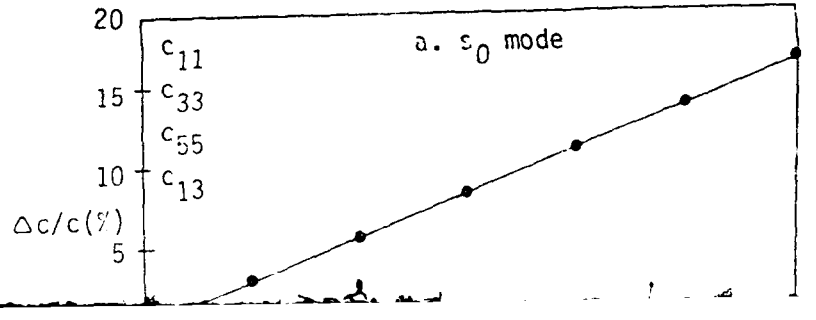

k_2(Nepers/cm) for aluminum in water

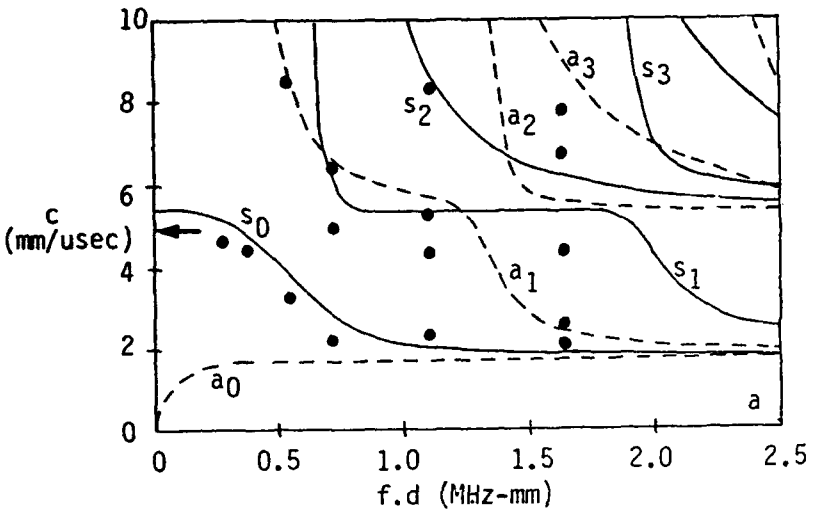

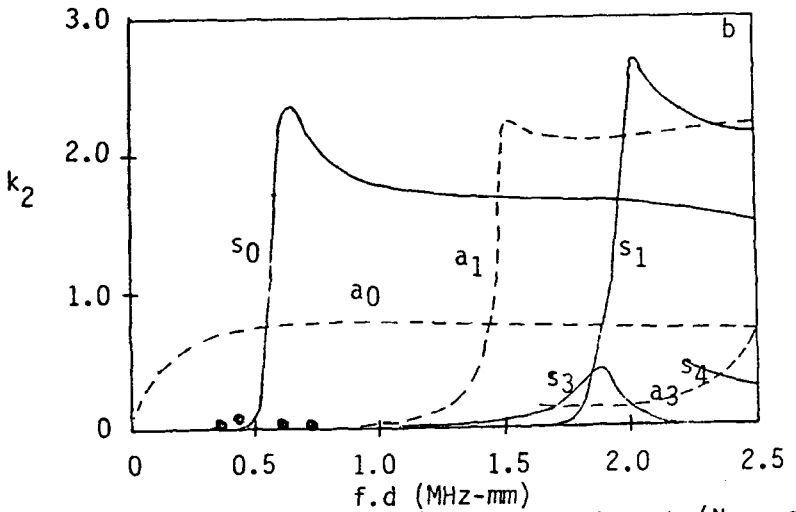

Figure 9 (a) Dispersion , (b) Attenuation, k_2(Nepers/mm) for $[0\ 90_3]_s$ laminate in water .
Arrow shows wavespeed determined from modulus obtained by tensile test.

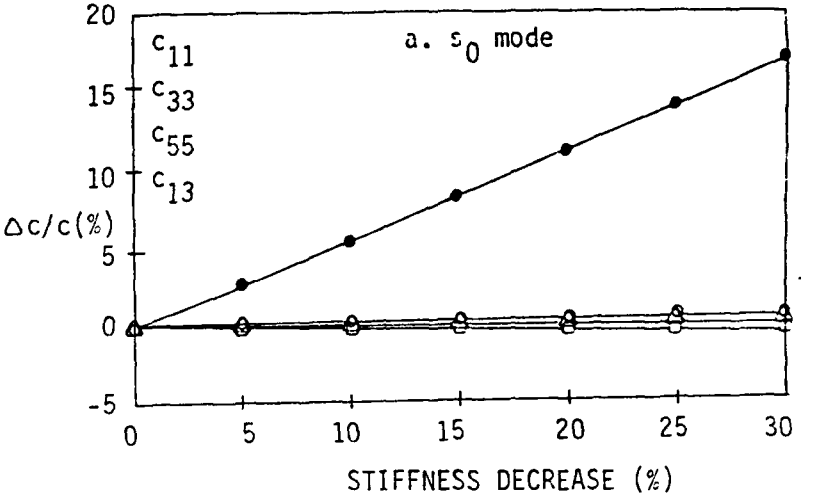

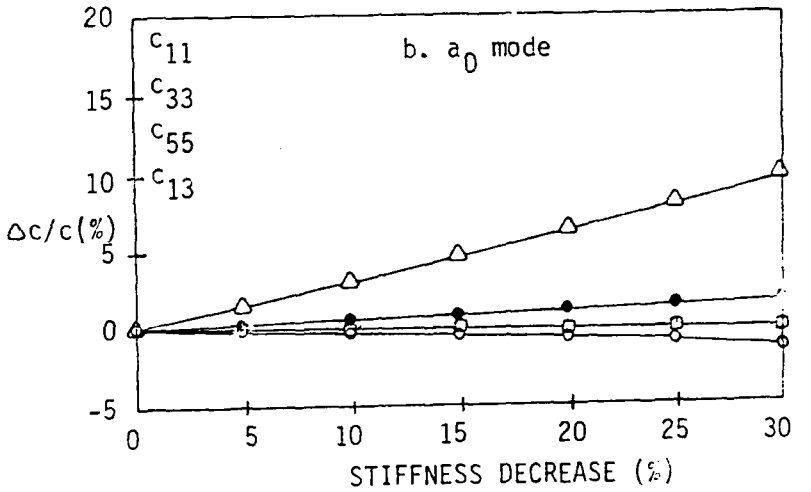

Figure 8 Effect of stiffness degradation on Lamb wave speed of $[0\ 90_4]_s$ laminate (a) on s_0 mode, (b) on a_0 mode

(A)

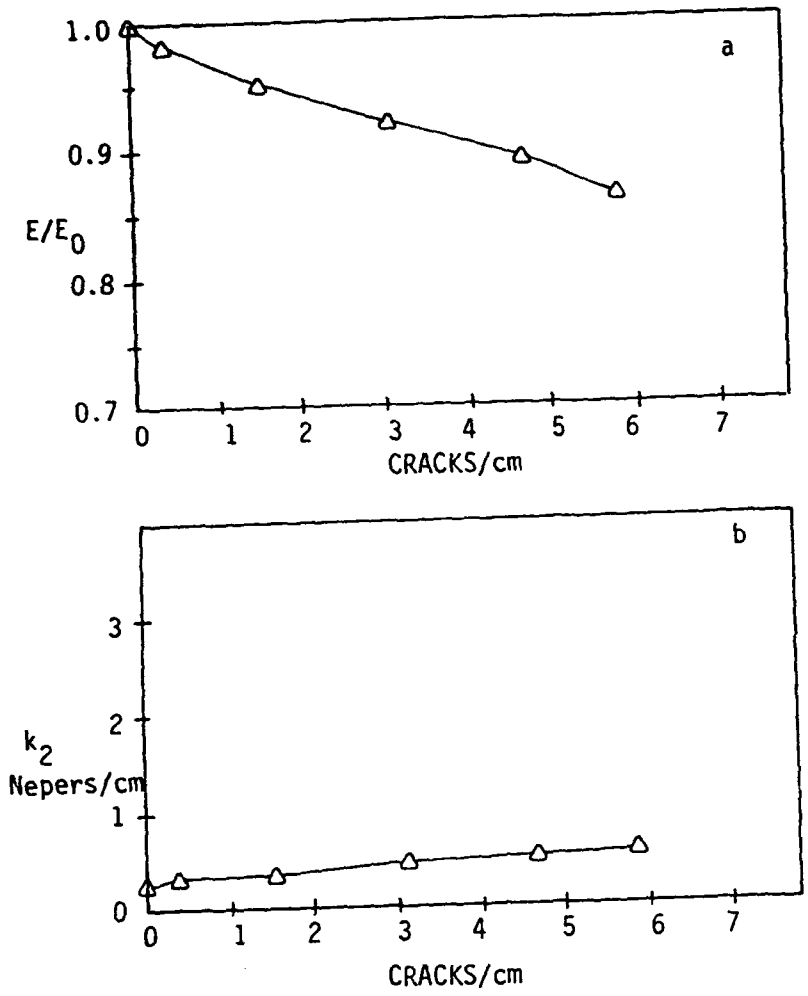

Figure 10 (a) Reduction in stiffness, (b) increase in attenuation in a [0 90_3]s laminate, f=0.5 MHz, d=0.55 mm.

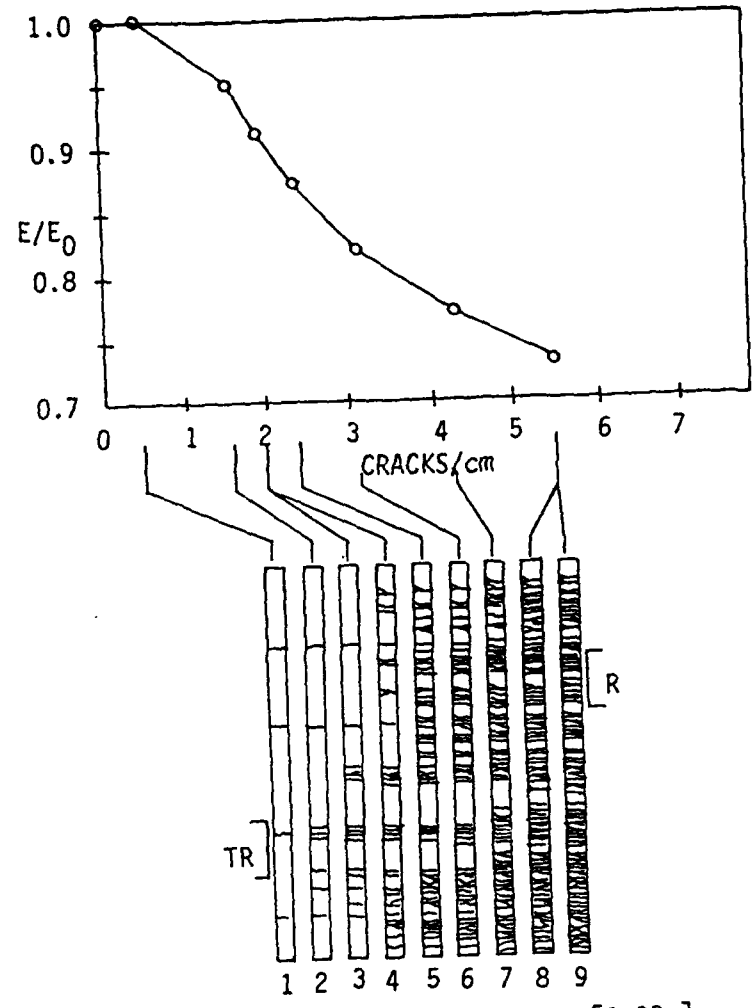

Figure 11 Reduction in stiffness in a [0 90_4]s laminate, f=0.5 MHz, d=0.71 mm.

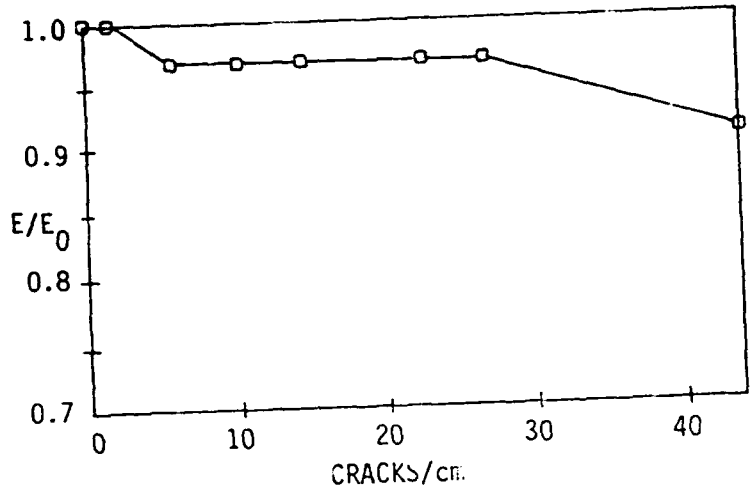

Figure 12 Reduction in stiffness in a $[0_2 90_2 0]$ laminate, f=0.5 MHz, d=0.55 mm.

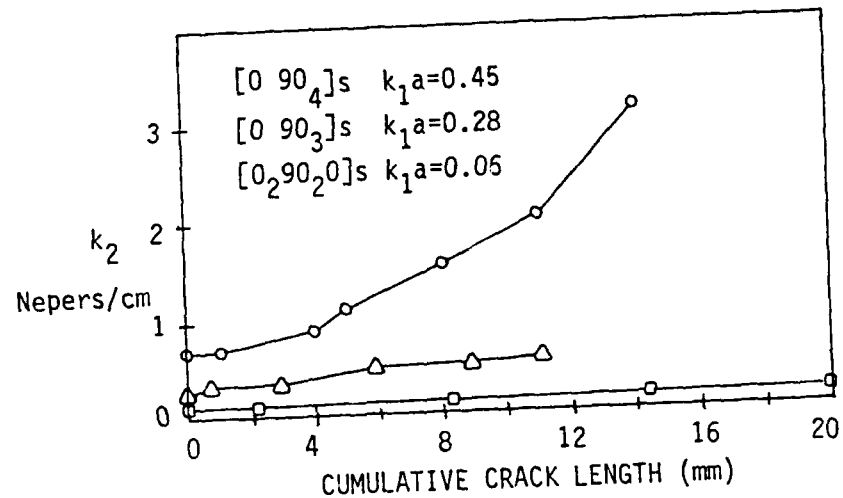

Figure 13 Increase in attenuation (k_2) with cumulative crack length for three laminates tested.

A New Technique for Ultrasonic-Nondestructive Evaluation of Thin Specimens

by V.K. Kinra and V. Dayal

Reprinted from EXPERIMENTAL MECHANICS, Vol. 28, No. 3, 288-297, September 1988

A New Technique for Ultrasonic-Nondestructive Evaluation of Thin Specimens

by V.K. Kinra and V. Dayal

ABSTRACT—Combining standard FFT methods with conventional ultrasonics, a method has been developed for measuring the phase velocity, the group velocity and the attenuation in ultra-thin specimens (submillimeter or subwavelength in thickness). A detailed description of this technique is given. The technique was used on four disparate materials: aluminum, an epoxy, a particulate composite and a graphite-fiber/epoxy composite. The method works equally well for thin or thick specimens, and for dispersive as well as nondispersive media.

List of Symbols

a = a characteristic length; half crack length or particle radius, mm
c, c_1 = longitudinal phase velocity in specimen, mm/μs
c_0 = longitudinal phase velocity of wave in immersion medium (water), mm/μs
c_g = group velocity in specimen, mm/μs
f = frequency, MHz
f_c = cut-off frequency, MHz
Δf = frequency resolution, MHz
$F^*(\omega)$ = Fourier transform of $f(t)$
$G^*(\omega)$ = Fourier transform of $g(t)$
h = plate thickness, mm
i = $\sqrt{-1}$
k = complex wave number = $k_1 + ik_2$, mm^{-1}
k_0 = wave number in water, real, mm^{-1}
k_1 = ω/c, wave number in specimen, mm^{-1}
k_2 = attenuation coefficient, nepers/mm
m = integer; number of complete round trips taken by the wave across the plate thickness
M = magnitude of a complex number
N = number of digitizing points
R_{ij} = reflection coefficient in medium i from medium j
T = sampling interval in time domain, ns
T_0 = signal length, μs
T_{ij} = transmission coefficient for a wave incident in medium i and transmitted into medium j
t = time, μs
u = particle displacement
x = distance
Ω = normalized frequency, $2\pi fa/c_1$
λ = wavelength, mm
ξ = normalized wave number, $2\pi fa/<c_1>$
ϱ = density of specimen, g/ml
ϱ_0 = density of water, g/ml
ϕ = phase of a complex number
ω = circular frequency, rad/μs
$< >$ = aggregate property of composite

Introduction

The classical method of measuring the speed of sound in nondispersive media is the time of flight method (see Ref. 1 for example). We note that in a nondispersive isotropic medium the phase velocity and the group velocity are identical.[2] When the material is either dispersive or exhibits frequency-dependent attenuation this method breaks down and a suitable method then is the so-called tone-burst method. Here, a *burst* of pure *tone*, typically about ten cycles in duration is used. This places a constraint on the specimen thickness; it must be thick enough so that the tone-burst reflections from the two faces of the specimen can be clearly separated in the time domain, i.e., it should be roughly five-wavelengths thick. For example in steel at, say, one-MHz frequency, the required minimum thickness would be about 30 mm. There are many situations of practical importance where one must conduct an ultrasonic examination of specimens which are considerably thinner than five wavelengths. For example, aircraft and aerospace structures using graphite/epoxy or metal-matrix composites employ panels as thin as one mm. Chang *et al.*[3] have developed a technique for the measurement of phase velocity in thin laminates. They perform an FFT of the front-surface and the back-surface reflections of a signal. The amplitude versus frequency curve is characterized by a series of resonance peaks. The peak spacing yields the phase velocity which is the same as the group velocity. The deviation between the group-velocity vector and the phase-velocity vector is zero for wave propagation parallel or perpendicular to the fibers; it is assumed that the material is nondispersive. This method requires human analysis of data. Further, one cannot measure attenuation by this method. More recently, Heyman[4] has developed a technique called phase-insensitive tone-burst spectroscopy. Although this technique yields excellent results, it requires the use of rather specialized and sophisticated transducers called acousto-electric transducers (AET) which are not yet commercially available.

By combining standard FFT methods with conventional ultrasonics (using commercially available broadband piezoelectric transducers) we have been able to develop a method by which one can measure the phase velocity, the group velocity and the attenuation in ultra-thin specimens (submillimeter or subwavelength in thickness). There are many situations in which one cannot obtain a series of resonance peaks required by the method of Chang *et al.*[3]

V.K. Kinra (SEM Member) is Associate Professor, Department of Aerospace Engineering, Texas A&M University, College Station, TX 77840. V. Dayal (SEM Member) is Assistant Professor, Department of Mechanical Engineering, North Carolina A&T University, Greensboro, NC 27411.

Original manuscript submitted: July 30, 1987. Final manuscript received: October 20, 1987.

Our method works even in the absence of a single resonance peak. A detailed description of this technique is the central objective of this paper. We will illustrate the use of this technique on four distinctly disparate materials: aluminum, an epoxy, a particulate composite and a graphite-fiber/epoxy composite. It will be demonstrated that this technique works equally well for thin or thick specimens, and for dispersive as well as nondispersive media.

Theory

Consider an infinite elastic plate immersed in an elastic fluid (water). A Lagrangian diagram indicating the space-time location of a wavefront which occupied the position $x = 0$ at time $t = 0$ is shown in Fig. 1. A plane-fronted finite-duration pulse, Ray 1, is normally incident on the plate. This results in an infinite series of reflected and transmitted pulses. The expressions for the reflection and transmission coefficients of a displacement wave for perfectly elastic media may be found in Achenbach's book.[5]

Let the displacement in the incident field be given by

$$u^{inc} = f_0(\omega t - k_0 x) \tag{1}$$

where $f_0(s) \equiv 0$ for $s < 0$. Here ω is the circular frequency and k_0 is the wave number of a monochromatic harmonic wave; $c_0 = \omega/k_0$. The displacement field along the various reflected rays may be written as

$$\begin{aligned} u_2 &= R_{12} f_0(s - s_2);\ s_2 = 2k_0 a \\ u_6 &= T_{12} R_{21} T_{21} f_0(s - s_6);\ s_6 = 2k_0 a + 2kh \\ u_{10} &= T_{12} R_{21}^2 T_{21} f_0(s - s_{10});\ s_{10} = 2k_0 a + 4kh \\ &\text{etc.} \end{aligned} \tag{2}$$

Here, $s = \omega t + k_0 x$, $h = b - a$ is the plate thickness, R_{ij} is the reflection coefficient in medium i from medium j, T_{ij} is the transmission coefficient for a wave incident in medium i and transmitted into medium j, $k = \omega/c$, c is the phase velocity in the plate, and

$$\begin{aligned} R_{12} &= \frac{\varrho_0 c_0 - \varrho c}{\varrho_0 c_0 + \varrho c} = -R_{21} \\ T_{12} &= \frac{2\varrho_0 c_0}{\varrho_0 c_0 + \varrho c} = 2 - T_{21} \end{aligned} \tag{3}$$

where ϱ_0 and ϱ are, respectively, the density of water and the plate material. The entire reflected field, $u^r = u_2 + u_6 + u_{10} + \ldots . \infty$, may be written as

$$\begin{aligned} u^r &= R_{12} f_0(s - s_2) + T_{12} R_{21} T_{21} \sum_{m=1}^{\infty} R_{21}^{m-1} f_0(s - s_m) \\ s_m &= 2k_0 a + m\, 2kh \end{aligned} \tag{4}$$

In an exactly analogous manner, one can write down the expressions for the transmitted pulses. With $s = \omega t - k_0 x$

$$\begin{aligned} u_4 &= T_{12} T_{21} f_0(s - s_4);\ s_4 = h(k - k_0) \\ u_8 &= T_{12} R_{21}^2 T_{21} f_0(s - s_8);\ s_8 = h(3k - k_0) \\ u_{12} &= T_{12} R_{21}^4 T_{21} f_0(s - s_{12});\ s_{12} = h(5k - k_0) \\ &\text{etc.} \end{aligned} \tag{5}$$

The total transmitted field may be written as

$$u^t = T_{12} T_{21} \sum_{m=0}^{\infty} R_{21}^{2m} f_0(s - s_m);\ s = h[(2m + 1)\, k - k_0] \tag{6}$$

In eqs (4) and (6) m is the number of *complete round trips* taken by the wave across the plate thickness h.

The Fourier transform of a function $f(t)$ is defined as

$$F^*(\omega) = \frac{1}{\sqrt{2\pi}} \int_{-\infty}^{\infty} f(t)\, e^{-i\omega t}\, dt,\ -\infty < \omega < \infty \tag{7a}$$

with the associated inverse transform given by

$$f(t) = \frac{1}{\sqrt{2\pi}} \int_{-\infty}^{\infty} F^*(\omega)\, e^{i\omega t}\, d\omega \tag{7b}$$

Analysis for Thick Specimens

We first consider the case of a relatively thick specimen such that various pulses in Fig. 1 can be clearly separated from each other in the time domain. Let $f(t)$ be the signal corresponding to Ray 2 and $g(t)$ be the signal corresponding to Rays 2 and 6 combined sensed by a transducer at $x = 0$. (This is the so-called pulse-echo mode.) Then

$$f(t) = R_{12} f_0(\omega t - 2k_0 a) \tag{8}$$

and

$$g(t) = T_{12} R_{21} T_{21} f_0(\omega t - 2k_0 a - 2kh) + f(t) \tag{9}$$

Let $F^*(\omega)$, $G^*(\omega)$ and $F_0^*(\omega)$ be the Fourier transforms of $f(t)$, $g(t)$ and $f_0(t)$, respectively. Then, a straightforward application of the shifting theorem for Fourier transforms yields

$$F^*(\omega) = R_{12} e^{-i2k_0 a} F_0^*(\omega) \tag{10}$$

$$G^*(\omega) = R_{12} F_0^*(\omega) e^{-i2k_0 a}[1 - T_{12} T_{21} e^{-i2kh}] \tag{11}$$

and

$$\frac{G^*(\omega)}{F^*(\omega)} = 1 - T_{12} T_{21} e^{-i2kh} \tag{12}$$

It is emphasized that in the foregoing it is assumed that the plate behaves in a perfectly elastic manner, i.e., the wave number k is real and $c = \omega/k$ is a constant. The

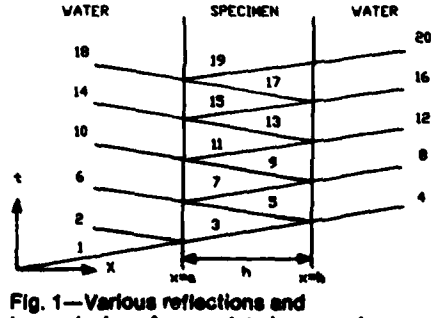

Fig. 1—Various reflections and transmissions from a plate immersed in water

key term in eqs (11) and (12) is e^{-i2kh} or $e^{-i2h\omega/c}$. Thus, in eq (11) if one plots $|G^*(\omega)|$ versus ω it will be characterized by a series of resonance peaks whose spacing is given by $\Delta(2h\omega/c) = 2\pi$, or, in view of $\omega = 2\pi f$,

$$c = 2h\,\Delta f \tag{13}$$

Measurement of c in aluminum using eq (13) is illustrated in Fig. 2. Here $F(\omega) = |F^*(\omega)|$ and $G(\omega) = |G^*(\omega)|$. Note that $G(\omega)$ consists of the transducer response, $F(\omega)$, superimposed by an oscillation due to $e^{-i2h\omega/c}$ term.

A further improvement in the measurement method can be achieved by plotting $[G^*(\omega)/F^*(\omega) - 1]$, eq (12). This is illustrated in Fig. 3. By taking out the shape of the transducer response we are left with oscillations due to the constructive and destructive interference between the front-surface (Ray 2) and back-surface reflections (Ray 6).

Even though eq (12) is derived for an elastic material it is rigorously valid for a linear-viscoelastic material provided the damping is small, i.e., in $k = k_1 + ik_2$, $k_2/k_1 << 1$. This elementary proof is deferred to the Appendix. We rewrite eq (12) as

$$e^{-i2kh} = -[G^*(\omega)/F^*(\omega) - 1]/T_{12}T_{21} = Me^{i\phi} \tag{14a}$$

Then, by equating real and imaginary parts,

$$k_1(\omega) = -\phi/2h$$

and

$$k_2(\omega) = (ln\,M)/2h \tag{14b}$$

where $M = |[(G^*(\omega)/F^*(\omega)] - 1]/T_{12}T_{21}|$. Since $k_1(\omega) = \omega/c$ and $\omega = 2\pi f$

$$c = \frac{4\pi h}{(-\phi/f)} \text{ and } k_2(\omega) = (lnM)/2h \tag{15}$$

These are the desired equations for calculating the phase velocity and the attenuation.

Now consider the *transmitted field* for a *thick* specimen. Two measurements are made. In the first, the specimen is removed from the water path, i.e., the wave travels solely through water. Let the receiving transducer be located at some $x = l > b$. Then $u^{inc}(l,t) \equiv f(t) = f_0(\omega t - k_0 l)$. The specimen is now inserted in the wavepath and the signal due to Ray 4 alone is recorded. Thus, $u^4(l,t) \equiv g(t) = T_{12}T_{21}f_0(\omega t - k_0 l - 2k_0 a - kh)$. Then,

$$\frac{G^*(\omega)}{F^*(\omega)} = T_{12}T_{21}e^{-i(kh+k_0h)} \tag{16}$$

If $\frac{G^*(\omega)e^{ik_0h}}{F^*(\omega)T_{12}T_{21}}$ is set equal to $Me^{i\phi}$ then

$$k_1(\omega) = -\phi/h \tag{17a}$$

and

$$k_2(\omega) = (ln\,M)/h \tag{17b}$$

where $M = \left|\frac{G^*(\omega)}{F^*(\omega)}\right| / T_{12}T_{21}$. Substituting $k_1 = 2\pi f/c$, we get

$$c = \frac{2\pi h}{(-\phi/f)} \text{ and } k_2(\omega) = ln\,M/h \tag{18}$$

Another variation of this technique is when signals for both Rays 4 and 8 are quite large. Then the following approach yields more accurate results because the data reduction can be done from a single experiment. Let $f(t)$ and $g(t)$ be the signals corresponding to Rays 4 and 8, let $F^*(\omega)$ and $G^*(\omega)$ be their Fourier transforms then

$$\frac{G^*(\omega)}{F^*(\omega)} = R_{21}^2\,e^{-i2kh} \tag{19}$$

as before, if we set $G^*(\omega)/F^*(\omega)\,R_{21}^2 = Me^{i\phi}$, then eq (15) can be used to calculate the wave speed and attenuation. In the following for brevity, these methods will be referred to as the second/first method.

We note that this method is equally effective for *dispersive* media. From eq (14) one plots k_1 versus ω. A secant to the curve yields inverse of the phase velocity (phase slowness). For dispersive media a quantity of interest is the group velocity. This is the speed with which energy propagates in a medium, $c_g = \partial\omega/\partial k_1$; this too can be computed from the phase plot, and eq (14b) yields frequency-dependent attenuation. Finally, we introduce a normalized attenuation $k_2\lambda$. This is the attenuation of a wave over one wavelength. The motivation for this particular normalization is that for a linear-viscoelastic material $k_2\lambda$ is independent of frequency.

Analysis for Thin Composites

In this paper the qualifiers 'thick' and 'thin' are used in the following sense. When various reflections or transmissions corresponding to a short-duration pulse can be separated in the time domain, the specimen is considered thick. However, the duration (or length) of the pulse depends on the center frequency of the transducer. Hence, with reference to the *absolute* dimensions of the specimen the use of the word 'thick' is quite arbitrary. On the other hand the word 'thick' is not arbitrary with

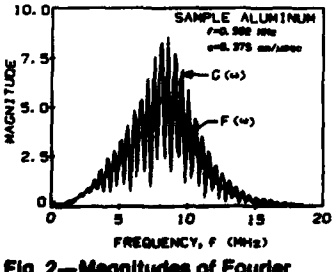

Fig. 2—Magnitudes of Fourier transforms of $f(t)$ and $g(t)$ when pulses can be separated

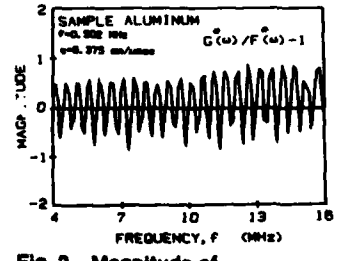

Fig. 3—Magnitude of $G^*(\omega)/F^*(\omega) - 1$ from Fig. 2. Resonance spacing can be measured easily from the zero line crossings

respect to the wavelength, i.e., a specimen is thick if, roughly, $h \geq 3\lambda$.

The *total* reflected field comprising Rays 2, 6, 10, 14 . . . ∞ at $x = 0$ is given by eq (12) as

$$u^r(o,t) \equiv g(t) = R_{12} f_0(\omega t - 2k_0 a) + T_{12} R_{21} T_{21} \sum_{m=1}^{\infty} R_{21}^{2(m-1)} f_0(\omega t - 2k_0 a - m2kh) \tag{20}$$

Note that Ray 2 cannot be used as the reference signal. One has to conduct a separate experiment as follows. The thin coupon is replaced by a thick coupon with the front surface precisely at $x = a$. Let the front-surface reflection be labeled $f(t)$. Then

$$f(t) = R_{12} f_0(\omega t - 2k_0 a)$$

$$F^*(\omega) = R_{12} e^{-i2k_0 a} F_0^*(\omega)$$

$$G^*(\omega) = F^*(\omega) + T_{12} R_{21} T_{21} \sum_{m=1}^{\infty} R_{21}^{2(m-1)} F_0^*(\omega) \cdot e^{-i[2k_0 a + m\,2kh]} \tag{21}$$

Let

$$Z = R_{21}^2 e^{-i2kh} \qquad |Z| < 1 \tag{22}$$

Then

$$\frac{G^*}{F^*} - 1 = \frac{T_{12} T_{21}}{R_{12} R_{21}} \sum_{m=1}^{\infty} Z^m$$

Observing that for $|Z| < 1$, $(1 - Z)^{-1} = 1 + Z + Z^2 + \ldots \infty$, and defining

$$\beta = \frac{R_{12} R_{21}}{T_{12} T_{21}} \left(\frac{G^*(\omega)}{F^*(\omega)} - 1 \right)$$

we get

$$Z = \frac{\beta}{1 + \beta} \tag{23}$$

From Z one can readily calculate the complex-valued wave number $k(\omega)$.

For completeness we include here a variation of this method. Suppose a *thick* coupon to obtain a reference signal is not available (this difficulty will be discussed later). One can then use a thick specimen of some other material; we have used a block of aluminum. Let the acoustic impedance of this material be $\varrho_1 c_1$. Let the front-surface reflection be $f(t) = R f_0(\omega t - 2k_0 a)$ where the reflection coefficient $R = (\varrho_0 c_0 - \varrho_1 c_1)/(\varrho_0 c_0 + \varrho_1 c_1)$, and $g(t)$ is still given by eq (18). As before with

$$\beta = \frac{R_{12} R_{21}}{T_{12} T_{21}} \left[\frac{R}{R_{12}} \frac{G^*(\omega)}{F^*(\omega)} - 1 \right] \tag{24}$$

$$Z = R_{21}^2 e^{-i2kh} = \beta/(1 + \beta) \tag{25}$$

In the following for brevity these methods will be referred to as the all/first method.

We now consider the transmitted field. Here a second transducer is used as a receiver at some $x = l > b$. To obtain a reference signal the specimen is removed and the signal through water is recorded.

$$f(t) = u^{inc}(l,t) = f_0(\omega t - k_0 l)$$

Let $g(t)$ be the *total* transmitted field, Rays 4, 8, 12, . . . ∞. Then from eq (6)

$$g(t) = T_{12} T_{21} \sum_{m=0}^{\infty} R_{21}^{2m} f_0[\omega t - k_0 l - h\{(2m + 1)k - k_0\}] \tag{26}$$

$$\frac{G^*(\omega)}{F^*(\omega)} = \frac{T_{12} T_{21} e^{-ih(k - k_0)}}{1 - R_{21}^2 e^{-i2kh}} \tag{27}$$

We note one major difference between eqs (23) and (27). Unlike eq (23), eq (27) is a *quadratic* in $Z = \exp(-ikh)$. This presents some additional numerical problems. These are discussed next. Equation (27) may be rewritten as

$$Z^2 + ZY - D_0 = 0$$

where

$$Y = \frac{T_{12} T_{21}}{R_{21} Z_0} \frac{F^*(\omega)}{G^*(\omega)} \tag{28}$$

$$Z_0 = \exp(-ihk_0)$$

$$D_0 = 1/R_{21}^2$$

and k_0 is the wave number in water. Since the phase velocity in water is known, Z_0 is known *a priori*. If the acoustic impedance of the plate, ϱc, was known, one could calculate T_{ij} and R_{ij}. However, c is precisely the unknown we are seeking to measure. This problem could be solved by a simple iteration procedure. An approximate phase velocity was initially used in the algorithm to estimate T_{ij} and R_{ij}. The quadratic equation (28) is solved and two roots of Z are obtained. The correct root is chosen based on the fact that the phase of Z *decreases* as frequency increases (for the other root the reverse is true). This velocity is used for the next iteration cycle. This procedure converges very rapidly. When we purposely supplied an initial phase velocity with a very large error (30 percent), the convergence was found to occur in about five iterations. More realistically, the wave speed can be estimated to within five percent. Here convergence to within 0.01 percent occurs within three or four iterations. When the value of c obtained by this procedure was substituted back into eq (28) to calculate attenuation, $k_2\lambda$ was found to be an oscillatory function of frequency for a linear viscoelastic material, namely, an epoxy. Now, it is well known that for such a material $k_2\lambda$ is a constant. The oscillating nature of $k_2\lambda$ could, however, be readily explained as follows. A detailed numerical examination of eq (28) revealed that the calculation of $k_2\lambda$ is very sensitive to small variation in the phase velocity c. The oscillations were due to the fact that the measured velocity was different from the true velocity. This problem could be resolved in the following manner. If one takes the absolute value of both sides, eq (25) can be rewritten as follows.

$$\cos \frac{4\pi hf}{c} + \frac{1}{2} \left(\frac{T_{12} T_{21}}{R_{21}} \right)^2 \left| \frac{F^*(\omega)}{G^*(\omega)} \right| = \frac{1}{2} \left[R_{21}^2 e^{q} + \frac{1}{R_{21}^2 e^{q}} \right] \tag{29}$$

where $q = 2h k_2\lambda/c$. The terms in eq (29) have been separated judiciously as follows. The left-hand side (LHS) is a function of wave speed only while the right-hand side (RHS) depends on both the wave speed and the attenuation. The RHS is a sum of two exponentials and, therefore, is *not* an oscillatory function of frequency f. On the other hand, the LHS is the sum of a cosine function of

frequency and the experimentally determined $F^*(\omega)/G^*(\omega)$ which was found to be oscillatory. Now if the correct value of c is not used in eq (29) the periods of the two terms do not match and the oscillatory parts do not cancel each other as they would for the correct value of c. With this in mind, the RHS is viewed as the reference curve and a numerical search is made around the value of c obtained by the iterative procedure described earlier, to minimize the root-sum-square of the LHS. This fixes c. Now we view the LHS as the reference curve and conduct a numerical search over a range of $k_2\lambda$ so as to minimize the root-sum-square between the LHS and the RHS. This fixes k_2.

Finally, it is noted that the theoretical procedures developed in this section are equally valid for both the longitudinal as well as the shear disturbances.

Experimental Procedures

Measurement Procedures

A schematic of the apparatus is shown in Fig. 4. The heart of the system is a pair of accurately matched, broadband, water-immersion piezoelectric transducers. An experiment is initiated at time $t = 0$ by a triggering pulse produced by a pulser/receiver; the pulse is used to trigger a digitizing oscilloscope; simultaneously the pulser/receiver produces a short-duration (about 100 ns) large-amplitude (about 200 V) spike which is applied to the transmitting transducer. In the reflection mode it also acts as a receiver. The received signal is post-amplified (to about one volt) and then digitized with maximum sampling rate of 100 MHz (or 10 nanoseconds per point). To reduce the ubiquitous random errors, each measurement is averaged over a sample size of 64. A laboratory computer controls *all* operations of the digital oscilloscope through an IEEE bus. The built-in signal processor of the oscilloscope performs FFT on the acquired signals and the relevant parts of the data are then transferred to the computer for further analysis.

Calibration Procedures

Since our objective in this research is to estimate damage in composite materials from a measurement of the ultrasonic parameters, accuracy is of prime importance. For example, one percent error in estimating the phase velocity may, for some typical laminates, correspond to a ten-percent error in estimating the remaining fatigue life. Typically each measurement was repeated about ten times. Based on *one* standard deviation we estimate the errors in our measurement as follows. We can determine velocity in monolithic materials to a precision of 0.1 percent, and velocity and attenuation in heterogeneous materials to a precision of 0.2 percent and 2 percent, respectively. The higher scatter in the composite materials is due to inherent spatial variation in the material properties. In order to achieve this precision the measurement system was subjected to systematic calibration procedures. These are described next.

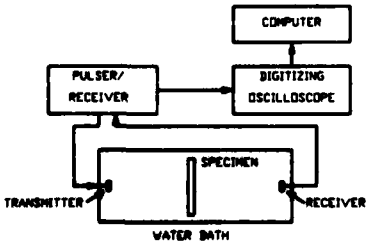

Fig. 4—Block diagram of the experimental setup

Sampling Interval

The analog signal from the transducer is digitized at a specified sampling interval by the digitizing oscilloscope. The object of this study was to determine an upper bound on the sampling interval below which the harmonic distortion was considered acceptable. We quote here the limits on the sampling interval as specified by the sampling theorem. "If the sampling interval T is chosen equal to $\frac{1}{2}f_c$, where f_c is the highest frequency component of the signal, aliasing will not occur."[7] Aliasing is defined as "the distortion of the desired Fourier transform of a sampled function".[7] An experimental verification of this statement is given here. Figures 5 and 6 show the amplitude and phase response of a 10-MHz transducer at sampling intervals of 10 nS (100 MHz), 20 nS (50 MHz), 40 nS (25 MHz), and 100 ns (10 MHz). The highest frequency content of this signal is about 10 MHz and so the sampling interval of 50 nS would be acceptable from the viewpoint of aliasing. It is obvious from Fig. 5 that at 10-nS or 20-nS sampling intervals, the frequency content of the signal is essentially the same. However at 40-nS sampling intervals, significant distortion of the amplitude is observed; but the phase remains relatively unaffected. At 100 nS, both the amplitude and the phase plots are completely distorted. This would come as no surprise for here we are sampling only one point per cycle. In this work we have used either a 10-nS or 20-nS sampling interval.

Frequency Resolution

It is seen from eqs (15) and (18) that wave speed can be calculated if the slope (ϕ/f) of the phase versus frequency curve can be obtained. The FFT algorithm provides the real and imaginary components of the transformed signals and from these the phase is calculated. The computer can provide the phase angle in the range of $-\pi/2$ to $+\pi/2$ from which the angle in the range of 2π can be deduced very easily, depending on the quadrant in which the phaser lies. Hence we obtain a sawtooth-type phase versus frequency plot. It was observed that for the signal under consideration, phase increases monotonically with the frequency. Thus the sawtooth plot has to be converted to a continuous phase versus frequency curve before its slope can be obtained to calculate the wave speed. The computer algorithm developed tracks the rotation of the phase vector and 2π radians are added to the phase each time the vector completes a cycle.

Let the sampling interval be T and the total number of sampled points be N. The total length of the signal is $T_0 = (N-1)T$. Let the frequency resolution be Δf, then $\Delta f = 1/T_0 = 1/(N-1)T$. The consideration of aliasing fixes T. Hence N is the only parameter that can be adjusted to obtain the desired frequency resolution. For example, if the desired $\Delta f = 0.05$ MHz/point, T is 10 nS, then $N = 2000$ or 2048. The length of a signal can be readily increased simply by adding zeros at the end of the signal. Of course, this is accompanied by an increased computation time.

Transducer Response

Consider a 10-MHz transducer in direct contact with an aluminum plate. An FFT of the back-wall reflection was obtained using the procedures outlined in the section 'Measurement Procedures' above. The results are presented in Fig. 7 in the form of magnitude and phase of the complex-valued Fourier transform. Experience indicated that satisfactory measurements can be made over a frequency range (or bandwidth) of 5 MHz to 11 MHz given by about 25 percent of the peak amplitude response as shown in the figure. It was observed that the phase versus frequency curve over this range is a straight line; outside this range it becomes nonlinear.

Results and Discussions

Wave Propagation in Nondispersive Media

The main objective of this work is to develop techniques suitable for very thin specimens. Therefore we subjected our techniques to the following critical test. A thick aluminum plate (2.807 ±0.0025 mm) was first tested using the conventional tone-burst method. Then the thickness was gradually machined down to 0.258 mm (about 10 mil, a very thin foil) in five steps. In nondimensional terms the thickness was reduced from about 4.4 to 0.4 wavelengths; a frequency of 10 MHz was used. At each step c was measured. We could have used five different samples. Instead we adopted the foregoing procedure in order to ensure that we are always testing exactly the same material. The density was measured by the Archimedes principle. Our estimate of the error in density is ±0.015 percent. The results are presented in Table 1. The first measurement was made using the conventional tone-burst method.[8,9] The time-domain signal is shown in Fig. 8(a). A particular peak (say the fourth peak) near the center of the tone burst is selected as the reference peak. The twice transit time, $2h/c$, could be measured to an accuracy of 1 nS. Our estimate of error in the phase velocity is 0.2 percent. See Ref. 10 for a detailed error analysis. In the second measurement the tone burst was reduced to about one cycle; see Fig. 8(b). Note that the pulses can be clearly separated. The second/first method, eq (15), was used to analyze these data. Since only the first two pulses are needed for data analysis, the remaining pulses are electronically gated out or nulled. In the third measurement, the data analyzed remain the same, i.e., Fig. 8(b). However, the all/first method, eq (27), is used. In other words, $g(t)$ is now viewed as the sum of all transmissions. For the remaining measurements the specimen was gradually machined down. The all/first method was used to analyze the data. The pulses for h = 1.686 mm are shown in Fig. 8(c). Note that the conventional tone-burst method can no longer be used. Though both methods developed in this work can be used, we used the all/first method. The pulse for the next three thicknesses, h = 1.001, 0.613 and 0.258 mm are shown in Figs. 8(d), 8(e), 8(f), respectively. Because of the reduced thickness the pulses cannot be separated in the time domain. Therefore, even the second/first method cannot be used; here we have to use the all/first method. For the thinnest specimen the round trip time is only

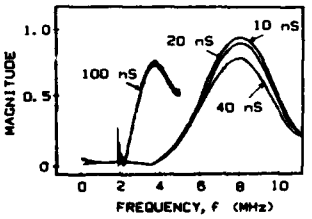

Fig. 5—Amplitude response of a 10-MHz transducer at different digitizing intervals

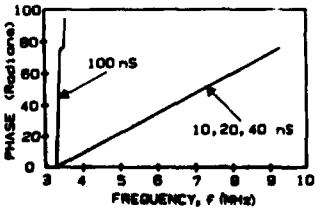

Fig. 6—Phase response of a 10-MHz transducer at different digitizing intervals

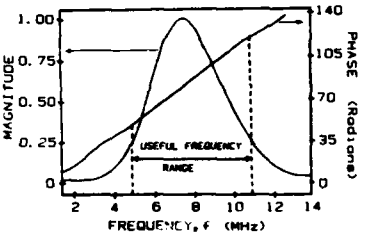

Fig. 7—Useful frequency range of a 10-MHz transducer

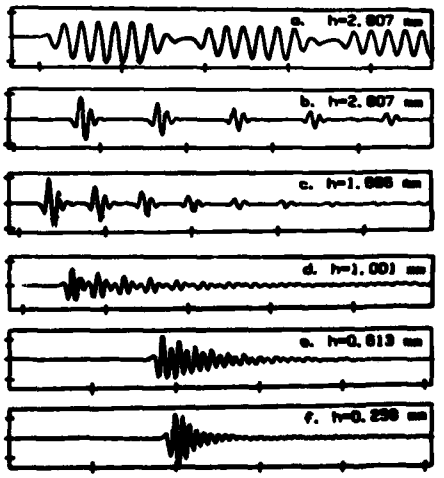

Fig. 8—10-MHz signal through aluminum plates of different thickness. (a) is for tone burst. Others are for a single pulse of signal. Plate thickness given on each signal

82 nS; the pulse duration is roughly 200 nS. This gives rise to what appears to be 'ringing' in Fig. 8(f).

With reference to Table 1, the average of all the measurements is 6.342 mm/μs $\pm$0.25 percent. We conclude that the all/first method developed for ultra-thin (subwavelength) specimens and the second/first method for moderately thin (about one wavelength) specimens yield results which agree to 0.25 percent with the conventional tone-burst method. (We hesitate to make absolute claims on accuracy because for the given piece of aluminum we do not know the *true value* of the phase velocity.)

The ideal method for 'calibrating' a new experimental technique is to use it to measure a quantity which is known with a ten times better accuracy. Unfortunately, the National Bureau of Standards has not yet developed a standard for acoustic velocity (or elastic modulii). Our laboratory did, however, participate in a six-laboratory ASTM round-robin conducted by Alan Wolfenden[11] (Department of Mechanical Engineering, Texas A&M University, College Station, TX 77843). This allowed us an opportunity to compare our error estimates with those of the others. The material tested were two nickel-based alloys; see Table 2 for a material and geometric description. Since these specimens are very, very 'thick' (several wavelengths), the second/first method, eq (15), was used. Furthermore, *shear velocity was also measured.* Here a shear (or Y cut) transducer was directly cemented onto the metal specimen using a shear couplant. Ignoring the 'main bang', the remaining reflected signal was collected. From the measurements of the longitudinal and shear velocity, c_1 and c_2, and density, ϱ, the elastic constants E and ν can be readily calculated. The results of the round-robin test are presented in Table 3. Reasonably good agreement (within 2.5 percent) is observed between the results obtained in different laboratories using different techniques.

Next, we have tested our experimental method on a medium which is nondispersive but attenuative. An epoxy (EPON 828Z) was selected for this purpose. The results are presented in Table 4. Note that three frequencies, spanning nearly a decade, were used. The phase velocity measured by the tone-burst method on a thick specimen is 2.915 mm/μs and agrees very well with that measured with the all/first technique.

TABLE 1—TEST RESULTS ON ALUMINUM SAMPLE

Material: Aluminum
Wave Type: Longitudinal
Mode: Transmission
Frequency: 10 MHz
Density: 2.8177 $\pm$ 0.0004 g/ml

h mm	h/λ	c mm/μs	$\bar{\sigma}/c$ percent	Technique	Reference Figure
2.807	4.4	6.3572		Toneburst	8a
2.807	4.4	6.3239	0.013	Second/First	8b
2.807	4.4	6.3275	0.010	All/First	8b
1.686	2.7	6.3461	0.040	All/First	8c
1.001	1.6	6.3536	0.030	All/First	8d
0.613	0.96	6.3594	0.130	All/First	8e
0.258	0.4	6.3231	0.140	All/First	8f

Wave Propagation in Dispersive Media

Finally, we tested our experimental procedures on a material which is simultaneously highly dispersive as well as highly attenuative. Towards this end we tested a random-particulate composite consisting of lead spheres in an epoxy matrix. These composites have been described in Refs. 12 and 13. Transducers with 0.25-MHz center frequency were employed. The second/first method in through-transmission mode, eq (16), was used.

Kinra[13] has shown that wave propagation in these composites occurs along two separate branches: (1) the low-frequency, slower, acoustical branch along which the particle motion is essentially in phase with the excitation, and (2) the high-frequency, faster, optical branch along which the particle motion is essentially out of phase with the excitation. The two are separated by a cutoff frequency which corresponds to the excitation of the rigid-body-translational resonance of the heavy inclusions. This occurs when $k_1 a = 0(1)$, where a is the inclusion radius. Around the cut-off frequency both the phase velocity and the attenuation change dramatically with frequency. This is what makes this composite such an interesting material to study using our technique which was developed especially for dispersive media.

The results for a dispersive material are presented now. In Fig. 9 $F^*(\omega)$ is the received signal with the specimen removed while $G^*(\omega)$ is the signal with the specimen in place; $\bar{c}$ is the volume fraction of inclusions. The dip in the amplitude of $G^*(\omega)$ corresponds to the cut-off fre-

TABLE 2—RESULTS OF ASTM ROUND-ROBIN TESTS OF NI-BASED ALLOYS

Sample 1: Inconel Alloy 600
Composition: Ni 37.46, C 0.01, Co 14.38, Nb 4.71, Ti 1.46, Fe 41.98
Test Frequency: 5.0 MHz
Mode: Reflection

Sample 2: Incoloy Alloy 907
Composition: Ni 74.91, Cr 15.48, C 0.08, Fe 9.53

Sample	h mm	ϱ g/ml	c_1 mm/μs	c_2 mm/μs	E GN/m^2	ν
1.2*	6.283	8.371	5.872	3.161	216.9 $\pm$ 0.14 percent	0.2960 $\pm$ 0.20 percent
1.4	6.365	8.373	5.877	3.163	216.6 $\pm$ 0.15 percent	0.2960 $\pm$ 0.20 percent
2.1	18.848	8.267	5.273	2.7308	163.0 $\pm$ 0.28 percent	0.3153 + 0.18 percent

*The first digit (1 or 2) refers to the alloy while the second digit (1-4) is merely to identify different physical specimens.

quency. The present measurement, $f_c = 0.21$ MHz, agrees quite well with the earlier measurement[12] using the conventional tone-burst method. We now introduce a normalized frequency $\Omega \equiv k_1 a = 2\pi f a / c_1$ and a normalized wave number $\xi = \langle k_1 \rangle a = 2\pi f a / \langle c_1 \rangle$ where $\langle\ \rangle$ refers to an aggregate property of the composite (an ensemble average). Figure 10 shows the frequency versus wave number plot. As expected,[12] along the acoustical branch at low frequencies the behavior is nondispersive; a straight line fitted through the data points passes through the origin ($\langle c_1 \rangle / c_1 = \Omega / \xi$). The same was noted at high frequencies along the optical branch. These two observations serve as critical checks on the accuracy of our measurement. The normalized phase velocity is given by the slope of the secant, $\langle c_1 \rangle / c_1 = \Omega / \xi$, and the group velocity is given by the slope of the tangent, $\langle c_g \rangle / c_1 = d\Omega / d\xi$. The discrete tone-burst data from the earlier work[12-14] are also plotted; the agreement is considered quite satisfactory. The present technique is tremendously faster. The entire dispersion and attenuation curve is produced in a single experiment. Another major advantage of this method is as follows. When one uses the tone-burst method, each point suffers a scatter due to random errors; see Fig. 10. In the present method the *whole curve* may shift up or down but the *shape* of the curve will not be altered by the random errors. Here we are mainly interested in the shape of the dispersion curve. Figure 11 shows the normalized phase velocity versus frequency. The arrow labeled HASHIN is the velocity calculated from the lower (appropriate) *static* bound due to Hashin and Shtrikman.[15] The agreement between the theory and the low-frequency results is considered quite satisfactory. As Ω increases the effective inertia of the lead spheres ($\sim \rho\omega^2$) increases and the phase velocity decreases. At very high frequencies (it is conjectured) the inertia becomes so large that the spheres become essentially motionless. Thus they no longer contribute to the inertia of the composite as perceived by the effective wave. Hence the velocity increases dramatically across the cut-off frequency and becomes frequency-independent at very high frequencies. Figure 11(b) shows the group velocity, i.e., the speed with which energy flows in a composite. As expected, the group velocity is

TABLE 3—COMPARISON OF ASTM ROUND ROBIN TESTS FOR THE YOUNG'S MODULUS, *E*

Lab/Sample	1.1	1.2	1.3	1.4	2.1	2.2	2.3
1	218.0 218.0 218.1	216.9	218.5	—	161.5	159.9	157.2
2	210.5	209.2	—	—	164.1	—	155.7
3	218.8	216.0	217.5 217.0 216.2 217.3	—	162.0 161.8 160.8	— —	158.4
4	212.0	—	205.0	—	156.0	—	172.0
5	215.6	—	214.2	—	156.0	—	162.0
6 [this work]	—	216.9	—	216.6	163.0	—	—
7	203.0	—	210.3	—	156.8	—	155.8 158.0

Units for above values: GN/m²
Techniques:
Lab. 1, 2, 7 Free-Free Beam
Lab. 3 Impulse Fourier
Lab. 4 Pulse-Echo-Overlap Ultrasonic
Lab. 5 Piezoelectric Ultrasonic Oscillation (PUCOT)
Lab. 6 This work

TABLE 4—TEST RESULTS ON EPON 828-Z EPOXY

Material: Epon 828-Z epoxy
Wave Type: Longitudinal
Mode: Transmission

Specimen thickness: 1.869 mm ± 0.0025
Specimen density: 1.2069 ± 0.0004 g/ml

Test Frequency MHz	Wave Speed mm/μs	$\bar{\sigma}$ percent	$k_2\lambda$	$\bar{\sigma}$ percent	Technique
1.0	2.874	0.1	0.1340	1.4	All/First
5.0	2.884	0.14	0.0924	1.5	All/First
10.0	2.915	0.08	0.0975	1.0	All/First
10.0	2.915	0.24	0.0979	2.2	Tone Burst

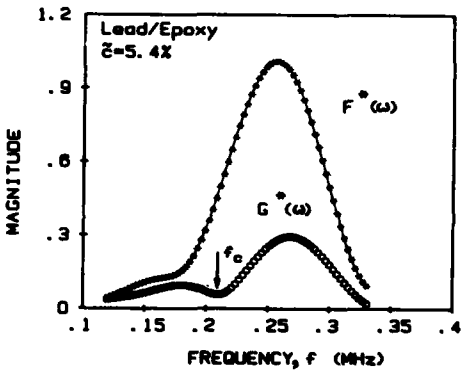

Fig. 9—Magnitude of $F^*(\omega)$ (FFT of signal through polystyrene delay rod) and $G^*(\omega)$ (FFT of signal through polystyrene and lead/epoxy specimen). Note the dip in amplitude at the cut-off frequency, f_c

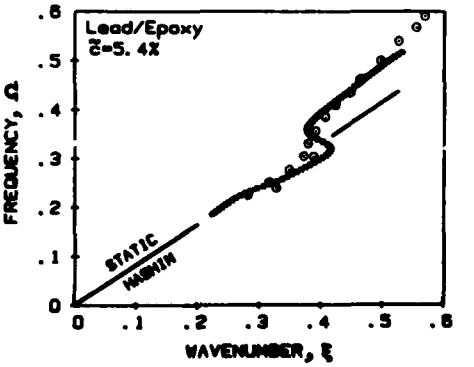

Fig. 10—Frequency $\Omega = k_1 a$, and wave number $\xi = \langle k_1 \rangle a$, curve for a dispersive lead/epoxy specimen. Circled points are data from Ref. 12-14

essentially constant at low and high frequencies. Around the cut-off frequency, Ω_c, it undergoes large fluctuations. Theoretically, $c_g \to \infty$ at two points around the cut-off frequency. Perhaps the most interesting feature is that the group velocity becomes negative around Ω_c, i.e., as the wave propagates in the positive x direction, the energy flows in the negative x direction. In Fig. 10 this corresponds to those points on the curve where the slope is negative.

In Fig. 12 we have plotted attenuation versus frequency. The peak in the curve defines the cut-off frequency. For comparison $k_2\lambda$ for the neat epoxy alone is 0.13 which is negligibly small compared to the peak attenuation. Thus all of $k_2\lambda$ may be attributed to the scattering effects.

QNDE of Damage in Composite Materials

We now demonstrate the application of our technique to fiber-reinforced composite materials. Graphite/epoxy AS4/3502 cross-ply $[0_s/90_4/0_2]_s$ laminates were tested. These were subjected to monotonic tensile loading. As a result transverse cracks develop. Edge replication was made to obtain a record of the transverse cracks. The loading was interrupted at several points along the load axis, the coupon was subjected to an ultrasonic examination and the loading was resumed. The second/first method in the reflection mode, eq (15), was used. In Fig. 13 we have also shown the portion of the edge replication which is illuminated by the ultrasonic beam. The number of cracks seen by the beam is also listed. Note that we have not plotted the attenuation $k_2\lambda$ but rather the changes in $k_2\lambda$ caused by this damage. To guard against fortuitous results three different frequencies were used, namely, 2.25, 5.00 and 7.50 MHz. We note that attenuation changes quite significantly and monotonically with the number of transverse cracks. We also note that in the range of frequency tested, the attenuation decreases with frequency. This may be attributed to the fact that these experiments were conducted at $k_1a = 1.23$, 2.70 and 4.02, where a is the half crack length, at 2.25, 5.00 and 7.50 MHz, respectively. Figure 14 shows the longitudinal phase velocity at the same three frequencies. Within the errors of measurement, ± 0.2 percent, the phase velocity remains constant with damage. This is not at all surprising in view of the fact that here the wave vector (or the particle displacement vector) is parallel to the crack face, i.e., the crack-wave interaction is very weak. Thus we

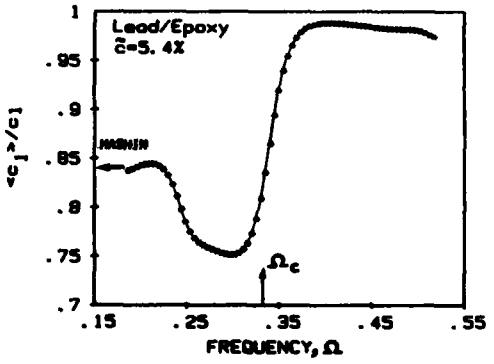

Fig. 11(a)—Normalized phase velocity and frequency curve for the dispersive lead/epoxy specimen

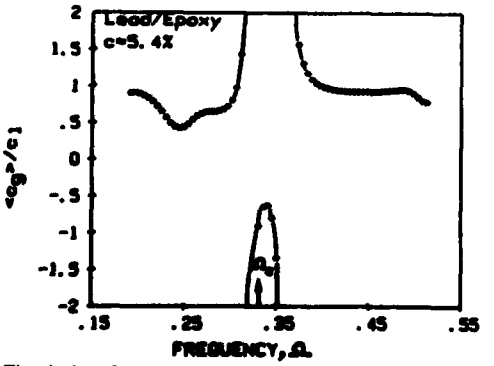

Fig. 11(b)—Normalized group velocity and frequency curve for lead/epoxy specimen

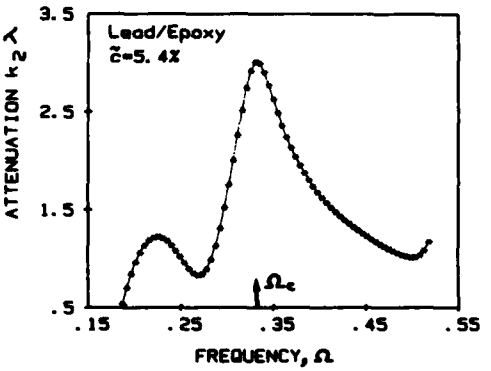

Fig. 12—Normalized attenuation and frequency curve. Note a very high attenuation (large energy absorption) due to dispersion at the cut-off frequency, Ω_c

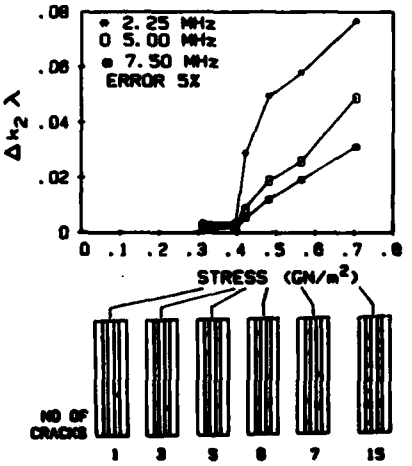

Fig. 13—Attenuation increases dramatically with transverse cracks in *Gr/Ep*, $[0_s, 90_4, 0_2]_s$ laminate at all three frequencies tested. Extent of damage is shown in the edge-replication sketches

conclude that for the present case while the attenuation is sensitive to the presence of transverse cracks, velocity is not. We have presented here just one example of the application of the new technique to ultrasonic NDE of fiber-reinforced composites. A detailed investigation of the problem has been carried out and the interested reader is referred to a follow-up paper.[16]

Conclusions

We have described a new experimental technique which can be used to measure phase velocity and attenuation of ultrasonic waves in very thin plates (down to a thickness which is three orders of magnitude smaller than the wavelength). We emphasize that in the development of this technique we have taken a 'black-box' approach, i.e., it would work for any material so long as it behaves in a linear-viscoelastic material and the attenuation is not large.

Acknowledgments

This research is supported by the Air Force Office of Scientific Research Contract No. F49620-83-C-0067. The continuing encouragement of Major Glasgow and Major Haritos is gratefully acknowledged.

References

1. Tauchert, T.R. and Guzelsu, A.M., "An Experimental Study of Dispersion of Stress Waves in a Fiber-Reinforced Composite," ASME J. Appl. Mech., 39, 98-102 (1972).
2. Kolsky, H., "Stress Waves in Solids," Dover (1953).
3. Chang, F.H., Couchman, J.C. and Yee, B.G.W., "Ultrasonic Resonance Measurements of Sound Velocity in Thin Composite Laminates," J. Comp. Mat., 8, 356-363 (Oct. 1974).
4. Heyman, J.S., "Phase Insensitive Acoustoelectric Transducer," J. Acoust. Soc. Amer., 64 (1), 243-249 (July 1968).
5. Achenbach, J.D., "Wave Propagation in Elastic Solids," North-Holland Publishing Company (1973).
6. Kolsky, H., "The Propagation of Stress Pulses in Viscoelastic Solids," The Phil. Mag., 8 (1), 693 (Aug. 1956).
7. Brigham, E.O., "The Fast Fourier Transform," Prentice Hall (1974).
8. Kinra, V.K., Petraites, M.S. and Datta, S.K., "Ultrasonic Wave Propagation in a Random Particulate Composite," Int. J. Solids Struct., 16, 301-312 (1980).
9. Kinra, V.K. and Anand, A., "Wave Propagation in a Random Particulate Composite at Long and Short Wavelength," Int. J. Solids, Struct., 18 (5), 367-380 (1982).
10. Kinra, V.K. and Ker, E.L., "Effective Elastic Moduli of a Thin-Walled Glass Microsphere/PMMA Composite," J. Comp. Mat., 16, 117-188 (March 1982).
11. Wolfenden, A., Harmouche, M.R., Blessing, G.V., Chen, Y.T., Terranora, P., Kinra, V.K., Dayal, V., Lemmens, J.W., Phillips, R., Smith, J.S. and Wann, R.J., "Dynamic Young's Modulus Measurements in Nickel-Based Alloys: Six Methods," to appear, J. Test. Eval.
12. Kinra, V.K. and Li, P.N., "Resonant Scattering of Elastic Waves by a Random Distribution of Inclusions," Int. J. Solids Struct., 22 (1), 1-11 (1986).
13. Kinra, V.K., "Dispersive Wave Propagation in Random Particulate Composites," Recent Advances in Composites in the United States and Japan, ASTM STP 864, ed. J.R. Vinson and M. Taya, 309-325 (1985).
14. Kinra, V.K. and Rousseau, C.Q., "Acoustical and Optical Branches of Wave Propagation: Some Additional Results," Proc. Multiple Scattering of Waves in Random Media and Random Rough Surfaces, The Penn. State Univ., ed. V.K. Vardan and V.V. Vardan, 603-613 (1985).
15. Hashin, Z. and Shtrikman, S., "A Variational Approach to the Theory of The Elastic Behavior of Multiphase Materials," J. Mech. Phys. Solids, 11, 127-140 (1963).
16. Dayal, V., Eden, J.G. and Kinra, V.K., "Ultrasonic Nondestructive Testing of Matrix Cracks in Fiber-Reinforced Composites," to be submitted to EXPERIMENTAL MECHANICS.

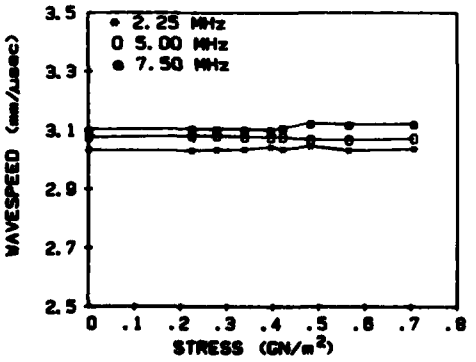

Fig. 14—Longitudinal wave-speed variation at three different frequencies with transverse cracks in a Gr/Ep, $[0, 90, 0_3]_s$ laminate

Appendix

Consider one-dimensional monochromatic, time-harmonic wave propagation along a rod made up of a linear-viscoelastic material, $e^{i(\omega t - kx)}$. At any frequency ω the *complex-valued* wave number is $k(\omega) = k_1(\omega) + ik_2(\omega)$. If attenuation is small the phase velocity $c = \omega/k_1$; k_2 is the attenuation, i.e., the amplitude of the wave decays as $e^{-k_2 x}$. Now suppose a pulse is propagating down this rod and is given at $x = 0$ by $f(t)$. Let

$$F^*(\omega) = \frac{1}{\sqrt{2\pi}} \int_{-\infty}^{\infty} f(t)\, e^{i\omega t}\, dt \qquad \text{(A1)}$$

Then

$$f(t) = \frac{1}{\sqrt{2\pi}} \int_{-\infty}^{\infty} F^*(\omega)\, e^{i\omega t} d\omega \qquad \text{(A2)}$$

For the sake of this discussion $f(t)$ may be viewed as an infinite sum of 'wavelets' of the type

$$f(t) = \left(\frac{F^*(\omega)\Delta\omega}{\sqrt{2\pi}}\right) e^{i\omega t} \qquad \text{(A3)}$$

Consider a propagating monochromatic 'wavelet' of complex amplitude, $\frac{F^*(\omega)\Delta\omega}{\sqrt{2\pi}}\, e^{i(\omega t - kx)}$. In eq (A3), $f(t)$ may be viewed as an infinite sum of such 'wavelets' at $x = 0$. Furthermore, at some arbitrary x the 'wavelets' may be summed up to yield

$$g(t) = \int_{-\infty}^{\infty} \left(\frac{F^*(\omega)d\omega}{\sqrt{2\pi}}\, e^{-ikx}\right) e^{i\omega t}$$

If $G^*(\omega)$ is the Fourier transform of $g(t)$, then

$$G^*(\omega) = F^*(\omega)^{-ikx}$$

or

$$\frac{G^*(\omega)}{F^*(\omega)} = e^{-ikx}$$

We have shown, therefore, that eq (12) which was originally derived for a perfectly elastic material is valid for a linear-viscoelastic material provided the attenuation is small ($k_2/k_1 < 0.1$) which is generally the case with engineering materials and certainly is the case for all materials tested during this work.

LEAKY LAMB WAVES IN AN ANISOTROPIC PLATE - AN EXACT SOLUTION AND EXPERIMENTS

BY

Vinay Dayal

Aerospace Engineering Department, Iowa State University, Ames, Iowa 50011

Vikram K. Kinra

Department of Aerospace Engineering and Mechanics and Material Center, Texas A&M University, College Station, TX 77843.

Received

ABSTRACT

We consider the propagation of Leaky Lamb waves in a plate consisting of a general balanced symmetric composite material. The problem has been examined both analytically as well as experimentally. An exact solution for the dispersion equation was obtained. Numerical results for complex-valued wavenumber were obtained for an isotropic material (aluminum) and a $[0/90_3]_s$ Graphite/Epoxy laminate. Excellent agreement for the isotropic case and a satisfactory agreement for the anisotropic case between the theory and experiment was observed.

Lamb waves are waves propagating in the plane of a plate with traction free boundaries. In the case of plane Lamb waves the particle displacement is in two directions: (1) the wave propagation direction, and (2) the thickness direction. The third component is zero because the plate is considered infinite in the plane of the plate. The governing equations for the Lamb waves were first derived by Prof. Horace Lamb in 1917 in his famous work[1]. These equations were quite complicated and a solution could be obtained only in the short and long wavelength limits. The first comprehensive solution was obtained by Mindlin[2] in 1950. Later, Viktorov[3] in his book dealt with the solution of Lamb waves in great detail. He provided the dispersion curves for a material with a Poisson's ratio of 0.34. According to Krautkramer et al[4] and Viktorov[3] the dispersion equations for Lamb waves in a plate immersed in a fluid were derived by Schoch[5]. Merkulov[6] has shown that if the density of the plate is large compared to that of the immersion fluid then the inertia effect of the fluid is negligible. He obtained a first order approximation solution for the complex part of the wavenumber i.e. attenuation. Plona et al[7] have shown that when the plate density is comparable to the fluid density, as in the case of plexiglas in water for example, then the inertial effects are significant and cannot be neglected.

Most of the work on Lamb waves has been motivated by the ultrasonic flaw detection of sheet material. Various researchers have studied the Lamb waves and used them for nondestructive evaluation (NDE) of homogeneous plates.[8,12] This is by no means an exhaustive list of the work in this field. With the advent of composites as a major structural material, especially in the aerospace industry, the attention of the NDE community has

shifted towards the composites and many of the NDE tools available for the testing of isotropic materials have been applied to the composites. Quite naturally, ultrasonics has also been used for the NDE of composites with varying degrees of success. The major difficulty in case of the composites arises from the fact that the theoretical analysis of wave propagation is considerably more difficult. For example, in an isotropic material the wave propagation and energy propagation directions are the same, in an anisotropic material the two are, in general quite different.

The general elastic wave problem in a layered composite is very complex and an exact solution is neither possible nor needed. Various simplified theories have been proposed which tend to make the calculation of dispersion relations manageable. The simplest ones to be proposed were the effective modulus theories.[13,15] Here, the geometrically weighted average of the constituent properties are used as the average material constants. Habegar et al[15], have replaced the composite plate with an equivalent homogeneous anisotropic plate and derived the Lamb wave displacement relations using the effective stiffness matrix. They have utilized these equations for the measurement of the nine elastic constants of paper.[16]

Some models[17-19] have been proposed to account for the dynamic effects of the propagating wave in the plates. These models incorporate the influence of the microstructure and anisotropy. One such 'effective stiffness" theory was proposed by Sun et al.[17] The fiber and matrix displacements are expressed as linear expansion about the mid-planes of the layers. The continuity relations take into account the dynamic interaction of the layers. Bedford et al[18] have proposed a diffusing continuum theory where the constituents are modeled as superimposed continua which undergo individual deformations. These deformations are then coupled together in a

dynamical process. The theory proposed by Chementi and Neyfeh[19] calculates the effective homogeneous transverse isotropic elastic behavior of a unidirectional composite in the long wavelength limit, using a two-step procedure based on alternating layered media. These results were then applied to a fluid-loaded anisotropic plate which is assumed to approximate the unidirectional fibrous composite laminate. The first limitations in all these theories is that they only consider ideal unidirectional composites with waves travelling in the fiber direction. Practical laminates, however, are cross-ply and angle-ply laminates and the effect of waves in these laminates becomes extremely complicated. The second limitation is that these theories have not considered the effect of fluid immersion and hence attenuation due to the leakage into the surrounding medium has been neglected.

As noted earlier, Habegar[15] calculated the dispersive equations for a balanced symmetrical laminate in vaccum (i.e. traction free boundary conditions). The object of the present work is to extend his analysis to the case of a laminate immersed in a liquid. The equations have been written in a form so that they can be used in conjunction with the effective stiffness matrix generated by any theory. The composite plate is replaced by an equivalent homogeneous anisotropic plate. Closed form dispersion equations are derived for both the symmetric and antisymmetric modes of Lamb wave propagation; an exact numerical solution is given. Due to particle displacement normal to the plate, waves are also set up in the surrounding fluid. This is the mechanism by which energy "leaks" from the plate into the liquid; hence the term "Leaky Lamb Waves". At the risk of stating the obvious, the wavenumber is complex; the imaginary part is the attenuation and is a measure of the energy leaked into the liquid. Stiffness matrix

calculated from the "effective modulus" theory has been used for the results presented here. Theoretical results obtained from the dispersion equation have been experimentally verified by tests performed on steel and aluminum plates. Excellent comparison between the theory and experiments was obtained. Finally, the theoretical solution for a composite laminate has been verified by tests performed on a $[0/90_3]_s$ Graphite/Epoxy composite plate.

I. THEORY

The development of the dispersion equations has traditionally been approached in two different ways. First, as developed by Lamb, the particle displacement U is written in terms of a scalar and a vector potential. A plane harmonic wave propagating in the plane of the plate is assumed, which allows the potential to be written so that the separation of variables technique can be used. The solution of potential equations is then used to satisfy the boundary conditions and the dispersion equation, linking wavespeed and frequency, is obtained. The second approach, namely, the method of partial waves, is more recent and is followed by Achenbach.[20] Harmonic waves can travel in a plate by reflecting back and forth between the two plane surfaces. These waves combine in such a manner that in the steady state a wave which consists of a travelling wave in the plane of plate and a standing wave in the thickness direction is obtained. This approach is more fundamental in that it directly provides the wave solution and results in a clearer picture of the nature of the wave propagation. In the following the second approach has been used. Since all the tests are performed under water, wave propagation in a plate immersed in a fluid is considered and suitable boundary conditions are applied.

A liquid-borne longitudinal wave incident on an unbounded plate is shown

in Fig. 1. Shown also are the mode-converted longitudinal and shear waves in the plate. The waves in the liquid along with the waves in the plate must sustain themselves to form a steady-state wave pattern in the plate. The conditions of the continuity of the displacements and equilibrium of forces at the plate-fluid interface have to be satisfied. The coordinate directions used here are the standard ones used in the composites literature: directions 1 and 2 in the plane of the plate while 3 normal to it.

For any symmetrical composite laminate the stress strain relation can be written as

$$\begin{bmatrix}\sigma_{11}\\ \sigma_{22}\\ \sigma_{33}\\ \sigma_{23}\\ \sigma_{31}\\ \sigma_{12}\end{bmatrix} = \begin{bmatrix}C_{11} & C_{12} & C_{13} & 0 & 0 & C_{16}\\ C_{21} & C_{22} & C_{23} & 0 & 0 & C_{26}\\ C_{31} & C_{32} & C_{33} & 0 & 0 & C_{36}\\ 0 & 0 & 0 & 2C_{44} & C_{45} & 0\\ 0 & 0 & 0 & C_{54} & 2C_{55} & 0\\ C_{61} & C_{62} & C_{63} & 0 & 0 & 2C_{66}\end{bmatrix} \begin{bmatrix}\varepsilon_{11}\\ \varepsilon_{22}\\ \varepsilon_{33}\\ \varepsilon_{23}\\ \varepsilon_{31}\\ \varepsilon_{12}\end{bmatrix} \tag{1}$$

The strain displacement relation can be written as

$$\varepsilon_{ij} = (U_{i,j}+U_{j,i})/2 \qquad \text{for } i,j=1,2,3 \tag{2}$$

The equation of motion in an elastic medium is

$$\sum_{j=1}^{3} \sigma_{ij,j} = \rho \ddot{U}_i \qquad i=1,2,3. \tag{3}$$

A plane wave travelling in an arbitrary direction, $\mathbf{x}$, may be written as

$$\mathbf{U} = \mathbf{U}_0 \exp[i(\mathbf{k}.\mathbf{x}-\omega t)] \tag{4}$$

where $\mathbf{U}$ is the displacement vector, $\mathbf{U}_0$ its amplitude and $\mathbf{k}$ is the wavenumber vector.

We now assume a plane strain condition considering an infinite plate. The displacement U_2 and all derivatives with respect to y vanish. Substituting Eqs.(1),(2) in Eq.(3),

$$\rho \ddot{U}_1 = C_{11}U_{1,11}+C_{13}U_{3,31}+C_{55}(U_{1,33}+U_{3,13}), \tag{5}$$

$$\rho\ddot{U}_3=C_{33}U_{3,33}+C_{13}U_{1,13}+C_{55}(U_{1,13}+U_{3,11}). \quad (6)$$

For a plane wave with displacements in the x and z directions only, the displacement components, U_1 and U_3, can be written from Eq.(4), as

$$U_1=U_{10}\exp[i(k_x x+k_z z-\omega t)], \quad (7)$$

and $$U_3=U_{30}\exp[i(k_x x+k_z z-\omega t)]. \quad (8)$$

where U_{10} and U_{30} are the wave amplitudes

Substituting Eqs.(5),(6) in Eqs.(7),(8)

$$\rho U_{10}\omega^2=C_{11}U_{10}k_x^2+(C_{55}+C_{13})U_{30}k_x k_z+C_{55}U_{10}k_z^2, \quad (9)$$

and $$\rho U_{30}\omega^2=C_{55}U_{30}k_x^2+(C_{55}+C_{13})U_{10}k_x k_z+C_{33}U_{30}k_z^2. \quad (10)$$

Let us define R as

$$R=U_{30}/U_{10}=(\rho\omega^2-C_{11}k_x^2-C_{55}k_z^2)/(C_{55}+C_{13})k_x k_z \quad (11)$$

Eliminating U_{10} and U_{30} from Eqs.(9),(10) we get a quadratic equation for k_z in terms of k_x and the elastic constants as

$$k_z^2=k_x^2\{-B\pm(B^2-4D)^{1/2}\}/2 \quad (12)$$

where,

$$B=[(C_{33}/\rho)(C_{11}/\rho-\omega^2/k_x^2)-(C_{13}/\rho)(2C_{55}+C_{13})/\rho-C_{55}\omega^2/\rho k_x^2]/\{(C_{33}C_{55})/\rho^2\}$$

and,

$$D=(\omega^2/k_x^2-C_{55}/\rho)(\omega^2/k_x^2-C_{11}/\rho)/\{(C_{33}C_{55})/\rho^2\}.$$

Let us define k_{zp} and k_{zm} as the two values of k_z obtained from Eq.(12) with + or - signs. Also R_p and R_m be the value of R when k_{zp} and k_{zm}, respectively, are substituted in Eq.(11). The equations derived above are for bulk waves travelling in an unbounded medium. These bulk waves travelling in the plate add up, such that, subject to the proper boundary conditions, the plate wave solution is obtained. The two possible plate wave displacements have the following forms

$$U_1=\exp\{i(k_x x-\omega t)\}[M\exp(ik_{zp}z)+N\exp(-ik_{zp}z)+P\exp(ik_{zm}z)+Q\exp(-ik_{zm}z)] \quad (13)$$

$$U_3=\exp\{i(k_x x-\omega t)\}[R_p\{M\exp(ik_{zp}z)-N\exp(-ik_{zp}z)\}+ +R_m\{P\exp(ik_{zm}z)-Q\exp(-ik_{zm}z)\}] \quad (14)$$

where M,N,P,Q are arbitrary constants.

The boundary conditions to be satisfied for a plate of thickness 2d are

$$\sigma_{33}=C_{33}U_{3,3}+C_{13}U_{1,1}=-p \quad \text{at } z=\pm d, \quad (15)$$

and,

$$\sigma_{31}=C_{55}U_{1,3}+C_{55}U_{3,1}=0 \quad \text{at } z=\pm d. \quad (16)$$

That is, the normal stresses in the plate and the liquid are equal and the shear stresses on the plate surface are zero as the fluid does not sustain shear. In addition, the continuity of diplacement demands,

$$U_3 = W_L \qquad \text{at } z=\pm d \quad (17)$$

where W_L is the displacement in the liquid.

Substituting Eqs.(13),(14) in Eqs.(15),(16), the following set of equations is obtained,

$$M\,G_p X + N\,G_p/X + P\,G_m Y + Q\,G_m/Y = ip(z=d) \quad (18.1)$$

$$M\,G_p/X + N\,G_p X + P\,G_m/Y + Q\,G_m Y = ip(z=-d) \quad (18.2)$$

$$M\,H_p X - N\,H_p/X + P\,H_m Y - Q\,H_m/y = 0. \quad (18.3)$$

$$M\,H_p/X - N\,H_p X + P\,H_m/Y - Q\,H_m Y = 0. \quad (18.4)$$

where $G_{p,m}=C_{33}k_{zp,m}+C_{13}k_x$; $H_{p,m}=k_{zp,m}+k_x R_{p,m}$;

and $X=\exp(ik_{zp}d)$; $Y=\exp(ik_{zm}d)$.

The wave motion in the fluid satisfies the equation

$$\frac{\partial^2\phi_L}{\partial x^2}+\frac{\partial^2\phi_L}{\partial z^2}+k_L^2\phi_L=0. \quad (19)$$

where $k_L=\omega/c_L$ is the wavenumber and c_L is the wavespeed in the fluid.

The form of the potential ϕ_L in the fluid to satisfy Eq.(19) is

$$\phi_L = \phi_0\exp[i(k_x x+k_z z-\omega t)]. \quad (20)$$

Substituting Eq.(19) in Eq.(18) it can be readily shown that

$$k_z^2 = k_L^2 - k_x^2.$$

The potential ϕ_L corresponds to a wave in the fluid which propagates along the plate in the x-direction and decays exponentially along the z-direction. This wave in the fluid has to be compatible with the Lamb wave in the plate. It means that this wave must pursue a path along the x-axis with a velocity equal to the phase velocity of the Lamb waves. The displacement in the fluid, W_L, can be calculated from the potential by

$$W_L = \frac{\partial \phi_L}{\partial z} = ik_z \phi_0 \exp[i(k_x x + k_z z - \omega t)]. \tag{21}$$

Applying the boundary conditions Eq.(17) to Eqs.(14),(21) and (18.2) we get

$$mM+nN+rP+sQ=ik_z\phi_0\exp(ik_z d) \tag{22}$$

$$-nM-mN-sP-rQ=-ik_z\phi_0\exp(-ik_z d) \tag{23}$$

where $m,n = \pm R_p \exp(\pm ik_{zp} d)$ and $r,s = \pm R_m \exp(\pm ik_{zm} d)$.

From Eqs (18.3) and (18.4) we can write

$$aM-bN+cP-eQ=0. \tag{24}$$

$$bM-aN+eP-cQ=0. \tag{25}$$

where $a,b = H_p \exp(\pm ik_{zp} d)$ and $c,e = H_m \exp(\pm ik_{zm} d)$.

From Eqs.(24) and (25) we get

$$N=[(ae-bc)P+(be-ac)Q]/(a^2+b^2)=N1.P+N2.Q \tag{26}$$

and,

$$M=[(be-ac)P+(ae-bc)Q]/(a^2+b^2)=N2.P+N1.Q \tag{27}$$

where $N1=(ae-bc)/(a^2+b^2)$ and $N2=(be-ac)/(a^2-b^2)$.

Substituting the values of M and N into Eqs.(22) and (23) we can write

$$(g+1)(P+Q)=ik_z\phi_0[\exp(ik_z d)+\exp(-ik_z d)] \tag{28}$$

where $g=mN2+nN1+r$ and $1=mN1+nN2+s$.

Similarly substituting the values of M and N into Eqs.(18.1) and (18.2),

$$P+Q=i\{p(z=d)+p(z=-d)\}/(F1+F2) \tag{29}$$

where $F1=N2.G_p.X+N1.G_p/X+G_m.Y$; $F2=N1.G_p.X+N2.G_p/X+G_m/Y$.

Comparing Eq.(28) with Eq.(29)

$$\frac{p(z=d)+p(=-d)}{F1+F2} = \frac{k_z\phi_0[\exp(ik_zd)+\exp(-ik_zd)]}{(g+1)} \tag{30}$$

The pressure in the fluid can be calculated from the potential ϕ_L from the relation

$$p = \lambda\left\{\frac{\partial_L^2\phi}{\partial x^2}+\frac{\partial_L^2\phi}{\partial z^2}\right\} \tag{31}$$

which gives

$$p(z=d) + p(z=-d) = -\lambda_L(k_x^2+k_z^2)\phi_0[\exp(ik_zd)-\exp(-ik_zd)] \tag{32}$$

Substituting Eq.(32) in Eq.(30)

$$\frac{[k_L^2-k_x^2]^{1/2}}{g+1} + \frac{\rho_L\omega^2}{F1+F2} = 0.$$

Simplification of F1+F2 and g+h, substitution into Eq.(33) and rearranging the equations give, for the symmetric mode,

$$\frac{\tan(k_{zp}d)}{\tan(k_{zm}d)} - \frac{G_p.H_m}{G_m.H_p} + \frac{i\rho_L\omega^2\tan(k_{zm}d)}{\rho(G_m/\rho)[k_x^2-k_L^2]^{1/2}}\left[-\frac{H_m}{H_p}R_p + R_m\right] = 0. \tag{34}$$

Similarly, we can show that for the antisymmetric mode the governing equation is

$$\frac{\tan(k_{zm}d)}{\tan(k_{zp}d)} - \frac{G_p.H_m}{G_m.H_p} + \frac{i\rho_L\omega^2\cot(k_{zp}d)}{\rho(G_m/\rho)[k_z^2-k_L^2]^{1/2}}\left[\frac{H_m}{H_p}R_p - R_m\right] = 0. \tag{35}$$

It is quite laborious, but not difficult, to show that for an isotropic material Eqs.(34) and (35) reduce to the equations (II.43) and (II.44) obtained by Viktorov.[3]

The first two terms of Eqs.(34) and (35) represent the dispersion relations for composite plate in vacuum. The third or the complex part of the equations is due to the immersion of plate in a liquid. It is observed

that almost all factors in the equations are complex and the required root, k_x, is also complex. These complex transcendental equations were solved by a numerical algorithm which is described next.

II. SOLUTION METHODOLOGY FOR DISPERSION EQUATIONS

The solutions of the dispersion equations for composite plates immersed in a fluid are obtained by the following two step procedure:

1. The correct value of k, of course is complex. However, as a point of departure, k is taken to be real and the dispersion equation for a plate in air is used. In other words, the imaginary part of Eqs.(34) and (35) is ignored. The roots for the remaining equation are obtained by a linear search method. The search is conducted in small steps varying either the wavespeed or the frequency while keeping the other fixed. Both modes of search are useful depending on the gradients of the dispersion curves in a particular region. The roots are then calculated precisely by the bisection technique.[22]

2. In the second step a search is made for the complex roots of k, i.e. for

$$k = k_1 + ik_2 \tag{36}$$

Substituting in the complete dispersion equation (34) or (35) for an immersed plate, we can write these equations in the form

$$\mathrm{Re}[k_1, k_2] + i\ \mathrm{Im}[k_1, k_2] = 0, \tag{37}$$

where Re and Im are the real and imaginary parts of the dispersion equation. Now for a solution to exist both the real and imaginary parts must be simultaneously zero, i.e.

$$\mathrm{Re}[k_1, k_2] = 0. \tag{38}$$

and

$$\mathrm{Im}[k_1, k_2] = 0. \tag{39}$$

Thus we have two transcendental equations with two unknowns k_1 and k_2. The modified Newton's (Secant) method is used to arrive at the roots of these equations. The initial estimate of the roots is: k_1 as obtained from step one (k_1 for the Lamb wave in the plate in air) and k_2=0. Now, k_1 is incremented in steps of 0.1 and k_2 in steps of 0.01. Since the Newton's method converges quadratically, the roots are obtained fairly rapidly. The nature of these equations is quite complicated and at places roots are close together. It is difficult to study the uniqueness and convergence of all the roots for such a complicated equation. Hence, it is quite possible that depending on the gradient of the equations and roots being close to each another, the solution may converge to some nearby root. To guard against this occurrence, we drew the complete dispersion curve diagram. It was found that in general the convergence was unique and rapid. Only at a few points the solution did not converge and some times it would converge at a nearby root. These points could be easily identified from the dispersion diagrams by using the following criterion: since the dispersion curves in air are smooth, it is reasonable to expect that the dispersion curves for the plate immersed in the fluid will also be smooth.

In the foregoing the effective elastic moduli of the plate were calculated using the classical laminate theory. Heuristically, when the wavelength is very large compared to the plate thickness, one would expect our calculations to be a fairly accurate representation of the reality. On the other extreme, when the wavelength is short compared to the plate thickness and, more importantly, where it is comparable to the plate thickness, clearly the theory is expected to break down for now the wave begins to "see" the individual plies. A question of practical significance is: Where does the transition occur? A systematic examination of the issue is

beyond the scope of the work. However, in the following we have probed this issue to a limited extent. This was the motivation for carrying out the experiments described next. It will be shown that the elementary "rule of mixtures" theory gives surprisingly good results upto $k_t d = 3.5$, where k_t is the shear wave number.

III. EXPERIMENTAL PROCEDURE

Shown in Fig.2 is a block diagram of the experimental setup. The pulse generator produces a trigger signal which is used to trigger the signal generator and also set the initial time (t=0) for the digitizing oscilloscope. The signal generator is used to produce a tone burst which is about 10-20 cycles long. This wave train is amplified to about 200 volts and fed into the transmitting transducer which launches a longitudinal wave in water. This wave is mode converted into a leaky Lamb wave in the specimen. These Leaky Lamb waves are sensed by the receiver which can be placed on either side of the specimen, see Fig. 3. Only the transmission mode (Fig. 3a) was used in this work. The signal from the receiver is amplified to about 1 volt and fed into a digital oscilloscope. All measurements are made with a reference peak near the center of the signal where it appears to have a steady-state. Note that a single cycle of signal will not be able to establish a good Lamb wave. When one cycle of sine wave is input into the transducer, due to the damping characteristics of the transducer, certain transient frequencies are produced. Since these frequencies do not correspond to the frequencies required to sustain Lamb waves in the plate, good Lamb waves will not be produced. Hence a long wave train is used which establishes the frequency of the signal and the effect of the transients can be ignored.

The transmitter and the receiver move on precision travelling mechanisms graduated to 0.001 in. The specimen is mounted on a turn table graduated to

0.1 degrees. When the specimen is rotated, the transducers are moved accordingly so that the same length of the specimen is always interrogated. The specimen is rotated in small steps and the peak amplitude and location a reference peak of the wave train is recorded.

The specimen is fixed at the angle identified as the Lamb angle for the measurement of attenuation. The receiver is moved by 0.5 inch (12.7mm) in steps of 0.05 (1.27mm) inch and the received signal is recorded. A exponential curve is fitted through this amplitude decay and the attenuation coefficient is estimated by the least-squares fit. The composite specimens tested during this work were fabricated using Magnamite AS4/3502 graphite/epoxy prepreg tapes manufactured by Hercules Inc.

IV. RESULTS AND DISCUSSION

The accuracy of our theory was checked in two ways: (1) against previous theories, and (2) against our own experiments.

The dispersion equations for a steel plate in water were solved with $c_{11}=c_{22}=c_{33}$; $c_{12}=c_{13}=c_{23}$ and $c_{11}=(E/\rho)^2$ and complex wavenumber was calculated. Figure 4(a) shows the dispersion curves for the steel plate. The solid lines are for the symmetric mode $(s_0, s_1, s_2, \ldots)$ and the dashed lines are for the asymmetric mode $(a_0, a_1, a_2, \ldots)$. Merkulov[6] did a corresponding analysis for an isotropic material but his solution was a first order approximation. Even then he was able to get good results because his assumption of $\rho_L/\rho \ll 1$ is valid for steel plate in water where $\rho_L/\rho \cong 0.128$. Figure 4(b) shows the attenuation for the first two modes. The approximate solution obtained by Merkulov is also shown and is fairly close to our exact solution. In conclusion, the approxi-mate analysis of Merkulov[6] serves to check our exact solution.

Next, the solution of the dispersive equations for an aluminum plate

are presented in Fig.5. (We note in passing that for aluminum $\rho_L/\rho = 0.37$ which is not negligible in comparison to one and, therefore, Viktorov's calculation may be quite inaccurate). The dispersion curves are exactly as obtained by Viktorov[3] but attenuation curves cannot be compared as no earlier work is available. Next, we describe the experimental results obtained with an aluminum plate. For a fixed frequency, $k_t d$, we measure the received amplitude as a function of the angle of incidence. The results are presented for three different values of $k_t d$ in Fig. 6. The peaks in the received signal correspond to the correct angle of incidence or "Lamb angle" which is governed by the Snell's Law;

$$\mathrm{Sin}(\theta_i)/\mathrm{Sin}(\theta_r) = c_w/c_L \qquad (40)$$

where θ_i is the angle of incidence, θ_r is the angle of refraction ($=\pi/2$ for Lamb waves), c_w is the wavespeed in water and c_L is the Lamb wavespeed. Thus,

$$c_L = c_w/\sin(\theta_i) \qquad (41)$$

It is noted that in Fig.6(a) at $k_t d$=1.0, two peaks are obtained. Converted to wavespeeds with Eq.(41) the values are shown as circled dots on the dispersion curves in Fig.5(a). The same comment applies to peaks in Fig.6(b)and 6(c). The attenuation was measured as described earlier. Measured values of the attenuation coefficient for an aluminum plate are shown as circles in Fig. 5(b). For the a_0 and a_1 modes the agreement between theory and experiments is excellent. For the s_0 mode the agreement is excellent as far as the lowest $k_t d$ (1.0) but becomes poorer as $k_t d$ increases. The reason for this becomes very clear when Figs.5(b) and 6 are examined together: The attenuation of the s_0 mode increases very rapidly with $k_t d \cong 2.0$ (Fig.5(b)). This results in a correspondingly small received signal for s_0 mode(Fig. 6) and a poor signal to noise ratio. Hence, a larger scatter in data is to be expected. The

importance of calculating attenuation curves becomes apparent: whenever possible the tests should be performed at low attenuation values to get accurate results.

Two questions arise at this stage regarding these measurements: (1) How do we ensure that the angle at which the measurement is made is the correct Lamb angle? and (2) Is the maximum amplitude criterion sufficient to guarentee that the angle is a Lamb angle? These questions are addressed here.

The angle of incidence for the Lamb waves can be checked by a very simple method. Shown in Fig. 7 is the schematic of the signal travelling through the specimen. When the receiver is at its initial location the total travel time is given by

$$t_i = l_1/c_w + l_2/c + l_4/c_w \tag{42}$$

As the receiver is moved by a distance x, the travel time becomes

$$t_f = l_1/c_w + l_2/c_L + l_3/c_L + l_5/c_w \tag{43}$$

The difference in the two arrival times is

$$\Delta t = t_f - t_i = l_3/c_L + (l_4 - l_5)/c_w = l_3/c_L - x\mathrm{Tan}(\theta)/c_w$$
$$= x/[c_L \cos(\theta)] - x\tan(\theta)/c_w \tag{44}$$

When Snell's law, Eq.(40), is substituted in Eq.(44), it is seen that $\Delta t = 0$. This means that at the correct Lamb angle when receiver is moved by any arbitrary distance, the total time taken by the wave to travel from the emitter to receiver remains unchanged and only its amplitude is reduced. Hence in a single experiment the attenuation is obtained and the correctness of the Lamb angle is verified. The precision of the procedure was found to be 0.1 degrees.

Next, tests were performed on a $[0/90_3]_s$ graphite/epoxy composite. The dispersion and attenuation curves for this specimen are shown in Figs. 8(a) and 8(b), respectively. (The derivation of elastic constants for this laminate

is deferred to the Appendix). The experimental results are shown as discrete circles in Fig.8. The comparison between the theory and experiments is considered reasonable. On the dispersion curves the comparison does not look very good, but the reason for this discrepancy is as follows. The stiffness coefficients used to solve the dispersion equations are for an ideal composite, with coefficients obtained by the rule of mixtures. Since the laminate used for the tests was fabricated by the author, it is expected that the properties of the laminate will not be as good as the theory suggests. The statically measured stiffness of the laminate is lower and the corresponding wavespeed is shown as an arrow on the figure. In view of the reduced value of c_{11} the entire dispersion curves will be shifted downwards and then an excellent agreement between theory and experiment will be observed. This also means that all the elastic constants to be used in the equations should be determined experimentally. Then only the solution of the dispersion curves will be truly representative of the response of the plate. The low attenuation values shown in Fig. 8(b) could be measured but then the attenuation rises very rapidly and cannot be measured at higher frequencies due to the reasons described earlier.

Finally, in this paper we have reported theoretical and experimental procedures for investigating Leaky Lamb Waves in composite laminates. The motivation for this work came from the Ultrasonic Nondestructive Evaluation (UNDE). As a composite laminate is damaged the stiffness decreases and the attenuation increases. Thus, from a measurement of stiffness and attenuation one can deduce the extent of damage. Measurement of these quantities in the through-the-thickness direction is a relatively straight forward matter and was the subject of a recent investigation by the present authors (Kinra and Dayal).[23] However, it is of equal, if not greater, interest to measure the

in-plane stiffness and attenuation. We have measured these quantities as a function of damage in graphite/epoxy laminates; this will be the subject of a follow-up paper by the authors.

V. CONCLUSIONS

We have considered the propagation of Leaky Lamb Waves in a balanced symmetric laminate immersed in a liquid. An exact solution for the dispersion equation has been derived. The wavespeed and the attenuation were also measured experimentally for a $[0/90_3]_s$ laminate. The agreement between the theory and experiment was found to be quite good.

ACKNOWLWDGEMENT

This research was supported by the Air Force of Scientific Research Contract No. F49620-83-C-0067 to Texas A&M University. The program managers were Dr. David Glasgow and Dr. George Haritos.

REFERENCES

[1]H. Lamb, *On Waves in an Elastic Plate,* Proc. Roy. Soc.(London), Ser.A., 93-114 (1917).

[2]R.D. Mindlin, *Waves and Vibrations in Isotropic Elastic Plates,* Structural Mechanics, ed. J.N.Goodier & N.J. Hoff, Pergamon Press, NY (1960).

[3]I.A. Viktorov, *Rayleigh and Lamb Waves*, Plenum Press, New York, (1967).

[4]J. Krautkramer and H. Krautkramer, *Ultrasonic Testing of Materials*, 3rd ed., Springer Verlag, Berlin, Ch:10-11 (1983).

[5]A. Schoch, "Der Schalldurchgang durch Platten (Sound transmission in Plates)", Acoustica, 2(1), 1-17 (1952).

[6]L.G. Merkulov, "Damping of Normal Modes in a Plate Immersed in a Liquid", Soviet Physics-Acoustics, 10(2) (Oct-Dec 1964.)

[7]T.J. Plona, M. Bahravesh and W.G. Mayers, "Rayleigh and Lamb Waves at Liquid Solid Boundaries", Ultrasonics, 171-174 (July 1975).

[8]E. Lehfeldt and P. Höller, "Lamb Waves and Lamination Detection" Ultrasonics, 255-257 (Oct 1967).

[9]R. Forito, W. Madigosky and H. Überall, "Resonance Theory of Acoustic Waves Interacting with an Elastic Plate", J. Acoust. Soc. Am., 66(6), 1857-1866 (Dec 1979).

[10]M. Hattunen and M. Luukala, "An Investigation of Generalized Lamb Waves using Ultrasonic Reflectivity Measurements", Applied Physics 2, 257-263 (1973)

[11]R.D. Fay and O.V. Fortier, "Transmission of Sound through Steel Plates Immersed in Water", J. Acoust. Soc. Am. 23(2), 339-346 (May 1951).

[12]A. Freedman, "Reflectivity and Transmissivity of Elastic Plates I. Comparison of Exact and Approximate Theories", J. Sound Vibrations, 59(3), 369-393 (1978).

[13]D.S. Choi and A. Bedford, "Transient Pulse Propagation in a fiber-reinforced Material", J. Acoust. Soc. Am. 54(3), 676-684 (1973)

[14]L.P. Solie and B.A. Auld, "Elastic Waves in Free Anisotropic Plates", J. Acoust. Soc. Am., 54(1), 50-65 (1973).

[15]C.C. Habegar, R.W. Mann and G.A. Baum "Ultrasonic Plate Waves in Paper", Ultrasonics, 57-62 (Mar. 1979).

[16]R.W. Mann, G.A. Baum and C.C. Habegar, "Determination of all nine Orthotropic Elastic Constants for Machine made Paper", TAPPI (Technical Assoc. of the Pulp and Paper Industry), 63(2), 163-166 (Feb. 1980).

[17]C.T. Sun, J.D. Achenbach and G. Herrmann, "Continuum Theory of Composite Materials", J. Appl. Mech., 467-475 (Sept. 1968).

[18]A. Bedford and M. Stern, "Towards a Diffusing Continuum Theory of Composite Materials", J. Appl. Mech., 8-14 (Mar. 1971).

[19]D.E. Chimenti and A.H. Nayfeh, "Leaky Lamb Waves in Fibrous Composite

Laminates", J. Appl. Phy., 58(12) 4531-4537 (1985).

[20]J.D. Achenbach, *Wave Propagation in Elastic Solids*, North-Holland Publishing Co., Amsterdam (1973).

[21]B.D. Agarwal, L.J. Broutman, *Analysis and Performance of Fiber Composites*, John Wiley & Sons, NY, Ch:5, 149 (1980).

[22]J.P. Holman, *Experimental Methods for Engineers*, McGraw Hill, NY, CH:3, 43(1978).

[23]V.K. Kinra, V. Dayal, "A New Technique for Ultrasonic NDE of Thin Specimen", to be published in Experimental Mechanics.

APPENDIX

The stiffness of an orthotropic lamina is fully defined by the following elastic constants,

$$E_{ijkl} = \begin{bmatrix} E_{1111} & E_{1122} & E_{1133} & 0 & 0 & 0 \\ E_{2211} & E_{2222} & E_{2233} & 0 & 0 & 0 \\ E_{3311} & E_{3322} & E_{3333} & 0 & 0 & 0 \\ 0 & 0 & 0 & E_{2323} & 0 & 0 \\ 0 & 0 & 0 & 0 & E_{3131} & 0 \\ 0 & 0 & 0 & 0 & 0 & E_{1212} \end{bmatrix} \tag{A1}$$

For a lamina with a fiber orientation in an arbitrary direction this stiffness tensor has to be written in the rotated coordinate directions. For a fourth order tensor, the transformation law is

$$T'_{ijkl} = a_{pi} a_{qj} a_{rk} a_{sl} T_{pqrs} \tag{A2}$$

where a_{ij} is the direction cosine between directions i and j.

Let directions 1 and 2 be in the plane of the plate and a rotation, θ, takes place about axis 3. Substituting the rotation angle in the transformation law and writing the stiffness in the contracted notation, the following non-zero terms are obtained,

$$E_{jkl} = \begin{bmatrix} C'_{11} & C'_{12} & C'_{13} & 0 & 0 & C'_{16} \\ C'_{21} & C'_{22} & C'_{23} & 0 & 0 & C'_{26} \\ C'_{31} & C'_{32} & C'_{33} & 0 & 0 & C'_{36} \\ 0 & 0 & 0 & C'_{44} & C'_{45} & 0 \\ 0 & 0 & 0 & C'_{54} & C'_{55} & 0 \\ C'_{61} & C'_{62} & C'_{63} & 0 & 0 & C'_{66} \end{bmatrix} \tag{A3}$$

Only the above terms will be effective when the stiffness matrix is synthesised.[21] Hence this matrix is used in deriving the governing equations for the Lamb waves. We observe from the main body of derivations of the dispersion equations that the terms left after simplifications are C_{11}, C_{13}, C_{33}, and C_{55}.

Relating the stiffness to modulus properties and the lamina being

transversely isotropic, with $E_3 = E_2$ and $\nu_{13} = \nu_{12}$, following relations are obtained,

$$\begin{aligned} C_{11} &= E_1/(1-\nu_{12}\nu_{21}) \\ C_{13} &= \nu_{12}E_2/(1-\nu_{12}\nu_{21}) \\ C_{33} &= E_2/(1-\nu_{12}\nu_{21}) \\ C_{55} &= G_{13} = G_{12} \end{aligned} \tag{A4}$$

For the AS4/3502 lamina, the following properties were measured,

E_1 = 1.48 E11 N/m2

E_2 = 1.10 E10 N/m2

ν_{12} = 0.27

ν_{21} = 0.0199

G_{12} = 4.83 E9 N/m^2.

and were used to estimate the laminate properties.

List of Figures:

Fig. 1. Generation of Lamb waves in a plate. Each reflection produces a longitudinal (solid line) and a transverse (dash line) wave.

Fig. 2. Block Diagram of the experimental setup.

Fig. 3. Generation and reception of Leaky Lamb waves, (a) transmission, and (b) Reflection modes.

Fig. 4. (a) Dispersion Curves and (b) attenuation curves for a steel plate immersed in water.

Fig. 5. (a) Dispersion curves and (b) attenuation curves for an aluminum plate immersed in water. Discrete points are experimental.

Fig. 6. Received signal amplitude as a function of angle of incidence, at $k_t d$ = 1.0, 2.25, 3.5 for aluminum plate in water.

Fig. 7. Travel time for a Lamb wave in a plate.

Fig. 8. (a) Dispersion curves, and (b) attenuation curves for a $[0/90_3]_s$ laminate in water. Discrete points are experimental.

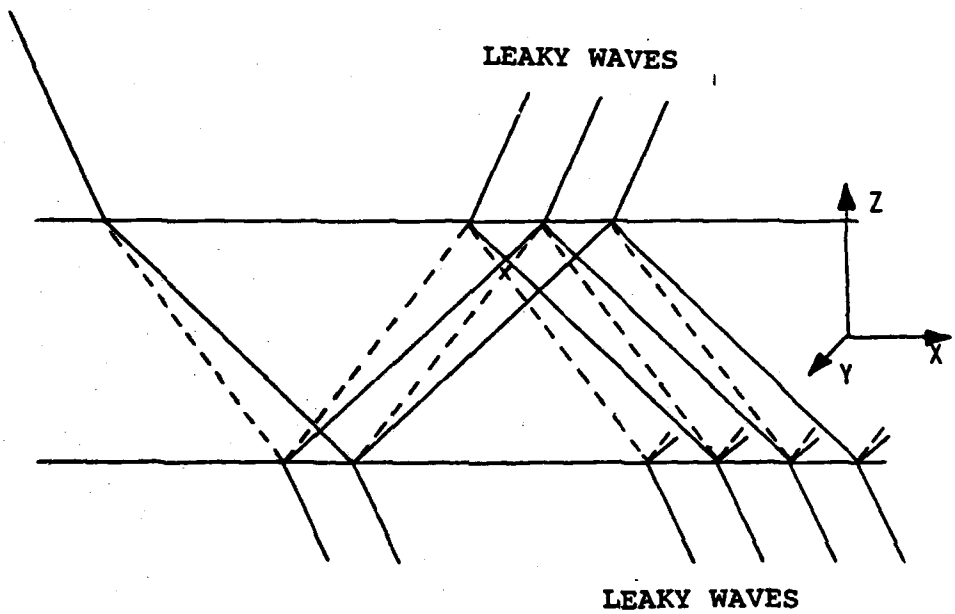

Fig 1

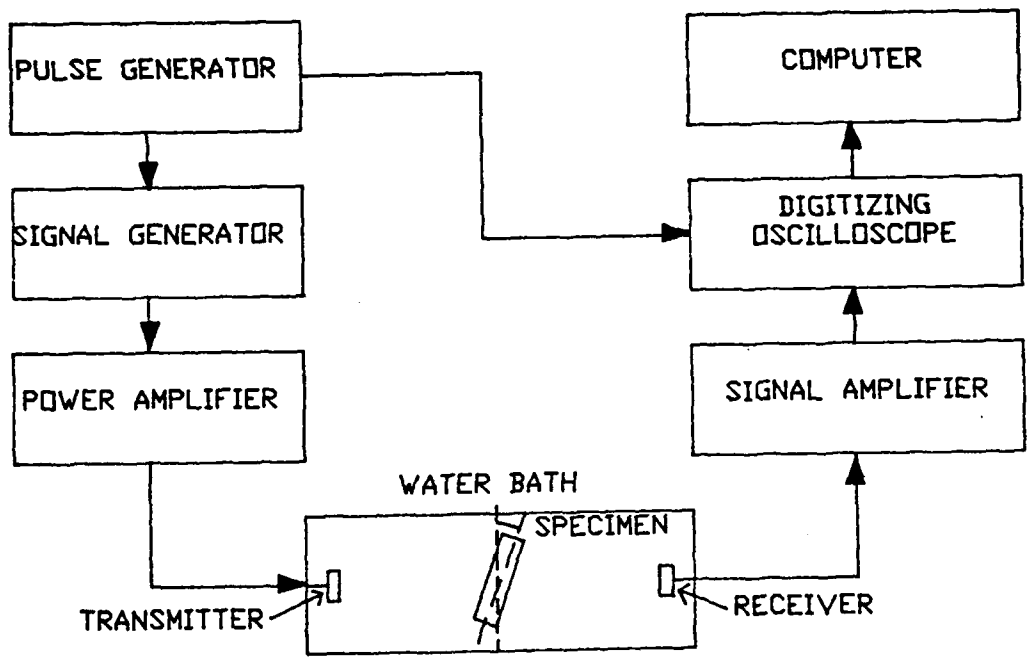
PULSE GENERATOR
SIGNAL GENERATOR
POWER AMPLIFIER
COMPUTER
DIGITIZING OSCILLOSCOPE
SIGNAL AMPLIFIER
WATER BATH
SPECIMEN
TRANSMITTER
RECEIVER

Fig 2

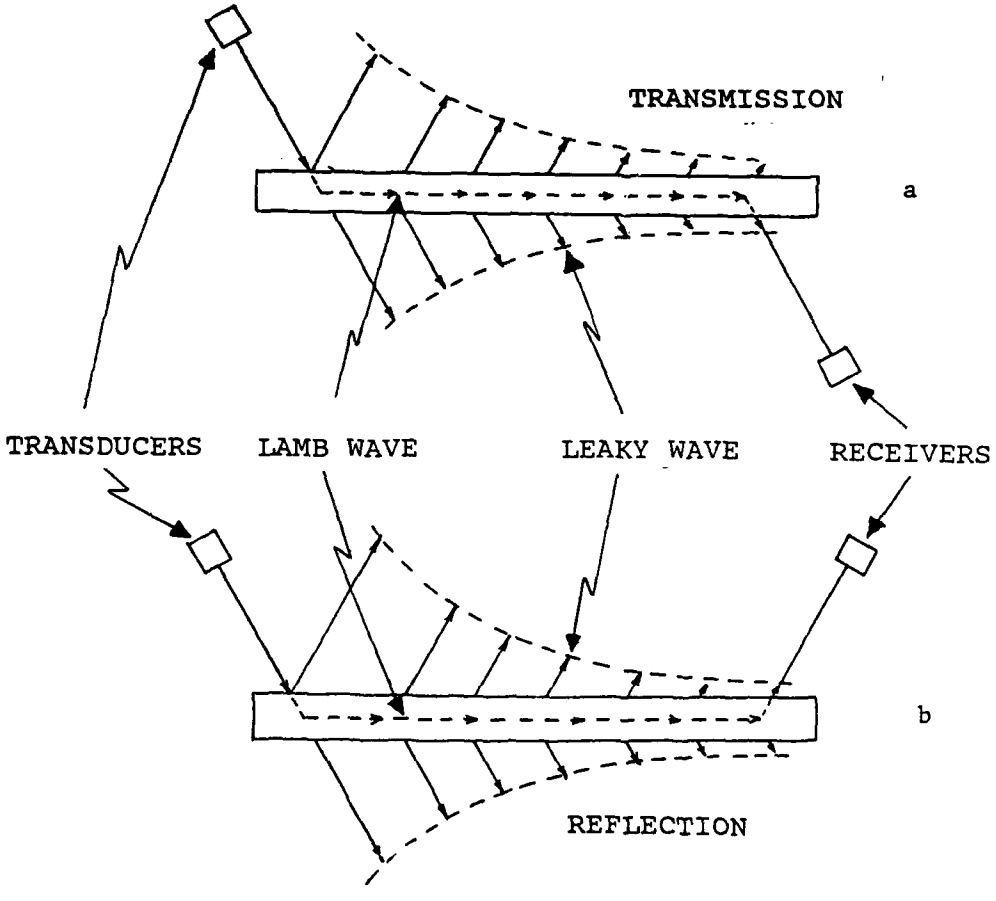
TRANSMISSION
a
TRANSDUCERS
LAMB WAVE
LEAKY WAVE
RECEIVERS
b
REFLECTION

Fig 5

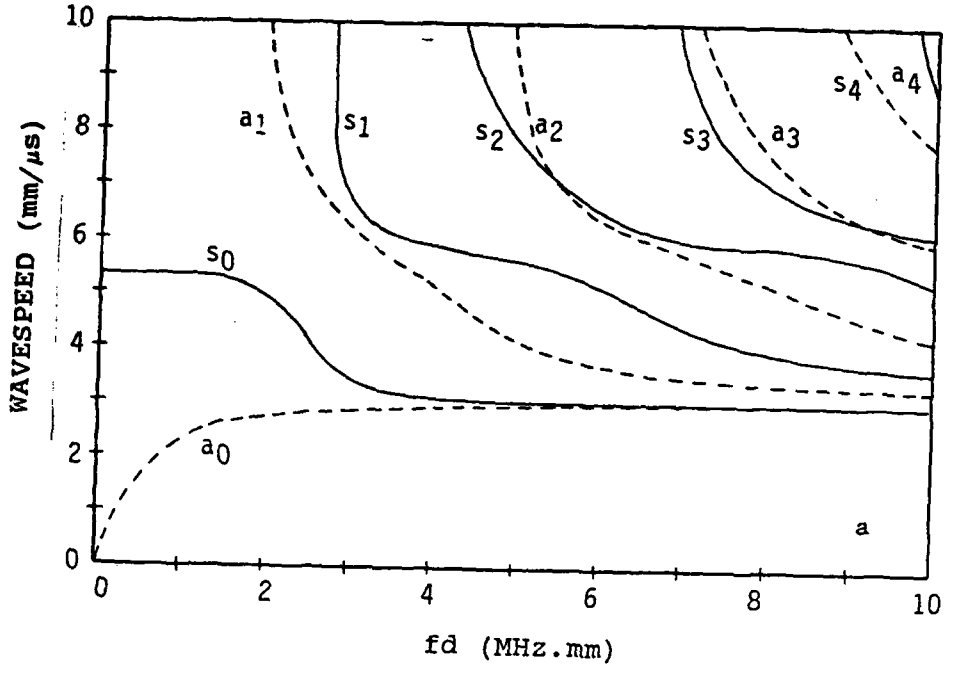
WAVESPEED (mm/μs)
fd (MHz.mm)
a0
s0
a1
s1
a2
s2
a3
s3
a4
s4
a
0
2
4
6
8
10

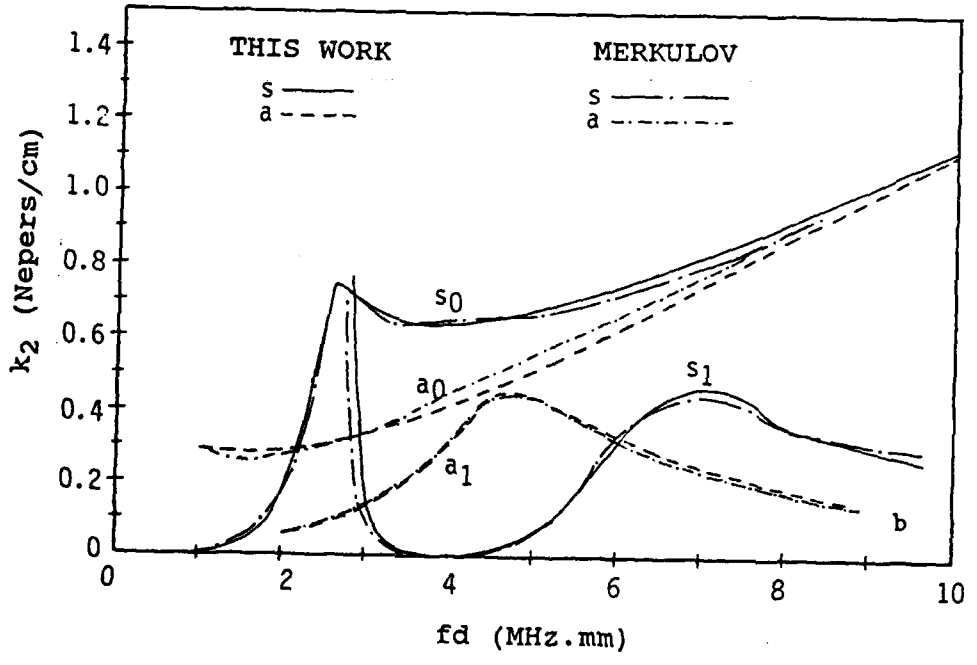
THIS WORK
MERKULOV
s
a
k2 (Nepers/cm)
fd (MHz.mm)
s0
a0
a1
s1
b
0
0.2
0.4
0.6
0.8
1.0
1.2
1.4
2
4
6
8
10

Fig 1

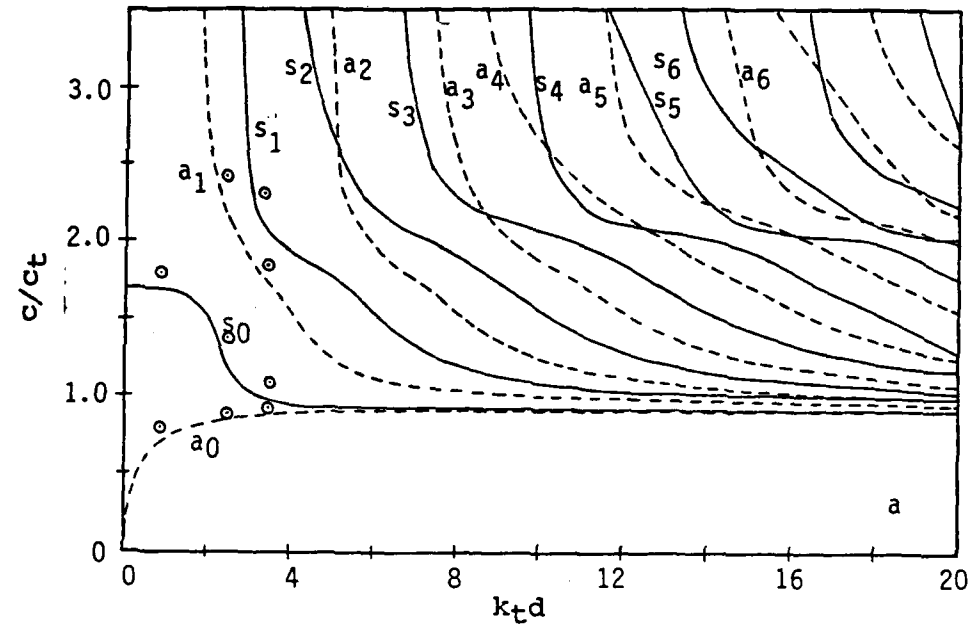
3.0
2.0
1.0
0
c/ct
s2
a2
s3
a3
a4
s4
a5
s6
s5
a6
s1
a1
s0
a0
a
0
4
8
12
16
20
ktd

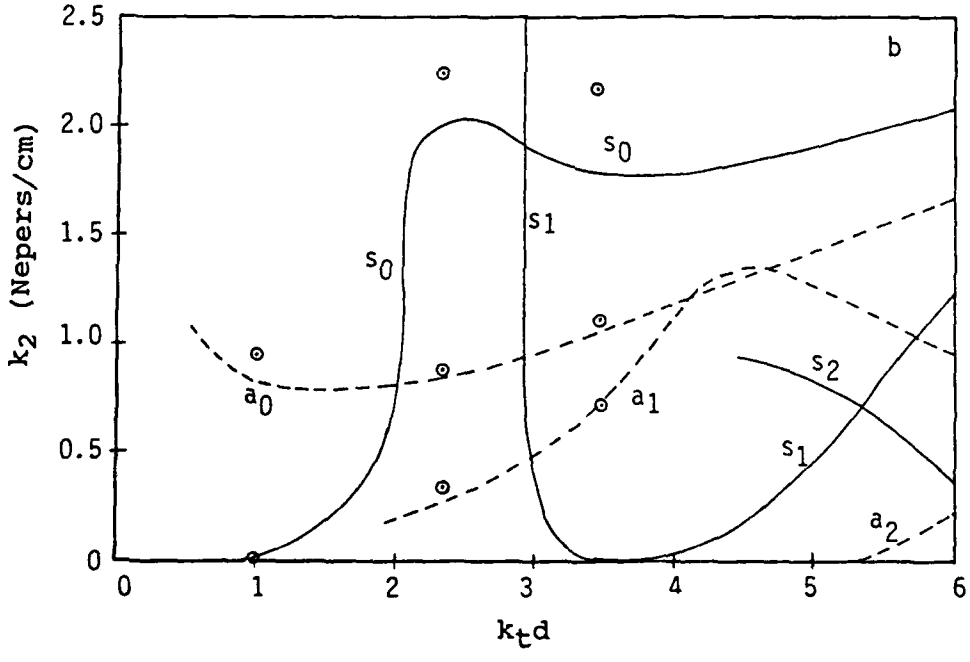
2.5
2.0
1.5
1.0
0.5
0
k2 (Nepers/cm)
b
s0
s1
s0
a0
a1
s2
s1
a2
0
1
2
3
4
5
6
ktd

Fig 5

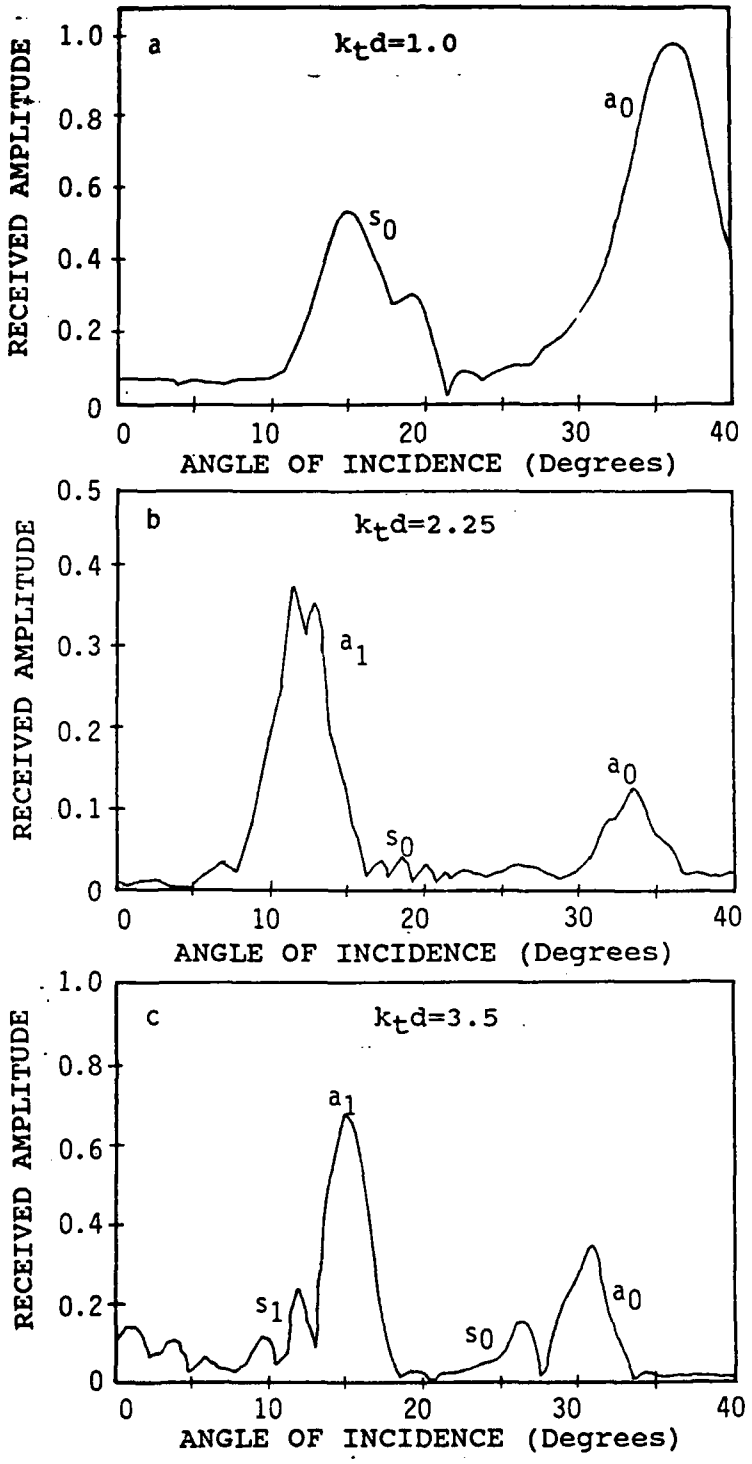
a
$k_t d$=1.0
a_0
s_0
RECEIVED AMPLITUDE
1.0
0.8
0.6
0.4
0.2
0
0
10
20
30
40
ANGLE OF INCIDENCE (Degrees)
b
$k_t d$=2.25
a_1
a_0
s_0
RECEIVED AMPLITUDE
0.5
0.4
0.3
0.2
0.1
0
0
10
20
30
40
ANGLE OF INCIDENCE (Degrees)
c
$k_t d$=3.5
a_1
s_1
s_0
a_0
RECEIVED AMPLITUDE
1.0
0.8
0.6
0.4
0.2
0
0
10
20
30
40
ANGLE OF INCIDENCE (Degrees)

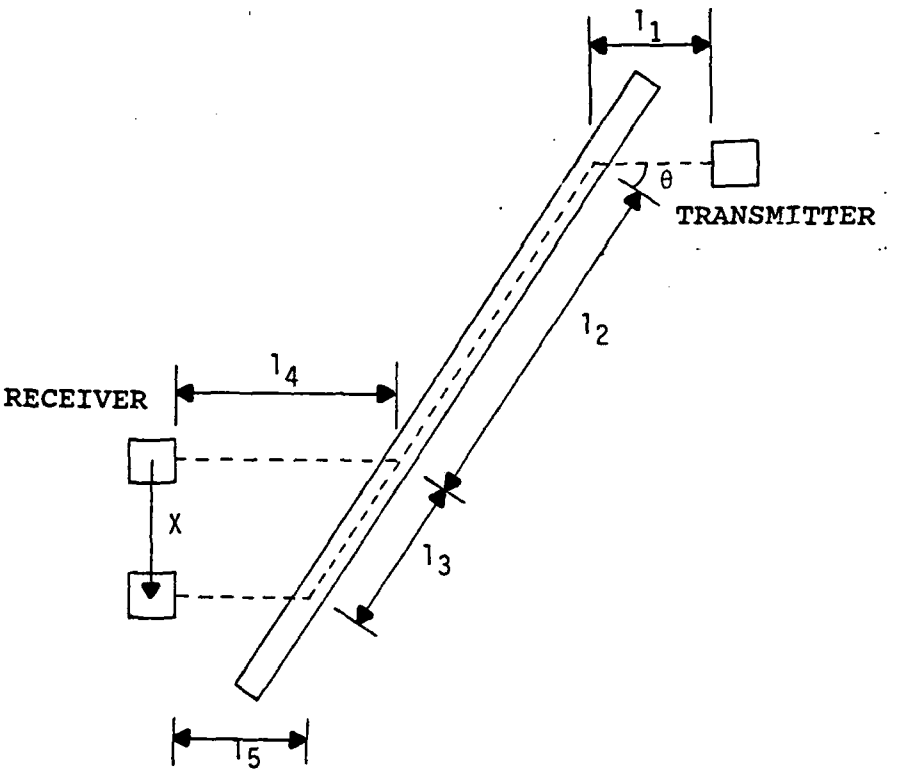

Fig. 7

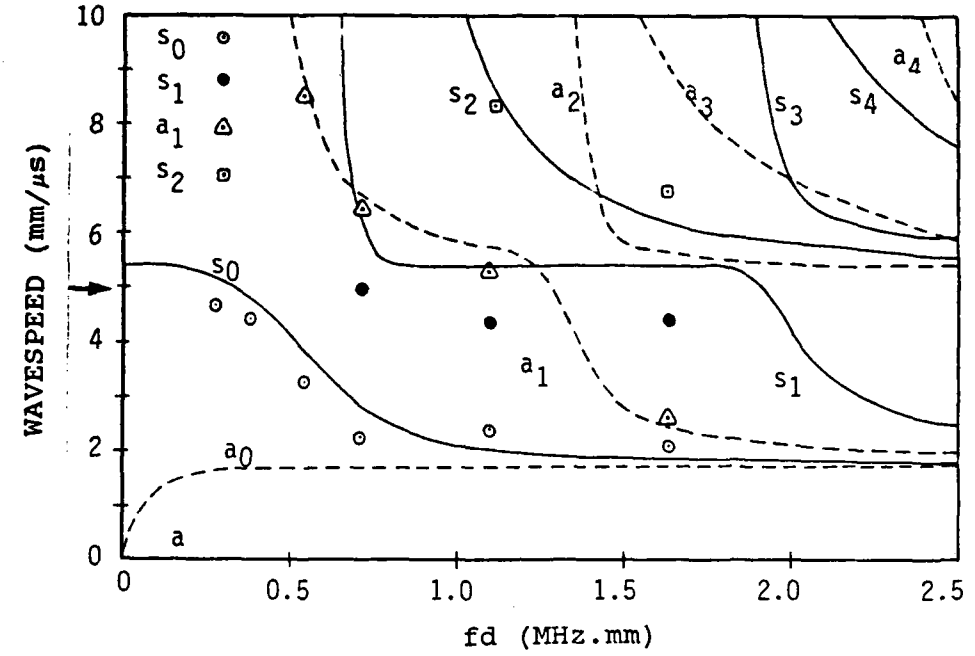
WAVESPEED (mm/μs)
fd (MHz.mm)
s_0
s_1
a_1
s_2
a_0
a_2
s_3
a_3
s_4
a_4
a

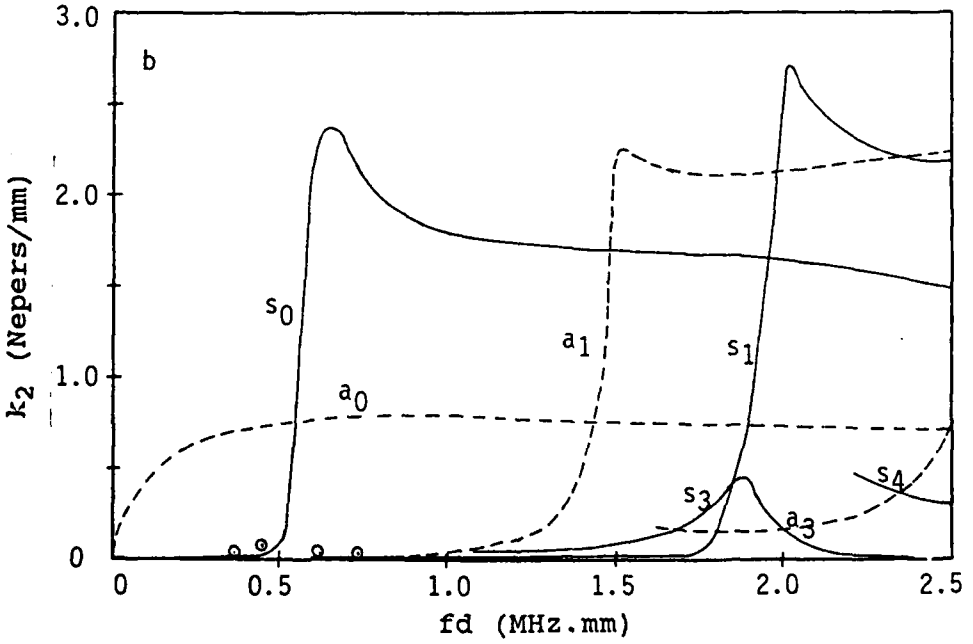
k_2 (Nepers/mm)
fd (MHz.mm)
b
s_0
a_0
a_1
s_1
s_3
a_3
s_4

LEAKY LAMB WAVES IN AN ANISOTROPIC PLATE-
NDE OF MATRIX CRACKS IN FIBER-REINFORCED COMPOSITES

Vinay Dayal

Aerospace Engg. Dept., Iowa State University, Ames, IA 50011

Vikram K. Kinra

Mechanics and Materials Center & Aerospace Engg. Dept.,

Texas A&M University, College Station, TX 77843

Received

ABSTRACT

This paper is concerned with the use of leaky Lamb waves for the Non-Destructive Evaluation (NDE) of damage in anisotropic materials such as fiber-reinforced composites. Two fundamental acoustic properties of the material, namely, the wavespeed and attenuation have been measured. Stiffness is deduced from the wavespeed. The damage mode selected for this study is matrix cracking. As expected, the in-plane stiffness decreases and the attenuation increases with an increase in the linear crack density.

ply laminates. The reason for this behavior becomes clear from Fig. 1a. In the through-the-thickness mode, the wave travels normal to the plate and the cracks also lie in the same plane. Obviously, the wave-crack interaction is low. As mentioned earlier, though changes in attenuation are measured, the wave-speed or stiffness is not effected. Moreover, out-of-plane stiffness is not of much use to the designer while in-plane stiffness is an important design criteria. Hence, ultrasonic waves travelling in the plane of the plate can be used to measure the relevant changes in wavespeed and attenuation. This mode of wave propagation is called the Lamb wave (or plate wave) mode. In this mode the waves travel in the plane of the plate or normal to the cracks, see Fig. 1b, and hence the crack-wave interaction will be large and it is expected that the in-plane stiffness can be measured.

When the plate is immersed in a fluid, the Lamb waves travelling in the plate leak energy into the surrounding fluid as shown in Fig. 2. These waves in the fluid have been named "Leaky Lamb waves". These leaky Lamb waves can be sensed by a transducer and the wavespeed and attenuation in the plate material can be measured. It may be noted here that in the Lamb wave mode of wave propagation, attenuation in undamaged specimens is due to; (1) energy leaked into the fluid, and (2) due to the material non-uniformity because of the damage. We assume that the attenuation due to leakage remains essentially constant but the attenuation due to damage increases with damage. Hence the measured increase in attenuation is attributed to the induced damage. The Lamb wavespeed, on the other hand, is related to the overall stiffness in the plane of the plate and hence the changes in wavespeed are due to the change in the in-plane stiffness as the damage increases.

Bar-Cohen and Chementi (4) have utilized the leaky Lamb waves for the non-destructive testing (NDT) of damage in fiber-reinforced composites. They have

shown that various forms of damage can be identified by a null-zone movement method. When a wave is incident upon the plate, the specular reflection from the plate takes place along with the generation of Lamb waves in the plate. Due to phase change in the leaky waves, the specular reflection and the leaky wave interfere and a well defined null zone is observed; this movement of the null zone has been related to various defects. They have used this in a C-Scan type setup to map the damage.

In this work we have taken an entirely different approach in utilizing Lamb waves for the NDE of composites. The receiving transducer is placed in such a position that the specular reflection is completely avoided and only the leaky waves are sensed. Shown in Fig. 2 is the relative position of the transmitter and the receiver. The wavespeed and attenuation in the specimen are measured from the received signal. The specimen is damaged and transverse cracks are introduced in the cross-ply laminates. We present here some results for the NDE of cross-ply laminates by leaky Lamb waves. It is observed that attenuation increases and in-plane stiffness decreases as damage is induced in the composites. The technique has a good potential for field application since it is non-destructive and is the only NDE technique available for the in plane stiffness measurement. Furthermore, as will be shown later, it yields <u>local</u> values of properties.

THEORY

The detailed derivation of the dispersion equations for a general balanced symmetrical composite laminate immersed in a fluid are reported in a companion paper (5). The basic symmetrical mode (s_0) has been selected for the tests. The reason for this selection will be described in details in the results section. It will suffice to mention at this stage that in this mode the wave travels as a plane-fronted wave. Also, the wavelength of the wave is large in comparison to the crack-size and therefore the composite can be treated as an anisotropic

homogenous material. In this mode it can be shown (6) that when fd is small,

$$c^2 = E_1/\rho(1-\nu_{12}\nu_{21}) \quad (1)$$

where f is the test frequency, 2d is the plate thickness, c is the Lamb wavespeed, E_1 is an in-plane modulus, and ν_{12} and ν_{21} are the two in-plane Poisson's ratios. For the composites tested during this investigation $\nu_{12}\nu_{21}<<1$ and hence Eq. (1) reduces to,

$$c^2 = E_1/\rho \quad (2)$$

The refraction of ultrasonic waves through a plate follow the Snell's law of refraction;

$$\mathrm{Sin}(\theta_i)/\mathrm{Sin}(\theta_r) = v_\omega/c \quad (3)$$

where v_ω is the wavespeed in water, θ_i and $\theta_r = \pi/2$ are the angles of incidence and refraction, respectively. Thus,

$$c = v_\omega/\mathrm{Sin}(\theta_i) \quad (4)$$

combining Eq.(4) with Eq.(2),

$$E_1 = \rho[v_\omega/\mathrm{Sin}(\theta_i)]^2 \quad (5)$$

This equation is used for the measurement of the in-plane stiffness in this work.

It is obvious from Eq. (5) that the measurement of θ_i will be an important factor in the accuracy of measurement. A very simple but elegant method has been devised to accurately ascertain the Lamb angle. As shown in Fig. 2 the receiver is moved by a distance, x. A very elementary calculation (5) shows that at the correct Lamb angle, total travel time from the emitter to the receiver is independent of x. Thus, though the receiver is moved on its travelling mechanism, the signal on the oscilloscope remains unchanged on the time scale: only its amplitude is reduced. It was determined that the Lamb angle could be measured with a precision of 0.1 degrees. The decrease in the amplitude of the signal as the receiver is moved, is recorded and by fitting an exponential curve through

the points, the attenuation coefficient is calculated. Thus, in one experiment the attenuation is obtained and the validity of the Lamb angle is also checked. The accuracy of measurement of modulus is estimated to be 2%, and for attenuation it is about 10%.

EXPERIMENTAL PROCEDURE

The block diagram of the experimental setup is shown in Fig. 3. The pulse generator produces a trigger signal which is used to trigger the signal generator and also set the initial time for the digitizing oscilloscope. The pulse generator produces a train of sinusoidal signal. Since these signals are typically of a few volts in amplitude, a power amplifier is used to amplify the signal to about 200 Volts. This amplified signal is then fed into the transmitting transducer. The transducer produces an ultrasonic wave which is transmitted through the water and specimen to the receiving transducer. The receiver sends the signal to the signal amplifier, which provides the oscilloscope with a signal of about one volt. The digitizing oscilloscope averages the signal over 64 samples and stores the average. On demand from the computer, the necessary information is provided by the oscilloscope over an IEEE-488 bus. The wavespeed and attenuation are then calculated. Entire operation of the oscilloscope is controlled by the computer.

Water is used as an acoustic couplant; the transducers are mounted inside a water bath. Transmitter and receiver are mounted on two travelling mechanisms graduated to 0.001 inch and the specimen is placed in a holder mounted on a turntable which is graduated to 0.1 degrees. When the specimen is rotated to achieve the correct Lamb angle, the length of the specimen between the transducer is increased. To offset this increase, the two transducers are moved laterally such that same length of the specimen is interrogated throughout the experiments. Since repeatability is very important in our measurements, the specimen holder

is designed so that exact replacement of the specimen is achieved every time. The specimen is carefully placed against a tab fixed on the specimen holder on each replacement. A typical plot of received signal as the specimen is rotated is given in Fig. 4.

All composite specimens are made of Magnamite AS4/3502 graphite/epoxy prepreg tapes manufactured by Hercules Inc. Transverse cracks were chosen to be the mode of damage for all the studies reported here. Towards this end cross-ply laminates with layups of the type $[0_m/90_n]_s$ were fabricated. Typically the specimen are plates of 1"X11" size.

All loading to induce damage in the specimen was performed on INSTRON Model 125 equipped with a 20,000 lb load cell. The tests were conducted in the stroke-control mode. The cross-head speed used was 0.05 in/min in the initial stages of damage. When nearing the ultimate strength of the specimen the speed was reduced to 0.02 in/min.

The edges of the specimens were polished with 5 and 1 micron alumina powder. This is done to get good quality edge replications. A record of the cracks developed in the specimen was maintained in the form of edge replications. In order to open the cracks, the specimens are loaded in the INSTRON machine to about 500 lbs. The replicating tape is softened by acetone and pressed against the edge of the specimen. The tape material flows into the crack and hardens in about 30 seconds. The tape is removed and the replica of the cracks can be viewed under a microfiche reader.

In the early stages of this work, water seepage into the cracks was found to be a major source of error and this was prevented by coating the edges with a strippable coat (Mfg. Sharwin Williams).

RESULTS AND DISCUSSIONS

Dispersion equations for Lamb waves in isotropic materials are available

in the published literature, they were solved (8) based on the assumption that the attenuation due to leakage is negligibly small. This assumption is reasonably valid as long as $\rho^1/\rho >> 1$ where ρ^1 and ρ are the densities of the plate and the immersion fluid, respectively. If one is studying steel/water system then ρ^1/ρ is, in fact, large compared to one. However, for the fiber-reinforced composites studied in this work, $\rho^1/\rho = 1.53$ and therefore, neglecting the inertial loading of water will result in gross error in the dispersion curves as also shown by Plona et al (9). Therefore, we have derived an exact solution for the dispersion equations for an anisotropic plate immersed in a fluid and have obtained the dispersion curves as well as the attenuation curves. These have been reported in an earlier paper (5). Some results from the work are shown in Fig. 7 for the sake of continuity.

Before embarking on the NDE of composites, we performed some numerical calculations to study the sensitivity of various wave speeds and frequencies on different components of the stiffness matrix. The four elastic constants c_{11}, c_{33}, c_{55}, and c_{13} are the contributors to the dispersion equations. In this study one stiffness coefficient is decreased at a time and the Lamb wavespeed calculated. The studies are made on a $[0/90_4]_s$ laminate. The effects of the degradation in stiffness constants on the basic symmetric and asymmetric modes, s_0 and a_0 respectively, are studied. The results for the symmetric mode at a fd = 0.25 MHz-mm (kd = 0.32) are shown in Fig. 5a. Quite expectedly, only c_{11} contributes significantly to the reduction in the wavespeed. The effect of c_{33} and c_{13} is very small and the effect of c_{55} is practically zero. An interesting result is that if the degradation takes place in c_{13} then the wavespeed increases; the effect is however very small. Shown in Fig. 5b is the effect of stiffness degradation on the a_0 mode at fd = 0.5 MHz-mm (kd = 0.63). Now a_0 is the fundamental flexural mode and is well known that shear deformation plays a significant role in the propagation of flexural waves. Accordingly, it is observed that the major

contributor in this case is c_{55} but contributions due to c_{11} and c_{33} are not negligible. A decrease in c_{33} results in an increase in Lamb wavespeed. However, c_{13} does not contribute to the change in wavespeed.

The results for the next higher modes, s_1 and a_1 are shown in Fig. 6. The effect of s_1 mode is studied at fd = 2.00 MHz-mm (kd = 2.53). For this mode the major contribution comes from the c_{33} and c_{11}. On the other hand degradation in c_{55} and c_{13} will tend to increase the wavespeed and their contributions are not negligible. The results for a_1 mode are at fd = 0.6 MHz-mm (kd = 0.76). Here c_{11} and c_{55} effects are of the same order and c_{33} and c_{13} effects are negligible.

The conclusions of this study are that the Lamb wave technique is useful in measuring the degradation in c_{11}, which can be made with tests in s_0 mode. To some extent, by using the a_0 mode the degradation in c_{55} can be studied. Since contributions from other modes will also affect the Lamb wave speed, the measurements will not be reliable for the case of a_0 mode. But a combination of tests may prove to be useful. For example, the degradation in c_{33} and c_{11} can be measured by tests in s_1 mode. If the ratio of these degradations is estimated, then the effect of c_{33} can be separated. Similarly, the effect of c_{55} can be measured by combining a_1 and s_0 modes. Based on this sensitivity study it was decided to carry out all measurements in the s_0 mode.

First, the tests were performed on a $[0/90_3]_s$ graphite/epoxy composite laminate. The dispersion curves for this specimen are shown in Fig. 7a. The solid lines are for symmetric mode and dashed lines for asymmetric modes. The attenuation curves for various modes are shown in Fig. 7b. The tests for Lamb wavespeed and attenuation in undamaged specimens, as described earlier, are performed and the results are shown as discrete points on Fig.7. The theoretical curves are from stiffness values calculated by the rule of mixtures (7); the agreement between

theory and experiments is considered satisfactory. The static stiffness of the laminate was also measured in a tensile testing machine and the corresponding wavespeed is shown as an arrow in Fig. 7a. This shows that if the experimentally determined values of the stiffness constant are used in the dispersion relations then a better correlation between the theory and experiments will be observed.

Now the same $[0/90_3]_s$ laminate is tested to study the effect of transverse cracks on the Lamb wave speed and attenuation. The tests are conducted at a frequency of 0.5 MHz with fd = 0.275 MHz-mm (kd = 0.34). The reduction in the normalized stiffness as a function of number of cracks per centimeter as damage progresses is shown in Fig. 8. The normalized stiffness is defined as E/E_0 where E_0 is the stiffness of the undamaged laminate and E is the stiffness of the damaged laminate. The figure also shows a dashed horizontal line which denotes the stiffness of the damaged laminate calculated by the ply-discount theory. In this theory the stiffness of the cracked lamina is assumed to be zero in the direction normal to the crack and the laminate stiffness is synthesized. The experimental results obtained by the Lamb wave technique are within the lower limit set by the theoretically obtained limit.

Next, a $[0/90_4]_s$ laminate is tested when damage is induced in it. The test is performed at 0.5 MHz with fd=0.355 MHz-mm (kd = 0.44). The reduction in stiffness for this laminate is shown in Fig. 9. Also shown in the figure is the damage state and the position of the transmitter (TR) and receiver (R) relative to the specimen. It is observed that in going from damage state 3 to state 4, though there was a substantial increase in the total number of cracks in the specimen, the number of cracks in the region interrogated by the transducer did not increase. As a consequence, no change in the stiffness of the specimen was recorded. This is very reassuring for it demonstrates that our measurement reflects local changes in the stiffness. For this specimen, stiffness reduced by about 30 % as compared

to the virgin state. The dashed line shows the stiffness reduction as calculated from the ply-discount theory but for this specimen the measured stiffness was slightly lower than the theoretically calculated value. In comparison to the reduction for the $[0/90_3]_s$ laminate it is observed that the stiffness reduction for this laminate is larger. The reason for this is that the net contribution of the eight-90° plies to the overall stiffness is more than the contribution of six-90° plies and hence failure of plies in the $[0/90_4]_s$ laminates results in a higher reduction in relative stiffness. Observe that the $[0/90_3]_s$ laminate has a crack length of 6-ply thickness long while the $[0/90_4]_s$ laminate has a larger crack length of 8-ply thickness long.

The next set of tests were performed on a $[0_2/90_2/0]_s$ laminate. For this laminate the crack size is very small; 2 ply-thickness long. The reduction in stiffness as transverse cracks are introduced is shown in Fig. 10. Observe a smaller reduction in stiffness. Even though this laminate has four-90° plies, they are divided into groups of two, and also, the total number of 0° plies in this laminate is increased three times. Thus the total contribution of the 90° plies to the overall stiffness is very low and hence their failure results in less reduction in stiffness.

The attenuation increase in the three laminates tested are combined together and shown in Fig. 11. Shown also in the figure are the k_1a for the three laminates. The purpose behind this presentation is to demonstrate the effect of the normalized scattering cross-section of the cracks, k_1a, on the attenuation. In this context we cite an excellent work by Tan (10) who has calculated the normalized scattering cross-section of a Griffith crack subjected to a longitudinal plane wave loading; see Fig. 12. Since Tan's calculation is for an unbounded medium, it cannot be applied quantitatively to the present case. However, it does provide an excellent background in which the present results can be explained

qualitatively. In $[0_2/90_2/0]_s$ laminate $k_1a = 0.06$. As is well known this is the so-called Rayleigh scattering regime where the scattering cross-section of a cracks is very small. The waves pass through the plate without seeing the cracks and as a result the increase in attenuation is very low. For $[0/90_3]_s$ laminate $k_1a = 0.26$ while for the $[0/90_4]_s$ laminate $k_1a = 0.45$ and the observed increase in attenuation is very high. The effect of k_1a on measured attenuation is very interesting. Kinra (11) has worked with composites consisting of Lead spheres in an epoxy matrix and has shown that the wave propagation in these composites occurs along two separate branches: (1) the low frequency, slower, acoustical branch along which the particle motion is essentially in phase with the excitation, and (2) the high frequency, faster, optical branch along which the particle displacement is essentially out of phase of the excitation. The two are separated by a cut-off frequency which corresponds to the excitation of the rigid-body-translation resonance of the heavy inclusion. This occurs when $k_1a = O(1)$, where a is the inclusion radius. Around the cut-off frequency both the phase velocity as well as the attenuation change very dramatically. This phenomenon is shown in Fig. 13 taken from our earlier work(12). It is our conjecture that a similar phenomenon is taking place in these laminates and the cracks act as inclusions.

These results forewarn against an arbitrary selection of the test frequencies. Depending on the flaw size, a, the test frequency and hence the k_1a has to be chosen such that a good signal amplitude decay curve is obtained. If the attenuation falls very slowly with damage then it will not be a sensitive measure of the damage. On the other hand if the attenuaton falls very rapidly then at a relatively low crack density the received signal will be lost and the measurement will be inaccurate.

CONCLUSIONS

Propagation of a leaky Lamb wave in its fundamental mode in three cross-ply

laminates; $[0_2/90_2/0]_s$, $[0/90_3]_s$, and; $[0/90_4]_s$, has been studied experimentally. The effect of matrix cracking on the speed (i.e. stiffness) and attenuation was studied in the long wavelength regime. As expected, it was found that the in-plane stiffness decreases while the attenuation increases with linear crack density. Therefore, either of these quantities may be used to measure the damage-induced degradation of the in-plane stiffness. A particular advantage of this method is that one can measure the local values (average over the transducer diameter) of stiffness. The attenuation, on the other hand, is averaged over the distance between the transmitter and receiver.

ACKNOWLEDGEMENT

This research was supported by the Air Force Office of Scientific Research under Grant No. AFOSR-84-0066 to Texas A&M University. The program managers were Dr. David Glasgow and Dr. George Haritos.

REFERENCES

1. H.I. Ringermacher, "Ultrasonic Velocity Characterization of Fatigue Damage in Graphite/Epoxy Composites", Proc. IEEE 1980 Ultrasonic Symp., Boston, 957-960 (Nov 1980).
2. J.H. Cantrell, Jr., W.P. Winfree, J.H. Heyman, and J.D. Whitcomb "Multiparameter Characterization of Fatigue Damage in Graphite/Epoxy Composite Material", Proc. IEEE 1980 Ultrasonic Symp., Boston, 1003-1005 (Nov 1980).
3. J.G. Eden, "The Application of Ultrasonics to assess Damage in Composite Materials", M.S. Thesis 1985, Texas A&M University, College Station, Tx 77843 (1985).
4. Y. Bar-Cohen, D.E. Chementi, "NDE of Defects in Composites using leaky Lamb waves", Proc. 15th. Symp. on NDE Sponsored by NTIAC & SWRI and South Texas Section of ASNT, San Antonio, TX, (Apr 1985)
5. V. Dayal, and V.K. Kinra, "Leaky Lamb Waves in an Isotropic Plate - An Exact Solution and Experiments" to be published in J. Acoust. Soc. Am.
6. C.C. Habegar, R.W. Mann,and G.A. Baum, "Ultrasonic plate waves in paper", Ultrasonics, 57-62, (Mar 1979)
7. B.D. Agarwal, L.J. Broutman, *Analysis and Performance of Fiber Composites*, John Wiley & Sons, NY, 20, (1980)
8. L.G. Merkulov, "Damping of Normal Modes in a Plate Immersed in a Liquid", Soviet Physics-Acoustics, 10(2) (Oct-Dec 1964).
9. T.J. Plona, M. Baharavesh and W.G. Mayers, "Rayleigh and Lamb Waves at Liquid Solid Boundaries", Ultrasonics, 171-174, (July 1975).
10. T.H. Tan, "Scattering of Plane Elastic Waves by a Plane Crack of Finite Width", J. Appl. Sci. Res., 33, 75-100.
11. V.K. Kinra, "Dispersive Wave Propagation in Random Particulate Composites", Recent Advances in Composites in the United States and Japan, ASTM STP 864,

ed., J.R. Vinson and M. Taya, 309-325 (1985).

12. V.K. Kinra and V. Dayal, " A New Technique for Ultrasonic Nondestructive Evaluation of thin Specimens", Expt. Mech., 28(3), 288-297, (Sept 1988).

LIST OF FIGURES

Fig. 1 Wave propagation direction, shown by arrows, with respect to transverse cracks in a cross-ply laminate.

Fig. 2 Generation and propagation of Lamb waves in a plate immersed in water.

Fig. 3 Block diagram of the experimental set up.

Fig. 4 Angle of incidence vs the received signal amplitude.

Fig. 5 Effect of degradation in stiffness coefficients in a $[0/90_4]_s$ laminate on Lamb wave wavespeed of (a) s_0 mode and (b) a_0 mode.

Fig. 6 Effect of degradation in stiffness coefficients in a $[0/90_4]_s$ laminate on Lamb wave wavespeed of (a) s_1 mode and (b) a_1 mode.

Fig. 7 Dispersion and attenuation curves for $[0/90_4]_s$ laminate. The circled data are experimental.

Fig. 8 (a) Reduction in stiffness, and (b) increase in attenuation of $[0/90_3]_s$ laminate, f=0.5 MHz, d=0.55 mm.

Fig. 9 Reduction in stiffness as transverse cracks increase in a $[0/90_4]_s$ laminate, f=0.5 MHz, d=0.71 mm. Line sketch shows damage state.

Fig. 10 Reduction in stiffness in a $[0_2/90_2/0]_s$ laminate, f=0.5 MHz, d=0.71 mm.

Fig. 11 Relative study of the increase in attenuation for the three laminates tested.

Fig. 12 Normalized plane-wave extinction cross-section for the scattering of a P-wave by a crack of finite width. (Ref. Tan (10))

Fig. 13 (a) Normalized phase velocity and, (b) Attenuation variation with normalized frequency, $\Omega(\Omega=k_1a$ where a is inclusion radius), in Lead Epoxy Composite at volume fraction $\tilde{c}$. (Ref. Kinra and Dayal (12)).

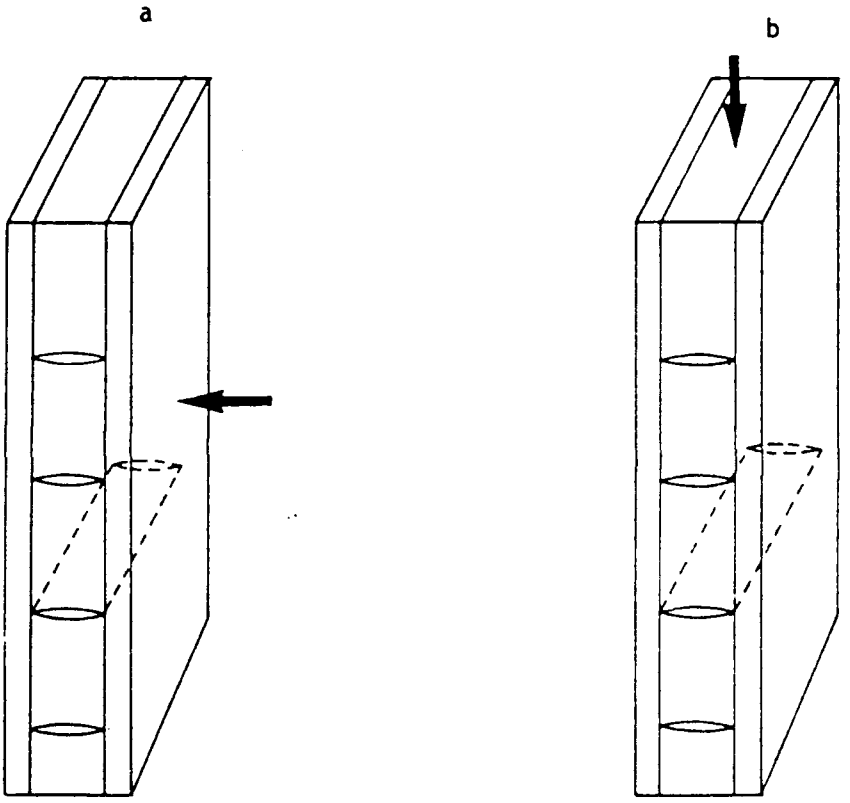

THROUGH-THE-THICKNESS MODE

LAMB WAVE MODE

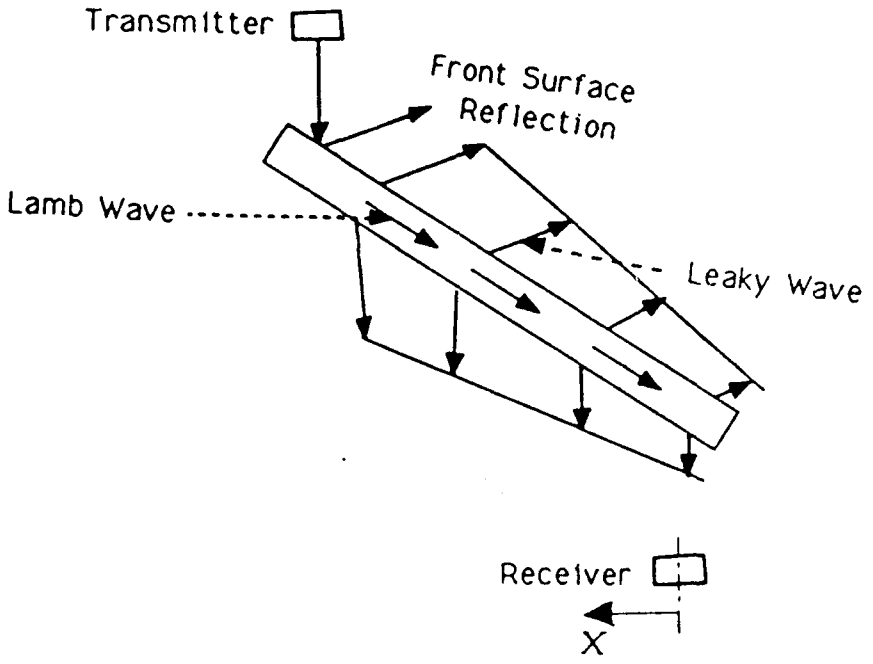
Transmitter
Front Surface
Reflection
Lamb Wave
Leaky Wave
Receiver
X

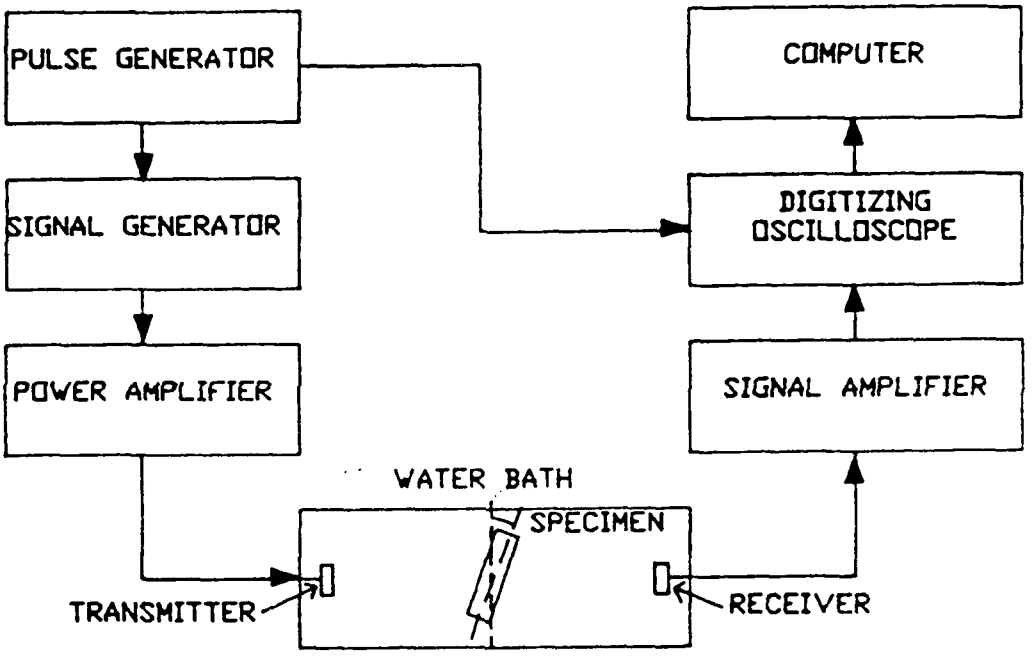
PULSE GENERATOR
SIGNAL GENERATOR
POWER AMPLIFIER
COMPUTER
DIGITIZING OSCILLOSCOPE
SIGNAL AMPLIFIER
WATER BATH
SPECIMEN
TRANSMITTER
RECEIVER

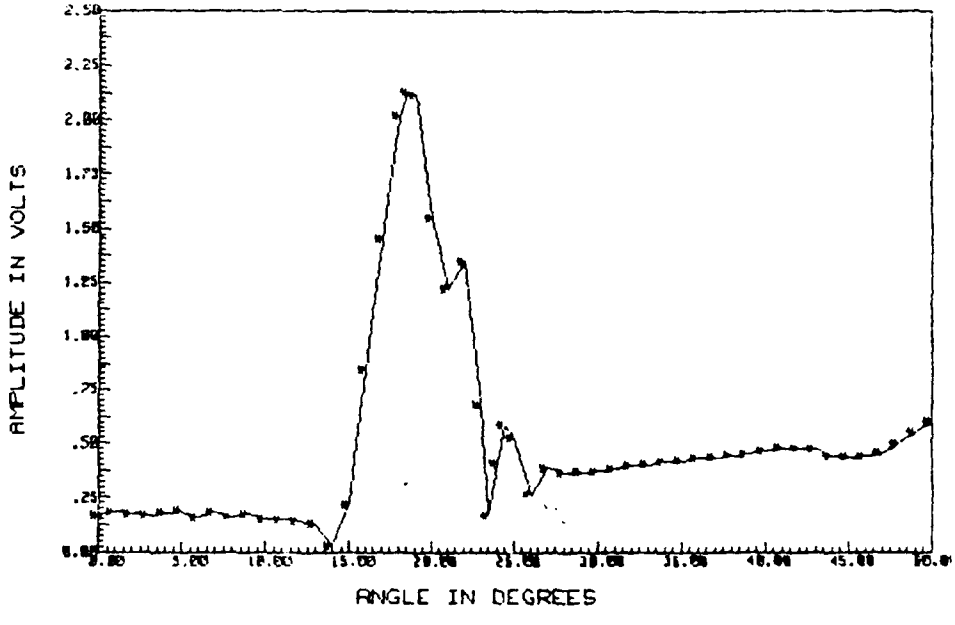
AMPLITUDE IN VOLTS
ANGLE IN DEGREES

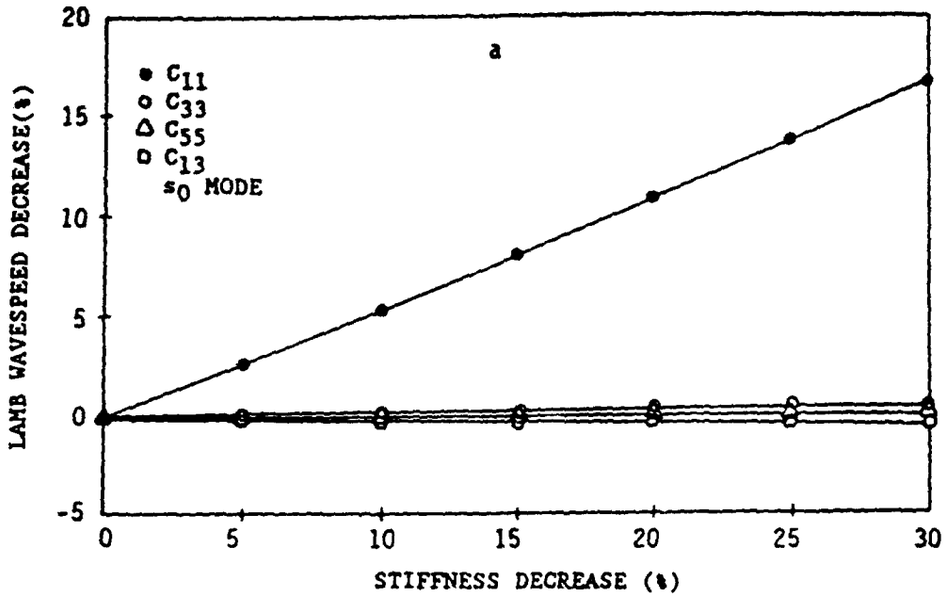
a
C_{11}
C_{33}
C_{55}
C_{13}
s_0 MODE
LAMB WAVESPEED DECREASE(%)
STIFFNESS DECREASE (%)
20
15
10
5
0
-5
0
5
10
15
20
25
30

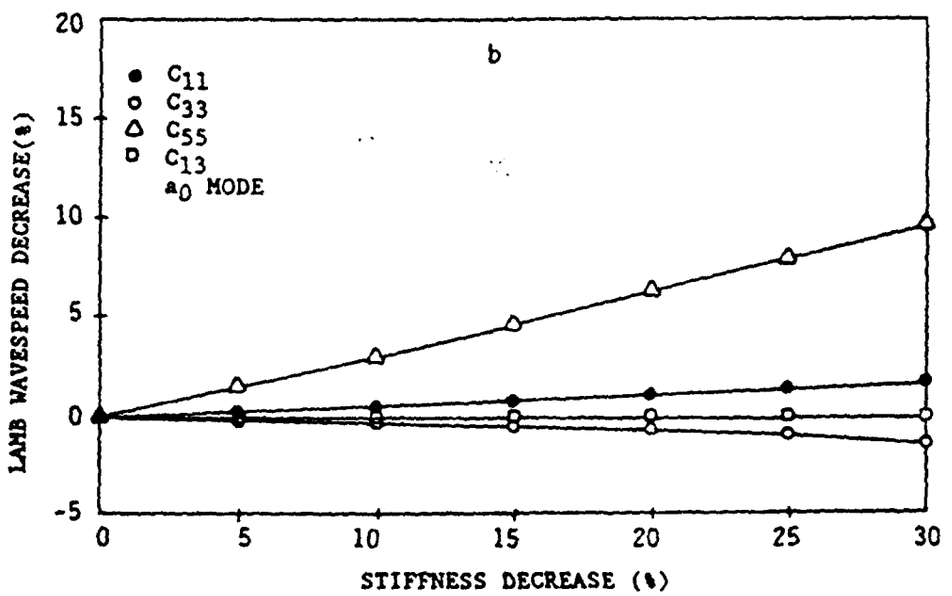
b
C_{11}
C_{33}
C_{55}
C_{13}
a_0 MODE
LAMB WAVESPEED DECREASE(%)
STIFFNESS DECREASE (%)
20
15
10
5
0
-5
0
5
10
15
20
25
30

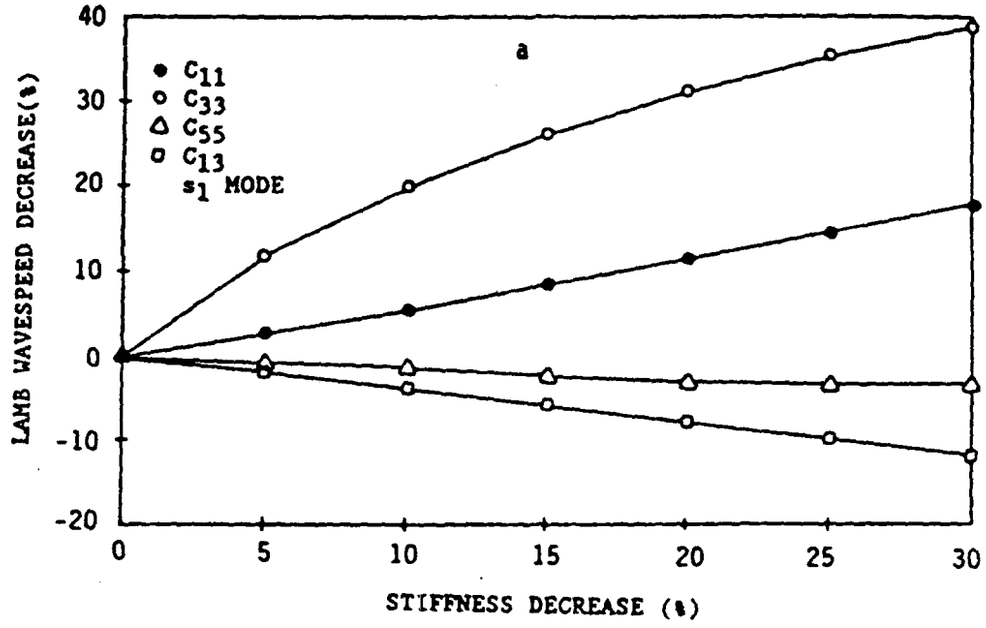
a
C_{11}
C_{33}
C_{55}
C_{13}
s_1 MODE
LAMB WAVESPEED DECREASE(%)
STIFFNESS DECREASE (%)
40
30
20
10
0
-10
-20
0
5
10
15
20
25
30

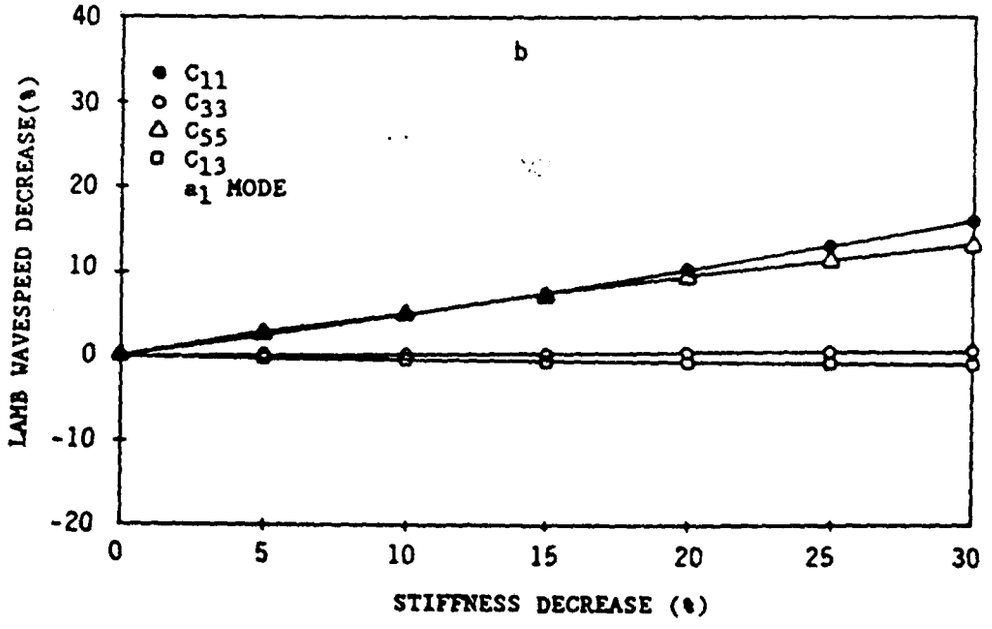
b
C_{11}
C_{33}
C_{55}
C_{13}
a_1 MODE
LAMB WAVESPEED DECREASE(%)
STIFFNESS DECREASE (%)
40
30
20
10
0
-10
-20
0
5
10
15
20
25
30

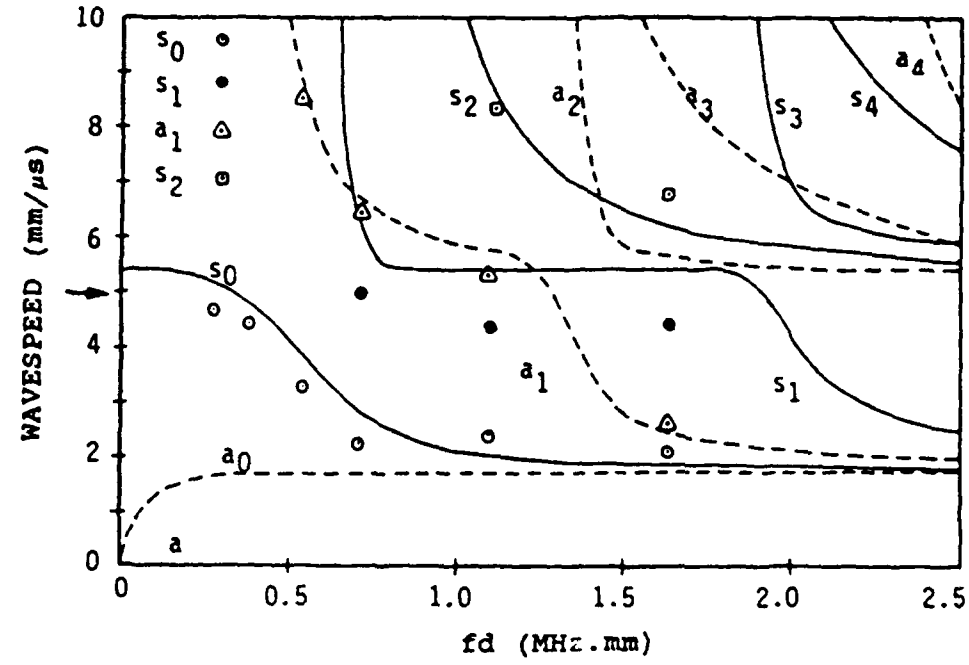
WAVESPEED (mm/μs)
fd (MHz.mm)
a
b
s_0
s_1
a_1
s_2
a_0
a_2
s_3
a_3
s_4
a_4

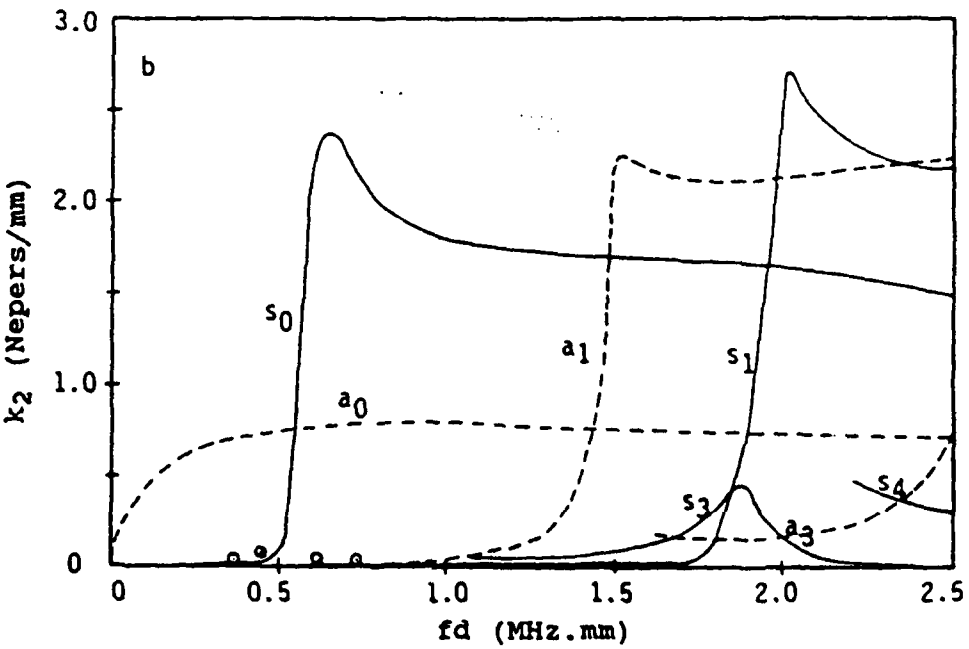
k_2 (Nepers/mm)
fd (MHz.mm)
b
s_0
a_0
a_1
s_1
s_3
a_3
s_4

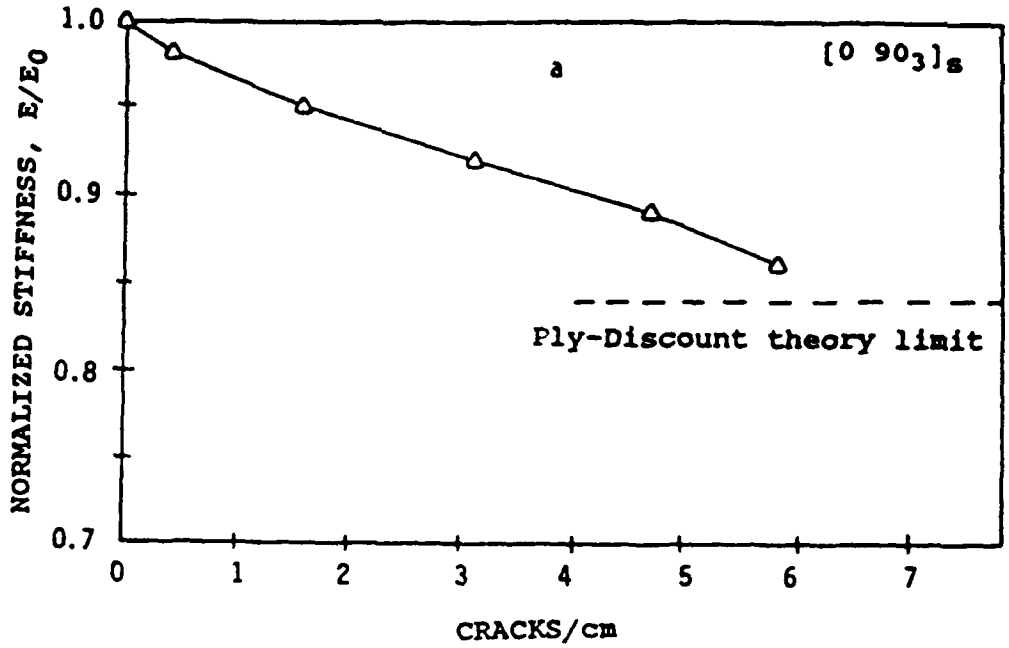
1.0
0.9
0.8
0.7
NORMALIZED STIFFNESS, E/E0
a
[0 90$_3$]$_s$
Ply-Discount theory limit
0
1
2
3
4
5
6
7
CRACKS/cm

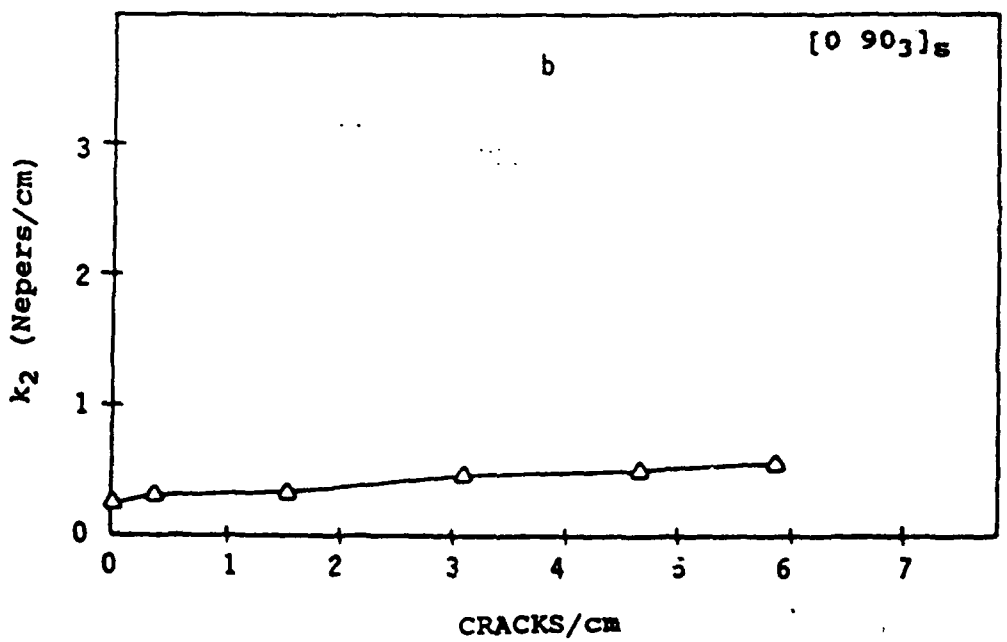
b
[0 90$_3$]$_s$
k_2 (Nepers/cm)
3
2
1
0
0
1
2
3
4
5
6
7
CRACKS/cm

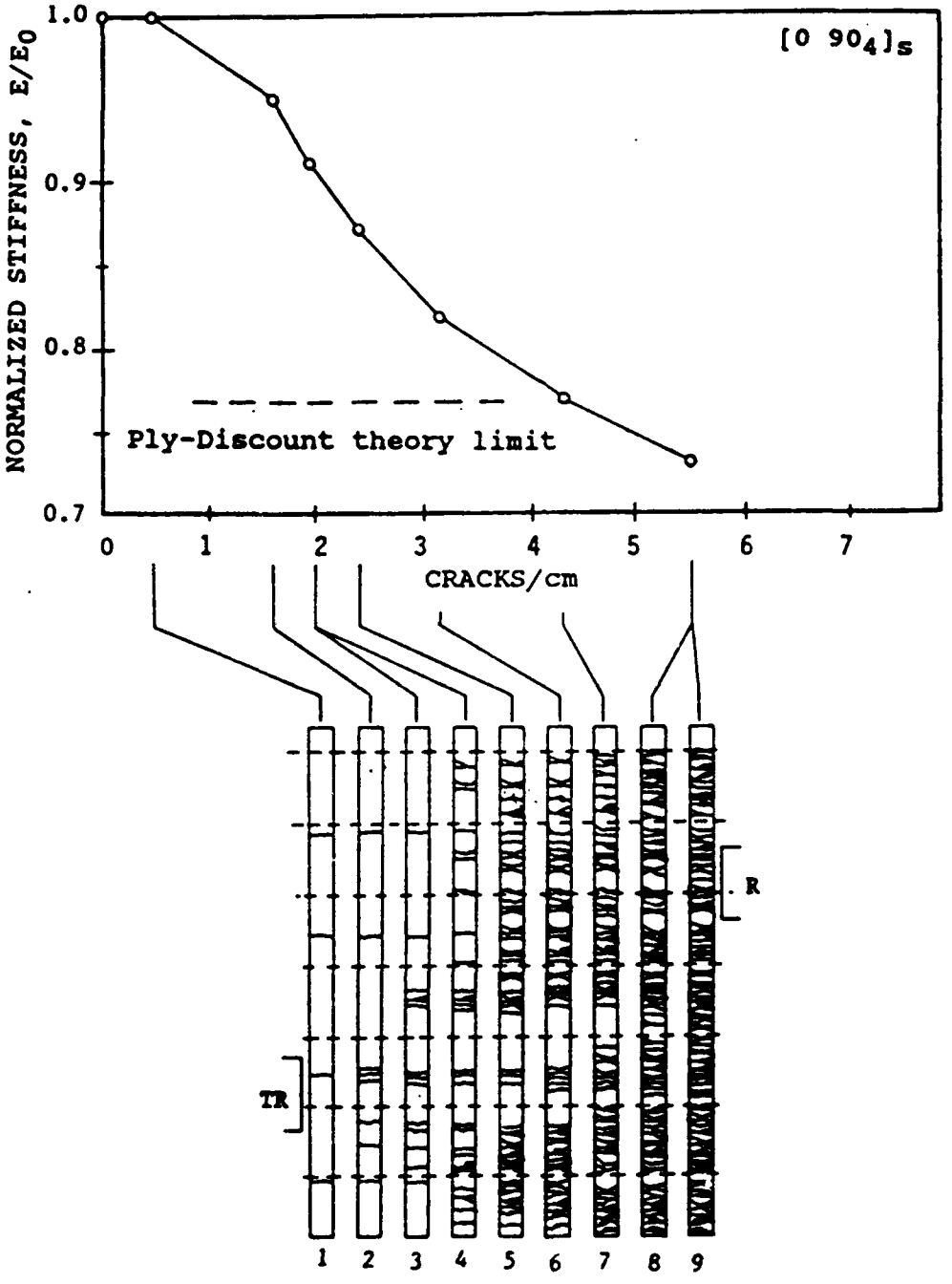
NORMALIZED STIFFNESS, E/E0
1.0
0.9
0.8
0.7
[0 90$_4$]$_s$
Ply-Discount theory limit
0
1
2
3
4
5
6
7
CRACKS/cm
TR
R
1
2
3
4
5
6
7
8
9

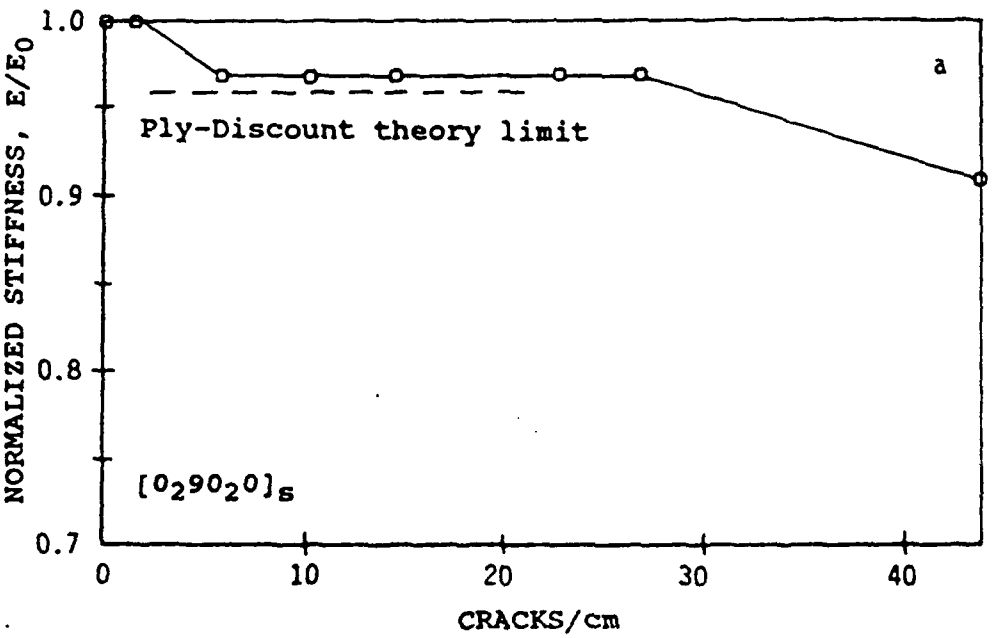
1.0
0.9
0.8
0.7
NORMALIZED STIFFNESS, E/E_0
a
Ply-Discount theory limit
$[0_2 90_2 0]_s$
0
10
20
30
40
CRACKS/cm

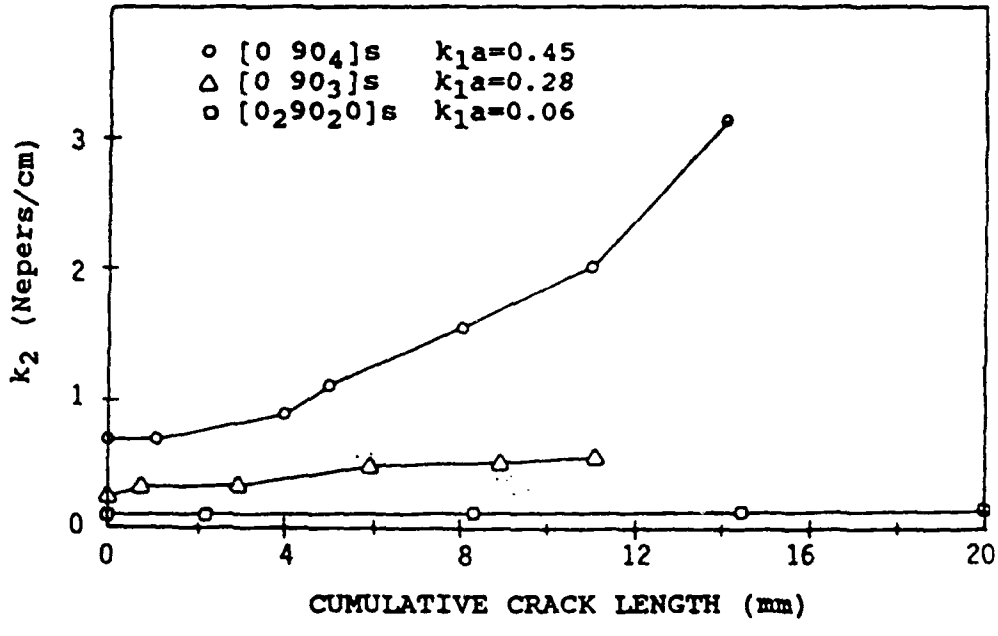
o [0 90$_4$]s k_1a=0.45
Δ [0 90$_3$]s k_1a=0.28
o [0$_2$90$_2$0]s k_1a=0.06
k_2 (Nepers/cm)
0
1
2
3
0
4
8
12
16
20
CUMULATIVE CRACK LENGTH (mm)

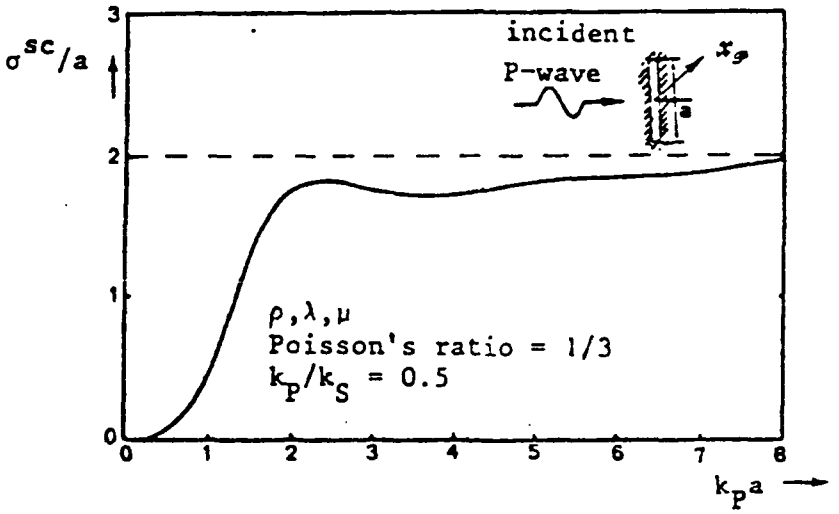
σ^{sc}/a
3
2
1
0
incident
P-wave
x_3
a
ρ, λ, μ
Poisson's ratio = 1/3
k_p/k_s = 0.5
0
1
2
3
4
5
6
7
8
$k_p a$

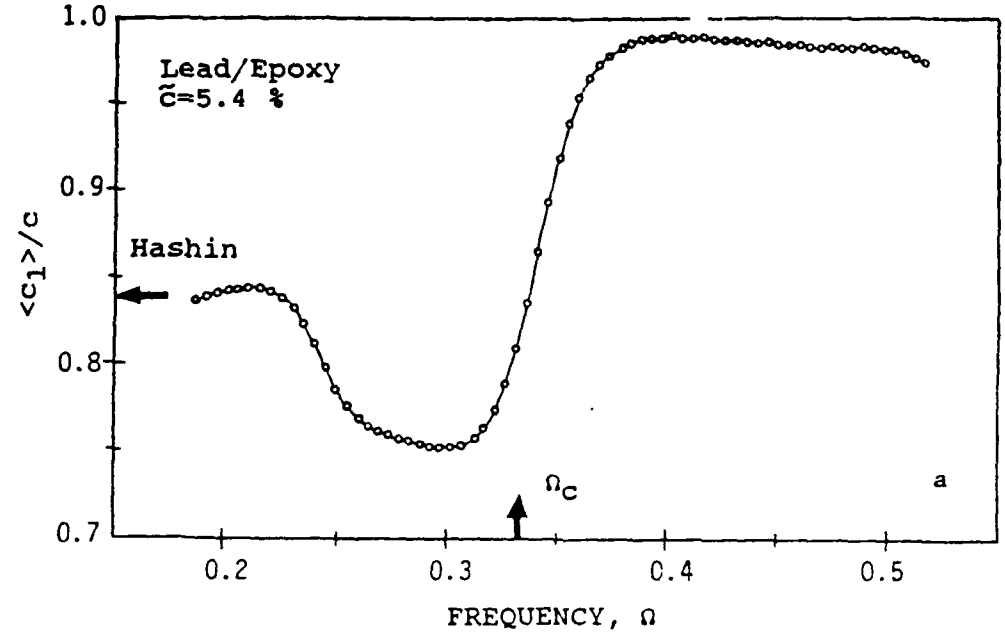
Lead/Epoxy
$\tilde{c}$=5.4 %
Hashin
$<c_1>/c$
1.0
0.9
0.8
0.7
Ω_c
a
0.2
0.3
0.4
0.5
FREQUENCY, Ω

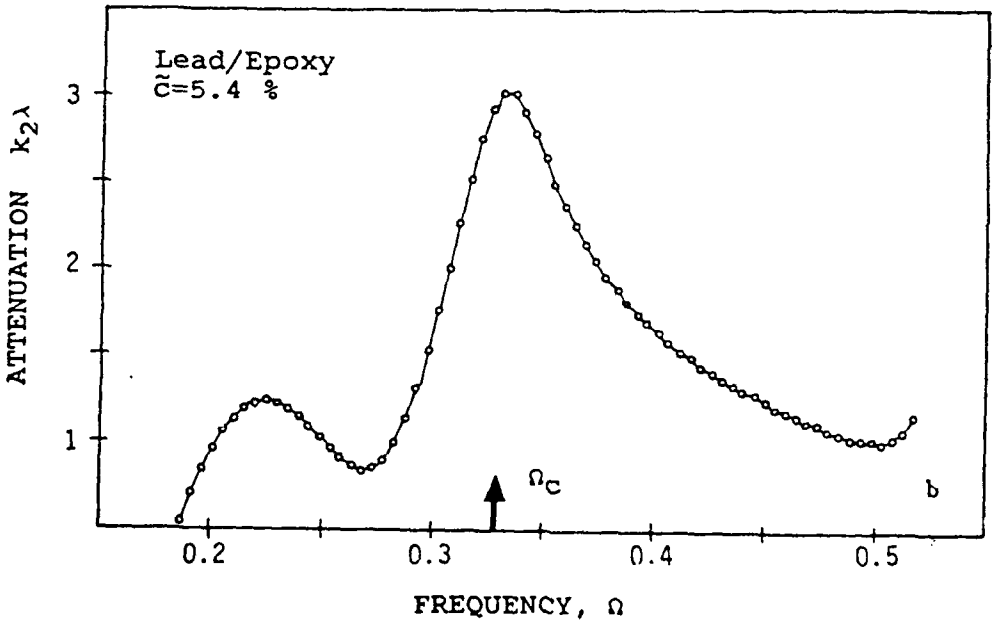
Lead/Epoxy
$\tilde{c}$=5.4 %
ATTENUATION $k_2\lambda$
3
2
1
Ω_c
b
0.2
0.3
0.4
0.5
FREQUENCY, Ω